Conference book of

19th International Conference on

Electrorheological Fluids and Magnetorheological Suspensions

July 7-10, 2025

Concordia University, Montreal, QC, Canada

Chairs: Ramin Sedaghati

Norman Wereley

Subhash Rakheja

Conference book of

19th International Conference on

Electrorheological Fluids and Magnetorheological Suspensions (ERMR 2025)

July 7-10, 2025

Concordia University

Montreal, QC, Canada

Chairs: Ramin Sedaghati

Norman Wereley

Subhash Rakheja

Editors:

Ramin Sedaghati
Concordia University
Montreal, QC, Canada

Norman Wereley
University of Maryland at College Park
MD, USA

Subhash Rakheja
Concordia University
Montreal, QC, Canada

Preface

Welcome to Montreal, Canada, and welcome to the 19th International Conference on Electrorheological Fluids and Magnetorheological Suspensions (ERMR2025).

International Conference on Electrorheological Fluids and Magnetorheological Suspensions (ERMR) is a premium and the longest-running international conference dedicated to the electrorheological fluids and magnetorheological suspensions. ERMR2025 is organized to delve into a spectrum of topics, related to ER and MR materials ranging from basic material science to the innovative engineering applications. For over 35 years, this biannual conference has provided a unique multidisciplinary platform to address ER and MR technology in various countries and now for the first time, it is held in Canada and in the beautiful city of Montreal.

ERMR aims at promoting research, development and application of electrorheological fluids and magnetorheological suspensions through the exchange of scientific results and insight from leading international scholars and specialists as well as the young researchers. The conference showcases the state of the art in this innovative and multidisciplinary area. It provides a forum for discussion of recent advances in the fields of smart materials and encourages the transfer of advanced scientific results from research to application. The main topics include functional ER and MR fluids, gels and elastomers; MR-based suspensions and devices; magnetoactive metamaterials materials; modeling and characterization; magnetoactive sensors and actuators; aerospace and ground technologies featuring MR and ER materials; smart fluid-based energy saving and harvest, etc.

ERMR maintains the tradition of a single-session format, and this intimate setting has furthered international understanding and launched long-lasting friendship. This year we look forward to welcoming over 90 participants who contributed 72 technical papers that are presented to you through plenary, oral and poster presentations.

We are pleased to acknowledge the support from National Research Council Canada, Concordia University, journals of Actuators (MDPI), journal of Smart material and Devices and the Canadian Society of Mechanical Engineering. The assistance from the members of the International Organizing Committee (IOC) and the Local Organizing Committee is much appreciated.

We are honored to host the 19th event of the ERMR this year and are delighted to welcome you to the metropolitan city of Montreal, the largest bilingual city in North America, and the cultural capital of Quebec. With your participation, we anticipate a valuable, enjoyable and memorable event. We wish you a great stay in this fascinating place!

Ramin Sedaghati (Concordia University), Norman Wereley (University of Maryland at College Park) and Subhash Rakheja (Concordia University)

ERMR2025 General and Co-Chairs

Conference Organization

Local Organizing Committee

General Chair	Ramin Sedaghati Concordia University
General Co-Chair	Subhash Rakheja Concordia University
General Co-Chair	Norman Wereley University of Maryland
Program Chair	Amin Fereidooni National Reseach Council Canada
Program Co-Chair	Viresh Wickramasinghe National Reseach Council Canada
Technical Chair	Alireza Moezi Concordia University
Technical Co-Chair	Amin Saber Concordia University

International Scientific Committee

Daniel Barber	Lord Corporation USA
Holger Boese	Fraunhofer Institute Germany
Antonio Jose Faria Bombard	Federal University of Itajubá Brazil

Georges Bossis	University of Nice France
Andrejs Cebers	Institute of Physics Latvia
Hyoung Jin Choi	Inha University South Korea
Seung-Bok Choi	The State University of New York (SUNY Korea) South Korea
Juan de Vicente	University of Granada Spain
Xufeng Dong	Dalian University of Technology China
Fernando Gonzalez-Caballero	University of Granada Spain
Faramarz Gordaninejad	University of Nevada, Reno USA
Daniel J. Klingenberg	University of Wisconsin, Madison USA
William Kordonski	QED Technologies Inc. USA
Evguenia Korobko	A. V. Lykov Heat and Mass Transfer Institute Belarus
Weihua Li	University of Wollongong Australia

Kunquan Lu	Chinese Academy of Science China
James E. Martin	Sandia National Laboratory USA
Masami Nakano	Tohoku University Japan
Stefan Odenbach	Technische Universitat, Dresden Germany
Subhash Rakheja	Concordia University Canada
Ramin Sedaghati	Concordia University Canada
Rongjia Tao	Temple University USA
Halil Ibrahim Unal	Gazi University Turkey
Xiaojie Wang	Chinese Academy of Science China
Weijia Wen	Hong Kong University of Science and Technology Hong Kong
Norman Wereley	University of Maryland USA
Jianbo Yin	Northwest Polytechnic University China

Miao Yu	Chongqing University China
Xiaopeng Zhao	Northwestern Polytechnical University China
Andrey Zubarev	Ural Federal University Russia

National Scientific Committee

Hamid Akbarzadeh	McGill University Montréal, Québec
Siamak Arzanpour	Simon Fraser University Burnaby, British Columbia
Ashutosh Bagchi	Concordia University Montréal, Québec
Yong Chen	National Research Council Canada Ottawa, Ontario
Javad Dargahi	Concordia University Montréal, Québec
Eric Diller	University of Toronto Toronto, Ontario
Mehdi Eshaghi	Carleton University Ottawa, Ontario
Masoud Hemmatian	Pratt & Whitney Canada Mississauga, Ontario
Amir Hooshiar	McGill University Montréal, Québec

Alice Jarry	Concordia University Montréal, Québec
Mehrdad R. Kermani	Western University London, Ontario
Hani Naguib	University of Toronto Toronto, Ontario
Muthukumaran Packirisamy	Concordia University Montréal, Québec
Jean-Sebastien Plante	Université de Sherbrooke Sherbrooke, Quebec
David Rancourt	University of Sherbrooke Sherbrooke, Quebec
Ion Stiharu	Concordia University Montréal, Québec
Afzal Suleman	University of Victoria Victoria, British Columbia
Hossein Vatandoost	National Research Council Canada Boucherville, Québec
Viresh Wickramasinghe	National Research Council Canada Ottawa, Ontario
Wen-Fang Xie	Concordia University Montréal, Québec

Table of Contents

Plenary Speakers – Abstracts

MR Metamaterials

MR Technology

MR Fundamentals

MR Fluid

Author Index

From Jacob Rabinow to David Carlson and Beyond: A Walk Down the MR Fluid and Devices History Lane

Mehdi Ahmadian

Center for Vehicle Systems & Safety, Virginia Tech, MC-0901, 3103 Commerce Street, Blacksburg, VA 24061, USA

ahmadian@vt.edu

Abstract

This presentation strolls down the magnetorheological (MR) fluids and devices memory lane by exploring their scientific and commercial progress from their discovery by Jacob Rabinow in 1948 to today. It recites some of the earlier MR patents in clutches and brakes to their reincarnation in the early 1990s, led by David Carlson. Dave's somewhat one-man effort to lead the crusade for convincing his employer, Lord Corporation, and the rest of the scientistic community to invest in and explore MR fluids is assessed. His efforts led to the rekindling of interest by the broader intelligent fluids and devices community to study, improve, and invent a new generation of MR fluids during the past two decades, which is also reviewed. Reflecting on some of the recent developments, the presentation provides a glimpse into some of the future discoveries in MR fluids and devices.

Development of Magnetorheological Elastomer Isolators with Metamaterial Structures

Weihua Li

School of Mechanical, Materials, Mechatronic, and Biomedical Engineering, University of Wollongong, Wollongong, New South Wales 2522, Australia

weihuali@uow.edu.au

Abstract

Semi-active isolators working with laminated magnetorheological elastomer (MRE) structures have found applications in vibration control. This work reports the development of new MRE isolators with metamaterial structures for enhancing vibration suppression capabilities suitable for wide frequency ranges. This novel design takes advantage of tunable vibration bandgaps from novel metamaterial structures. Specifically, metamaterial MRE isolators were designed and prototyped. The mechanism of the formation of vibration bandgaps, for both infinite and finite periodic structures, was theoretically analysed, which details the equivalent negative stiffness of the metamaterial MRE isolator. Experiments were conducted to evaluate bandgaps of the metamaterial MRE isolators and their vibration isolation capacity. Results demonstrate that the new metamaterial MRE isolators are capable of offering enhanced vibration isolation performance with controllable bandgaps.

Multifunctional and Metamaterials for Warfighter Protection

Ken Loh

Department of Structural Engineering, University of California San Diego, La Jolla, CA, United States

kjloh@ucsd.edu

Abstract

The safety, resiliency, and survivability of the warfighter, whether in a training or forward deployed environment, are of utmost importance for the military. For instance, musculoskeletal injuries are the leading cause of military disability discharge, which amount to ~1.6 million injuries per year within the U.S. Department of Defense. At sea, sailors and damage control personnel perform duties in hazardous conditions, especially when responding to shipboard emergencies because of smoke, fire, flood, and/or radiation. Similarly, resiliency at sea is further put to test during search and rescue of sailors fallen overboard. The goal of this presentation is to highlight three unique ongoing efforts in multifunctional and metamaterials development in the ARMOR Lab, all aimed at enhancing warfighter performance and protection. First, graphene nanosheet (GNS) piezoresistive sensors were integrated with firefighting equipment, specifically the self-contained breathing apparatus. The GNS sensors were strategically placed to measure the health, activities, and surrounding conditions of shipboard personnel during shipboard damage control operations. Laboratory and shipboard human subject tests were conducted and showed that gait, movement, and respiration rate could be accurately measured. The second example is the design of a wearable, passive, antenna uniform patch that changes shape (and thus its antenna signature) when a sailor falls overboard, so that the identity, location, and condition of the sailor could be quickly determined using remote sensing. Termed Active Skins, these additively manufactured mechanical metamaterials incorporated specific stimuli-responsive materials to detect parameters such as temperature changes and exposure to seawater. The last example showcases an additively manufactured field-responsive mechanical material (FRMM) that exhibits dynamic control and on-the-fly tunability. Specifically, complex structures of polymeric tubes were printed and infilled with magnetorheological fluid suspensions. Modulating applied magnetic fields resulted in rapid, reversible, and sizable changes of the FRMM's effective stiffness, which could be potentially used as a wearable adaptive armor.

Energy Absorption Strategies for Occupant Protection in Aerospace and Automotive Vehicles

Norman Wereley

Department of Aerospace Engineering, University of Maryland, College Park, MD 20742, USA

wereley@umd.edu

Abstract

The ability to dissipate energy in vehicle systems, especially with the goal of protecting occupants from potentially injurious vibration, repetitive shock, crash and blast loads, is becoming a critical issue as the cumulative impact of these load spectra on chronic health and acute injury are becoming better understood. The objective of this talk is to discuss what properties are optimal for energy absorption (EA) applications such as impact or shock load mitigation. Two primary strategies will be discussed in this talk: passive vs. semi-active energy absorbers. The first focus is the use of crushable materials to absorb energy. Two classes of passive materials will be discussed for EA applications including sintered and composite hollow glass foam materials, as well as elastomeric or plastic cellular materials. The second focus is the use of magnetorheological fluids (MRFs) or magnetorheological elastomers in EA applications. The properties of the MRF can be optimized for a particular application. A number of key nondimensional parameters can be used to gain insight into how to define optimality for various applications including: Bingham number, Hedstrom number, Reynolds number, Mason number, dynamic range. Also, the trade-offs associated in designing an optimal MRF for a particular application are discussed. The advantages of passive versus semi-active EA strategies will be discussed.

Microstructure as a key to understand the behavior of magnetorheological elastomers

Stefan Odenbach

Chair of Magnetofluiddynamics, Measuring and Automation Technology, TU Dresden, 01069 Dresden, Germany

stefan.odenbach@tu-dresden.de

Abstract

X-ray microtomography has been proven to be an excellent tool for analyzing the inner structure of magnetic hybrid materials. Using sophisticated methods of digital processing, it has become possible to track changes in the microstructure over numerous steps of changing external stimuli. By combining microstructural investigations with macroscopic characterization of the materials, one can correlate microstructural changes and macroscopic behavior using single descriptors.

In the talk, the techniques and image processing methods will be discussed, along with the experimental procedures used to correlate microstructural aspects with macroscopic behavior. In an outlook, methods to experimentally evaluate the dynamics of structure formation will be outlined.

Clutching Magnetorheological Actuators: an Enabling Technology for Haptic-Robots and High-Performance Machines

Jean-Sébastien Plante

Department of Mechanical Engineering, Université de Sherbrooke, Sherbrooke, QC, Canada

jean-sebastien.plante@usherbrooke.ca

Abstract

In today's era of artificial intelligence, the progress of human-robot physical interaction is now limited by robotic hardware, notably, actuators. Unlike human muscles, the gearmotors used in most robots on the planet cannot perform strong, powerful tasks as well as gentle, dexterous ones in the same package. This presentation will show how clutching actuators based on magnetorheological (MR) fluid clutches repel conventional gearmotor limitations and open the door to new "haptic-robots" capabilities. Functioning of the MR clutching technology is first explained and current applications to active suspension seats and automotive active suspensions are reviewed. Then, an analytical and experimental performance assessment of today's prominent robotic actuator technologies, that is, harmonic drives and quasi-direct-drives, is conducted in comparison with the MR clutching technology. Analytical models of five key performance metrics are developed for torque-to-mass, torque-to-inertia, backdriving loads, rendering stiffness, and power consumption. Finally, the design space of the three actuation technologies is drawn and performance potential in robotics is compared. Results show how MR actuators resolve a gearing conflict by decoupling the motor inertia through a fluidic interface, enabling gearing ratios between 50 to 100:1 with minimal output inertia, and thus, best in class accelerations. Results also show that MR actuators resolve a damping conflict by exploiting the serial positioning of the fluidic interface to tailor damping rates on demand, thus enabling rendering stiffnesses from null up to five times stiffer than harmonic drives. These unique dynamic characteristics combined with best-in-class torque densities in the 100 to 200 N.m/kg range, low backdriving torques, and low power consumption open the door to unseen robotic performance such as cobots capable of human-like haptic tasks.

High performance magnetorheological fluids based on cross-scale particles

Xufeng DONG

School of Materials Science and Engineering, Dalian University of Technology, Dalian 116024, People's Republic of China

dongxf@dlut.edu.cn

Abstract

The vibration reduction of critical engineering structures is closely linked to their longevity, safety, and reliability. Magnetorheological (MR) fluid based intelligent vibration reduction technology offers significant advantages, including a wide range of applicable frequencies, low energy consumption, and excellent stability. Currently, the critical performance indicators of MR fluids, such as shear yield strength, sedimentation stability, and zero-field viscosity, exhibit mutual constraint effects. Achieving a balance among these key performance indicators and developing MR fluids with exceptional comprehensive performance presents a bottleneck problem that hampers the progress of intelligent vibration reduction technology in structural engineering. This study demonstrates that by incorporating homemade, high-saturation magnetization (208.0 emu$\cdot$g^{-1}) nanoparticles as a secondary component in cross-scale bidisperse MR fluids, the performance drawbacks experienced by monodisperse micron particles can effectively be mitigated, leading to a more stable equilibrium between performance factors. The main reason is that nanoparticle addition heightens chain structure density under magnetic fields, while reducing overall particle density when no magnetic field is applied. By substituting some micron particles with nanoparticles, the significant increase in zero-field viscosity caused by direct nanoparticle introduction can be circumvented. The optimal proportion of nanoparticles in MR fluids was preliminarily explored, and it was found that the Micro-Nano bidisperse MR fluids exhibit high shear yield strength (58.3 kPa at 436 kA$\cdot$m^{-1}), excellent sedimentation stability (82.6% at 7 days), suitable zero-field viscosity (1.25 Pa$\cdot$s at 100 s^{-1}), and ideal reversibility. Most notably, the method used to prepare these MR fluids is simple, bestowing considerable value for engineering applications.

Dynamic response of functionally graded graphene origami-enabled auxetic metamaterial sandwich plates embedded with GPLs-reinforced MRE: Experimental, Modeling, and Finite Element Analysis

Reza Aboutalebi[1], Mehdi Eshaghi[2] and Ramin Sedaghati[3]

[1] Department of Mechanical Engineering, Amirkabir University of Technology, Tehran, Iran
(E-mail: reza.aboutalebi@aut.ac.ir)
[2] Department of Mechanical and Aerospace Engineering, Carleton University, Ottawa, Canada
(E-mail: mehdi.eshaghi@carleton.ca)
[3] Department of Mechanical, Industrial and Aerospace Engineering, Concordia University, Montreal, Canada
(E-mail: ramin.sedaghati@concordia.ca)

Short abstract: Magnetorheological elastomers (MREs) are smart materials with tunable viscoelastic properties. Reinforcing MREs with graphene platelets (GPLs) enhances stiffness while preserving tunability. This study analyzes the dynamic response of a sandwich plate with an MRE-GPL core and functionally-graded (FG) graphene origami (GOri)-enabled auxetic metamaterial (GOEAM) face layers. The viscoelastic properties of MREs are modeled based on the experimental data using the Generalized Maxwell approach and validated via the nonlinear least-squares method. GOri's mechanical properties are determined using novel micromechanical approaches. The problem is solved using the finite element method (FEM) and first-order shear deformation theory (FSDT).
Keywords: MRE-GPL, GOEAM, FEM, Generalized Maxwell Model, FSDT

1. INTRODUCTION

Magnetorheological elastomers (MREs) are smart materials with tunable mechanical properties that make them highly effective in vibration control applications. Comprising elastomeric matrices embedded with magnetically responsive particles, MREs exhibit field-dependent stiffness and damping characteristics, enabling adaptive vibration mitigation in engineering systems [1]. Recent studies have explored the potential of MREs in dynamic absorbers, isolators, and tunable structures, demonstrating their ability to enhance system stability and reduce undesired oscillations [2]. Auxetic metamaterials have a negative Poisson's ratio, expanding laterally when stretched. Designed through unique geometries, they offer superior energy absorption, fracture resistance, and flexibility. Used in aerospace, biomedical, and impact-resistant applications, they distribute stress effectively, enhancing durability and performance [3]. Zhao et al. [4] developed a formula to predict the mechanical behavior of graphene origami (GOri)-enabled auxetic metallic metamaterials (GOEAMs) using machine learning and molecular dynamics. They introduced a novel micromechanical method based on the Halpin-Tsai approach, which enables the tuning of the negative Poisson's ratio.

2. MRE's MODEL DEVELOPMENT

In the present investigation, a three-element Maxwell model incorporating the omission of one dashpot is introduced and elaborated upon. Subsequently, the constitutive equation delineating the relationship between shear stress and shear strain is formulated as follows.

$$\tau + p_1\dot{\tau} + p_2\ddot{\tau} = q_0\gamma + q_1\dot{\gamma} + q_2\ddot{\gamma} \tag{1}$$

While, τ and γ represent shear stress and shear strain, respectively. The coefficients are:

$$p_1 = \frac{\mu_1}{G_1} + \frac{\mu_2}{G_2}, p_2 = \frac{\mu_1\mu_2}{G_1G_2}$$

$$q_0 = G_3, q_1 = G_3\left(\frac{\mu_1}{G_3} + \frac{\mu_2}{G_3} + \frac{\mu_1}{G_1} + \frac{\mu_2}{G_2}\right), q_2 = G_3\left(\frac{\mu_1\mu_2}{G_1G_2} + \frac{\mu_1\mu_2}{G_1G_3} + \frac{\mu_1\mu_2}{G_2G_3}\right) \tag{2}$$

By mathematical manipulation, the storage and loss moduli based on the Generalized Maxwell model can be derived in the subsequent format.

$$G' = G_3 + \frac{G_1\mu_1^2\omega^2}{G_1^2+\mu_1^2\omega^2} + \frac{G_2\mu_2^2\omega^2}{G_2^2+\mu_2^2\omega^2}, G'' = \frac{G_1^2\mu_1\omega}{G_1^2+\mu_1^2\omega^2} + \frac{G_2^2\mu_2\omega}{G_2^2+\mu_2^2\omega^2} \quad (3)$$

The obtained model then can be validated by comparing experimental data and the unknown coefficiants of the storage and loss moduli can be determined.

3. GOEAM -BASED MICROMECHANICAL MODEL

The mechanical properties of FG-GOEAM face layers are obtained based on the Halpin–Tsai model and rule of mixture:

$$E = f_E E_{Cu}\frac{1+\varsigma_1\varsigma_2 V_{Gr}}{1-\varsigma_2 V_{Gr}}, \nu = f_\nu(\nu_{Cu}V_{Cu}+\nu_{Gr}V_{Gr}), \varsigma_1 = 2\frac{l_{Gr}}{t_{Gr}}$$

$$\rho = f_\rho(\rho_{Cu}V_{Cu}+\rho_{Gr}V_{Gr}), \alpha = f_\alpha(\alpha_{Cu}V_{Cu}+\alpha_{Gr}V_{Gr}), \varsigma_2 = \frac{\left(\frac{E_{Gr}}{E_{Cu}}\right)-1}{\left(\frac{E_{Gr}}{E_{Cu}}\right)+\varsigma_1} \quad (4)$$

f_E, f_ν, f_ρ, and f_α are correction functions for modulus of elasticity, Poisson’s ratio, mass density, and coefficient of thermal expansion, respectively.

4. THEORETICAL FORMULATIONS

The displacement field of the sandwich plate based on the FSDT can be expressed as follows.

$$u_i = u_{0_i} + z_i\theta_{x_i}$$
$$v_i = v_{0i} + z_i\theta_{y_i}$$
$$w_i = w_0 \quad (5)$$

where the subscript *i* refers to to bottom, core, and top layers of the sandwich plate.
The kinetic energy (*T*) and strain energy (*V*) of the structure can be determined in the following format:

$$T_i = \frac{1}{2}\int_{\frac{-a}{2}}^{\frac{-a}{2}}\int_{\frac{-b}{2}}^{\frac{b}{2}}\int_{-h_i/2}^{h_i/2}\rho_i((\dot{u}_i)^2+(\dot{v}_i)^2+(\dot{w}_i)^2)dz_i dy dx$$

$$V_i = \frac{1}{2}\int_{\frac{-a}{2}}^{\frac{a}{2}}\int_{\frac{-b}{2}}^{\frac{b}{2}}\int_{-h_i/2}^{h_i/2}\left(\sigma_{x_i}\varepsilon_{x_i}+\sigma_{y_i}\varepsilon_{y_i}+\tau_{xy_i}\gamma_{xy_i}+\tau_{xz_i}\gamma_{xz_i}+\tau_{yz_i}\gamma_{yz_i}\right)dz_i dy dx \quad (6)$$

The equation of motion of the sandwich plate then can be calculated using Hamilton's principle.

$$\delta\int_{t_1}^{t_2}(T-V)\,dt = 0 \quad (7)$$

The final format of the equation of motion can be determined using FEM in the following manner.

$$[M]\{\ddot{D}\} + [K]\{D\} = 0 \quad (8)$$

REFERENCES

[1] R. Aboutalebi, A new higher-order shear deformation theory for flutter instability of a hybrid sandwich panel resting on a viscoelastic foundation, Engineering Structures 309 (2024) 118089.
[2] J.M. Ginder, M.E. Nichols, L.D. Elie, S.M. Clark, Controllable-stiffness components based on magnetorheological elastomers, Smart structures and materials 2000: smart structures and integrated systems, SPIE, 2000, pp. 418-425.
[3] K.E. Evans, A. Alderson, Auxetic materials: functional materials and structures from lateral thinking!, Advanced materials 12(9) (2000) 617-628.
[4] S. Zhao, Y. Zhang, Y. Zhang, J. Yang, S. Kitipornchai, Graphene origami-enabled auxetic metallic metamaterials: an atomistic insight, International Journal of Mechanical Sciences 212 (2021) 106814.

Controllable Properties of the Representative Structure of Negative Stiffness Mechanical Metamaterials Filled with Magnetorheological Fluids

Fangping Yan[1], Ya'nan Zhang[2], Qingchao Chen[1], Chengkai Gu[1] and Xuli Zhu[1]

[1] College of Mechanical and Electronic Engineering, Shandong University of Science and Technology, China
(E-mail: yfp232086@163.com, 18263821719@163.com, sdust22@126.com, zhuxuli@tsinghua.org.cn)
[2] College of Mechatronics Engineering, Henan University of Science and Technology, China
(E-mail: 9906442@haust.edu.cn)

Short abstract: Representative structures of negative stiffness mechanical metamaterials filled with magnetorheological fluids were designed and fabricated, and the controllable properties were investegated experimentally. The results show that the negative stiffness of the representative structures and the corresponding regions decrease in the presence of magnetic field, the pressing force and the negative stiffness of the structures can be controlled by the external magnetic field.
Keywords: Negative stiffness, Mechanical metamaterials, Controllable properties, Magnetorheological fluids

1. INTRODUCTION

Mechanical metamaterials are structural materials that are microscopically designed to achieve unique mechanical properties without changing the chemical composition[1]. Negative stiffness mechanical metamaterials (NSMMs) are comprised of negative stiffness (NS) elements[2]. Mechanical metamaterial with controllable properties is an emerging field attracting great attention. Chibar developed a tactile sensor with high properties based on NS honeycomb metamaterials[3]. Zhakatayev presented a design method for metamaterial consisting of negative stiffness beams assembled in a honeycomb structure[4]. Chen designed and fabricated a novel metamaterial magnetorheological elastomer vibration isolator with a controllable vibration bandgap[5].

2. OBJECTIVES

Real-time tunable NS allows NSMMs to be adapted to different conditions without changing the physical structures. The properties of NSMMs depend on their constituent elements, which are representative structures. The performance of magnetorheological fluids (MRFs) can be controlled by the external magnetic field. Therefore, it can be expected that representative structures containing MRFs can achieve properties real-time control of NSMMs.

3. MATERIALS AND EXPERIMENTS

3.1. DESIGN AND FABRICATION

The investigated representative structures of NSMMs were formed by injecting MRFs into the dome structures as shown in Fig. 1a. The cross-section view of the dome structure is shown in Fig. 1b, which was made of silicon rubber Sylgard 184. The MRFs were mixed by carbonyl iron powder and silicone oil.

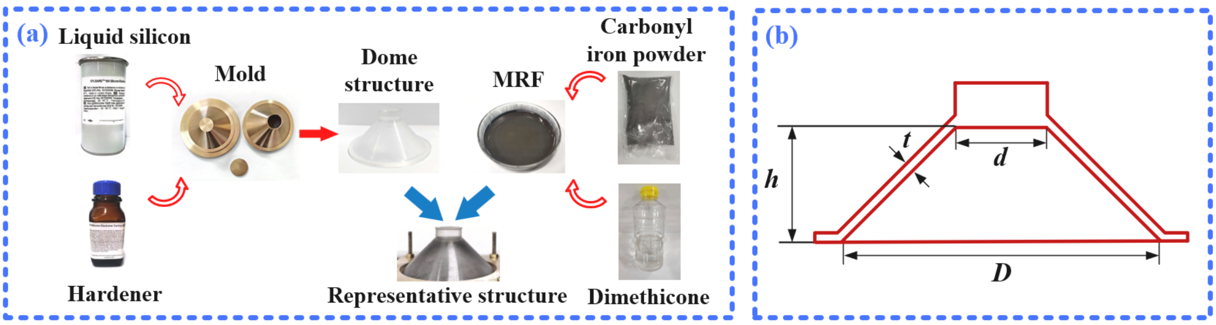

Figure 1: Preparation process (a) and cross-section view (b) of the representative structure.

3.2. EXPERIMENTS

The electronic universal material testing machine WDW-200 was used to carry out compression experiments, and the compressing speed was set to 2 mm/min. The permanent magnets were used to generate a magnetic field. The magnetic field strength was 60 mT measured by Tesla meter HT20. The compression experiments include three types: the hollow dome structures, the dome structures containing MRFs without an external magnetic field, and the dome structures containing MRFs in the presence of an external magnetic field.

4. RESULTS AND DISCUSSION

The experimental results are shown in Fig. 2a. The NS is defined by calculating the slopes of straight line segments with displacement between 4 mm and 7 mm. The absolute values of NS and the peak forces are shown in Fig. 2b. The results show that the external magnetic field can increase the peak force, decrease the value of NS, and reduce the displacement region of NS. The performances of the representative structures can be controlled when the external magnetic field changes continuously.

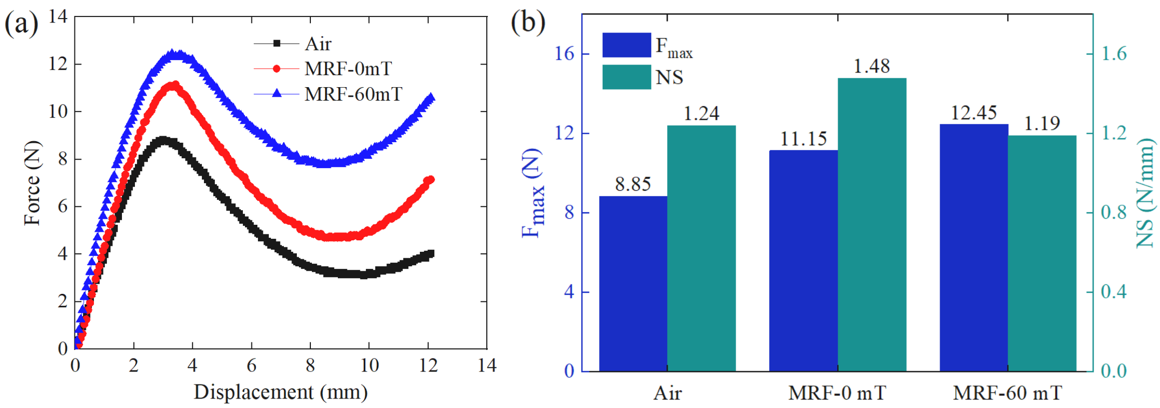

Figure 2: The dependence of force on compressive displacement (a) and the peak pressing forces and absolute values of NS (b).

5. CONCLUSION

Representative structures of NSMMs filled with MRFs were developed, and the controllable properties of the structures were investigated experimentally. In the presence of external magnetic field, the peak pressing force of the structure increases, the NS value decreases, and the NS displacement region reduces.

ACKNOWLEDGEMENT

The Project Supported by National Natural Science Foundation of China No. 52375192 and 52305190.

REFERENCES

[1] Tan X, Cao B, Liu X, et al. Negative stiffness mechanical metamaterials: a review. Smart Materials and Structures, 2025 Jan 1;34(1):013001.
[2] Dwivedi A, Banerjee A, Bhattacharya B. Simultaneous energy harvesting and vibration attenuation in piezo-embedded negative stiffness metamaterial. Journal of Intelligent Material Systems and Structures, 2020 May; 31(8):1076-1090.
[3] Chibar R, Kostyukova V, Khajikhanov S, et al. Honeycomb-Inspired Metamaterial for Tactile Sensors With Variable Stiffness. IEEE Sensors Journal, 2025 Jan 1;25(1):577-586.
[4] Zhakatayev A, Kappassov Z. Analytical modeling and design of negative stiffness honeycombs. Smart Materials and Structures, 2020 Apr;29(4):045024.
[5] Chen Z, Sun S, Deng L, et al. Investigation of a new metamaterial magnetorheological elastomer isolator with tunable vibration bandgaps. Mechanical Systems and Signal Processing, 2022 May 1;170:108806.

Jamming transition in magnetorheological suspensions made of iron and calcium carbonate particles

G.Bossis[1], Y.Grasselli[2],O.Volkova[3]

[1, 3] InPhyNi, UMR 7010, CNRS, Université Côte d'Azur, France
(E-mail: bossis@unice.fr, Olga.VOLKOVA@univ-cotedazur.fr)
[2] SKEMA Business School 60 rue Dostoievski, BP085, 06902 Sophia Antipolis, France
(E-mail yan.grasselli@skema.edu)

Short abstract: The jamming transition, also known as discontinuous shear thickening (DST), is observed in very concentrated suspensions of solid particles, with a size of about one micron or greater. This study focuses on the use of a magnetic field to trigger this transition which is characterized by a sharp increase of viscosity. We show that this transition is very dependent on the coverage of the particle surface by a layer of adsorbed polymers. We present some results in terms of shear stress versus shear rate or shear strain for a suspension made of a mixture of iron and calcium carbonate particles.
Keywords: Suspension, jamming, superplasticizer, viscosity jump.

1. INTRODUCTION

Highly concentrated suspensions of microparticles in a carrier liquid can undergo a sharp transition under flow with a sudden jump in viscosity when the hydrodynamic stress is large enough to break the lubrication film and bring particles surface into solid contact. This phenomenon called "discontinuous shear thickening" (DST) is most often undesirable in applications such as concrete casting in the construction industry or metal pastes for 3D printers or composite parts but can be useful if it can be controlled by an external mean like a magnetic field. This is the case of magnetorheological suspensions (MRS) that can also transform into a solid in the presence of a magnetic field, but their yield stress is quite low except at high applied magnetic field. In the case of the DST transition, the application of a weak field on a flowing suspension can generate a yield stress which would require a field of at least two orders of magnitude larger than in an ordinary MRS [1]. Due to the use of magnetic microparticles with high density their high sedimentation can cause phase separation and/or aggregation. A simple way to reduce the sedimentation is to mix lighter non-magnetic particles with magnetic particles and, despite the decrease in magnetic materials, the MRS suspension can maintain a high field induced yield stress due to the transmission of stresses by nonmagnetic particles [2]. In the same vein it has been shown that a small quantity of iron particles dispersed among much lighter calcium carbonate particles is sufficient to control the DST transition while maintaining the same large increase in effective viscosity [3]. In this way sedimentation and the risk of irreversible aggregation of magnetic particles are reduced. We will emphasize the determining role of the volume fraction of particles and of functionalization of their surfaces to explain and control the DST transition. We shall also present some results showing the relationship between the instability of jets of concentrated suspensions of magnetic particles and the DST transition.

2. OBJECTIVES

The aim of this paper is to demonstrate the relationship between the coverage ratio of the surface of the particles, both for iron and calcium carbonate, with the critical stress required to trigger the jamming transition and to present some results obtained using the same superplasticizer molecule with a mixture of iron and calcium carbonate particles. These results will concern the rheological curves: shear stress as a function of shear rate, but also the behaviour of the viscoelastic moduli, G, G" and some preliminary results on the influence of the jamming transition on the MRS suspension jet.

3. MATERIAL AND METHODOLOGY

We used carbonyl iron (CI) particles obtained from BASF (grade HQ) with a density $\rho = 7.7$ g/cm^3 and calcium carbonate(CC) grade BL200 from Omya $\rho = 2.72$ g/cm^3.The suspending liquid was a mixture of ethylene glycol and water in a mass ratio 85/15, minimizing evaporation. The superplasticizer molecule, whose trade name is Optima100 (Opt), consists of a short polyethylene oxide (PEO) chain and a negatively charged diphosphonate head that bind to ferrous ions and calcium ions. Rheological curves are measured with a rheometer MCR502 from Anton Paar. The magnetic field is imposed through a coil whose center coincides with the sample in a plate-plate geometry.

4. RESULTS AND DISCUSSION

From the shear stress versus shear rate curves at different proportions $F_{CI}=V_{CI}/(V_{CI}+V_{CC})$ and a total volume fraction of solid Φ=0.705, we measured the evolution of yield stress and Bingham viscosity with the magnetic field for a superplasticizer mass concentration relative to the particle mass of 0.2%.[4]. Although quite counterintuitive, the largest variation of yield stress and viscosity was obtained at a low iron particle fraction: F_{CI} between 5 and 10%. This is explained by the fact that non-magnetic particles transmit the stress induced by the formation of linear aggregates of CI particles [2] and because a low concentration of CI particles decreases the magnetic permeability and thus the demagnetizing field in a plate-plate geometry. An other finding is related to the role of the superplasticizer polymer on the jamming transition (cf. Fig. (2)) where we see that, for a pure suspension of iron particles, increasing its concentration from 0.1% to 0.4% strongly increases the critical stress where the jamming transition appears but that beyond 0.4% the critical stress decreases. By measuring the adsorption isotherm of this molecule on the surface of iron particles and CC particles we have seen that the concentration of 0.4% corresponds to a dense layer of polymer giving the

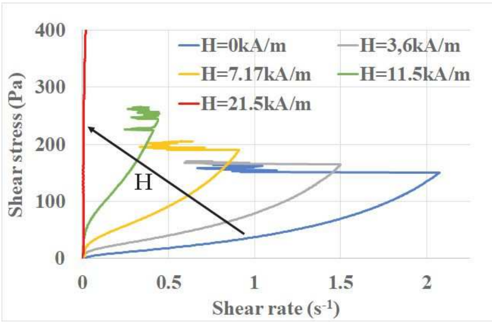

Fig.1 Shear stress versus shear rate. Total volume fraction: Φ=70.5%; with 5% Fe: and 95% $CaCO_3$ in volume;C_{opt}=0.2%

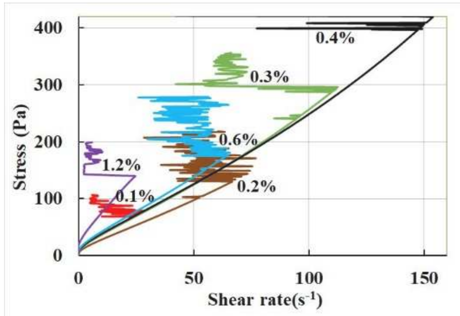

Fig.2 Suspension of iron particles at Φ=64% for different concentrations, C_{opt}, of superplasticizer

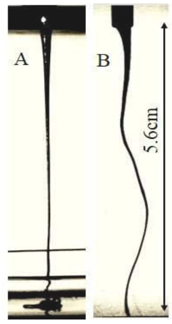

Fig.3A:Φ=0.62
Fig 3B:Φ=0.63

maximum repulsive force between particles. A higher concentration will lead to the formation of micelles inside the interparticle space that will facilitate the desorption of polymer from the particle surface and thus decrease the critical stress. Unlike usual MR fluids where it is mainly the yield stress which increases with the magnetic field, here, as can be seen in Fig.1, it is the shear thickening that increases the viscosity. This effect probably comes from an increase in the entanglement between the polymer chains of each individual coating layer. Finally it is not only the behaviour of a very dense MR suspension inside a container which depends on the jamming transition, but also the instability of the jet of such suspensions. In Fig.3A, for the same imposed pressure, the jet is steady for a suspension of iron particles at Φ=0.62 but unstable at Φ=0.63. We try to relate this behaviour to the extensional stress at the output of the capillary

5. CONCLUSIONS

The mechanism of the jamming transition in concentrated suspensions is governed by the percolation of a network of frictional contacts between particles that depends on the balance between attractive (hydrodynamic and/or magnetic) and repulsive forces coming from the polymer layers. Due to the stress transmission between solid particles (magnetic or not) this transition can be triggered by a small magnetic field even with a low volume fraction of magnetic particles, opening the way to a new class of MRS

ACKNOWLEDGEMENT

The authors want to thank the Centre National d'Etudes Spatiales (CNES, the French Space Agency) for having supported this research

REFERENCES

[1] Bossis G, Volkova O, Grasselli Y, Ciffreo A. The role of volume fraction and additives on the rheology of suspensions of micron sized iron particles. Frontiers in Materials. 2019.Vol 6 Article 4,1- 6
[2] Wilson BT, Klingenberg DJ. A jamming-like mechanism of yield-stress increase caused by addition of nonmagnetizable particles to magnetorheological suspensions. Journal of Rheology. 2017, 61:601–611
[3] Bossis G, Ciffreo A, Grasselli Y, Volkova O, Analysis of the rheology of magnetic bidisperse suspensions in the regime of discontinuous shear thickening. Rheologica Acta. 2023,62:205-223)

Three-Dimensional Numerical Analysis of Thermal Flow of Temperature-Sensitive Magnetic Fluid around a Single Heated Cylinder

Y. Iwamoto[1], R. Suzuki[1] and Y. Ido[1]

[1] Department of Mechanical Engineering, Nagoya Institute of Technology, Japan
(E-mail: iwamoto.yuhiro@nitech.ac.jp)

Short abstract: A temperature-sensitive magnetic fluid (TSMF) is a magnetic nanofluid with ferromagnetic nanoparticles having a low Curie temperature. Its unique "temperature-sensitive magnetization" causes magnetization to drop sharply as temperature rises near room temperature. This property has been explored in self-circulating heat transport devices. In this study, numerical simulations using the lattice Boltzmann method visualized the thermal flow of TSMF around a heated cylinder. Results showed that applying a magnetic field causes magnetic buoyancy to eject heated fluid, enhancing heat transfer.
Keywords: Temperature-sensitive magnetic fluid, Heat transfer, Lattice Boltzmann method, Thermomagnetic pump, Energy conversion.

1. INTRODUCTION

With the increasing demand for miniaturization and energy efficiency in electronic devices, the development of self-circulating heat transport devices without mechanical driving components, such as heat pipes, has become increasingly important. In particular, magnetically-driven heat transport devices using temperature-sensitive magnetic fluids (TSMFs) hold promise as cooling technologies for low-temperature heat sources (below 373 K) with high heat generation density. TSMFs are magnetic nanofluids that stably disperse magnetic nanoparticles with a low Curie temperature (e.g., MnZnFe) in solvents such as oil. These fluids exhibit a temperature-sensitive magnetization, and their magnetization significantly decreases with rising temperatures in ambient conditions. By utilizing this property, applying both a magnetic field and heat to the TSMF induces a self-driven flow due to the imbalance of magnetic body forces, simultaneously enabling heat transfer[1].

To date, numerous experimental[2] and numerical studies[3, 4] have investigated heat transport devices utilizing TSMFs. The heat flow characteristics of these fluids differ significantly from conventional Newtonian fluids, being highly influenced by the shape of heat transfer surfaces and the distribution of the magnetic field. However, since magnetic fluids are black and opaque, experimental visualization of heat flow is challenging. As a result, numerical simulations have been widely used to visualize heat flow, though most analyses are limited to two dimensions. Considering that magnetic fields are distributed in three dimensions, understanding the three-dimensional heat flow phenomena is essential for advancing heat transport devices using TSMFs. In this study, we performed a thermal flow analysis of TSMFs around a single heated cylinder using the lattice Boltzmann method. We investigated the influence of the magnetic field on heat flow behavior in detail.

2. NUMERICAL ANALYSIS

The analysis model is shown in Figure 1, and the magnetic field distribution is presented in Figure 2. The flow channel is a three-dimensional rectangular channel containing a single heated cylinder. The fluid is assumed to be an incompressible Newtonian fluid, and the equations of motion consider both magnetic body force and buoyancy. The lattice Boltzmann method was used to solve the equation of motion, the finite difference method was used for the energy equation, and the immersed boundary method was used for momentum exchange between the heated cylinder and the fluid. The physical properties of the fluid were based on a kerosene-based TSMF [1]. The boundary conditions are indicated in Figure 1.

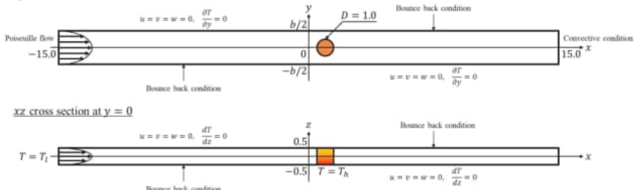

Figure 1: Analysis model.

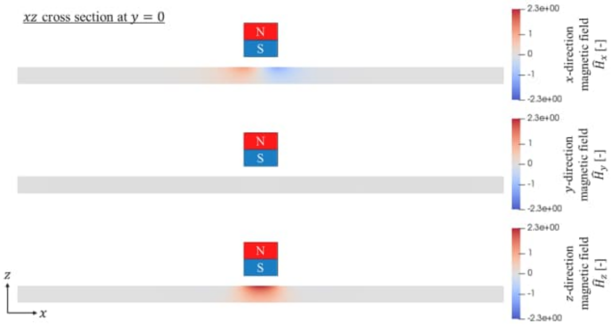

Figure 2: Magnetic field distribution.

3. RESULTS AND DISCUSSION

Figure 3 presents a representative result of the thermal flow analysis. The TSMF flowing in from upstream moves in the +z direction in front of the heated cylinder and then rapidly descends in the -z direction behind the cylinder. In general, for non-magnetic Newtonian fluids, the heated fluid rises in the +z direction due to buoyancy. In contrast, in the case of TSMF, the magnetic body force causes the lower-temperature magnetic fluid to flow toward regions with a stronger magnetic field, specifically in the +z direction. Additionally, as the fluid temperature increases due to heating, the magnetization of the TSMF decreases. Consequently, the heated fluid is ejected from the strong magnetic field region and flows in the -z direction. This mechanism allows the heat-absorbed TSMF to be efficiently excluded from the magnetic field, enabling effective heat recovery through its flow behavior.

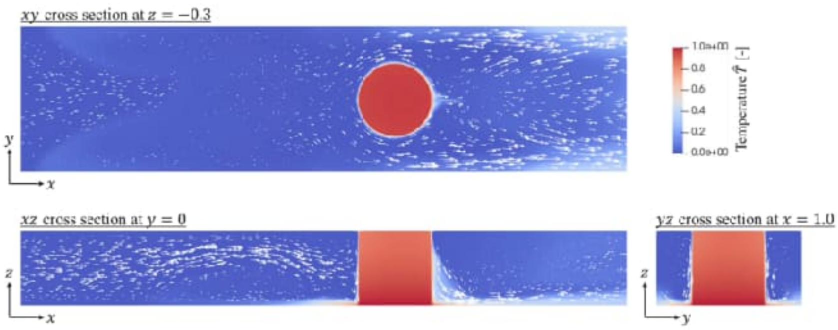

Figure 3: Typical results of the thermal and fluid flow analysis.

ACKNOWLEDGEMENT

This work was supported in part by the Nitto Foundation, Japan.

REFERENCES

[1] Iwamoto Y, Yamaguchi H, Niu XD. Magnetically-driven heat transport device using a binary temperature-sensitive magnetic fluid, Journal of Magnetism and Magnetic Materials. 2011; 323: 1378.
[2] Iwamoto Y, Nakasumi H, Ido Y, Yamaguchi H. Long-distance heat transport based on temperature-dependent magnetization of magnetic fluids. International Journal of Applied Electromagnetics and Mechanics. 2020; 62: 711.
[3] Pattanaiki MS, Varma VB, Cheekati SK, Chaudhary V, Ramanujan RV, Optimal ferrofluids for magnetic cooling devices. Scientific Reports. 2021; 11: 1.
[4] Hangi M. Bahiraei M, Rahbari A. Forced convection of a temperature-sensitive ferrofluid in presence of magnetic field of electrical current-carrying wire: A two-phase approach. Advanced Power Technology. 2018; 29(9): 2168.

Chain-to-layer transition in sheared magnetorheological fluids

J. R. Morillas[1], O. Martínez-Cano[1], J. F. Morris[2] and J. de Vicente[1]

[1] Magnetic Soft Matter Group, Department of Applied Physics, University of Granada, Spain
(E-mail: jmorillas@ugr.es, omcano@ugr.es, jvicente@ugr.es)
[2] Benjamin Levich Institute, The City College of New York, United States of America
(E-mail: morris@ccny.cuny.edu)

Short abstract: The evolution of the internal structure of a magnetorheological fluid under simple shear flows and magnetic fields applied along the velocity gradient direction is investigated. Using videomicroscopy, we observe that field-induced chains transition into a layered pattern oriented perpendicular to the vorticity direction once a characteristic Mason number is exceeded. The threshold value and the pattern period show a strong dependence on the shearing gap. To explain this behaviour, a toy model based on chain-chain interactions is proposed, which successfully captures the qualitative aspects of the experimental observations.
***Keywords*:** lamellar structures, rings, microstructure, rheo-microscopy, SALR interaction.

1. INTRODUCTION

Currently, the rheology of magnetorheological (MR) fluids under simple shear flows and magnetic fields applied along the velocity gradient direction is successfully described by the so-called chain model [1]. According to this model, the characteristic shear-thinning behaviour arises from the progressive breakup of field-induced aggregates (ideally, chains aligned with the field direction) as the shear rate increases. In this context, chain length and orientation are governed by the balance between shear forces, which tilt and elongate the chains, and magnetic forces, which tend to keep the chain particles together. This balance is quantified by the Mason number, Mn. Within this framework, as Mn approaches zero, chains percolate throughout the system, giving rise to a yield stress. Conversely, at sufficiently high Mn values (i.e., above the critical Mason number, Mn_c) [2], chains are totally disrupted, resulting in a suspension of disaggregated and homogeneously dispersed particles, beyond which no further viscosity evolution is expected.

Despite the widespread use of the chain model in magnetorheology, it is well known that structure evolution under shear flow is not limited to chain disruption leading to a fully disaggregated state. Instead, at high Mn, particles rearrange into layers oriented perpendicular to the vorticity direction, forming a well-defined macro-pattern [2,3]. This phenomenon has received relatively little attention. It has been suggested that the pattern emerges once Mn_c (~ 1) is exceeded [2], but the underlying mechanism remains unclear. Moreover, it is not well understood why layers appear, whether the pattern vanishes at higher Mn values or which system parameters govern pattern morphology.

2. OBJECTIVES

This work aims to track the in-situ formation of layers in MR fluids and correlate these microstructural changes with the sample's rheological behavior. Additionally, a toy model is proposed to reproduce this phenomenon and identify the key control parameters governing layer formation and morphology.

3. MATERIAL AND METHODOLOGY

Experiments were performed on conventional MR fluids based on carbonyl iron microparticles (3 µm diameter, BASF) dispersed in glycerol (86-88%, viscosity of 106 mPa·s, Scharlau) at 10 vol%. Specifically, the flow curve under a 10 kA/m magnetic field was obtained using a torsional rheometer with plate-plate geometry for different shearing gaps. The bottom plate was made of glass to allow a high-speed camera positioned beneath it to capture the microstructural projection on the flow/vorticity plane. Camera and rheometer were synchronized to correlate each recorded image with the corresponding data point in the steady state flow curve, enabling precise identification of the shear rate at which layer formation occurs. The captured images were further analyzed to extract pattern morphology parameters, such as its period [4].

4. RESULTS AND DISCUSSION

Figure 1 shows the main experimental findings regarding (a) the Mn needed to trigger the chain-layer transition, $Mn_{c\text{-}l}$, and (b) the period of the resultant pattern, d, as a function of the shearing gap, h. The results show that $Mn_{c\text{-}l}$ decreases while d increases with increasing gap size. However, neither of these behaviours is adequately explained by existing theories. The chain model, for instance, does not predict any dependence between Mn_{c-l} and the shearing gap [2]. Similarly, current models for pattern period suggest that d should scale with the square root of the gap [5], which does not fully account for the observed trend.

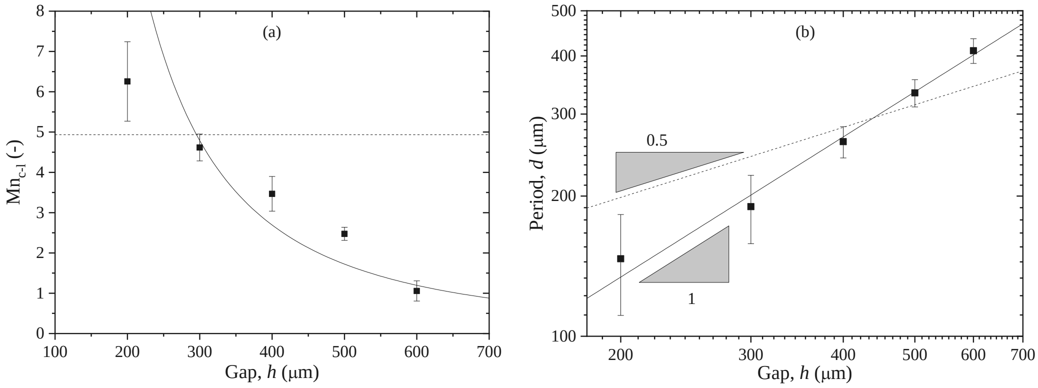

Figure 1: Mason number required to induce layer formation (a) and pattern period (b) as functions of the shearing gap. Points: Experimental results. Dashed lines: fits based on published models from [2] (a) and [5] (b). Solid lines: fits obtained using the proposed model based on chain-chain interactions.

To explain these experimental trends, based on the visual observation of the microstructure, it was hypothesized that layer formation does not necessarily occur once all particles are fully disaggregated, but rather while they still form linear chains tilted by the shear flow. By computing the magnetic interaction between these chains (treating them as single entities rather than as assemblies of individual particles) a SALR (short attractive/long repulsive)-like force was obtained. This is characterized by a localized attractive region near the chain, which extends as the chain tilts under shear flow.

Based on this assumption, layer formation can be understood in terms of the interplay between two length scales: the typical distance between chains (l_0, determined by the particle concentration) and the attractive range of the chain-chain force (l_a, controlled by the chain tilt angle which in turn is given by the product $h \cdot$ Mn [1]). Layers will form only when $l_a > l_0$ so that the attractive region is sufficiently long to encompass a sufficient number of neighbouring chains. Since l_a increases with $h \cdot$ Mn, it can be concluded that: (i) layers will form only when Mn exceeds a threshold value (Mn_{c-l}), and (ii) the larger the gap h, the smaller the Mn required to reach the $l_a > l_0$ regime (so Mn_{c-l} should decrease with h, as shown in Figure 1a). Finally, once layers are formed, it is important to note that the only relevant length scale is the shearing gap h, which controls the tilt angle and the range of the attractive region. Thus, it is expected that all other lengths in the system (including the pattern period) will scale with h, explaining the linear dependence seen in Figure 1b.

5. CONCLUSIONS

In-situ visualization of the microstructural evolution during shear has shown that MR fluids develop a layered pattern, with the period and triggering Mason number increasing and decreasing, respectively, with the shearing gap. These behaviours are successfully explained by a model that accounts for the interactions between percolating tilted chains.

ACKNOWLEDGEMENT

Financial support by (EFST)-H2020-MSCA-IF-2020 (Grant 101030666) fellowship is acknowledged.

REFERENCES

[1] Martin JE, Anderson RA. Chain model of electrorheology. The Journal of Chemical Physics. 1996 Mar; 104(12):4814-27.
[2] Volkova O, Cutillas S, Bossis G. Shear banded flows and nematic-to-isotropic transition in ER and MR fluids. Physical Review Letters. 1999 Jan; 82:233-6.
[3] Henley S, Filisko FE. Flow profiles of electrorheological suspensions: An alternative model for ER activity. Journal of Rheology. 1999 Sep; 43:1323-36.
[4] Martínez-Cano Ó, Morillas JR, Cvek M, Ramírez J, de Vicente J. High-speed video microscopy of sheared carbonyl iron suspensions. Smart Materials and Structures. 2022 Dec; 32(2):025004.
[5] Cutillas S, Bossis G, Cebers A. Flow-induced transition from cylindrical to layered patterns in magnetorheological suspensions. Physical Review E. 1998 Jan; 57(1):804.

Retrieving the relevance of packing efficiency in MR fluids: Prof. Zinoviy P. Shulman team

Eduardo O. Resek[1], Júlio G. F. Manuel[1], Antonio J. F. Bombard[1]

[1] Instituto de Física e Química, Universidade Federal de Itajubá, Brazil
eresek@unifei.edu.br, julio.gabriel98@gmail.com, bombard@unifei.edu.br

Abstract: The concept of packing efficiency is fundamental in dispersion rheology to reduce the viscosity of concentrated slurries or increase the content of the dispersed phase, even without applying any external (electric or magnetic) field. However, packing efficiency can also affect the yield stress of electrorheological or magnetorheological fluids, under an applied field. This was first described by Prof. Shulman's group in the 1980s, but the concept seems to have been forgotten. This work aims to retrieve the relevance of this concept to the ERMR community.
***Keywords*:** Magnetorheology, packing efficiency, aggregate susceptibility, Zinoviy P. Shulman.

1. INTRODUCTION

The original idea of using the packing efficiency of particles in physical models to estimate the value of the static yield stress of magnetorheological fluids (with the same value of the volumetric fraction of the magnetic phase), was first described in the middle of the 1980s, by the group of Prof. Zinoviy P. Shulman and collaborators [1–3]. Interestingly, the importance of this concept seems to have been forgotten, or perhaps not well understood. The same idea was revisited and incorporated into the model proposed by Tang and Conrad in 2000 [4]. The last time we found the same concept in literature (to the best of our knowledge) was in Kordonski et al 2001 model [5]. The original equation proposed by Rosensweig in his model for MRF yield stress in 1995 [6] is:

$$\sigma_y = \frac{\mu_0}{4}\phi H_0^2\left[\frac{(1-\phi)\chi^2}{1+(1-\phi)\chi}\right], \tag{1}$$

where μ_0 is the magnetic permeability of the free space ($4\pi \times 10^{-7}$ N.A^{-2}), ϕ is the volume fraction of the magnetic powder (dispersed phase in MRF), $\boldsymbol{H_0}$ is the magnetic field strength, and χ is the susceptibility of a magnetic material laminae, proposed by Rosensweig in his "*laminae model*" [6].

Kordonski et al [5], following the "laminae model" proposed by Rosensweig [6] for MRF, assumed that such magnetic laminae are formed by compact aggregates, consisting of particles with a certain "*packing degree ξ* ", and following Shulman et al [3], they assumed $\xi = 0.7$ as the value for the "*greatest packing degree*". They describe the term related to the susceptibility of a magnetic material laminae in the Rosensweig model as: $\chi_m = \frac{M_S}{H}\xi$. Here, $\mathbf{M_s}$ is the saturation magnetization of carbonyl iron powder and ξ is the packing efficiency of the iron spheroidal particles inside the magnetic laminae. On the other hand, Rosensweig's model did not consider the possible effects of particle packing. Kordonski, Gorodkin, and Zhuravski (2001) proposed this, modifying the Rosensweig model [5,6]. Tang and Conrad, also incorporated in their "Analytical model for MRF" [4], a distinction between ϕ (the total volume fraction of the particles), Φ_c (the volume packing density, conceptually equivalent to the "*packing degree* ξ" by Kordonski *et al* [5]), and φ_s (the volume fraction occupied by the aggregates). We called this ϕ_{RCP} in Manuel *et al* 2023 [7].

$$\varphi_a = \frac{\varphi}{\Phi} \text{ (Shulman et al), or } \Phi_c = \frac{\phi}{\varphi_s} \text{ (Tang \& Conrad)} \tag{2}$$

2. OBJECTIVES

To visually demonstrate that packing efficiency affects the magnetic susceptibility of a column of particles. To recall and recover the *"aggregate susceptibility"* concept by Shulman *et al* [3].

3. MATERIAL AND METHODOLOGY

Chrome steel spheres with 2 mm and ½ inch were employed for the packing efficiency experiments. The spheres were carefully weighed on an analytical scale (± 0.1 mg), maintaining identical masses of spheres in each of the three tubes. As the material (AISI 52100) is the same in all cases, the only difference was the organization of the balls in each tube. Next, 4290 µL of synthetic polyalphaolefin oil (Synfluid® PAO 2) was added to each tube, using a micropipette, filling the interstices, totalling 8.58 mL. Immediately after the preparation, the magnetic susceptibility χ of each tube was measured with an SM150L magnetic susceptibility meter (ZH Instruments, Brno, Czech Republic), operating at a frequency of 68 Hz, and applying a field of 80 A/m.

4. RESULTS AND DISCUSSION

The steel spheres were arranged manually, as shown in Figure 1, without applying any magnetic field. Only in the middle tube, some care was necessary to ensure the observed packing. Figure 1 illustrates three arrangements with chrome steel spheres, with the same chemical composition, and only two sizes: 2.0 mm or ½”. In the left tube, there are 4 half-inch spheres. In the central tube, there is an ordered mixture of many 2 mm spheres, interspersed with 3 half-inch spheres. And in the right tube, there are only 2.0 mm spheres. All three tubes contain the same volumes of steel and oil, according to Table 1. The volume fraction of solids ($\phi = vol_{steel}/vol_{steel + oil}$) was kept fixed and equal to 0.50. The difference in packing efficiency resulting from the three tubes is noticeable. Table 1 shows that the higher the packing efficiency, the greater the magnetic susceptibility. The most direct and simple explanation for this result, as well established in the literature, is the concept of reluctance in magnetism. Just as the flow of electrical charges (current) always seeks the path of least electrical resistance, magnetic field lines (magnetic flux) also concentrate on the path of least reluctance.

Figure 1: Three tubes with Cr steel balls.

Table 1: Packing efficiency and magnetic susceptibility of the tubes in Fig. 1

Tube Fig. 1	Balls N	Balls mass (g)	Cr Steel volume (cm^3)	PAO volume (cm^3)	v_{steel}/v_{total} ϕ (-)	App. Vol (cm^3)	Packing ξ (-)	Susceptibility χ_{SI} (-)
Left (½ in.)	4 L	33.4231	4.290	4.290	0.50	7.7	0.56	2.53 ± 0.02
Center (mix)	3 L + 256 S	33.4286	4.290	4.290	0.50	6.0	0.72	3.34 ± 0.01
Right (2 mm)	1024 S	33.4198	4.290	4.290	0.50	7.2	0.60	2.89 ± 0.01

5. CONCLUSIONS

The notion that *“the degree of filling of the aggregate”* [3] (packing efficiency) affects the *“aggregate susceptibility”* of magnetorheological fluids, introduced by Prof. Shulman’s group, is revisited. We devise a simple experiment showing that higher packing efficiency enhances magnetic susceptibility. Future research could explore the practical implications of this to improve the magnetorheological effect.

ACKNOWLEDGEMENT

AJFB acknowledges FAPEMIG for the Grants APQ-00620-23 and APQ-00297-24.

REFERENCES

[1] Shulman ZP, Kordonskii VI, Zaltsgendler EA, Prokhorov IV, Khusid BM, Demchuk SA. Structure and magnetic and rheological characteristics of a ferro-suspension (Experiment). *Magnetohydrodynamics*. 1985. 20(3):223-229.
[2] Shulman ZP, Kordonskii VI, Prokhorov IV, Khusid BM. “Magnetic relaxation in ferrosuspensions”. *Magnetohydrodynamics*. 1986. 21(3):218-224.
[3] Shulman ZP, Kordonsky VI, Zaltsgendler EA, Prokhorov IV, Khusid BM, Demchuk SA. *International Journal of Multiphase Flow*. 1986. 12(6):935-955.
[4] Tang XL, Conrad H. “An analytical model for magnetorheological fluids”. *J. Phys. D: Appl. Phys*. 2000. 33:3026-3032.
[5] Kordonski W, Gorodkin S, Zhuravski N. “Static yield stress in magnetorheological fluid”. *Intl. J. Modern Physics B*. 2001. 15(6&7):1078-1084.
[6] Rosensweig RE. “On magnetorheology and electrorheology as states of unsymmetric stress”. *J. Rheology.* 1995 Jan 1st; 39(1):179-192.
[7] Manuel JGF, Bombard AJF, Weeks ER. “Effect of polydispersity in concentrated magnetorheological fluids”. *Smart Mater. Struct* 2023. 32:045014.

Optimized material behaviour of magnetic gels and elastomers

Lukas Fischer[1] and Andreas M. Menzel[1]

[1] Theory of Soft Matter / Biophysics, Institute of Physics, Otto von Guericke University Magdeburg, Germany
(E-mail: lukas.fischer@ovgu.de, a.menzel@ovgu.de)

Short abstract: Our long-term scope is to optimize magnetic gels and elastomers concerning their material behaviour. In our work, we focus on theoretical materials design. To this end, we develop and entangle theoretical-analytical and computational simulation tools. Using basic spherical and cubical model systems we optimize the internal structuring in terms of the spatial arrangement of magnetisable inclusions. We identify structures that maximise and minimise modes of magnetostrictive deformation and rheological effects. Future collaborative endeavours are planned to transfer these results to reality.
Keywords: Magnetic gels and elastomers, materials design, magnetostriction, magnetorheological effect, internal structure.

1. INTRODUCTION

Magnetorheological gels and elastomers, here briefly called magnetic gels and elastomers, consist of micrometre-sized inclusions in soft elastic, reversibly deformable carrier media [1]. We address reversibly magnetisable inclusions that, upon magnetization in homogeneous external magnetic fields, transmit the induced interactions between them to deformations of the surrounding elastic medium [2]. These microscopic distortions couple to the overall, macroscopic material behaviour. Specifically, they lead to macroscopic deformations, that is, changes in overall shape. Moreover, they affect the mechanical resistance against overall deformations, that is, the moduli of elasticity. Respectively, we distinguish between magnetostrictive (changes in shape) and magnetorheological (changes in mechanical properties) effects. For magnetically soft inclusions, both variations in material properties are induced reversibly and switched off upon release of the external magnetic fields. Direct applications are conceivable and discussed extensively, for instance, in the context of soft actuators or magnetically tunable damping devices.

2. OBJECTIVES

Our goal is to identify and demonstrate the potential of magnetic gels and elastomers in view of their magnetostrictive and magnetorheological behaviour, see Figure 1. To this end, we determine maximal or minimal magnitudes of deformation in homogeneous external magnetic fields by adjusting the positioning of the magnetisable inclusions within the elastic carrier material. Similarly, we maximize or minimize the magnetically induced changes in stiffness under imposed mechanical deformations by finding most appropriate spatial arrangements of the magnetisable inclusions. In this way, we contribute to corresponding materials design.

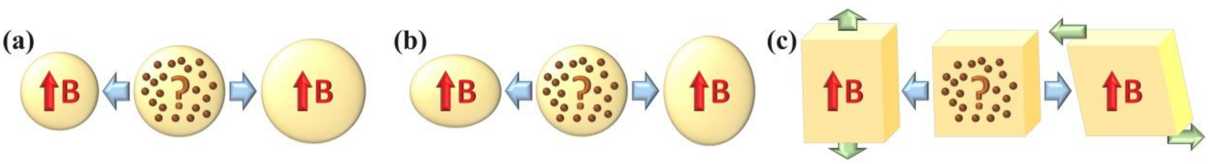

Figure 1: We optimize the internal structure of magnetic gels and elastomers, that is, the spatial arrangement of magnetisable inclusions (brown) for (a) maximized decrease (left) or increase (right) in volume, (b) maximized contraction (left) or extension (right) along the magnetization direction, and (c) maximized increase or decrease in Young modulus (left) or shear modulus (right) upon deformation (green arrows) when magnetized by a strong external magnetic field (red).

3. MATERIAL AND METHODOLOGY

We base our study on analytical calculations in the framework of elasticity theory combined with numerical evaluations and adapted simulation tools to perform optimization procedures. Particularly, we solve the equations of linear elasticity for a finite-sized example object, namely the free-standing homogeneous and isotropic elastic sphere [3]. Possibly compressibility is taken into account. The solution in terms of a Green's function allows to evaluate everywhere within and on the surface of the sphere the displacement field in response to force distributions applied to its inside. In our case, these forces result from magnetic interactions. Evaluations on the surface of the sphere define the overall deformation [3]. Analytical expressions are derived for specific modes of surface deformation as a function of the positions of the magnetic force centres within the elastic sphere [4]. Adaptations of simulated annealing maximize or minimize these modes of deformation by determining the optimized spatial arrangements of the magnetic force centres [5]. To determine maximized mechanical hardening or softening of the materials, we again work with numerical optimization procedures [5]. Yet, instead, we evaluate changes in overall energy upon deformation and magnetization for cubical example systems of finite size.

4. RESULTS AND DISCUSSION

4.1. MAGNETOSTRICTIVE EFFECTS

We determine the optimized spatial arrangements of magnetisable inclusions within free-standing elastic spheres that maximize increase or decrease in volume upon magnetization [5], see Figure 1(a). Moreover, we consider maximized elongation or contraction along the magnetization direction [5], see Figure 1(b). The identified structures depend on the number of inclusions and the degree of compressibility of the elastic material, as do the magnitudes of the induced deformations. Generally, our approach identifies structures resembling layers of hexagonally arranged inclusions to maximize increase in volume and to maximize contraction along the magnetic field direction upon magnetization. In contrast to that, the outer parts of the arrangements within the sphere become less regular when we maximize elongation of the sphere along the magnetization direction. Rather branched and fuzzy spatial arrangements of the inclusions are found to maximize decrease in overall volume upon magnetization. In view of later experimental realizations, for instance, using 3D printing techniques, we set a lower bound for the distance between the inclusions.

4.2. MAGNETORHEOLOGICAL EFFECTS

To maximize or minimize the elastic Young or shear moduli upon magnetization [5], see Figure 1(c), we proceed in a similar way, however, for cubical incompressible systems. We here numerically evaluate the energy of the system upon magnetization and deformation instead of calculating the magnitudes of modes of deformation. Specifically, we find that the Young modulus for stretching along the magnetization direction is mostly enhanced upon magnetization by arrangements of the inclusions close to fcc lattices. Instead, the shear modulus is mostly increased by layer-like structures with the layer normals parallalel to the directions of shear displacement. Likewise, maximized softening, that is, decrease in shear modulus is achieved by layer-like structures. Yet, the layers here coincide in orientation with the shear plane. Contrarily, decrease in Young modulus upon magnetization is maximized for lower to moderate numbers of inclusions by chain-like arrangements forming hollow tubes with the tube direction along the magnetization and stretching direction.

5. CONCLUSIONS

In conclusion, we demonstrate that entangled theoretical-analytical and computational simulation methods serve to optimize the magnetostrictive and magnetorheological performance of magnetic gels and elastomers. Through future collaborative projects, we are starting to work on ways that transfer our concepts to reality [6].

ACKNOWLEDGEMENT

We thank the Deutsche Forschungsgemeinschaft (German Research Foundation, DFG) for support through the Research Unit FOR 5599 via grants nos. ME 3571/10-1 and ME 3571/11-1.

REFERENCES

[1] Menzel AM. Mesoscopic characterization of magnetoelastic hybrid materials: magnetic gels and elastomers, their particle-scale description, and scale-bridging links. Archive of Applied Mechanics. 2019 Jan 15;89:17-45.
[2] Puljiz M, Huang S, Auernhammer GK, Menzel AM. Forces on rigid inclusions in elastic media and resulting matrix-mediated interactions. Physical Review Letters. 2016 Dec 2;117(23):238003.
[3] Fischer L, Menzel AM. Magnetostriction in magnetic gels and elastomers as a function of the internal structure and particle distribution. The Journal of Chemical Physics. 2019 Sep 21;151(11).
[4] Fischer L, Menzel AM. Analytical expressions for the two basic modes of surface displacement and overall deformation of a free-standing or elastically embedded sphere. ArXiv preprint arXiv:2407.09291. 2024 Jul 12.
[5] Fischer L, Menzel AM. Maximized response by structural optimization of soft elastic composite systems. PNAS Nexus. 2024 Sep;3(9):pgae353.
[6] FOR 5599. From production processes of structured magnetic elastomers to their macroscopic material behaviour. https://gepris-extern.dfg.de/gepris/projekt/511114185. 2024.

Evaluate the influence of particle shape on magnetorheological elastomer using large amplitude oscillatory shear test

Dipalkumar Patel[1] and Ramesh V Upadhyay [2]

[1] Department of Mechanical Engineering, C. S. Patel Institute of Technology, Charotar University of Science and Technology (CHARUSAT), Changa-388421, Gujarat, India (Email: dipal8404@gmail.com)
[2] Dr K C Patel Research & Development Centre, Charotar University of Science &Technology, CHARUSAT campus, Changa-388421, Gujarat, India. (Email: rvu.as@charusat.ac.in)

***Short abstract*:** Magnetorheological elastomer (MRE) is smart soft solid composite material consist of rubber matrix and iron particles, which can tune its viscoelastic properties in presence of magnetic field. Mostly non-LVE region of MRE can be better explain by the large amplitude oscillatory shear test (LAOS). In this study, influence of particle shape is evaluated using LAOS parameters. For development of MRE spherical shape iron particle and irregular shape iron particles are used. LAOS parameters are derived for the different strain and magnetic field to evaluate the iron particle shape on MRE performance.
***Keywords*:** Magnetorheological elastomer, viscoelastic properties, large amplitude oscillatory shear test.

1. INTRODUCTION

Magnetorheological elastomer is soft solid composite material which consist of silicone rubber and iron particles. Present day, MRE is gaining its popularity in different applications like as vibration isolation and sensors. Basically, MRE is viscoelastic material, which can tune its viscoelastic properties in presence of magnetic field. Viscoelastic properties of MRE can be evaluated using amplitude sweep, frequency sweep and magneto sweep. However, all these methods are used to characterize the MRE under the liner viscoelastic region (LVE) and can be better to explain the behaviours at small amplitude but cannot used for the non-LVE region. For non-LVE region most common technique used is large amplitude oscillation shear (LAOS). LAOS gives the real time stress- strain curve (Lissajous curves) which can be helpful for micro level study of MREs. LAOS is accommodating the dynamics study to understand the relative contribution of elastic and viscous stress in non-liner region.

Different researchers use LAOS study for different materials like MR grease and MR plastomer to understand the micro structure behavior under the magnetic field at large strain amplitude. Recently few researchers also used LAOS method for the MR elastomer. Dargahi et al (2019) performed the dynamic test and generate stress-strain curve for six different sample having different volume fraction of iron particle and silicone rubber. Result revealed that, slope an area of the hysteresis loop increase with increase in magnetic field [1]. Tahir et al. (2022) used two different type of elastomer one consists of iron and cobalt as filler material and other one is iron and nickel in equal quantity. Hysteresis study is carried out using hydraulic dynamic testing machines and result shows that MR elastomer with nickel iron combinations have higher MR effect compared to cobalt and iron combination. Magnetic field is applied using N52 Neodymium magnets [2]. Vatandoost et al. (2024) developed new method for dynamics study under large amplitude for MR elastomer to explain the strain hardening and strain softening behavior of MR elastomer under the large amplitude oscillatory axial (LAOA) loading. In this they used oscillatory axial loading with the help of compression and tension in sample using hydraulic operated dynamic mechanical testing machine [3]. All the above-mentioned research were carried out using carbonyl iron particles (CIP) or other magnetic particles which is available in spherical shape. Recently some researcher used flake shape based MRE and reported storage modulus of flake shape based MRE is higher compared to spherical shape particles due to higher particle matrix interaction [4]. Thus, in this study to better understand the particle matrix interaction LAOS study is carried out for the spherical shape particle based MRE and flake shape particle based MRE.

2. OBJECTIVES

Main objective of this paper is to explain the particle matrix interaction of MRE using LAOS parameter like strain softening and stiffening behaviour of MRE. For this study MRE are developed using spherical shape iron particle and flake shape iron particle and evaluate its performance using LAOS test on rheometer and LAOS parameter are derived. For detail understanding of particle shape influence LAOS study carried out at different strain and magnetic field.

3. MATERIAL AND METHODOLOGY

Magnetorheological elastomer is fabricated using liquid silicon rubber and iron particle. In this study two types of iron particles are used one is spherical shape and other is flakes shape. MRE is fabricated with 60% weight of iron particle added in liquid silicon rubber and stir it at 400 rpm up to 60 min. After that curing agent is added in the solution to cure it in plastic mould for 24 hrs. After that desired shape of shape is cut for LAOS testing. Spherical shaped iron particles sample is mentioned as MRES-60 and flake shape iron particle sample is mentioned as MREF-60.

4. RESULTS AND DISCUSSION

The stress strain hysteresis loop for the MRES-60 and MREF-60 sample at different strain of 0.5%, 1% and 3% at fixed frequency of 1Hz at 0mT and 640 mT magnetic field as shown in figure 1. Major axis of elliptical shape and its inclination with horizontal axis indicate the elastic behaviour of MRE. Figure 1 (a) at 0 mT MREF-60 major axis inclination is higher than MRES-60 which indicate the MREF-60 is more elastic than MREs-60. Same behaviour is also observed (figure 1(b)) at 640mT magnetic field but the change in inclination is more than 200% more in MREF-60 at 640mT compared to 0mT, where this change in inclination in MRES-60 is nearly 60%. Thus MREF-60 is more elastic compared to MRES-60 due to higher particle matrix interaction which is result of particle shape irregularity.

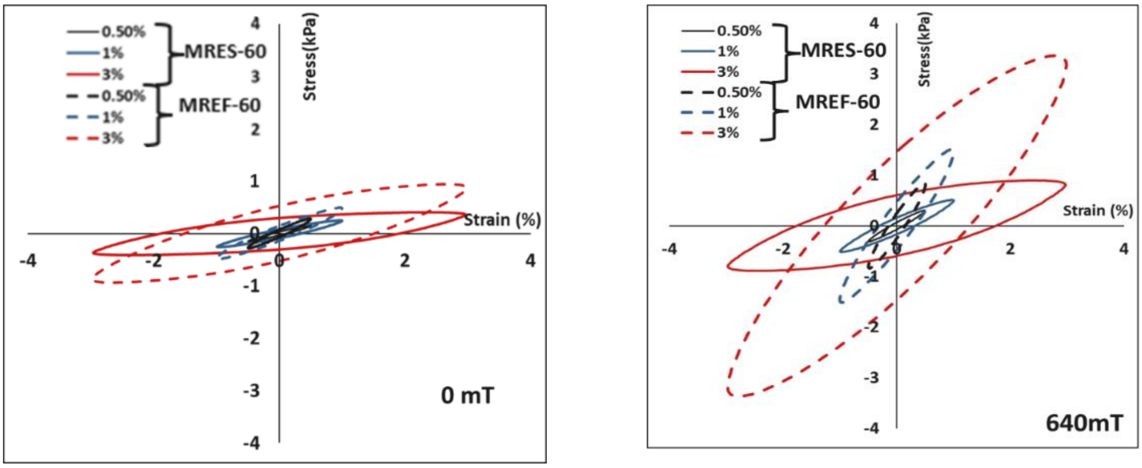

(a) (b)

Figure 1. Stress- strain hysteresis curve for MREF-60 and MRES-60 for different strain 0.5%, 1% and 3% at fixed frequency of 1 Hz

5. CONCLUSIONS

In this study MRE with different shape of iron particles are fabricated and its performance is evaluated using LAOS at non-LVE region. LAOS experiment reveals that flaked shaped iron particle based MRE is more elastic compared to the spherical shape iron particle based MRE.

ACKNOWLEDGEMENT

The Charotar University of Science and Technology (CHARUSAT) supported the work and provided all experimental facilities.

REFERENCES

[1] Dargahi A, Sedaghati R, Rakheja S. On the properties of magnetorheological elastomers in shear mode: Design, fabrication and characterization. Composites Part B: Engineering. 2019 Feb 15;159:269-83.
[2] Tahir S, Usman M, Umer MA. Effect of volume fraction on shear mode properties of Fe-Co and Fe-Ni filled magneto-rheological elastomers. Polymers. 2022 Jul 21;14(14):2968.
[3] Vatandoost H, Sedaghati R, Rakheja S. A new method to characterize the nonlinear magneto-viscoelasticity behavior of magneto-active elastomers under large amplitude oscillatory axial (LAOA) loading. Nonlinear Dynamics. 2024 Mar;112(5):3319-56.
[4] Patel D, Upadhyay RV, Mazlan SA. Particle-reinforced elastomer model to analyse viscoelastic properties of flake-shaped electrolyte iron particle-based magnetorheological elastomer. Smart Materials and Structures. 2023 Jul 28;32(9):095011.

Advancing Magnetorheological Elastomers: Printability and Rheological Properties via Vat Photopolymerization

Mohd Aidy Faizal Johari[1], Saiful Amri Mazlan[1,2], Nur Azmah Nordin[1,2], Muhammad Hariz Zubir[1] and Michal Sedlacik[3]

[1] Engineering Material & Structures (eMast) iKohza, Malaysia-Japan International Institute of Technology (MJIIT), Universiti Teknologi Malaysia, 54100 Kuala Lumpur, Malaysia.
(E-mail: ma.faizal@utm.my, amri.kl@utm.my, nurazmah.nordin@utm.my, muhammad-93@graduate.utm.my)
[2] Automotive Development Centre, Institute for Sustainable Transport (IST), Universiti Teknologi Malaysia, 81310 Skudai, Johor, Malaysia.
(E-mail: amri.kl@utm.my, nurazmah.nordin@utm.my)
[3] Centre of Polymer Systems, University Institute, Tomas Bata University in Zlín, Trida T. Bati 5678, 760 01 Zlín, Czech Republic.
(E-mail: msedlacik@utb.cz)

Short abstract: Additive manufacturing (AM) of magnetorheological elastomers (MREs) has gained attention for efficiently producing complex designs. This study investigates vat photopolymerization as an alternative to fused deposition modeling (FDM), eliminating the need for intricate feedstock preparation. A liquid elastomer resin mixed with carbonyl iron particles (CIPs) is UV-cured via 3D printing, with optimized exposure times ensuring successful printing and adhesion. Rheometer testing identified 30 wt.% CIPs as the optimal composition, demonstrating significant magnetorheological (MR) effects. Results confirm vat photopolymerization as a viable, efficient method for MRE fabrication, with potential applications in automotive systems, such as vibration damping and adaptive components.
Keywords: 4D printing; Additive manufacturing, Magnetorheological elastomer, Rheology, Vat photopolymerization.

1. INTRODUCTION

Additive manufacturing (AM), or 3D printing, has transformed fabrication with its ability to produce complex designs efficiently and reduce waste [1]. Vat photopolymerization has emerged as a promising method for fabricating magnetorheological elastomers (MREs), which consist of elastomers embedded with magnetic particles and exhibit tunable stiffness under magnetic fields. These materials have diverse applications, with potential use in advanced automotive systems such as vibration damping, adaptive suspensions, and noise reduction. Traditional MRE fabrication is reliant on molds and limits design flexibility. Early AM methods like fused deposition modeling (FDM) showed potential but faced challenges such as nozzle clogging, limited material options, and poor resolution [2]. Vat photopolymerization addresses these issues by curing a liquid resin mixed with carbonyl iron particles (CIPs) using UV light, embedding the particles directly into the elastomer matrix [3]. This study investigates optimal CIP compositions and exposure times (normal and bottom) to enhance printability and performance. Preliminary findings suggest 30 wt.% CIPs as the optimal composition, achieving a magnetorheological (MR) effect comparable to conventional methods. Vat photopolymerization offers superior design flexibility, improved mechanical properties, and enhanced MR performance, establishing it as a viable alternative for MRE manufacturing, particularly for automotive applications.

2. OBJECTIVES

This study aims to investigate the potential of vat photopolymerization as an alternative additive manufacturing technique for fabricating MREs. The research focuses on optimizing CIP composition, exposure times, and printability parameters to achieve MREs with enhanced magnetorheological performance and mechanical properties comparable to conventional methods.

3. MATERIAL AND METHODOLOGY

The 4D-printed MRE was made by mixing Magma photopolymer resin with 30 wt.% CIPs and curing it using UV light in a Creality LD-002H 3D printer. The process included: pre-processing, where 30 wt.% CIPs were selected for fast curing under 10 seconds, and CAD models were converted to G-code; processing, where exposure times were optimized for printability; and post-processing, which involved cleaning with isopropyl alcohol, air drying, and final UV curing. Various sample shapes were printed and evaluated for design flexibility and printability. The rheological properties of 4D-printed MREs were tested at 25 °C using a Physica MCR 302 rheometer, analyzing shear strain effects through amplitude sweep (0.001–10% strain at 1 Hz) and magnetorheological effects via current sweep (0–4 A, up to 750 mT) under on-state and off-state conditions.

4. RESULTS AND DISCUSSION

The 4D printing process was optimized with a normal exposure time of 9 seconds and a bottom exposure time of 80-90 seconds, ensuring successful prints. Two tests were performed: amplitude sweep and current sweep, to observe how the material responds to changing magnetic fields. The amplitude sweep test showed that the material's storage modulus (stiffness) decreased with increased shear strain. In the off-state (without a magnetic field), the material was less stiff (0.3 MPa), but the storage modulus increased when a magnetic field was applied.

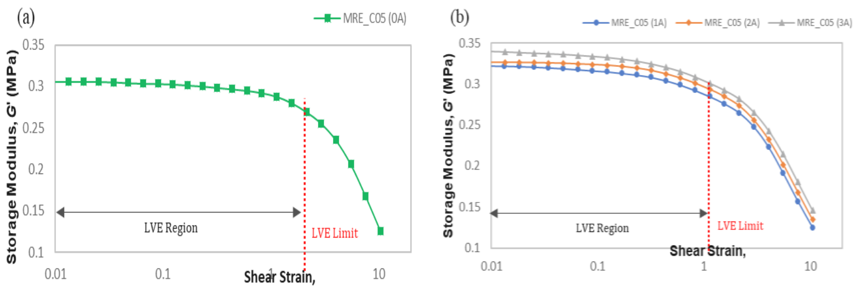

Figure 1: Amplitude sweeps for 4D-printed MRE: (a) off-state and (b) on-state conditions.

This increase was due to the alignment of magnetic particles (CIPs) within the matrix, which made the material stiffer. The LVE (linear viscoelastic) limit was shorter in the on-state than the off-state, meaning the material became less flexible when exposed to a magnetic field. The current sweep test confirmed that higher magnetic flux densities led to increased storage modulus, which is a common behavior in MREs. The 4D-printed MRE showed a relative MR (Magnetorheological) effect of 8.7%, similar to conventional MREs with 30 wt.% CIPs. Despite differences in fabrication methods, the 4D-printed MRE exhibited comparable performance regarding stiffness changes under magnetic fields. In conclusion, 4D printing can be used to produce MREs with similar properties to those made using traditional methods, offering a promising alternative for future MRE applications.

5. CONCLUSIONS

This study confirmed the feasibility of 4D printing magnetorheological elastomers (MREs) using vat photopolymerization, achieving performance comparable to conventionally manufactured MREs. Printability depended on exposure times, with higher CIP content increasing curing time and causing defects at 60–70 wt.%. An optimal composition of 30 wt.% CIP ensured successful printing with minimal defects. Magnetorheological tests validated the functionality of 4D-printed MREs, highlighting the potential to customize properties through UV exposure adjustments. This approach opens new possibilities for advanced MRE applications and further exploration of tailored rheological behaviors.

ACKNOWLEDGEMENT

This work was supported by the Higher Institution Centre of Excellence (HiCOE) program of the Ministry of Higher Education (MOHE) Malaysia under the HiCOE Research Grant. This research work also supported and funded by Universiti Teknologi Malaysia (UTM) under Fundamental Research (Vot. No. 22H14).

REFERENCES

[1] Ren L, Wu Q, Li J, He Y, Zhang Y, Zhou X, et al. 4D printing of customizable and reconfigurable mechanical metamaterials. Int J Mech Sci 2024;270:109112.
[2] Bastola AK, Paudel M, Li L. Dot-patterned hybrid magnetorheological elastomer developed by 3D printing. J Magn Magn Mater 2020;494:165825.
[3] Mondal S, Katzschmann R, Clemens F. Magnetorheological behavior of thermoplastic elastomeric honeycomb structures fabricated by additive manufacturing. Compos B Eng 2023;252:110498.

Multifunctional Magnetic Graphene Oxide with Morphable Reconfiguration

Jun Cai[1], Yiwen Chen[2], Alireza Seyedkanani[3], Marta Cerruti[4], and Hamid Akbarzadeh[5]

[1,3,5] Department of Bioresource Engineering, McGill University, Canada
(E-mail: jun.cai2@mail.mcgill.ca, alireza.seyedkanani@mail.mcgill.ca, hamid.akbarzadeh@mcgill.ca)
[2,4] Department of Mining and Materials Engineering, McGill University, Canada
(E-mail: yiwen.chen2@mail.mcgill.ca, marta.cerruti@mcgill.ca)

Short abstract: Responsive materials that convert energy into mechanical work have diverse applications. Among these materials, graphene oxide (GO) stands out due to its exceptional responsiveness to light, heat, and humidity, but challenges like slow response and environmental limitations persist. This study presents a magnetic GO (MGO) bilayer actuator, incorporating hard-magnetic microparticles to enhance actuation capabilities through a magnetic field, offering fast response and precise control, and demonstrating stability in aqueous environments. The MGO film enables the low-cost and straightforward manufacturing of customized geometries through post-fabrication processes including cutting and folding, facilitating complex structural morphing under a certain magnetic actuation.
***Keywords*:** Magnetic graphene oxide, Magnetic actuation, Shape morphing, On-demand manufacturing.

1. INTRODUCTION

Graphene oxide (GO), an important graphene derivative, has been extensively utilized as building blocks to construct GO-based actuators. GO is often combined with other materials to obtain bilayer structures [1]. Due to the distinct physical/chemical properties of the assembled bilayer structures, when subjected to external stimuli (e.g., light, heating, and humidity) [1], a strain mismatch typically occurs at the interface of the bilayer, leading to a noticeable bending deformation. Although these approaches can efficiently actuate GO-based bilayer systems, they encounter several practical challenges, such as difficulty in precise stimuli control [2], slow response speed [1], and limited functionalities. Inspired by magnetically-actuated soft machines [2-4], we propose a novel GO-based bilayer actuator, termed magnetic GO (MGO) to address the aforementioned issues that GO-based actuators are encountered. Actuated by magnetic fields and remaining stable in the water, MGO actuators differ from previous GO-based actuators, enabling their utilization in water to fulfil various functionalities. Additionally, magnetic actuation offers untethered and precise control and a large penetration range, making it advantageous for various applications [2, 3]. Distinguished from traditional fabrication methods for magneto-active soft materials [4], the unique flexibility of MGO film allows for effortless creation of diverse designs through simple cutting and origami folding, offering the freedom to obtain complex structures and generate various functionalities.

2. Results and Discussion

Figure 1a shows the fabricated MGO film, which consists of one GO layer and one composite layer containing dispersed hard-magnetic microparticles and GO/poly(acrylic acid)(PAA). The MGO films are stable in deionized water for up to 30 days due to the crosslinking of GO layer by Ca2+ and the presence of PAA that effectively binds the GO and the embedded particles together. After creating creases in the MGO films with appropriate patterns, MGO films can be folded into various origami structures. A fully magnetized MGO film retains a large magnetic hysteresis due to NdFeB's significant remanence and coercivity [4]. To illustrate the magnetic actuation performance of MGO, we investigate the magnetically controllable shape morphing of the origami structures fabricated by MGO films. Different from other conventional fabrication methods for realizing magnetic soft materials [4], our magnetic origami fabrication approach exploits pre-existing MGO films, which allows for swift adaptation to desired structures through straightforward cutting and folding post-process, thereby eliminating the need for predefined designs and significantly reducing fabrication time and complexity. To illustrate the magnetic actuation performance of MGO, we design a Miura-ori pattern (Fig. 1b) with programmed magnetization patterns (Fig. 1c). To achieve this magnetization pattern, the MGO Miura-ori is magnetized in its fully folded state, with the magnetic field applied parallel to the Miura-ori panels. MGO Miura-ori demonstrates rapid folding/unfolding under an applied magnetic field, either a uniform field generated by a Helmholtz coil (Fig. 1d(i)) or a non-uniform magnetic field applied by a permanent magnet (Fig. 1d(ii)).

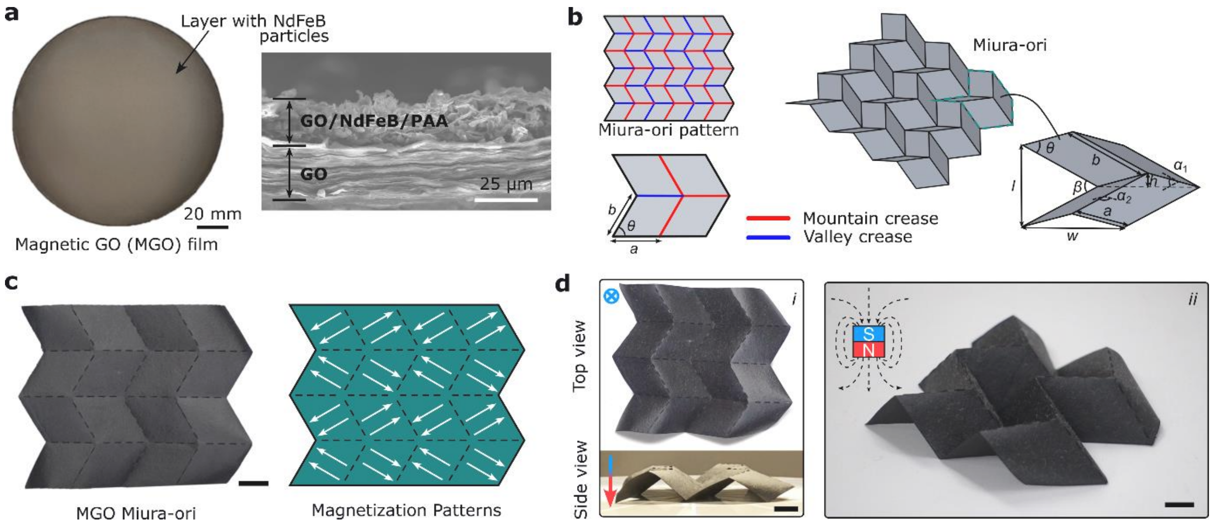

Figure 1. Magnetic graphene oxide origami. (a) MGO film and SEM image of an MGO film. (b) Miura-ori pattern. $a = b = 10$ mm and $\theta = 60^{\circ}$. (c) MGO Miura-ori sample and schematic showing the magnetization patterns. (d) Folding of MGO Miura-ori actuated by magnetic fields generated by (*i*) a Helmholtz coil or (*ii*) a permanent magnet.

3. CONCLUSIONS

In summary, the developed MGO film represents a notable advancement in the field of responsive materials. These lightweight MGO films demonstrate magnetically-driven rapid shape morphing and enable precise remotely-controlled structural reconfigurations. While the magnetization pattern introduced in the MGO structure is currently permanent, further research could focus on developing efficient, low-energy strategies for reprogramming the magnetization pattern.

ACKNOWLEDGEMENT

The authors acknowledge financial support by New Frontiers in Research Fund (NFRFE-2022-00507), the Canada Research Chairs program in Multifunctional Metamaterials, Natural Sciences and Engineering Research Council of Canada through NSERC Discovery Grant (RGPIN-2022-04493), and the Quebec Research Fund Nature and Technologies (FRQNT) doctoral awards (B2X).

REFERENCES

[1] Dong, Y., Wang, J., Guo, X., Yang, S., Ozen, M. O., Chen, P., ... & Liu, B. F. (2019). Multi-stimuli-responsive programmable biomimetic actuator. Nature communications, 10(1), 4087.
[2] Hu, W., Lum, G. Z., Mastrangeli, M., & Sitti, M. (2018). Small-scale soft-bodied robot with multimodal locomotion. Nature, 554(7690), 81-85.
[3] Kim, Y., Yuk, H., Zhao, R., Chester, S. A., & Zhao, X. (2018). Printing ferromagnetic domains for untethered fast-transforming soft materials. Nature, 558(7709), 274-279.
[4] Kim, Y., & Zhao, X. (2022). Magnetic soft materials and robots. Chemical reviews, 122(5), 5317-5364.

Morphological Characterizations of Magnetoactive Foams Incorporated with Different Composition of Magnetic Iron Particles

Nur Azmah Nordin[1,2], Noor Sahirah Muhazeli[1], Saiful Amri Mazlan[1,2], Mohd Aidy Faizal Johari[1], Noriyuki Kuwano[3], Satoshi Hata[3,4], Hiroshi Akamine[4]

[1] Engineering Material & Structures (eMast) iKohza, Malaysia-Japan International Institute of Technology (MJIIT), Universiti Teknologi Malaysia, 54100 Kuala Lumpur, Malaysia.
(E-mail: ma.faizal@utm.my, amri.kl@utm.my, nurazmah.nordin@utm.my)

[2] Automotive Development Centre, Institute for Sustainable Transport (IST), Universiti Teknologi Malaysia, 81310 Skudai, Johor, Malaysia.
(E-mail: amri.kl@utm.my, nurazmah.nordin@utm.my)

[3] The Ultramicroscopy Research Center, Kyushu University, 744 Motooka, Nishi-ku, Fukuoka 819-0395, Japan.
(E-mail: noriyuki.kuwano.577@m.kyushu-u.ac.jp, hata.satoshi.207@m.kyushu-u.ac.jp)

[4] Faculty of Engineering Sciences, Kyushu University, 6-1 Kasugakoen, Kasuga, Fukuoka 816-8580, Japan
(E-mail: hata.satoshi.207@m.kyushu-u.ac.jp, akamine.hiroshi.331@m.kyushu-u.ac.jp)

***Short abstract*:** Magnetoactive (MA) foam, made of carbonyl iron particles (CIPs) that were embedded in an absorbent matrix of polyurethane (PU) foam, shows a strong magnetic responsiveness and controllable properties respective to the stimuli. This study investigates the morphological and elemental changes in MA foam using VPSEM and EDX spectroscopies. Samples with 0, 35, and 75 wt.% CIPs were fabricated via in situ method. Results reveal that increasing CIP concentrations have reduced average pore sizes and altered the foam density as well as stiffness, offering insights into tailoring MA foam properties for semi-active devices and advanced applications.
***Keywords*:** Magnetoactive foam; Carbonyl iron particles; Morphology; Struts; Porosity.

1. INTRODUCTION

Magnetoactive (MA) foam is a magnetic field-responsive material comprising micron-sized magnetically permeable particles, such as carbonyl iron particles (CIPs) embedded within a porous absorbent foam matrix during the foaming process. MA foam exhibits properties that can be continuously, rapidly, and reversibly tuned by altering the external magnetic fields [1]. With its lightweight and porous structure, MR foam holds potential applications in automotive, aerospace, and robotics, particularly in semi-active, lightweight components. By adjusting the strength of magnetic field, the magnetic particles would be attracted and tend to align according to the direction of magnetic fields, causing the foam structure to be slightly changed, enabling the manipulation of wave energy as it passes through the material. MR foam normally can be fabricated via two primary methods: ex situ and in situ. The ex situ method, encompassing MR fluid foam, MR elastomer foam, and MR plastomer foam, involves introducing a mixture of magnetic particles and a suspension medium (e.g., fluid or elastomer liquid) into a preformed foam [2]. This method often leads to agglomeration, with magnetic particles trapped in foam pores, compromising uniformity. In contrast, the in situ method integrates magnetic particles directly with the absorbent foam matrix, achieving enhanced particle distribution and stronger bonding within the matrix [3]. As a result, in situ MA foam offers superior responsiveness to magnetic fields and becomes a promising candidate for smart sound control and other advanced applications. Both methods however result in different localization of magnetic particles in the foam structure.

2. OBJECTIVES

This study aims to investigate the morphological and elemental characterizations of MA foams fabricated via in situ method, focusing on the CIP’s distribution in the porous absorbent matrix which would affect the resultant physicochemical performance of this smart foam.

3. MATERIAL AND METHODOLOGY

The in-situ fabrication of MA foam samples involved with dispersing carbonyl iron particles (CIPs) into an absorbent foam matrix of polyurethane (PU) that composed of two components; polyether polyol (RG135NFDH1) and 4,4′-diphenylmethane diisocyanate (4,4′-MDI). Three concentrations of CIPs which were 0 wt.% (reference sample), 35 wt.%, and 75 wt.% were used to investigate their effects on the morphological changes in MA foams. Morphological analyses were conducted using VPSEM and EDX, while porosity test was carried out utilizing toluene absorption method until saturation following the ASTM D792. Porosity percentage then was calculated based on the weight differences of pre- and post-absorption foam. The findings highlight the influence of CIP's concentration on the foam structure, density and porosity, providing insight into tailoring resultant MA foams performance.

4. RESULTS AND DISCUSSION

Figure 1 shows the VPSEM micrograph of MA foams with different concentration of CIPs; (a) Sample A (0 wt.% CIPs), (b) Sample B (MR foams with 35 wt.% CIPs), and (c) Sample C (MR foams with 70 wt.% CIPs). As observed in the figure, all the fabricated samples are categorized as closed-pore structures since the pores are fully enclosed and do not interconnect to the other pores. In fact, as per-layer of pore structures has been observed, while the other layers could not be seen clearly from the micrographs, the closed-pores which are basically transparent, show overlapping to one another. Besides, it was observed that pores structures of sample B and C were more tightly packed compared to Sample A, which correlated to the dense structure, compact particles attributed to the increment in the concentrations of CIPs in the foam structure. In fact, the measurements of pore sizes show that the Sample A has larger pores compared to Sample B (35 wt.% CIPs) and Sample C (75 wt.% CIPs), reflecting the varying CIP concentrations in the foam matrix. Notably, Sample C exhibited the smallest pore sizes and the highest pore density correspond to the higher CIP content.

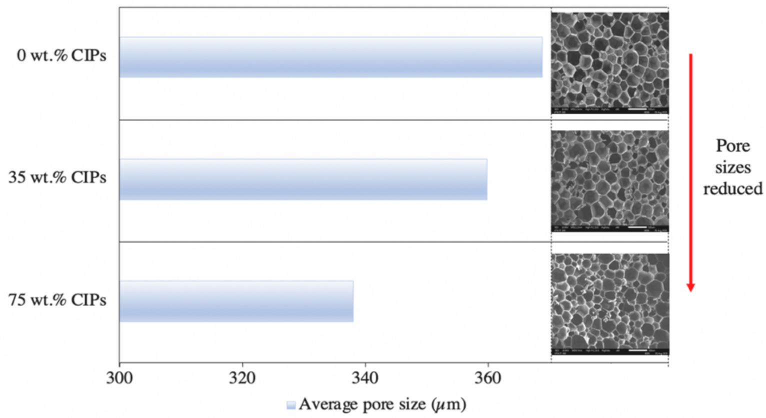

Figure 1: Average of pore sizes of MA foams with regards to various concentration of CIPs.

5. CONCLUSIONS

In brief, the study fabricated MA foams with 0, 35 and 75 wt.% CIPs via the in-situ method and explored morphology-porosity correlations. Results showed smaller, more compact pores with increased CIP concentrations, successfully embedded into foam struts. Porosity and density improved, advancing MA foams as a smart, controllable material with enhanced properties, for various applications.

ACKNOWLEDGEMENT

This work was supported by the Higher Institution Centre of Excellence (HiCOE) program of the Ministry of Higher Education (MOHE) Malaysia under the HiCOE Research Grant. This research work was also supported by Universiti Teknologi Malaysia (UTM) under Fundamental Research (Vot. No. 23H17).

REFERENCES

[1] A.A. Marzuki, **N.A. Nordin**, S.A. Mazlan, M.A.F. Johari, R.E.M. Khaidir, M. Sedlacik and Ubaidillah, Enhancement of the Rheological Properties of Magnetorheological Foam Via Different Constraint Volumes Foaming Approach, Polymer Testing, 128, 2023, 108235.

[2] Muhazeli NS, Nordin NA, Mazlan SA, Abdul Aziz SA, Ubaidillah, Nazmi N. Mini review: an insight on the fabrication methods of smart magnetic polymer foam. Journal of Magnetism and Magnetic Materials, 534, 2021,168038.

[3] Guo Q, Ghadiri R, Weigel T, Aumann A, Gurevich EL, Esen C, Medenbach O, Cheng W, Chichkov B, Ostendorf A. Comparison of in situ and ex situ methods for synthesis of two-photon polymerization polymer nanocomposites, Polymers, 6(7), 2037-50.

Hybrid Torque Control Strategy with Gaussian Process Feedforward for a Novel MRF Dual-Clutch of an Electric Vehicle Transmission

Huan Zhang[1], Lei Deng[1*], Weihua Li[2], and Haiping Du[1*]

[1] School of Electrical, Computer and Telecommunications Engineering, University of Wollongong, Wollongong, New South Wales 2522, Australia
(E-mail: hz994@uowmail.edu.au, leideng@uow.edu.au, hdu@uow.edu.au)
[2] School of Mechanical, Materials, Mechatronic and Biomedical Engineering, University of Wollongong, Wollongong, New South Wales 2522, Australia
(E-mail: weihuali@uow.edu.au)

Short abstract: Modelling and controlling MRF clutches in EV transmission is challenging due to the nonlinear and rate-dependent hysteresis. Feedback control can address model errors and uncertainties but fails to resolve rate-dependent hysteresis. This study proposes a Gaussian Process (GP) hysteresis inverse model for a Magnetorheological Fluid Dual Clutch (MRFDC) of an EV transmission to capture the nonlinear and rate-dependent hysteresis. A hybrid controller integrating the PI feedback control with a GP hysteresis inverse model-based feedforward compensator is designed. Experiments on an MRFDC EV transmission platform demonstrate that the hybrid controller outperforms conventional PI control, achieving superior torque tracking and clutch-shifting performance.

***Keywords*:** Magnetorheological Fluid Clutch, Electric vehicle transmission, Nonlinear and rate-dependent hysteresis, Hysteresis compensation, Gaussian process

1. INTRODUCTION

As a critical component responsible for power transmission, the clutch directly influences the overall vehicle performance, in terms of dynamics, efficiency, safety, and comfort. For EV transmissions based on MRF clutches, clutch engagement and disengagement are managed by adjusting the input current to the clutches, allowing for connecting different gears and altering the transmission ratios [1]. However, MRF clutches exhibit pronounced nonlinear and rate-dependent hysteresis between the input current and output torque [2], significantly affecting the accuracy of the MRF clutch's torque output [3], especially when precise control is requested quickly, such as dynamic torque tracking and clutch-shifting. Therefore, developing a precise torque control strategy that can address the nonlinear rate-dependent hysteresis issues associated with MRF clutches is crucial.

This study focuses on developing a precise torque control strategy for a novel MRFDC of an EV transmission, considering its inherent hysteresis on the current control input as well as its changing rate. The strategy is a hybrid control strategy combining a pure PI feedback control and a GP-based hysteresis inverse model compensator. The pure PI controller is employed to mitigate the effects of model errors, uncertainties, and disturbances. Meanwhile, a GP-based hysteresis inverse model, with the required torque and its change rate serving as the input, is proposed as a feedforward compensator to obtain compensation current commands considering the rate-dependent hysteresis. The effectiveness of the proposed hybrid control strategy is validated through a series of dynamic tracking and clutch-shifting experiments performed on a prototype MRFDC EV transmission platform.

OBJECTIVES

- Investigate the rate-dependent hysteresis phenomenon in MRFDC
- Establish GP hysteresis inverse model and validate its effectiveness in describing MR Clutches
- Build a hybrid torque control of the MRFDC
- Evaluate the torque tracking performance of the hybrid torque control in tracking defined torque signals and gear shifting.

4. RESULTS AND DISCUSSION

The prototyped MRFDC transmission is demonstrated in **Figure 1(a)**, and the designed hybrid controller for the MRFDC is illustrated in **Figure 1(b)**. The controller is proposed by combining the pure PI feedback controller with a feedforward compensator: the GP-based hysteresis inverse model.

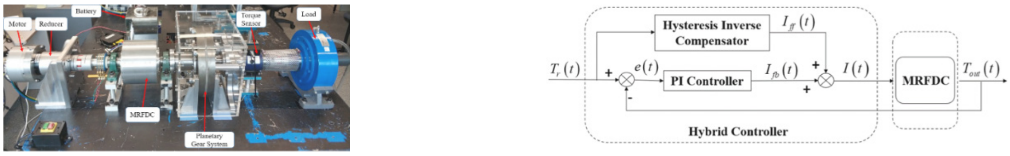

(a) (b)

Figure 1: Block diagram of (a) experimental setup and (b) the hybrid controller.

In the experimental evaluation, tracking signals, including step and arbitrary signals, were selected to assess the dynamic torque tracking performance of the hybrid controller for both internal and external clutches. Additionally, the control performance during the clutch shifting between the internal and external clutches was examined using a predefined shift sequence. The results presented in **Figures 2 and 3** demonstrated that the proposed hybrid control achieved enhanced tracking performance in step and arbitrary signals compared to PI control. This superior controllability is also observed in the clutch-shifting process presented in **Figure 4**.

(a) (b)

Figure 2: Control performance of under the step tracking signal. (a) Internal clutch. (b) External clutch.

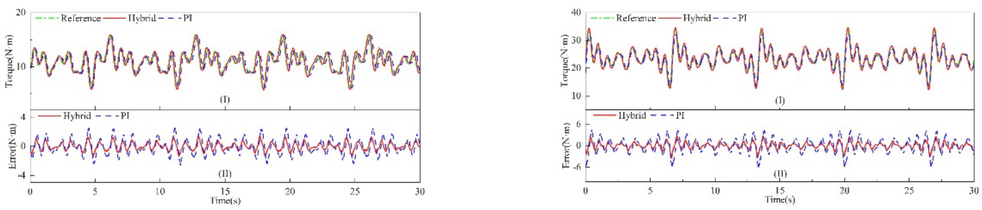

(a) (b)

Figure 3: Control performance under the multi-frequency arbitrary tracking signal. (a) Internal clutch. (b) External clutch.

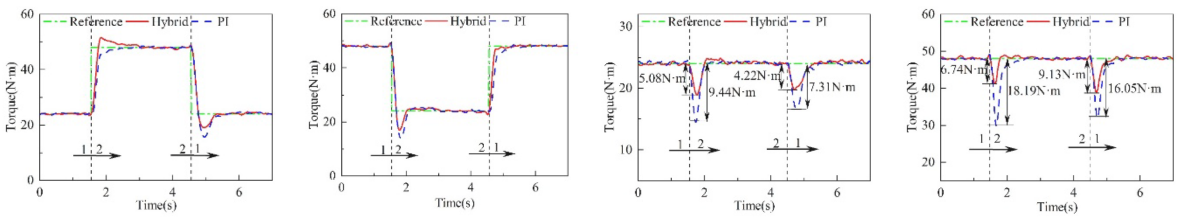

(a) (b) (c) (d)

Figure 4: Control performance for the clutch-shifting process. Shifting process with changing transmission output torque of (a) internal and (b) external clutches. Shifting process with constant output torque of (a) internal and (b) external clutches

REFERENCES

[1] H. Zhang, H. Du, S. Sun, J. Zhao, D. Ning, W. Li, Y. Wang, A novel magneto-rheological fluid dual-clutch design for two-speed transmission of electric vehicles, Smart Materials and Structures, 30 (2021) 075035.

[2] h. zhang, L. Deng, J. Zhao, W. Li, H. Du, Comparative analysis and optimization of nonlinear hysteresis models for a magnetorheological fluid dual-clutch of an electric vehicle transmission, Smart Materials and Structures, (2024).

[3] G. Chen, X. Xiong, Y. Lou, Z. Li, Modeling and observation of rate-dependent hysteresis and creep phenomena in magnetorheological clutch, IEEE/ASME Transactions on Mechatronics, 27 (2022) 2053-2061.

Field Test of Skyhook Controlled Damping System on Real Railway Vehicle

Zbyněk Strecker[1], Filip Jeniš[2], Michal Kubík[3], Ondřej Macháček

[1, 2, 3, 4] Faculty of Mechanical Engineering, Brno University of Technology, Czech Republic
(E-mail: zbynek.strecker@vutbr.cz, Filip.Jenis@vutbr.cz, Michal.Kubik@vutbr.cz, Ondrej.Machacek@vutbr.cz)

Short abstract: The paper presents the comfort improvement of a real railway vehicle equipped with skyhook-controlled magnetorheological dampers riding on three different tracks (corridor with normal wear, regional track, and new corridor). The railway unit consisted of 5 carriages. The comfort was measured in the second carriage, which was equipped with magnetorheological dampers, and the fourth carriage with standard passive dampers mounted by the manufacturer. This setup enabled the evaluation of comfort increase in comparison to the original setup with passive dampers directly during the same ride. The results showed significant improvement of 30% on the worst track.

Keywords: skyhook, semiactive suspension, magnetorheological dampers, railway vehicle, ride tests

1. INTRODUCTION

Traditionally, railway vehicles have relied on passive suspension systems to mitigate vibrations and improve ride comfort. However, these systems often struggle to adapt to varying track conditions and vehicle speeds, leading to suboptimal performance across different operational scenarios. The utilization of semiactively controlled magnetorheological (MR) dampers has proven to increase passenger comfort for various road vehicles. Although a couple of research studies simulating the use of such suspension on railway vehicles have been published with promising results, only a few simulations were verified by experiments. All of the simulations were simplified (reduced degrees of freedom, neglected response time of semiactive dampers, neglected noise from sensors etc.), so the quantification of real comfort improvement remained unclear.

2. OBJECTIVES

The main goal is to quantify an improvement in comfort of real railway vehicle equipped by magnetorheological dampers in semiactive secondary suspension riding on different types of real track.

3. MATERIAL AND METHODOLOGY

3.1. EXPERIMENT SETUP

The test rides were conducted using railway unit Škoda 10 EV Interpanter. The unit consists of 5 carriages. In the second carriage weighting 54 tons, instead of the original vertical and lateral passive dampers, the magnetorheological (MR) dampers were installed. All remaining 4 carriages remained in original state.

The MR dampers maximum force at 7 A and piston velocity 0.1 m/s was 8 kN, while the force for the same piston velocity and 0 A was below 400 N. The primary response time of the dampers was τ_{63} = 8.5 ms for force rise and 4 ms for force drop. For the rides, three different track types were selected: Corridor without curves with max. speed 160 km/h and standard rail wear, regional track with max speed 120 km/h and curves with smallest radius R = 800 m and new corridor track with smallest radius R = 300 m with maximum speed 100 km/h. Each MR damper was connected to its own control unit together with the encoder stroke sensor and sprung mass accelerometer. The control loop period was 1 ms.

3.2. ALGORITHM

The control law for electric current I to the MR damper coil was based on a linear skyhook algorithm and was calculated according to the equation (1):

$$I = \begin{cases} sat(k \cdot |\dot{y}_2|), & \dot{y}_2(\dot{y}_d) \geq 0 \\ 0\,A, & \dot{y}_2(\dot{y}_d) < 0 \end{cases} \tag{1}$$

The sprung mass velocity $\dot{y}_2$ was calculated by summation from sprung mass acceleration signal. A high-pass IIR filter with cutting frequency of 0.2 Hz was set to remove DC component of the sprung mass velocity. The relative velocity between sprung and unsprung mass $\dot{y}_d$ was calculated bydifferentiation of stroke sensor signal. Coefficient k was experimentally set to the highest value ($k = 0.05$ for lateral dampers and $k = 0.1$ for vertical dampers) that did not cause random current switching due to the measured signal noise. The saturation current was set to 4 A (force at 0.1 m/s was 6 kN) for lateral damper and 7 A for vertical damper.

3.3. COMFORT EVALUATION

The comfort was evaluated using vertical and lateral accelerometers positioned above the bogies in the second (with MR dampers) and fourth (with original passive dampers) carriages according to the standard EN 12299 "Railway applications - Passenger comfort - Measurement and evaluation." The ride comfort is evaluated as the N_{MV} parameter, which is calculated according to equation (2).

$$N_{MV} = 6 \cdot \sqrt{\left(a_{XP95}^{W_d}\right)^2 + \left(a_{YP95}^{W_d}\right)^2 + \left(a_{ZP95}^{W_b}\right)^2} \tag{2}$$

Where $a_{XP95}^{W_d}$, $a_{YP95}^{W_d}$, $a_{ZP95}^{W_b}$ are 95% percentiles rms acceleration of 60 5s long segments in longitudinal, lateral and vertical direction, weighted by weight functions W_d a W_b defined in EN12299.

4. RESULTS AND DISCUSSION

The overall comparison of the ride quality parameter N_{MV} in relation to algorithm and track is presented in Fig. 1. The improvement was largest (approximately 30%) for the traction bogie and the track with the highest excitation (caused by the combination of track wear and vehicle speed). Although the track quality of the regional track was lower than the corridor with normal wear, the lower ride speed caused lower bogie excitation, and therefore, the absolute values of the comfort parameter N_{MV} were also lower. Again, the comfort improvement using semiactive control was more than 25%. The smallest comfort improvement was in the case of the new curvy corridor, where the bogie excitation was very small and the ride was very comfortable (N_{MV} under 1) for both carriages. The biggest amplitude reduction (42%) was observed at the natural frequency of the vehicle at 1.8 Hz in the vertical direction. Although vibrations at this frequency were very clearly felt by the passengers, the weight function W_b suppresses the influence of this frequency on the parameter N_{MV}. The performance of semiactive suspension was also reduced by the construction of the vehicle. The secondary suspension air spring was connected with an external air reservoir by pipes with a relatively small cross-section, which caused quite high damping that can not be removed within experiments. Removing of this parasitic damping when $\dot{y}_2(\dot{y}_d) < 0$ would decrease the force that increases the velocity of the sprung mass, thus decreasing overall vibrations.

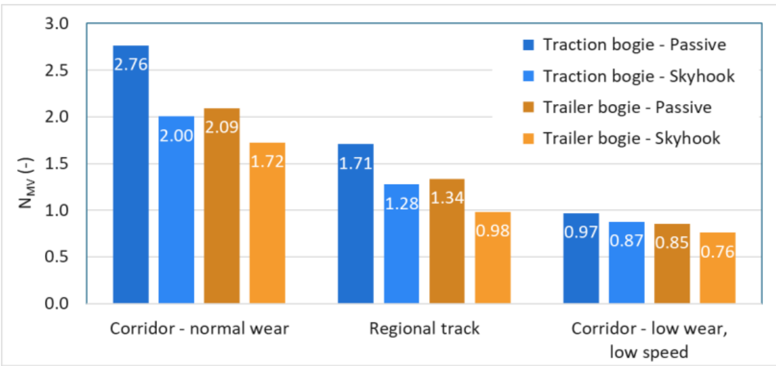

Figure 1: Comparison of ride comfort parameter on different tracks and different control algorithms

5. CONCLUSIONS

The measurement on the real railway vehicle demonstrated a significant improvement of the comfort parameter N_{MV} in the carriage with skyhook-controlled secondary suspension compared to the carriage with passive suspension designed by the railway vehicle producer. The improvement (up to 30%) was higher for higher bogie excitation but it was significant for all track types.

ACKNOWLEDGEMENT

This work was supported by Technology Agency of the Czech Republic under grant CK04000210.

Evaluation and Improvement of Miniature MR Fluid Device for Lightweight Haptic Interface

Asahi Higashiguchi[1], Isao Abe[2] and Takehito Kikuchi[3]

[1] Graduate School of Engineering, Oita University, 700 Dannoharu, Oita 870-1192, Japan
[2, 3] Faculty of Science and Technology, Oita University, 700 Dannoharu, Oita 870-1192, Japan
(E-mail: abe-isao@oita-u.ac.jp, t-kikuchi@oita-u.ac.jp)

Short abstract: Magnetorheological (MR) fluids are composite materials comprising ferromagnetic particles, medium oils, and several types of additives. Their rheological properties change rapidly, stably, and repeatedly when applying magnetic fields. Therefore, we focus on the development of MR fluid devices for haptics. In this paper, we have evaluated the characteristics of a miniature MR fluid device for a lightweight haptic interface. In addition, we redesigned the device structure to control the magnetic flux path for the second prototype. As results, we succeeded in designing the device with higher torque performance than that of the first prototype.
***Keywords*:** Magnetorheological fluid, Haptic interface, Teleoperation

1. INTRODUCTION

Teleoperation systems are installed in disaster-affected areas, under water, and in surgical robots. However, the sensitive nature of their tasks causes psychological stress to operators. Therefore, we have investigated haptic devices using the controllability of magnetorheological (MR) fluids. Owing to the rapid and reversible property change, the MR fluid works effectively in haptic devices with a high responsiveness. In our previous study, we developed the 0.3 Nm-Class MR fluid device based on the multi-layered disc structure [1]. However, the size and weight of the device is excessive for handheld haptic devices. For these reasons, we developed a miniature-size MR fluid device with a cylindrical rotor structure [2]. In addition, as related study, Wellborn et al. achieved high braking torque based on a serpentine magnetic flux path in a small-scale device [3]. In this study, we evaluated the first prototype of a miniature MR fluid device. Furthermore, to achieve higher torque performance, we developed the second prototype with serpentine magnetic flux path. In addition, we compared it with the first prototype using magnetic field analysis and mechanical testing.

2. MINIATURE MR FLUID DEVICE

2.1. DESIGN

We developed two types of miniature MR fluid devices. Figure 1(a) shows their appearance. The dimensions of the two devices are the same. Figures 1(b) and 1(c) show the cross-sections of the first and second prototypes, respectively. A ball bearing and a bearing ball made of nonmagnetic materials hold the output shaft that connects to the rotor. The rotor is located between the inner and outer electromagnetic cores, and the gap is filled with MR fluids. In addition, the second prototype has the Aluminum-ring on the magnetic flux path. This design is expected to increase the intensity of magnetic flux passing through the MR fluid layers, thereby achieving higher torque.

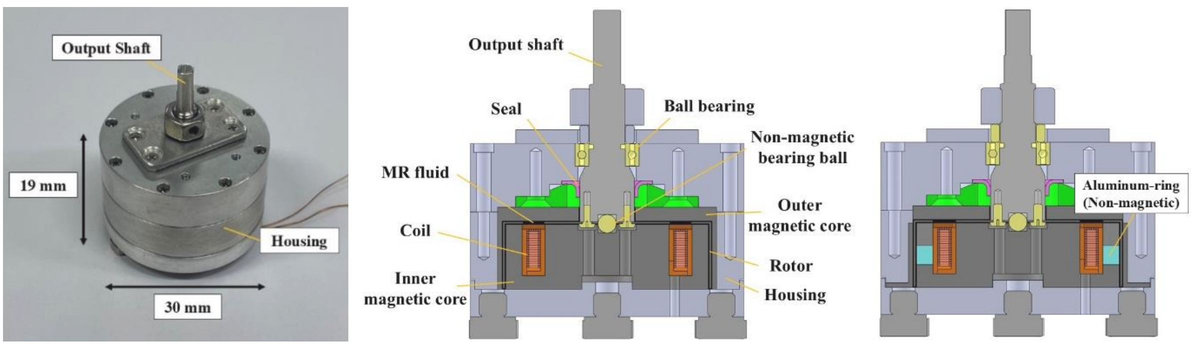

(a) Dimensions (b) First prototype (c) Second prototype

Figure 1: Miniature MR fluid device (appearance (a), and cross-section (b) and (c))

2.2. ANALYSIS

To estimate the performance of both devices, we conducted magnetostatic analysis using the finite-element-method analysis software (ANSYS). The analyzed components include the inner and outer electromagnetic cores as well as the rotor section. The number of turns of the coil and the diameter of the magnetic wire were 100 and 0.2 mm, respectively. We used the B-H properties of the measured MR fluid sample (132DG, Lord Corp.) in this study. Figure 2 shows the magnetic flux density distribution at 1.2 A. Based on these results, we calculated the regional average values of the magnetic flux density, which serves as the source of the MR effect, as well as the output torque values of each device caused by the MR effect (Figure 3).

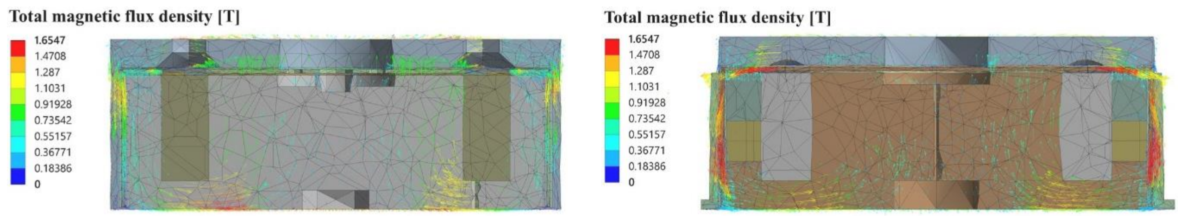

(a) First prototype (b) Second prototype

Figure 2: Analytic results for the miniature MR fluid device

3. EVALUATION

The torque responses of the devices were measured using our experimental setup. For the static torque tests, the electric current was controlled between 0.0 and 1.2 A for 6 seconds. The average torque for each condition was calculated. Figure 3 shows the estimated and experimental torque values of the first and second prototypes. The horizontal and vertical axes represent the current input (A) and the output torque (Nm), respectively. In the first prototype, the experimental results were close to the simulation values, indicating high reliability. Additionally, the torque performance of the second prototype exceeded that of the first prototype. The experimental results of the second prototype will be presented in our conference presentation.

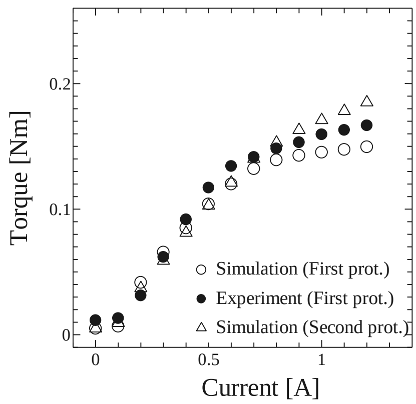

Figure 3: Analytic and experimental results for static torque

4. CONCLUSIONS

In this study, we evaluated the first prototype of a miniature MR fluid device. Subsequently, we developed the second prototype with an aluminum ring to enhance the magnetic flux compared to the first prototype. As a result of the analysis, we successfully designed a second prototype with higher static torque performance.

ACKNOWLEDGEMENT

This study was partially supported by Kurata Grants of the Hitachi Global Foundation (1555) and the Fund Program for Creating Research-based Startups from Academia (Grant Number JPMJSF23DW).

REFERENCES

[1] Takano T., Ikeda A., Abe I., Kikuchi T., "Improvement of Haptic Interface for Teleoperation Endoscopic Surgery Simulators Using Magnetorheological Fluid Devices," Journal of Robotics and Mechatronics, 34 (6), pp.1268-1276, 2022.

[2] Higashiguchi A., Abe I., Kikuchi T., "Design and Analysis of Miniature Magnetorheological Fluid Device for Handheld Haptic Interface," in 2024 IEEE International Conference on Advanced Intelligent Mechatronics, pp.367-372, 2024.

[3] Wellborn P. S., Mitchell J. E., Pieper N. J. and Webster R. J., "Design and Analysis of a Small-Scale Magnetorheological Brake," in IEEE/ASME Transactions on Mechatronics, 27 (5), pp. 3099-3109, 2022.

Development of a novel compact magneto-rheological impact damper featuring shear-mode twin-tube structure

Huu-Quan Nguyen[1], Quoc-Duy Bui[2,*], Duc-Nam Nguyen[3,*], Thanh Danh Lam[4] and Quoc Hung Nguyen[5,*]

[1, 2, 3] Faculty of Mechanical Engineering, Industrial University of Ho Chi Minh City, Ho Chi Minh City, Vietnam
(E-mail: nguyenhuuquan@iuh.edu.vn, buiquocduy@iuh.edu.vn, nguyenducnam@iuh.edu.vn, lamthanhdanh@iuh.edu.vn)
[5] Institute of Engineering, Ho Chi Minh City University of Technology, Ho Chi Minh City, Vietnam
(E-mail: nq.hung@hutech.edu.vn)
* Corresponding author. Tel.: +84 938485812 (Q. H. Nguyen)

Short abstract: In this study, we develop a novel magneto-rheological (MR) damper for impact damping applications. The MR impact damper (MRID) functions in shear mode, employing a twin-tube structure to expand the operational area of MRF, thereby enhancing damping performance. Modeling and optimization are carried out to attain a compact and optimal design. Experimental tests and evaluations are scheduled to verify the feasibility of the proposed MRID. This research aims to deliver an effective and compact MRID capable of producing a soft-landing effect, thereby minimizing harm during collisions.
Keywords: damper, impact, magneto-rheological, soft-landing, twin-tube.

1. INTRODUCTION

Impacts, such as those encountered in high-speed aircraft landings, vehicle accidents, or machine tool operations, present significant risks to human safety and structural integrity. One of the most effective strategies for mitigating detrimental effects of impact shocks and vibrations is to use impact dampers.

MRF, a smart material responsive to magnetic fields, has recently emerged as a promising candidate for semi-active suspension systems. By adjusting the intensity of the magnetic field applied to the MRF, the damping properties can be controlled in real-time. Over the past few years, numerous studies on MRIDs have been undertaken [1-4]. In this paper, we propose a novel compact MRID with superior damping performance for impact damping applications. This innovative MRID incorporates a twin-tube structure operating in shear mode, with multiple magnetic coils strategically positioned along the stroke to expand the active area of MRF in a specific operational space, resulting in enhanced damping force and dynamic range.

2. OBJECTIVES

Building upon the previous analyses, the objectives of paper are as follows:

- Develop a novel MRID featuring shear-mode twin-tube structure to improve damping performance.
- Conduct the modeling and optimization to attain the optimal design for a specific impact case study.
- Verify the feasibility of the shear-mode twin-tube MRID through experiments and assessments.

3. MATERIAL AND METHODOLOGY

Figure 1 depicts the configuration of the novel shear-mode twin-tube MRID. A cylinder relatively slides to a piston core and an outer housing at the same time, forming a twin-tube structure. The two coaxial annular ducts on the inner and outer faces of the cylinder are filled with MRF, which can be activated by magnetic coils positioned on the cylinder. When subjected to magnetic fields, the MRF in the twin ducts solidifies, leading to the expected damping force produced by increased friction between the cylinder and MRF.

The total damping force F_d is determined as the sum of yield stress damping force F_τ, viscous damping force F_η and Coulomb friction force at O-ring F_{or}:

$$F_d = F_\tau + F_\eta + 2F_{or} \tag{1}$$

$$F_\tau = \sum A_{l.j}\tau_{y.j} = 2\pi \sum r_j l_j \tau_{y.j} \tag{2}$$

$$F_\eta = \eta \frac{v}{t_g} \sum A_j = 2\pi\eta \frac{v}{t_g} \sum r_j l_j \quad (3)$$

where τ_y and η are the MRF properties, v is the shear velocity, and A_l, r, l and t_g are geometric dimensions.

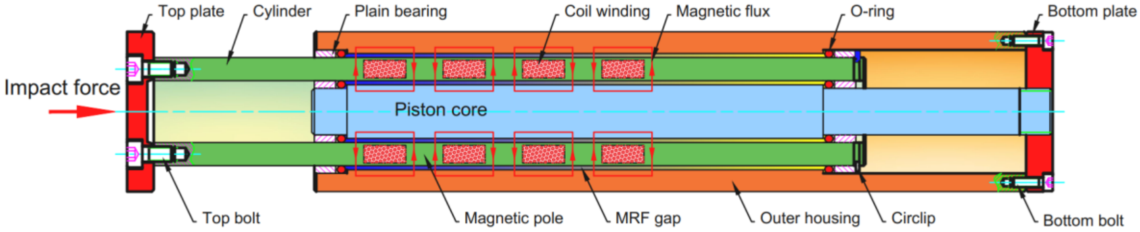

Figure 1: Configuration of the shear-mode twin-tube MRID.

The methodologies planned to be implemented in the paper include:

– Analysis and review. Configurations of MRIDs are initially reviewed, followed by analyses of their respective advantages and disadvantages. Subsequently, the shear-mode twin-tube structure is proposed.

– Modeling, simulation and comparison. Based on the mathematical model, a design optimization problem is formulated. The shear-mode twin-tube MRID model is simulated and optimized using ANSYS software. The results are then compared with previous studies.

– Experimental verification. The MRID is designed, prototyped and experimentally validated on a test rig.

4. RESULTS AND DISCUSSION

Figure 2 illustrates the simulation results for the shear-mode twin-tube MRID. It is observed that the magnetic flux is distributed throughout the twin MRF ducts, thereby improving the damping force. Building upon these modeling and simulation, a design optimization is scheduled to be conducted, taking into account performance criteria such as damping force, dynamic range and inductive time constant.

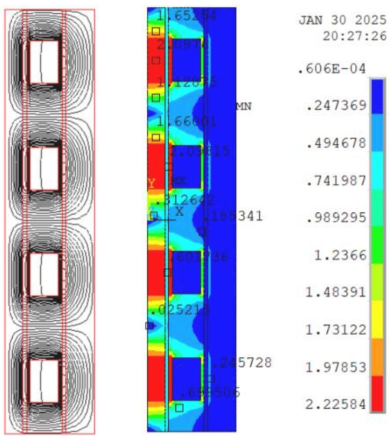

Figure 2: Simulation of magnetic flux lines and magnetic flux density.

5. CONCLUSIONS

In this work, a novel compact shear-mode twin-tube MRID for impact applications is introduced. The modeling and simulation results initially show the feasibility of this concept. In the next phase, the proposed MRID will be optimized, prototyped, experimentally tested, and evaluated for functionality validation.

REFERENCES

[1] Choi YT, Robinson R, Hu W, Wereley NM, Birchette TS, et. al. Analysis and control of a magnetorheological landing gear system for a helicopter. Journal of the American Helicopter Society. 2016;61(3):1-8.

[2] Wang M, Chen Z, Wereley NM. Adaptive magnetorheological energy absorber control method for drop-induced shock mitigation. Journal of Intelligent Material Systems and Structures. 2021;32(4): 449-461.

[3] Maeda T, Otsuki M, Hashimoto T. Protection against overturning of a lunar-planetary lander using a controlled landing gear. Proceedings of the Institution of Mechanical Engineers, Part G: Journal of Aerospace Engineering. 2019;233(2):438-456.
[4] Zheng J, Zhao J, Wang L, Li Z, Dong W, E S. Optimal control for soft-landing in elevator emergency crash using multiple magnetorheological shock absorbers. Journal of Intelligent Material Systems and Structures. 2022;33(19):2454-2469.

Fatigue Damage Degradation and Dynamic Characteristics of Periodic-Structured Anti-Yaw Magnetorheological Elastomer Isolator

Leizhi WANG[1], Feng SUN[2] and Bo ZHANG[3]
[1, 2, 3] School of Mechanical Engineering, Ningxia University, Yinchuan 750021, China;
(E-mail: wangleizhi@outlook.com, sfeng@nxu.edu.cn, zhangb@nxu.edu.cn)

***Short abstract*:** The anti-yaw isolator in bogie systems effectively suppress lateral vibrations caused by hunting motion. To adapt to multifrequency excitation loads induced by track irregularities, operational speeds, and bogie wheelset structures, this study proposes a periodic-structured anti-yaw isolator employing interface-modified magnetorheological elastomer (MRE) for broadband lateral vibration suppression. However, long-term service leads to thermal aging and fatigue damage in MRE components of these isolators, resulting in degradation of dynamic properties and potential safety hazards for high-speed vehicles. This project investigates the fatigue-induced performance degradation and dynamic characteristics of MRE anti-yaw isolator. Considering thermal fatigue effects, a thermal-magneto-mechanical viscoelastic model was established, systematically analysing the viscoelastic mechanical properties of interface-enhanced anisotropic MRE. It's used to analyse dynamic load and bandgap regulation, proposing an inverse dynamic modelling algorithm with thermal fatigue compensation to achieve optimized lateral vibration control.

***Keywords*:** anti-yaw isolator, MRE, thermal fatigue, dynamic degradation, bandgaps

Performance Evaluation of Control Approaches for An MR Damper Prosthetic Leg

Afrouz Hajimoradi[1], Hossein Vatandoost[2], Ramin Sedaghati[3]

[1, 3] Department of Mechanical Engineering, Concordia University, Montreal, QC, Canada
(E-mail: afrouzhajimradi@gmail.com, ramin.sedaghati@concordia.ca)
[2] National Research Council of Canada, Boucherville, QC, Canada
(E-mail: hossein.vatandoost@nrc-cnrc.gc.ca)

Short abstract: Magnetorheological (MR) fluid dampers can have extensive applications for prosthetic legs due to their compact size and rapid response time. In this regard, control approaches play a crucial role for the effective implementation of such technology. In this study, we investigate the performance of three control strategies: namely, feed forward, adaptive and robust inverse dynamics controllers. We evaluate the performance of the controller in one gait cycle through simulation experiments. Finally, we present the performance results of each controller.
***Keywords*:** MR damper, prosthetic leg, control approach, gait cycle.

1. INTRODUCTION

Magnetorheological (MR) fluid dampers have emerged as a transformative technology in prosthetic leg design, offering adaptable damping properties that enhance user mobility and comfort. These dampers utilize a controllable fluid whose viscosity can be rapidly changed in response to an applied magnetic field, allowing for real-time adjustments to dynamic loads and gait variations. Despite their potential, the effectiveness of MR dampers heavily depends on the control strategy employed to regulate the damping force. In this study, we investigate the performance of three control approaches for MR damper prosthetic legs.

2. OBJECTIVES

This paper evaluates the performance of three control methods—Feed Forward Controller (FFC), Inverse Dynamic Adaptive Controller (IDAC), and Inverse Dynamics Robust Controller (IDRC)—in minimizing knee angle tracking error in a prosthetic leg during a single gait cycle.

3. METHODOLOGY

To achieve concrete results toward the presented objective, we perform simulation experiments by deriving a dynamic model of the prosthetic leg shown in Fig. 1(a). To measure the tracking error of the knee angle, the discrepancy between the actual and the desired knee angle is evaluated. However, the desired knee angle of the prosthetic leg cannot be directly measured due to lack of thigh in the amputees. Therefore, in the second step, we estimate this angle using a function approximator. Finally, using the developed dynamic model and the function approximator, we implement each controller in MATLAB.

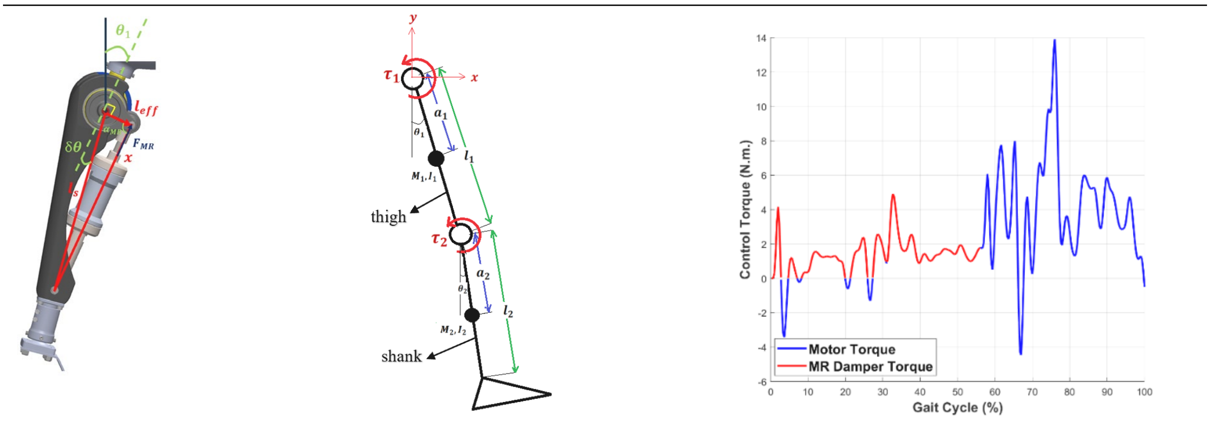

(a) (b) (c)

Figure 1. (a) Prosthetic leg, (b) Schematic model of human leg as a double pendulum, and (c) The control torque using combination of MR Damper and DC Motor for one gait cycle

3.1. Dynamic Model of the Leg Prosthetic

The leg prosthesis is modeled as a double pendulum as shown in Fig. 1 (b) and the Lagrange method is used to obtain the dynamic equation as:

$$M_{12}\ddot{\theta}_1 + M_{22}\ddot{\theta}_2 + C_2 + G_2 = \tau \tag{1}$$

In this equation, θ_1, θ_2 denote the hip joint angle and the knee joint angle, respectively. Also, $(\dot{\ })$ and , $(\ddot{\ })$ denote the first and second derivative of the variables (angular speed and acceleration). Mass matrices M_{12}, M_{22}, the Coriolis matrix C_2 and the gravity matrix G_2 are function of the length of the thigh, shank, knee and the hip angles. The control torque on the knee is denoted by $\tau = \tau_2$ which is generated by combination of MR damper and DC motor. It is assumed the amputee controls their hip comfortably. The objective of control strategies is to generate control torque τ through control of MR damper and DC servo motor to minimize error, $e(t)$, between the desired and the actual knee angle.

3.2. Approximation of the Desired Knee Angle

Inspired by [1], we approximate the knee angle as a polynomial of the hip angle:

$$\hat{\theta}_2 = \sum_{i=0}^{n} c_i\, \theta_1^i = C^T[1,\ \theta_1^i, \dots, {\theta_1^i}^n], \tag{2}$$

where the superscript denotes the value of the variable at the ith sample and $C = [c_0 \dots c_n]^T$ denotes the vector coefficients. The data from one gait cycle was obtained and then the optimal coefficients are identified by solving a least-square minimization technique to minimize the error between the estimates and actual values of the knee angle. In this study, we use polynomial of order $n = 3$.

3.3. Performance Evaluation of the Control Approaches

The controllers' performance was evaluated using two metrics derived from simulation experiments over a single gait cycle. First, we compute the root mean square error (RMSE) of the knee angle across all sampled data points. We denote this metric by e. Second, the control energy is calculated as the sum of the squared knee torque values and denoted by u. To compare the control approaches, we define a control cost as the sum of the squared normalized RMSE and the normalized control energy ($e_n^2 + u_n^2$), where normalization is performed relative to the maximum observed values of each metric. The quadratic form of this cost function is inspired by the traditional formulation used in optimal control [2].

4. RESULTS AND DISCUSSION

Table 1 illustrates the results of the simulation experiments. As observed, the robust control approach (IDRC) provides the minimum value of the control cost among the three approaches. This implies that IDRC may be the optimal choice to provide high control accuracy with relatively minimal amount of control effort. The control cost can be tailored according to our task-specific requirements. For instance, if higher accuracy of the controller is required, we can reflect this with a weighted sum as $we_n^2 + u_n^2$ where higher values of the weight indicate the importance of accuracy, whereas lower values of weight indicate the importance of control energy. Finally, Fig 1. (c) illustrates the generated control torque for one gait cycle. This torque is provided by a combination of the MR damper and a DC motor during walking as depicted in this figure.

Table 1: Comparison of the Performance of the Control Approaches

Method	RMSE	Normalized RMSE	Control Energy	Normalized Control Energy
FFC	2.14	1.00	1.78×10^4	0.91
IDAC	1.47	0.72	1.71×10^4	0.881
IDRC	1.54	0.69	1.94×10^4	1.00

5. CONCLUSIONS

This work evaluated three control approaches for MR prosthetic legs, introducing metrics to assess control cost based on accuracy and control effort. Future research may explore a wider range of methods and real-world implementation on MR damper prosthetic legs.

REFERENCES

[1] Park J, Yoon GH, Kang JW, Choi SB., "Design and Control of a Prosthetic Leg for Above-knee Amputees Operated in Semi-active and Active Modes," *Smart Materials and Structures*. 2016 Jul 11;25(8):085009.
[2] Lewis FL, Vrabie D, Syrmos VL., "Optimal Control," *John Wiley & Sons*; 2012 Mar 20.

Research of a passive-tuned magnetorheological damper for whole-spacecraft vibration isolation

Lifan Wu[1], Xiaomin Dong[2] and Kaixiang Wang[3]

[1, 2, 3] State Key Laboratory of Mechanical Transmission, Chongqing University, Chongqing 400044, The People's Republic of China
(E-mail: 1140286676@qq.com, xmdong@cqu.edu.cn, 1047638597@qq.com)

***Short abstract*:** During the launch stage of a carrier rocket, the rocket-borne satellite will be subjected to complex vibrations from the rocket body. Based on this special condition, a magnetorheological (MR) damper using permanent magnet and MR composite was proposed. The mechanical model of the proposed damper was derived by analyzing the squeeze strengthening effect of composite. Furthermore, the mechanical performances of the damper were tested and the results showed that the damper can generate a damping force exceeding 800N. Finally, a simulation system for the whole-spacecraft vibration isolation was setup and the results showed that the damper had a good performance.
***Keywords*:** whole-spacecraft vibration isolation, magnetorheological composite, passive-tuned damper, squeeze strengthening

1. INTRODUCTION

When the carrier rocket is launched, the rocket-borne satellite is subject to a variety of quasi-static and dynamic loads. It is easy to cause the satellite and the precision equipment on the rocket to be affected by vibration and shock, and even lead to the serious consequences of satellite launch failure. Therefore, in order to ensure the normal launch of the carrier rocket and the normal operation of the satellite carried by the rocket, it is necessary to take vibration isolation measure to dissipate the vibration energy of the satellite during the launch stage of the rocket and ensure the normal operation of the satellite [1, 2].

Current studies have shown that whole-spacecraft vibration isolation technology can effectively inhibit the transmission of vibration energy between the rocket and the satellite, and can effectively improve the harsh mechanical environment [3]. The whole-spacecraft vibration isolation technology is a kind of satellite and rocket vibration isolation measure that does not change the satellite or launch vehicle's own structure, but only adds a set of vibration isolation system to the adapter structure, so as to reduce the vibration response of the satellite [4].

2. OBJECTIVES

The influence of factors such as magnetic flux density, matrix density of the MR composite, and squeeze on the MR composite was investigated for wideband vibration, and a modified H-B model was established to characterize the mechanical properties of the MR composite.

The mechanical model of the proposed damper was derived by analyzing the squeeze strengthening effect of the MR composite and the influence of non-uniform radial gap on the damping force.

A simulation system for the whole-spacecraft vibration isolation was setup and the results showed that the proposed damper had a good isolation performance.

3. MATERIAL AND METHODOLOGY

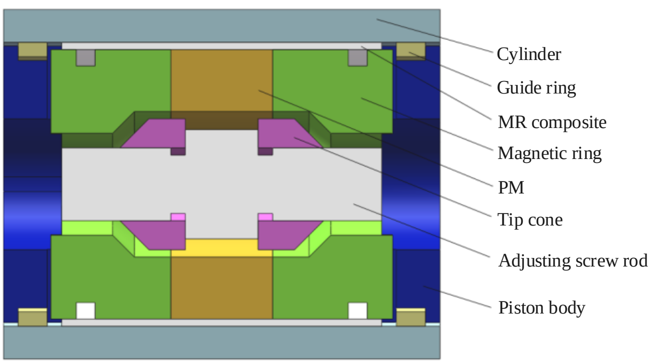

Figure 1: Schematic diagram of damper.

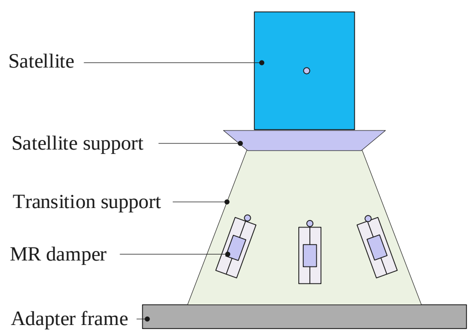

Figure 2: Platform framework.

Unlike traditional MR fluid, the MR composite use non-woven fabric as the matrix, so the magnetic particles in the composite will be bound by the fibers in the non-woven fabric, even if no magnetic field is applied, it is not easy to change the spatial position of the magnetic particles on the matrix. As shown in Figure 1, because the damping gap size of the proposed damper is adjustable, the output damping force can theoretically be adjusted from zero (frictionless state), and the dynamic range is large. Moreover, because of the squeeze strengthening effect of the MR composite, the output damping force of the MR damper can be greater than that of the traditional shear type MR dampers with the same size. Finally, the simulation model of the vibration isolation platform was built according to the framework shown in Figure 2.

4. RESULTS AND DISCUSSION

It can be seen from the results in Table 1 that after the MR damper was installed, both the maximum acceleration and the root mean square of acceleration of the satellite decrease to a certain extent, and the decrease degree is affected by the angle of the adjusting screw rod. The maximum acceleration value of the satellite decreases from 0.2358 to 0.1628, with a decrease of 30.96%. The root mean square (RMS) value of satellite acceleration decreased from 0.0806 to 0.0528, a decrease of 34.49%.

Table 1: Simulation results of vibration isolation effect.

Condition	Maximum acceleration value (*g*)	RMS value (*g*)
Without damper	0.2358	0.0806
Damper, 0°	0.1825	0.0563
Damper, 120°	0.1848	0.0568
Damper, 240°	0.1687	0.0558
Damper, 288°	0.1628	0.0528
Damper, 336°	0.1643	0.0533
Damper, 384°	0.1669	0.0562

5. CONCLUSIONS

A MR damper using permanent magnet and MR composite was proposed, which has stable performance. The mechanical performances of the proposed damper were tested and the results showed that the damper can generate a damping force exceeding 800 N. Compared with the satellite without the proposed damper, the root mean square value (simulated) of the satellite vibration acceleration decreases by about 34.49%.

ACKNOWLEDGEMENT

This research is supported financially by the National Natural Science Foundation of People's Republic of China (52075056).

REFERENCES

[1] Wilke PS, Johnson CD, Fosness ER. Payload isolation system for launch vehicles. Symposium, San Diego, Ca, F: Conference on Passive Damping and Isolation, at the Smart Structures and Materials 1997 Symposium. 1997: 20-9.

[2] Evert ME, Janzen PC, Anderson EH, et al. Active vibration isolation system for launch load alleviation. San Diego, CA, F: proceedings of the Smart Structures and Materials 2004 Conference, 2004: 62-14.

[3] Wilke PS, Johnson CD, Grosserode PJ, et al. Whole-spacecraft vibration isolation on small launch vehicles, Newport Beach, Ca, F: proceedings of the Smart Structures and Materials 2000 Conference, 2000: 20-9.

[4] Deng X, Dong X, Xing J, et al. Nonlinear dynamics of magnetorheological whole-satellite with variable parameters under small amplitude and medium-high frequency vibration. Smart Materials and Structures, 2021; 31(1): 015038.

Integration of Metal 3D-Printed Magnetorheological Clutches in a Backdrivable High-Power Density Robotic Actuator

Pierre Lhommeau[1] and Jean-Sébastien Plante[1]

[1] Faculty of engineering, University of Sherbrooke, Createk, Canada.
(E-mail: Pierre.Lhommeau@USherbrooke.ca, Jean-Sebastien.Plante@USherbrooke.ca)

***Short abstract**: Dynamic robots such as humanoid or walking robots require high power density but backdrivable actuators for smooth and rapid movements. Geared magnetorheological actuators are promising for such purposes but underexplored for high-power density robots applications. This paper investigates using miniature, nested 3D-printed magnetorheological clutches combined with highly geared high-speed motors to achieve this. An actuator prototype experimentally shows a power density above 1 kW/kg with high output speeds over 250 rpm and good backdrivability. This work also highlights that while nested 3D printing is functional in laboratory conditions, it still has challenges to solve before becoming a practical manufacturing process.*

***Keywords**: Additive manufacturing, Magnetorheological clutches Power density, Backdrivability, Dynamic Actuators.*

1. INTRODUCTION

Walking and humanoid robots are designed to replicate animal-like dynamic performance, pushing back the limits of conventional actuation technology. In such applications, classic gearmotors fall in a classic design conflict by having to trade between torque/power density and backdrivability [1].

Geared MR actuation is an alternative actuation approach resolving the traditional design conflict found in gearmotors by using fluidic clutches to decouple the motor inertia from the actuator output. The fluidic decoupling therefore allows the use of high-gearing levels for compactness while staying backdrivable. The performance reached on actuators developed for serial chain robotic arms is promising, with torque density of 90 N.m/kg while staying highly backdrivable [2]. However, geared MR actuators have not been explored for high-power density applications such as walking and humanoid robots.

Maximizing simultaneously the torque/power density of geared MR actuators AND the backdrivability requires using MR clutches with minimal inertia and viscous losses. Low clutch inertial and viscous losses reduce backdriving loads, allowing higher gearing for better torque/power density. This is achieved by keeping the MR clutch shear interfaces close to the rotation axis, which is best done with multi-disk clutches [3]. Manufacturing multi-disk MR clutches, particularly on small scales (~10 mm) is challenging. Nested metal 3D printing has been proposed as a manufacturing process to simplify the assembly of miniature multi-disk MR clutches. A proof-of-concept prototype proved the approach viable on simplified individual components [3]. To date, it is unclear if we can, and how to use nested 3D printing for geared MR actuators.

2. OBJECTIVES

Objectives of the paper are found across the disciplines of manufacturing and robotics. A first objective is to investigate the design and manufacturing process for nested 3D printed MR clutches on small scales that can be used in fully functional actuators. A second objective is to clearly assess the potential of nested 3D printing as a practical manufacturing approach. A third objective is to verify if a geared MR actuator can meet performance requirements for walking/humanoid robot with power density above 1 kW/kg.

3. MATERIAL AND METHODOLOGY

3.1. Actuator requirements

Performance requirements are based on MIT's Cheetah 3 actuators [1], a gold standard in dynamic legged robotics, with a torque density estimated around 115 N.m/kg and output speeds of 200 rpm. The study uses existing components from Exonetik's serial-chain robotic arm to ensure reliability, focusing on the critical nested 3D-printed clutches. However, this comes at the cost of imposing the gearing ratio. Here, the gearing of 61.12:1 allows reaching output speeds of 250 rpm when coupled to Hobbywing 1400kv brushless motors operating on 3S. Another constraint is that the 3D-printed MR clutches have to fit in the housing, imposing 32 mm as the maximal diameter.

3.2. Nested 3D-printed Clutch design and manufacturing

Efforts focus on making an operational 3D-printed clutch that fits the existing joint. Figure 1 shows the main clutch components as well as a CT scan of the nested 3D-printed parts. The CT scan puts in evidence that the limits of the 3D printer used were reached. Although the laser parameters were tuned for thin features, some geometries are not accurate like the output disks warping due to thermal residual stresses.

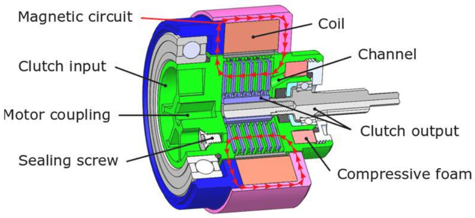

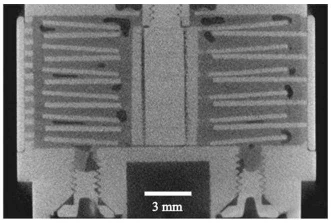

Figure 1: Left, CAD view of the MR clutch components. Right, CT scan of the MR clutch shear interface.

Due to the rough and uneven surface finish of the 3D printer, all functional surfaces such as bearing fits or sealing surfaces have to be post-machined using a CNC. Precisely machining the 3D-printed clutches is a challenge due to the difficulty to reliably reference the part, the small size of the features, and the low rigidity of some of the 3D-printed features causing vibration. But 3D printing process also enables unique features like nested 3D printing, printing small threads or channels inside the parts that eases the assembly process.

4. EXPERIMENTAL CHARACTERIZATION

The performances of the actuator prototype are characterized on a test bench. The backdriving torque, torque-to-current relationship, bandwidth and viscous drag of the actuator are measured. Figure 2 shows the actuator and its bandwidth characterization up to 20 Hz. (*Dues to some constraints on the test bench, we couldn't measure at higher frequencies but this will be fixed soon, and a bandwidth over 60 Hz is expected.*)


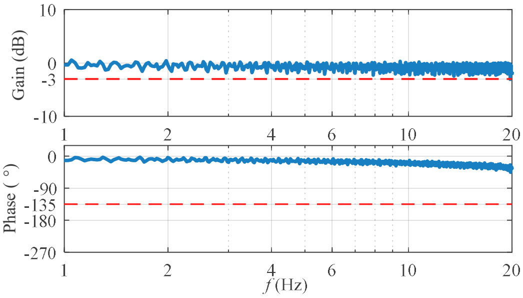

Figure 2: Left, picture of the robotic actuator next to the 3Dprinted clutch and a pin. Right, experimental bandwidth characterization of the actuator.

5. CONCLUSIONS

This work demonstrates the possibility of using nested 3D printing to create an actuator suitable for dynamic robots with high power density and backdrivability. The proposed methodology is functional but not ready for production yet. 3D printing process brings some complexities that could be overcome by future generations of 3D printers with better accuracy, and featuring on-board machining.

REFERENCES

[1] P. M. Wensing, A. Wang, S. Seok, D. Otten, J. Lang, and S. Kim, “Proprioceptive Actuator Design in the MIT Cheetah: Impact Mitigation and High-Bandwidth Physical Interaction for Dynamic Legged Robots,” *IEEE Trans. Robot.*, vol. 33, no. 3, pp. 509–522, Jun. 2017, doi: 10.1109/TRO.2016.2640183.

[2] A. St-Jean, F. Dorval, J.-S. Plante, and A. Lussier-Desbiens, “Magnetorheological-Actuators: An Enabling Technology for Fast, Safe, and Practical Collaborative Robots,” *IEEE Trans. Robot.*, vol. 40, pp. 1261–1272, 2024, doi: 10.1109/TRO.2023.3341573.

[3] P. Lhommeau, M. Lamy, and J.-S. Plante, “Design and characterization of a miniaturized low inertia and low viscous friction magnetorheological clutch using 3D metal printing for human-robot applications,” *J. Intell. Mater. Syst. Struct.*, 2023, doi: 10.1177/1045389x221147675.

Simulation and experimental study on the influence of magnetic field on the surface roughness in magnetorheological polishing

Thanh-Danh Lam[1], Quoc-Duy Bui[1], Quoc Hung Nguyen[2] and Duc-Nam Nguyen[1,*]

[1] Faculty of Mechanical Engineering, Industrial University of Ho Chi Minh City, Ho Chi Minh City, Vietnam
(E-mail: lamthanhdanh@iuh.edu.vn, buiquocduy@iuh.edu.vn, nguyenducnam@iuh.edu.vn)
[2] Institute of Engineering, Ho Chi Minh City University of Technology, Ho Chi Minh City, Vietnam
(E-mail: nq.hung@hutech.edu.vn)
*Corresponding Author: Duc-Nam Nguyen (E-mail: nguyenducnam@iuh.edu.vn)

Short abstract: Magnetorheological polishing (MRP) is a surface finishing method that uses non-Newtonian fluids to improve the surface quality of workpieces. In this study, the influence of magnetic field on MR polishing slurry will be simulated and experimented on SKD11 steel. A simulation model to analyze the effect of the working gap between the workpiece and the polishing tank on the magnetic field distribution during machining was carried out. As a result, the optimal working gap for polishing process is 2mm. Based on the simulation results, an experimental model was conducted. The surface roughness of the workpiece (Ø30 mm) was rapidly reduced from Ra = 120 nm to Ra = 22 nm.

Keywords: *MR polishing, surface roughness, working gap, magnetic field, non-Newton fluid.*

1. INTRODUCTION

Surface finishing is an important step in the process of improving the surface quality of a product. Traditionally, the product surfaces are finished through grinding and lapping process [1-4]. To improve the surface quality, the polishing process with MR fluids for complex surface have been developed [5-8]. The MRF polishing technology uses a flexible abrasive tools formed by rheological properties in a magnetic field to polish the surfaces of the workpiece. In this study, a polishing process for spherical workpiece with MRF is proposed. The influence of magnetic field on MR polishing slurry will be simulated and experimented on SKD11 spherical steel. When the magnetic field is applied, the rheological properties of MRP fluid will be changed in the machining process. The viscosity and shear yield stress of MRP fluid was greatly improved under applied electric current. The simulation process will be performed to analyze and determine the ability of the magnetic field to affect the machining process. Based on the simulation results, the experimental process is established. As a results, the surface roughness of the workpiece has been significantly improved.

2. OBJECTIVES

Study on influence of the working gap between a workpiece and polishing tank on the magnetic field distribution. The shear stress depends on the field distribution affecting the polishing process. Therefore, design of the magnetic field generation component of the MRP process should be optimized.

3. MAGNETORHEOLOGICAL POLISHING AND SIMULATION MODEL

3.1. PRINCIPLE OF MAGNETORHEOLOGICAL POLISHING

The principle of polishing spherical workpiece by MRP process is shown in Fig. 1.

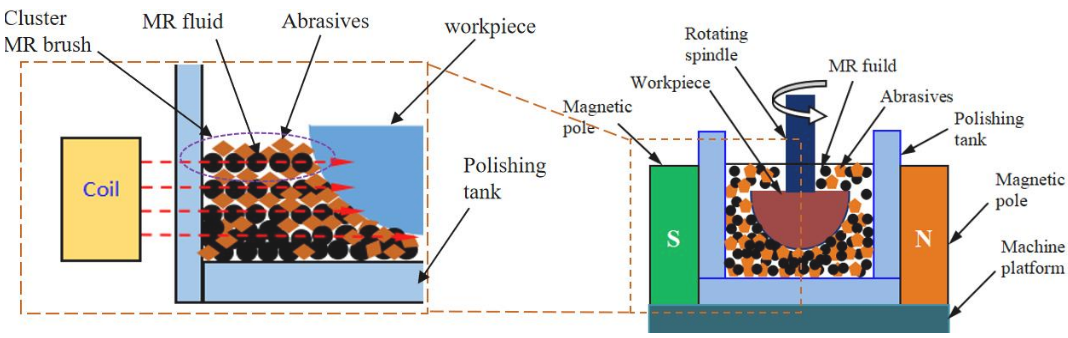

Figure 1: Principle of MR polishing process

3.2. SIMULATION MODEL AND RESULTS

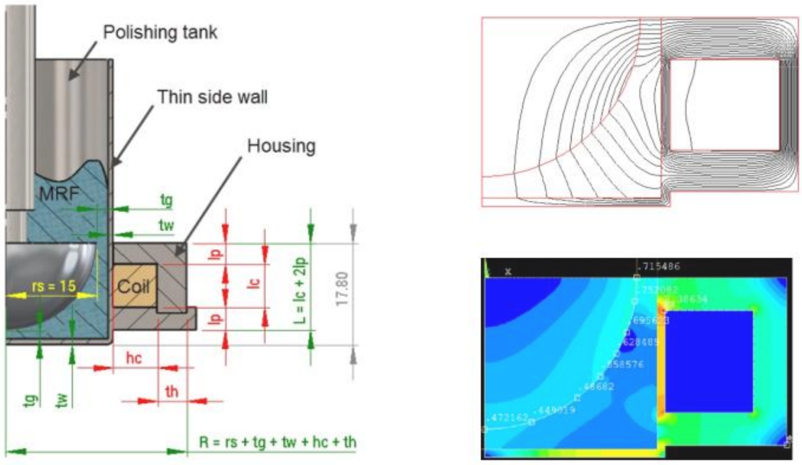

a. Simulation model b. Optimal results

Figure 2: Simulation results

In order to improve the MRF shear stress-based polishing performance, design of the magnetic field generation component (MFGC) of the MRP device should be optimized. The Multi-Objective Genetic Algorithm (MOGA) optimization method is employed for the MFGC optimization problem. As a results, the yield stress of the MFGC was significant improved with working gap of 2 mm.

4. EXPERIMENTAL RESULTS AND DISCUSSION

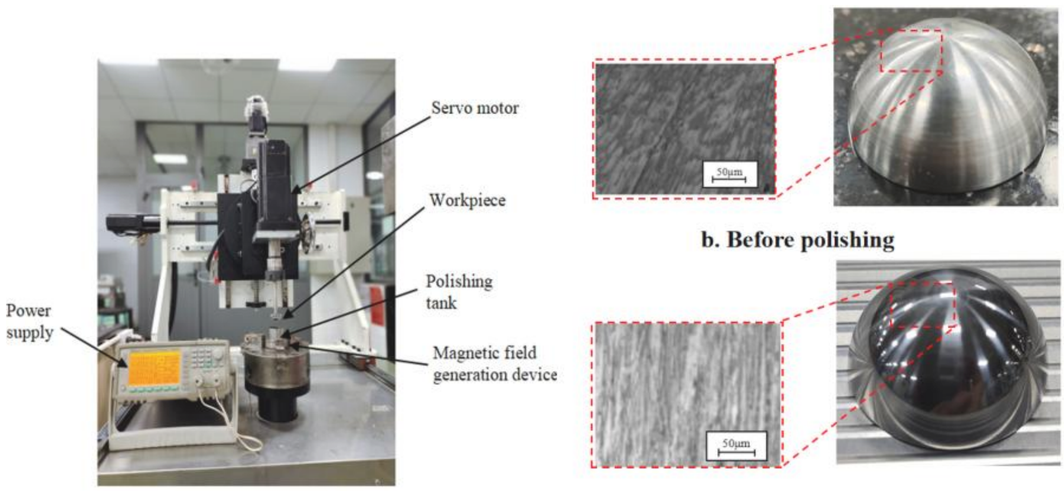

a. Experimental model **c. After polishing**

Figure 3: Experimental model and results

Based on optimal simulation results, an experimental model is proposed. Therefore, surface roughness (Ra) of workpiece was significantly reduced from 120nm to 22nm under suitable machining conditions.

5. CONCLUSIONS

- A simulation model was designed and optimized for working gap in MR polishing.
- The Ra was significantly reduced from 120nm to 22nm under optimal machining condition.
- This machining process can polish the complex surfaces with simple and high efficient.

REFERENCES

[1] Wegener K, Bleicher F, Krajnik P, Hoffmeister HW, Brecher C. Recent developments in grinding machines. CIRP Annals Manufacturing Technology. 2017; 66(2): 779-802.

[2] Nguyen DN, Chau NL, Dao TP, Chander P, Sunpreet S. Experimental study on polishing process of cylindrical roller bearings. Measurement and Control. 2019; 52(1): 1272-1281.

Experimental study of a magnetorheological torque limiter for dog type automated manual transmission

Félix Palardy[1], Tim Dumais[2], Marc Denninger[3], Guillaume Rochette-Marion[4] and Jean-Sébastien Plante[5]

[1,2,4,5] Faculty of Engineering, Université de Sherbrooke, Sherbrooke, Canada.

Felix.palardy@usherbrooke.ca, Tim.dumais@usherbrooke.ca, Guillaume.rochette-marion@usherbrooke.ca and Jean-sébastien.plante@usherbrooke.ca

[3] Exonetik, Sherbrooke, Canada (Marc.denninger@exonetik.com)

Short abstract: Automated manual transmissions (AMTs) are a cost-effective and energy efficient transmission option for small vehicles such as urban micro-cars. However, performing fast and smooth shifts with AMT's can be challenging when using conventional friction clutches. To overcome these challenges, this study presents an AMT concept featuring a programmable magnetorheological torque limiter managing the torque transferred to the wheels after each dog engagement. A fully functional prototype is built on an all-terrain vehicle (ATV) platform and open-loop torque-control strategies are tested to evaluate shift quality and comfort metrics. Experimental results highlight fast shift times averaging 24.5 ms (best of 9 ms) and high torque control responsiveness, showcasing the potential of MR technology for performant and responsive AMTs.

Keywords: Magnetorheological, Automated Manual Transmission (AMT), Shift quality, Dog clutch.

1. INTRODUCTION

Complex control and low responsiveness of conventional friction clutches found in AMTs frequently lead to poor shift quality [1]. A notable example from the automotive industry is the first generation Smart ForTwo AMT, frequently criticized by customers for "seriously not shifting properly". The integration of magnetorheological (MR) clutches in AMTs design could address these challenges since MR clutches are known for their superior torque controllability and fast responsiveness [2]. Although MR clutches seem to naturally fit in automotive powertrains, they have scarcely been investigated in the literature for such applications, and to the authors knowledge, have not been tested on road in an actual test vehicle. The closest reported work on MR clutches usage in powertrains explored their potential as manual transmission synchronizing clutches on a test bench [3]. The goal of this paper is to experimentally study the capability of a MR clutch coupled to a dog-shifted AMT to provide two fundamental requirements for successful AMTs, that is having: (1) low shift duration for best acceleration performance, and (2) high torque controllability to maximize comfort during shifts. A detailed prototype of an AMT-MR transmission is presented with emphasis on the MR clutch design and the high-speed shifting mechanism. The prototype is integrated into an instrumented and modified all-terrain vehicle (ATV) to explore the effects of different control strategies.

2. AMT-MR design

The AMT-MR prototype is composed of three major systems: (I) the MR clutch assembly, (II) the dog type multi-speed transmission and (III) the high-speed shifter mechanism. The powertrain schematic is presented at Figure 1a and its integration into a BRP Traxter 2001 ATV is shown in Figure 1b. Two 15 kW high-speed electric motors (1) deliver power to the MR clutch assembly (4) via a timing belt system (2-3). The MR clutch regulates torque transfer to the multi-speed Yamaha R1 2001 transmission (12), which then transmits torque to the rigid axle (6) and wheels (4) through a two-stage chain reduction (7-11).

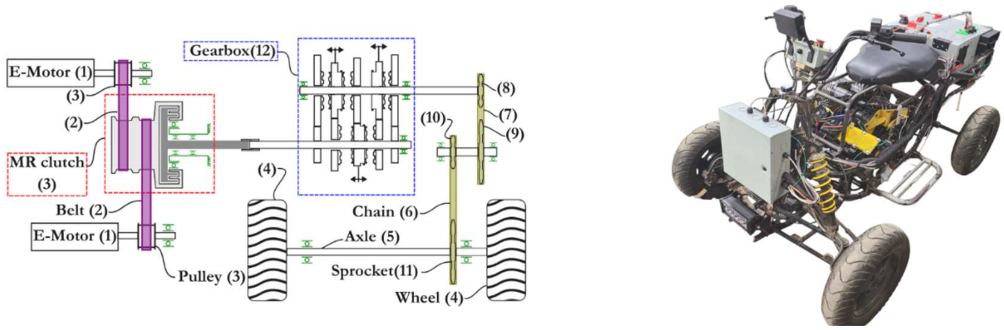

(a) (b)

Figure 1: AMT-MR powertrain schematic **(a)** and vehicle implemented **(b)**

3. METHODOLOGY

Three open-loop control strategies are implemented: (I) Ramp, (II) Step, and (III) Powershift. The Ramp and Step are comfort oriented modes where the control sequence involves a step-down setpoint of the desire MR clutch torque limit. The gearbox ratio is then shifted, and the torque is restored either gradually (Ramp) or instantly (Step) to its original setpoint after a specified period. The powershift strategy is a performance-oriented mode and differs from the Ramp and Step by keeping the clutch torque setpoint to a constant value during the entire shifting sequence and, shifting as fast as possible, without even interrupting the motor command. All tests are conducted on an asphalt drag strip with a randomly chosen sequence of control strategies, clutch torque limits and re-engagement durations to minimize risks of biasing errors. Vehicle sensors recorded shifter position, vehicle acceleration, MR clutch current, and shaft speeds. Data acquisition and control are managed using a LabJack-T7 and an ESP32. Time normalized version of the longitudinal acceleration VDV (VDV*) [4], 3Hz low pass filtered jerk of the longitudinal acceleration, and the vehicle's pitch angular acceleration (PAA) are used to quantified shift performance and comfort.

4. EXPERIMENTAL RESULTS AND ANALYSIS

Clutch re-engagement duration significantly impacts VDV* and PAA, revealing a trade-off between shifting duration and comfort. The MR clutch torque limit setpoint has greater influence during fast shifting sequence. Higher torque limits setpoint increase VDV* at low re-engagement durations, while angular acceleration peaks at both low and high torque limits, with lower values at a mid-range setpoint. Figures 2a and 2b respectively show the VDV* and PPA results.

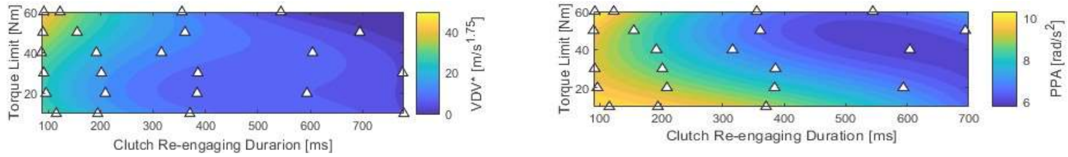

(a) (b)

Figure 2: Effect of torque setpoint and re-engaging time on **(a)** VDV* and **(b)** PPA

For power-shift sequences, a lower MR clutch setpoint reduces the filtered peak jerk across all tested shift sequence. The system shows an average shift time of 24.5 ms, with a fastest recorded shift duration of 9 ms, significantly surpassing the performance of the Graziano ISR transmission, which, at 50 ms, represents the shortest shift duration currently achievable by an AMT in a production car [5].

5. CONCLUSIONS

The extensive tests conducted on the AMT-MR prototype suggest the approach to have the potential for high shift quality by achieving fast shifts for performance and high torque controllability for comfort. Shifting comfort is subjective and complex. The aim of the work is limited to demonstrate feasibility using basic control schemes, not to optimize comfort. Future work should focus on understanding and optimizing the torque control logic of the clutch during shifting sequences.

ACKNOWLEDGEMENT

This research is supported by the Université de Sherbrooke and Exonetik inc.

REFERENCES

[1] Ahssan, M., Ektesabi, M., & Asghari Gorji, S. (2018). Electric vehicle with multi-speed transmission: A review on performances and complexities. *SAE International Journal of Alternative Powertrains, 7*.
[2] Chen, G., & Lou, Y. (2022). Recurrent-neural-network-based rate-dependent hysteresis modeling and feedforward torque control of the magnetorheological clutch. *IEEE/ASME Transactions on Mechatronics, 27*(5), 2875–2886.
[3] Hegger, C., & Maas, J. (2022). Automatic two-speed transmission based on a combined MRF coupling element. *IEEE/ASME Transactions on Mechatronics, 27*(5), 3019–3028.
[4] Walker, P., Fang, Y., & Zhang, N. (2017). Dynamics and control of clutchless automated manual transmissions for electric vehicles. *Journal of Vibration and Acoustics, 139*.
[5] Oerlikon Graziano and Vocis Driveline Controls develop step change in transmission technology for new Lamborghini flagship – Oerlikon Graziano. (n.d.). *Oerlikon*. Retrieved November 28, 2018

A novel gimbal magnetorheological semi-active inerter with self-powering capability.

Kim Thach Tran[1], Lei Deng[2] and Weihua Li[1]

[1]School of Mechanical, Mechatronics, Materials and Biomedical Engineering, University of Wollongong, 2522, NSW, Australia
(E-mail: ktt757@uowmail.edu.au, weihuali@uow.edu.au)
[2] School of Electrical, Computer and Telecommunication Engineering, University of Wollongong, 2522, NSW, Australia
(E-mail: leideng@uow.edu.au)

***Short abstract**: This study presents a novel gimbal magnetorheological semi-active inerter (GMRSI) with self-powering capability for 2-degree-of-freedom vibration control. The GMRSI-based building vibration control system was designed and equipped with a semi-active control strategy to minimise seismic vibration transmission from the ground to the top floor of a scaled building. Numerical simulations and experimental validation under harmonic and seismic excitation were conducted to evaluate the performance of the proposed system.*

***Keywords**:* Magnetorheological semi-active inerter, Self-Powering, Vibration Control.

1. INTRODUCTION

Earthquakes cause serious damage to civil structures, leading to loss of lives and properties. To protect buildings from catastrophic failures, vibration control strategies are employed. The mechanical inerter has emerged as a two-terminal device for vibration control, where the force applied between its terminals is proportional to their relative acceleration. This proportional relationship is governed by inertance, measured in kilograms [1]. While passive inerters feature fixed inertance, semi-active inerters incorporate mechanisms to dynamically control inertance [2]. Semi-active inerters are beneficial over passive inerter in vibration control applications due to its ability to broaden the effective frequency range of inerter-based vibration control systems. Compared to other semi-active components, such as springs and dampers, the application of semi-active inerters in vibration control remains underexplored [3,4].

This study introduces a gimbal magnetorheological semi-active inerter (GMRSI) with self-powering capability for vibration control in a scaled three-story building structure. The self-powering capability of the GMRSI is beneficial as it eliminates the need for an external power supply. This enhances the system's autonomy and reliability, especially during power outage or in remote applications. Firstly, the research includes the design and fabrication of the GMRSI and the scaled building model, providing the foundation for vibration control testing. Secondly, control algorithms are developed to achieve two primary objectives: minimising transmissibility to the top floor and enhancing self-powering capability through effective energy harvesting. Lastly, numerical simulations and experimental validation are conducted under harmonic and seismic excitation to evaluate the performance of the GMRSI.

2. DESIGN OF SEMI-ACTIVE INERTER SYSTEM

Figure 1(a) illustrates the CAD design of the GMRSI. The GMRSI features a gimbal structure composed of a "Yoke" and a "Joystick". The Yoke features a slotted arch and two coupling joints, which connects to the motor and flywheel through overdriving gearboxes. The Joystick has a T-shaped configuration, with bearings incorporated to allow sideways motion. A universal joint divides the longer section of the Joystick, facilitating integration with the scaled building structure via a linear bearing. The shorter section of the Joystick includes coupling joints to interface with the flywheel and motor through gearboxes.

The GMRSI operates by transmitting motion through its gimbal structure. When the bottom half of the Joystick's longer section rotates about the x-axis, the bearing allows free rotation around this axis, while the Yoke's constraints drive Flywheel 1 to create inertance and Motor 1 for energy harvesting. Similarly, rotation about the y-axis engages the Yoke's slot and the Joystick's bearings to drive Flywheel 2 and Motor 2. This dual-axis capability enables the GMRSI to generate inertance and harvest energy simultaneously in two degrees of freedom. The inertance is dynamically regulated by magnetorheological variable inertia flywheels (MRVIF) serving as Flywheels 1 and 2. These MRVIFs can adjust their net inertia by engaging or disengaging the outer casing from the inner casing using a magnetorheological (MR) clutch mechanism. Energy harvested from DC Motors 1 and 2 powers the MR clutches, ensuring self-sufficient operation.

Figure 1(b) presents the CAD model of the GMRSI-based building vibration control system, integrating the GMRSI with a scaled building structure designed following Mill's scaling laws [5]. The Joystick is connected to the ground floor plate via a linear bearing, while the scaled building structure and the GMRSI are mounted on a plywood ground plate. This ground plate is fixed on a 6-DOF vibration test platform capable of generating sinusoidal and seismic excitations along the x and y axes. These excitations induce motion of the ground floor plate, activating the GMRSI to mitigate vibrations and harvest energy in both axes. The semi-active control strategy implemented in the GMRSI is designed to minimise the transmissibility of ground excitations to the top floor, enhancing vibration control and energy efficiency.

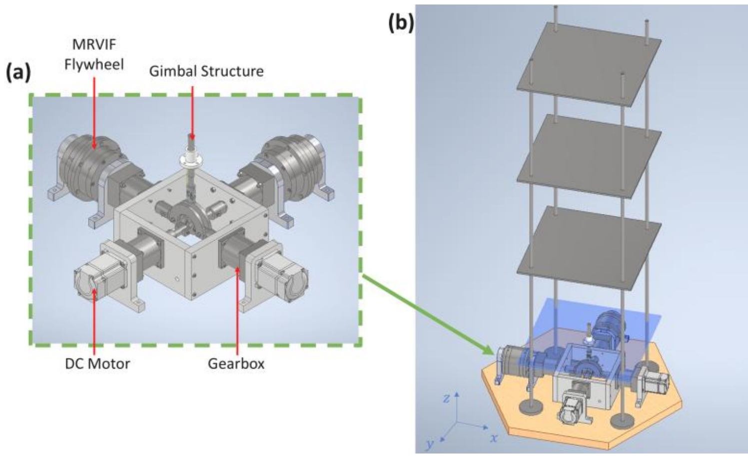

Figure 1. CAD model of: (a) The Gimbal Magnetorheological Semi-active Inerter (GMRSI); (b) The GMRSI-based building vibration control system.

3. METHODOLOGY

The prototype of the GMRSI was fabricated, and experimental testing was conducted under sinusoidal excitation to establish the mathematical relationship between the current supplied to the MRVIF and the inertance of the semi-active inerter. Subsequently, numerical simulations were carried out to calculate the top floor transmissibility under sinusoidal excitation with continuously varying inertance. These simulations identified the optimal inertance that minimises top floor transmissibility within the 0-10 Hz frequency range. Using this optimal inertance and the experimentally derived inertance-current relationship, a control strategy for the GMRSI's inertance was developed. The strategy uses the frequency of oscillation, calculated from the measured ground acceleration signal via Fast Fourier Transform, as the input. Concurrently, a control strategy for the energy harvesting system was devised to enable self-sufficiency. Finally, numerical simulations were conducted to evaluate the performance of the GMRSI-based structural vibration control system under sinusoidal and seismic excitations. The GMRSI-based building vibration control system prototype was then constructed and experimentally tested to validate its performance.

ACKNOWLEDGEMENT

The authors acknowledge the financial support provided by the Australian Government Research and Training Program (AGRTP) Scholarship, and the Australian Research Council (ARC) Discovery Project Grant (Number: DP240101050).

REFERENCES

[1] Smith, M. C. (2002). Synthesis of mechanical networks: the inerter. IEEE Transactions on automatic control, 47(10), 1648-1662.
[2] Chen, M. Z., Hu, Y., Li, C., & Chen, G. (2014). Semi-active suspension with semi-active inerter and semi-active damper. IFAC Proceedings Volumes, 47(3), 11225-11230.
[3] Jin, S., Chen, Z., Sun, S., Deng, L., Yang, J., Du, H., & Li, W. (2024). Development of a semi-active MR inerter for seismic protection of civil structures. Journal of Intelligent Material Systems and Structures, 35(15), 1231-1244.
[4] Tran, K. T., Jin, S., Deng, L., Du, H., Nguyen, H. Q., & Li, W. (2024). Semi-active inerters: a review of the literature. *Frontiers in Materials*, *11*, 1347060.
[5] Mills, R. S. (1979). *MODEL TESTS ON EARTHQUAKE SIMULATORS--DEVELOPMENT AND IMPLEMENTATION OF EXPERIMENTAL PROCEDURES*. Stanford University.

Seismic response control of a long-span cable-stayed bridge with spatially variable ground motion using MR-based semi-active systems

Zahrasadat Momeni [1] and Ashutosh Bagchi [2]

[1, 2] Department of Building, Civil and Environmental Engineering, Concordia University, Montreal, Canada
(E-mail: zahra.momeni24@yahoo.com, ashutosh.bagchi@concordia.ca)

Short abstract: Cable-stayed bridges are important lifeline structures that are very sensitive to vibration, and semi-active control systems could be very useful to ensure their high performance and adaptability. The present study takes a novel approach where an evolutionary algorithm named the nondominated sorting genetic algorithm (NSGA-II) has been used and further developed to create an optimal replicator dynamic controller for magnetorheological (MR) dampers to achieve an effective system for vibration control. The proposed methodology has been applied to a benchmark cable-stayed bridge and found to be very effective.

Keywords: Data-driven approach, Semi-active control, Game theory, Replicator dynamic, Optimization.

1. INTRODUCTION

Long-span cable-stayed bridges are slender structures with high flexibility and low structural damping, which make them vulnerable to vibration. Also, due to wide spacing of their supports, Spatially Varying Ground Motions (SVGM) during earthquakes are important to consider in the seismic analysis [2]. Magnetorheological (MR) dampers could be effective in reducing the dynamic response of cable-stayed bridges under non-uniform seismic loads [3]. Dyke et al. [3] proposed the use of a clipped-optimal algorithm to calculate the command voltage applied to magnetorheological (MR) dampers during earthquakes. To account for the nonlinear behaviour of MR dampers, researchers have recently developed intelligent controllers that rely on data-driven approaches with artificial intelligence and game theory. Soto et al. conducted comprehensive research on the vibration control of high-rise structures and highway bridges with MR dampers [5, 6]. They developed an innovative intelligent data-driven control algorithms based on agent technology and replicator dynamics concept of evolutionary game theory integrated with a multi-objective optimization algorithm, NSGA-I [7]. While the replicator dynamic controller has proven effective for controlling structures other than highway bridges and has been successfully used for high-rise building structures, its efficiency for cable-stayed bridges is yet to be determined.

2. OBJECTIVES

The aim here is to develop an optimal data-driven control technique that combines replicator dynamics from evolutionary game theory and a multi-objective optimization evolutionary algorithm to maximize control system performance by addressing multiple objectives. To achieve it, a replicator dynamics algorithm has been integrated with the Non-dominated Sorting Genetic Algorithm II (NSGA-II).

3. MATERIAL AND METHODOLOGY

An international ASCE benchmark for a controlled cable-stayed bridge is considered here as a case study. The overall view of the cable-stayed bridge is shown in Fig. 1. The bridge has a total length of 1205.8 m, is composed of two towers, 128 cables, and additional 12 piers on the approach bridge from the Illinois side. The main span is 350.6 m in length, the length of the side spans is 142.7 m each, and the approach on the Illinois side extends to 570 meters [1].

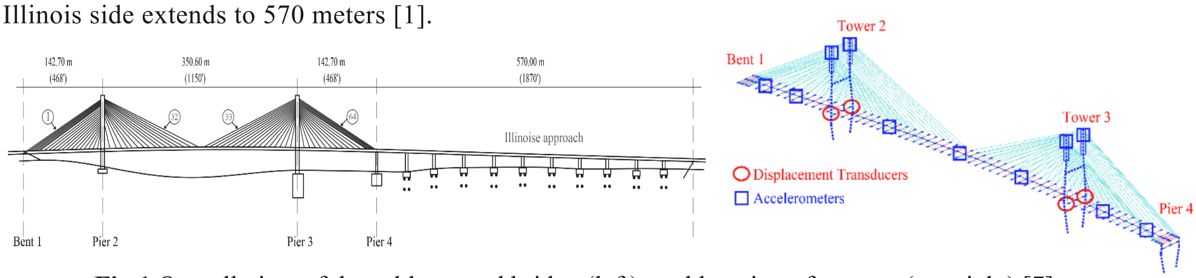

Fig.1. Overall view of the cable-stayed bridge (left); and location of sensors (top-right) [7]

Dampers are installed between the deck and the towers; eight between the deck and Pier 2, and another eight between the deck and Pier 3. In this case, Piers 2 and 3 are treated as towers. All dampers are oriented to provide forces in the longitudinal direction. The well-known modified Bouc–Wen model is employed to simulate the mechanical behavior of MR damper [8]. To compare the control performance of different available control systems, a total of 18 evaluation criteria (J_1 to J_{18}) provided in the benchmark problem [1] is considered here.

4. RESULTS AND DISCUSSION

Non-stationary ground motions, characterized by differences in time and amplitude, are considered here for SVGM analysis. The following ground motions have been used with time delays to the different supports: El Centro (1940), Mexico City (1985), and Gebze (1999).

Table 1: Comparison of evaluation criteria among different control strategies (for El Centro earthquake)

Evaluation criteria	Active control	Passive	PNS	Semi active MR-RC control
	[0,0.05, 0.16, 0.20] s at 15°C			
J_{1x} (shear at tower base X)	0.331	0.357	0.365	**0.222**
J_{1z} (shear at tower base Z)	1.022	1.023	1.020	**0.921**
J_{2x} (shear at deck level X)	0.810	0.988	0.976	**0.476**
J_{2z} (shear at deck level Z)	0.967	0.964	0.961	**0.864**
J_{3x} (moment at tower base X)	0.324	0.338	0.287	**0.135**
J_{3z} (moment at tower base Z)	1.097	1.091	1.094	**0.985**

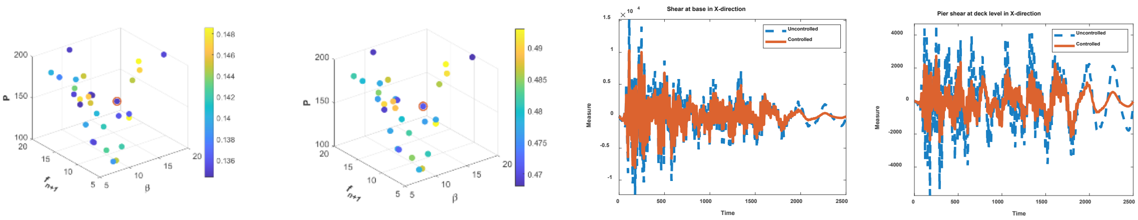

Fig.2. From left to right: 3D plot of the trade-off between dynamic parameters and performance criteria – the maximum shear at base ($J_{1\text{-}x}$) and the maximum pier shear at deck level ($J_{2\text{-}x}$); and the vibration responses.

5. CONCLUSIONS

Traditional structural control methods often consider a single performance criterion and overlook the potential conflicts between multiple objectives. To address this, a multi-objective approach that combines replicator dynamics with the Non-dominated Sorting Genetic Algorithm II (NSGA-II) was proposed here. For the selected case study, the proposed control system resulted in: (a) 46% reduction in deck displacement compared to passive control systems during the El Centro earthquake; (b) 33% reduction in shear forces at the tower base compared to active control systems during the same event; (c) significant reductions in peak shear forces and moments at critical sections in all cases; and (d) improved overall deck displacement under various seismic excitations.

REFERENCES

[1] Caicedo, J. M., Dyke, S.J., Moon, S. J., Bergman, L.A., Turan, G. and Hague, S. (2003), "Phase II benchmark control problem for seismic resp. of cable-stayed bridges." J. of Str. Contr. 10(3-4): 137-168.

[2] Hu, Z.L., Wei, B., He, X.H., Jiang, L.Z. and Li, S.S. (2022), "Effects of spatial variation of ground motion (SVGM) on seismic vulnerability of ultra-high tower and multi-tower cable-stayed bridges." J. of Earthquake Engineering 26(16): 8495-8524.

[3] Ze-bing, D.A.I., Huang, J., and Wang, H. (2004), "Semi-active control of a cable-stayed bridge under multiple-support excitations." J. of Zhejiang University-Science A 5: 317-325.

[4] Dyke, S. J., Spencer Jr, B. F., Sain, M. K. and Carlson, J. D. (1996), "Modeling and control of magnetorheological dampers for seismic response reduction." Smart mat. and str. 5(5): 565.

[5] Soto, M. G., and Adeli, H. (2018), "Vibration control of smart base-isolated irregular buildings using neural dynamic optimization model and replicator dynamics." Engineering Structures 156: 322-336.

[6] Hormozabad, S. J., and Soto, M.G. (2021), "Load balancing and neural dynamic model to optimize replicator dynamics controllers for vibration reduction of highway bridge structures." Engineering Applications of Artificial Intelligence 99: 104138.

[7] Momeni, Z. and Bagchi, A. (2023), "Intelligent Control Methodology for Smart Highway Bridge Structures Using Optimal Replicator Dynamic Controller." Civil Engineering Journal 9(1): 1-16.

[8] Jung, H., Spencer Jr, B.F. and Lee, I. (2003), "Control of seismically excited cable-stayed bridge employing magnetorheological fluid dampers." J. of Structural Engineering 129(7): 873-883.

Low temperature viscosity optimisation of automotive grade MRF

T. Featherstone, E. Mutter[2] and X. Peng[3]

[1, 2, 3] Authors' MagnetoRheological eXperience, Enabling Electrification, Infineum UK Ltd, United Kingdom
(E-mail: thomas.featherstone@Infineum.com, ellis.mutter@Infineum.com and xinyan.peng@infineum.com)

Short abstract: Magnetorheological devices are expected to operate across wide temperatures in automotive applications. As temperatures decrease the magnetorheological fluid viscosity will increase near-exponentially which will reduce the difference between on state and off state behaviour of the fluid, and in turn reduce the range of control possible for the MR device. This paper quantifies the low temperature viscosity and explores approaches to reducing low temperature viscosity

Keywords: Low temperature viscosity, additive

1. INTRODUCTION

MagnetoRheological Fluids (MRF) in their simplest definition are magnetically responsive particles suspended in a carrier fluid which can near-instantaneously [1] change from a fluid to a solid in the presence of a magnetic field. This behaviour is valuable in the transmission or absorption of force, such as in damping and isolation applications, or in torque transmission. In these applications it is preferable to have a large difference between the fluid behaviour in the absence of a magnetic field, and the solid behaviour in the on state as this enables device control over a wide range of conditions and inputs. The solid behaviour of a magnetorheological fluid is determined almost entirely by the volume fraction of magnetically responsive particles, and the strength of the magnetic field, while the factors influencing fluid behaviour in the absence of a magnetic field include, but are not limited to the amount and size of magnetically responsive particles, the type and quantity of supplemental chemical additives, the type and quality of the carrier fluid and, critically, the operating temperature.

A common commercial example of such a device using magnetorheological fluids is the automotive shock absorber [2]. Automotive applications have a wide temperature operating range, the lower limit of which is determined by the lowest plausible ambient temperature conditions and the upper of which is determined by highest plausible ambient temperature combined by heat from work done either by the component in question, or a neighbouring component which can result in device temperature excursions far greater than the ambient temperature alone.

MRF carrier fluids can be diverse, and span aqueous, hydrocarbon and silicone fluids, however all are characterised by having a liquid viscosity which is highly sensitive to temperature, demonstrating a negative, exponential relationship between temperature and viscosity [3]. A consequence of this temperature – viscosity relationship is that the off-state viscosity can drastically increase in low temperature conditions, while the on-state performance is broadly unchanged. This results in a narrower device control range. This paper describes the research and optimisation of magnetorheological fluids to improve fluid behaviour at low temperature.

2. OBJECTIVES

The objectives of this paper is to quantify the low temperature viscosity of ~25 % (v) iron magnetorheological fluids in the absence of a magnetic field, and improve on the state of the art by making changes to the carrier fluid and additive chemistry to enable wider device control ratios in low temperature conditions.

3. MATERIAL AND METHODOLOGY

A number of magnetorheological fluid formulations were tested with ~25 % (v) CIP concentration. These are fully formulated fluids containing thixotropic and performance additives in a hydrocarbon carrier fluid. The hydrocarbon carrier fluid, performance additives and thixotropic additive were modified in turn to quantify the impact on low temperature viscosity.

Low temperature viscosity measurements were taken on an Anton Paar MCR 302e equipped with a Peltier device and 50mm diameter plate on plate geometry

4. RESULTS AND DISCUSSION

Modification of the MRF carrier fluid from a 4 cSt to a 3 cSt fluid yielded an 18 % decrease in viscosity at – 40 deg. C. A further 30 % reduction was possibly with inclusion of supplemental low temperature flow additive chemistry taking the overall reduction in low temperature viscosity to 44 %.

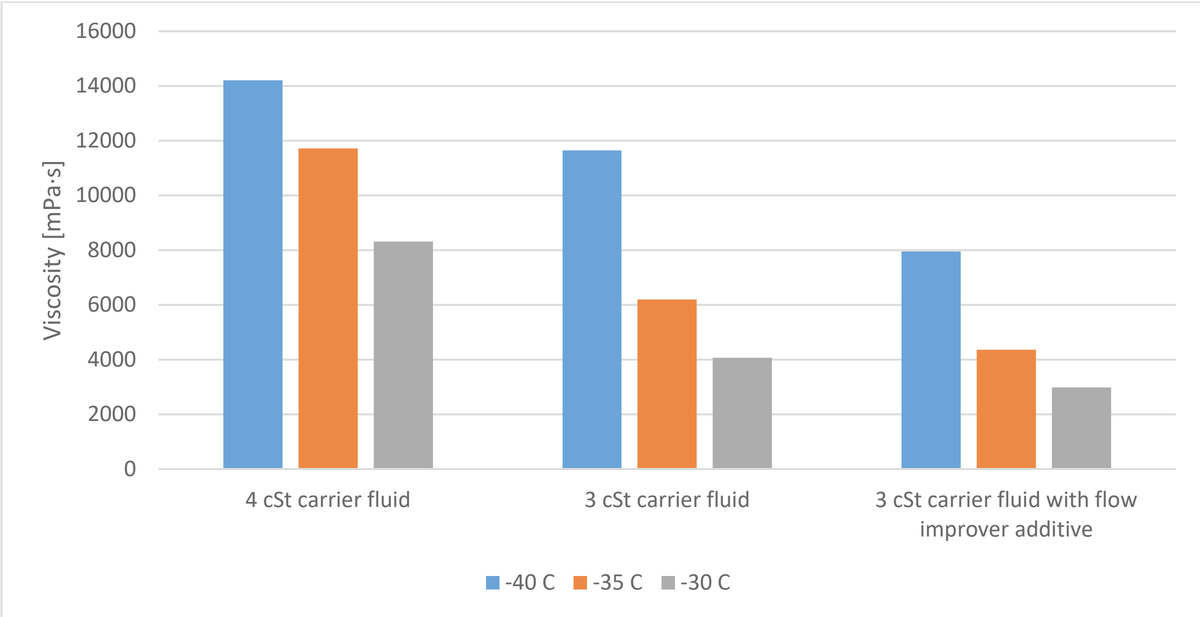

Figure 1: Low temperature viscosity measurements of baseline and optimised MRFs

5. CONCLUSIONS

It is obvious that a reduction in off-state viscosity of a magnetorheological fluid enables a wider device control ratio and as a consequence, many magnetorheological fluids use low viscosity, highly refined or synthetic hydrocarbon carrier fluids to minimise fluid viscosity. We can see from work here that there is significant further optimisation possible though selection and evaluation of suitable supplementary additive chemistry. These findings have important implications for commercial application in automotive and aeronautical where the ability to maintain performance in low temperature is a critical acceptance factor.

ACKNOWLEDGEMENT

This project is part of a broader range of commercial magnetorheological material development activity by Infineum.

REFERENCES

References have to be provided inside the full text as serial numbers within square brackets. They should be presented in the reference section in the serial order of appearance in APA format as shown below.

[1] Vicente, J, Klingenberg DJ, Hidalgo-Alverez R. Magnetorheological fluids: a review. Soft Matter, 2011, 7, 3701

[2] https://www.magneride.com/ accessed 2025/01/25

[3] Seeton, CJ. Viscosity–temperature correlation for liquids. Tribology Letters, 2006, 22, 67-78

[4] Wereley NM, Pang L, Kamath GM. Idealized hysteresis modeling of electrorheological and magnetorheological dampers. Journal of Intelligent Material Systems and Structures. 1998 Aug;9(8):642-9.

Development of a Constitutive Model for Characterizing Electrorheological Fluid Material under Large Amplitude Oscillatory Shear Strain

F. Mohammadi[1], R. Sedaghti[2]

[1, 2] Concordia University, Department of Mechanical and Industrial Engineering, Canada
(E-mail: farough.mohammadi@gmail.com, ramin.sedaghti@concordia.ca)

Short abstract: In this paper a constitutive model is presented for characterizing electrorheological fluid material under large amplitude oscillatory shear strain. Compared with the previously developed constitutive models, the present model provides more accurate predictions of dynamic mechanical properties for both small and large shear strain amplitudes in both time and frequency domains.

Keywords: Dynamic mechanical properties, ER fluids, Large strain amplitude, Constitutive model.

1. INTRODUCTION

Due to the ability of electrorheological (ER) and magnetorheological (MR) fluids to provide field-dependent rheological behaviour and reversible and rapid response, they have been used in many applications particularly in development of adaptive vibration absorption and isolation devices. For large amplitude oscillatory shear, dynamic properties of the ER fluid material not only depends on the electric field intensity (E) and frequency (ω), it also depends on the shear strain amplitude $\tilde{\gamma}$. The Fourier transformation technique is generally widely used method to quantify the behavior of viscoelastic material [1]. According to this method, the output stress response under the harmonic shear strain input can be written as:

$$\begin{aligned}\tau &= \tilde{\gamma}(G_1'(\omega,E,\tilde{\gamma})\sin(\omega t) + G_1''(\omega,E,\tilde{\gamma})\cos(\omega t)) \\ &+ \tilde{\gamma}\sum_{n=1}^{\infty}\left[G_{2n+1}'(\omega,E,\tilde{\gamma})\sin((2n+1)\omega t) + G_{2n+1}''(\omega,E,\tilde{\gamma})\cos((2n+1)\omega t)\right]\end{aligned} \tag{1}$$

Under small amplitude oscillation, G'_{2n+1} and G''_{2n+1} in Eq. (1) are negligible compared with their counterparts G'_1 and G''_1 which represent storage and loss moduli in linear viscoelastic region. The nonlinear behavior of ER and MR fluid materials were also previously investigated by other researchers. For instance, for a single field intensity and frequency, Laun et al. [2] applied the Bingham-Hooke model to describe the material properties of MR fluids in both linear and nonlinear regimes as:

$$\tau = \begin{cases} G_0(\gamma - \gamma_B) & |\tau| \le \tau_y \\ \mathrm{sign}(\gamma)\tau_y + \eta_B\dot{\gamma} - \lambda\dot{\tau} & |\tau| > \tau_y \end{cases} \tag{2}$$

where τ_y , G_0 , η_B, λ and γ_B represent yield stress, elastic modulus, Bingham viscosity, relaxation time and constant shear deformation, respectively. While the model provided reasonable accuracy for small amplitude motion, it deviated from the experimental data for large deformation [2]. In the present paper, the linear and nonlinear viscoelastic properties of an ER fluid material is investigated under small and large amplitude oscillatory shear strains for low to moderate excitation frequencies and different applied electric field intensities. A constitutive model is then formulated to predict the experimental data and extrapolate the mechanical behavior in regions hat cannot be measured due to test setup limitations.

2. PROPOSED CONSTITUTIVE MODEL

Building upon Eq (2), the following model is proposed for the stress response under the oscillatory shear strain to achieve more accuracy particularly in the nonlinear regime:

$$\tau = \begin{cases} \dfrac{\mu(\dot{\gamma} - \dot{\gamma}_R)}{\tilde{\dot{\gamma}}} + (K + \dfrac{D}{\tilde{\gamma}})(\gamma - \gamma_R) & \tau\dot{\gamma} > 0 \\ \tilde{\tau}\,\mathrm{sgn}(\tau) + G_0(\gamma - \tilde{\gamma}) + \eta\dot{\gamma} & \tau\dot{\gamma} \le 0 \end{cases} \tag{3}$$

in which η, μ, K, D and G_0 are frequency and field dependent characteristic parameters, $\tilde{\tau}$, $\tilde{\gamma}$ and $\tilde{\dot{\gamma}}$ are the shear stress, strain amplitudes and shear strain rate amplitude ($\tilde{\dot{\gamma}} = \omega\tilde{\gamma}$), respectively. The typical stress-shear strain rate hysteresis loop based on Eq. (3) is shown in Figure 1 for frequency of 0.1 Hz and electric field of 1.9 KV/mm. In the nonlinear regime ($\tau\dot{\gamma} > 0$), an amplitude-dependent relationship defines the shear stress response, governing the material's behaviour from the initial loading stage through unloading. Thus, the yielding stress is considered to be negligible. The model, however, can predict the transition between the linear and nonlinear regimes.

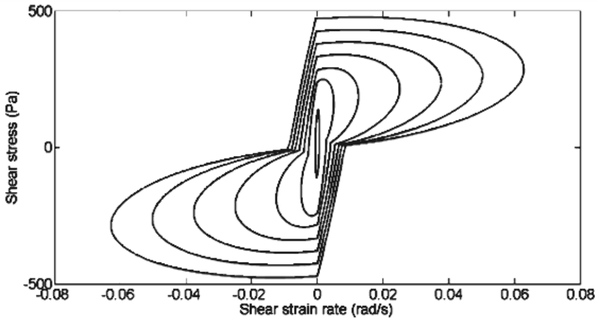

Figure 1: Typical hysteresis loop of the proposed model, f= 0.1 Hz, E=1.9 KV/mm for stress-strain rate.

Using the experimental data provided in Ref [3] for the ER fluid formulated by dispersing cornstarch in corn oil (40 mPa·s viscosity) with a particle weight fraction of 30%, the frequency and field dependent model parameters are identified using least square minimization technique.

3. RESULTS AND DISCUSSION

Sample results for loss and storage moduli vs shear strain amplitude and shear force vs time responses are shown in Figures 2 and 3. As it can be realized, results using presented predictive model is capable of capturing the dynamic properties of the ER fluid material resonably well in boh time and frequency domains at different electic filed filed intensities and shear starin amplitudes small and large strain amplitudes. Detailed discussion are available in Ref [3].

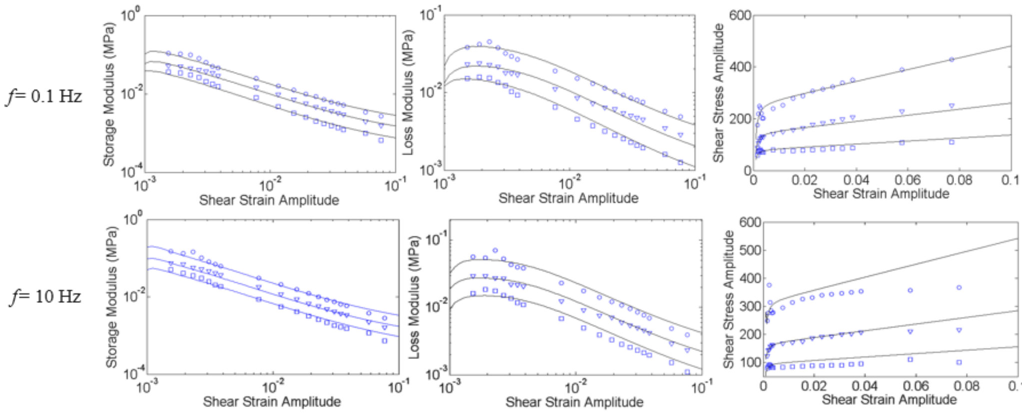

Figure 2. Complex modulus and shear stress of the ER fluid versus $\tilde{\gamma}$ for different electric field intensities and frequencies; Symbols represent the experimental results and the solid lines represent simulation results using the proposed model. □ E=0.7 KV/mm; ∇ E=1.3 KV/mm; ○ E=1.9 KV/mm.

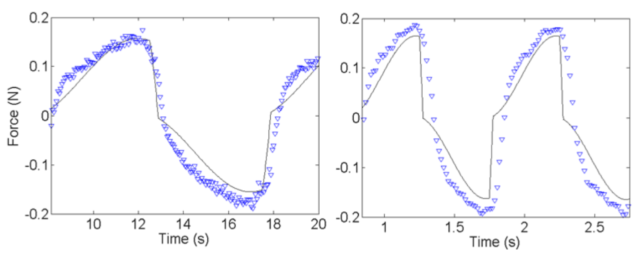

Figure 3: Time history of the shear force for $\tilde{\gamma} = 3.8462\%$ and E=1.3 KV/mm

5. CONCLUSIONS

The proposed constitutive model can be effectively used to predict linear and nonlinear viscoelastic properties of MR/ER fluids damper under large deformation.

REFERENCES

[1] M. Wilhelm, Fourier-transform rheology. Macromolecular Materials and Engineering, 2002; 287: 83–105.
[2] H. M. Laun, C. Gabriel, and C. Kieburg. Magnetorheological fluid in oscillatory shear and parameterization with regard to MR device properties. Journal of Intelligent Material Systems and Structures, 2010; 21:1479-1489.
[3] F. Mohammadi and R. Sedaghati, "Dynamic mechanical properties of an electrorheological fluid under large-amplitude oscillatory shear strain," Journal of Intelligent Material Systems and Structures, 2012; 23 (10): 1093–1105.

Theoretical and Experimental Study on the Influencing Factors of Yield Stress of MR Fluid under Squeeze-Shear Mode

Haopeng Li[1], Fei Chen[2] and Zuzhi Tian[3]

[1, 2, 3] School of Mechanical and Electrical Engineering, China University of Mining and Technology, Xuzhou, China
(E-mail: haopeng.li@cumt.edu.cn, xzcumtcf@126.con, tianzuzhi@cumt.edu.cn)

Short abstract: This study investigates the factors influencing the yield stress of magnetorheological (MR) fluids under squeeze-shear through theoretical modelling and experimental analysis, including squeeze stress, magnetic field strength, particle concentration and magnetic field intensity. In the squeeze-shear mode, the yield stress of the MR fluid increases with the increase in squeeze stress, magnetic field strength, and particle size, while it decreases with the rise in temperature.

***Keywords*:** MR fluid, yield stress, squeeze-shear mode, influencing factors.

1. INTRODUCTION

Magnetorheological (MR) fluids are widely used in intelligent drive equipment because of their controllable rheological reaction. Yield stress is one of the most important performance parameters of MR fluids, and its magnitude determines the performance of MR devices. There are three main working modes of MR Fluids: squeeze, shear and flow. The yield stress of MR fluids in a single mode is low, and it is found that the introduction of squeeze pressure can greatly increase the yield stress of MR fluids. However, the theoretical research on yield stress of magnetorheological fluids in squeeze-shear mode is insufficient, and there is a lack of instruments to measure yield stress of MR fluids in composite mode. This work aims to study the influencing factors of yield stress in MR fluids under squeeze-shear mode.

2. CALCULATION OF YIELD STRESS UNDER SQUEEZE-SHEAR MODE

The classical dipole method, finite element method, and magnetic energy analysis are used to analyse the interaction between particles in the squeeze-shear composite mode, and a fusion dipole model is proposed. A mathematical model of the magnetic energy density of the particle chain under the combined magnetic field and squeeze was established by analysing the characteristics of the particle chain (Figure1). By analysing the micro yield process of MR fluid, the yield stress of MR fluid in composite mode is calculated and then the constitutive model of MR fluid in composite mode is established (Equation 1).

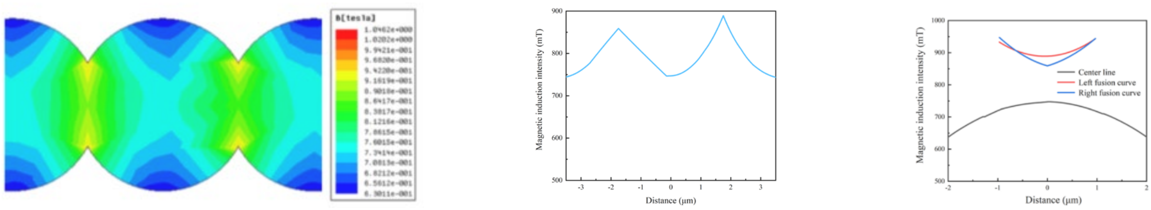

(a) magnetic field distribution (b) X-axis distribution (c) Y-axis distribution

Figure 1: Magnetic field distribution of particles

$$E_{\mathrm{u}} = \frac{E_{\mathrm{c}}}{L} = \frac{8N_{\mathrm{c}}\pi r^6 \mu_0 \chi^2 H^2}{9Ll^3}\left[C(1-3\cos^2\theta)\cos^3\theta\right]$$

$$\tau_u = \frac{\partial E_{\mathrm{u}}}{\partial \gamma} = \frac{\partial E_{\mathrm{u}}}{\partial(\tan\theta)} \qquad \tau_y = \sum_{i=1}^{P}\tau_u \qquad (P = \frac{\phi SL}{(4\pi R^3/3)N_{\mathrm{c}}S}) \tag{1}$$

3. MEASUREMENT OF YIELD STRESS UNDER SQUEEZE-SHEAR MODE

The structure of the measuring system is designed, and the mathematical expression of yield stress in the measuring system is derived. The magnetic circuit of the measuring system is simulated by Ansys Maxwell software, and the rationality of the magnetic circuit is verified. The accuracy and stability of the system are proved by experiments. The test system is shown in Figure 2.

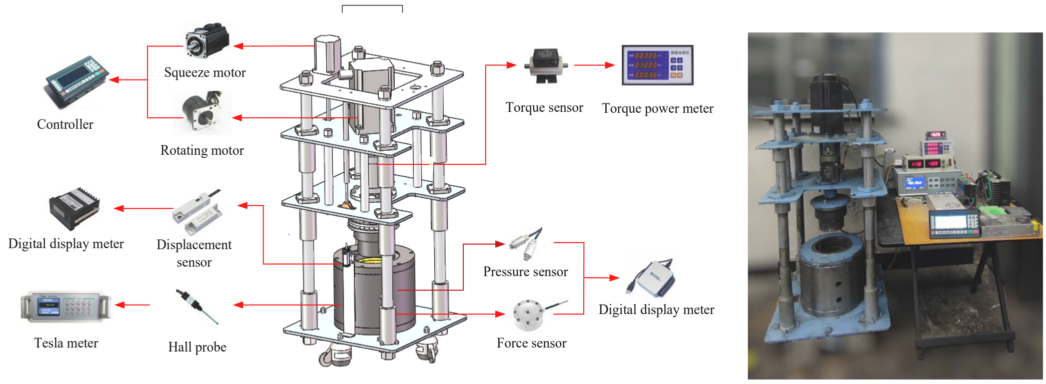

Figure 2: Yield stress measurement system under squeeze-shear composite mode

4. RESULTS AND DISCUSSION

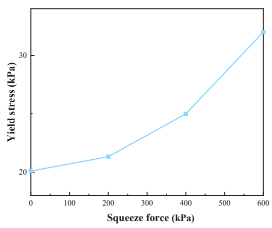

Figure 3: Yield stress under different squeeze stress

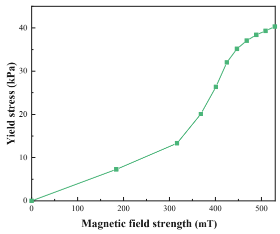

Figure 4: Yield stress under different magnetic field strengths

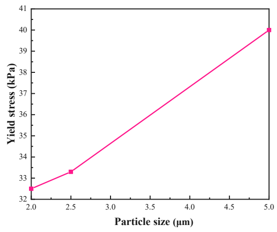

Figure 5: Yield stress under different particle size

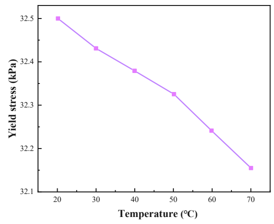

Figure 6: Yield stress at different temperatures

4.1.SQUEEZE STRESS

When the squeeze pressure is 600 kPa, the yield stress of the MR fluid is 1.5 times that of the yield stress without squeeze. As the squeeze stress increases, the increasing trend becomes more pronounced because with the increase in squeeze, the intermolecular forces and frictional forces between the particles rise .

4.2. MAGNETIC FIELD STRENGTH

The shear yield stress of MR fluid increases with the increase of magnetic field strength, but the increase speed slows down. This is because the magnetic interaction between particles becomes stronger with the increase of magnetic field strength. When the magnetic field strength reaches a certain level, the interaction between magnetic particles approaches saturation, which slows down the growth rate of yield stress.

4.3. PARTICLE SIZE

In the squeeze-shear mode, the yield stress of the MR fluid increases with the increase in particle size. This is because the surface area of the particles increases gradually with the radius, and the increased surface area will receive more electromagnetic force, which leading to more magnetic energy.

4.4. TEMPERATURE

With the increase in temperature, the yield stress of the MR fluid gradually decreases. However, the change in yield stress with temperature is relatively small. As the temperature rises, the magnetization intensity of the soft magnetic particles gradually decreases, which leads to a reduction in the yield stress.

5. CONCLUSIONS

In the squeeze-shear mode, the stress of the MR fluid increases with the increase in squeeze stresss, magnetic field, and particle size, while it decreases with the rise in temperature.

ACKNOWLEDGEMENT

This research was supported by the National Natural Science Foundation of China (52305078, 52375069)

Synthesis, Rheological Characterization, and Tunable Viscoelasticity of Magnetorheological Elastomers in Compression

Tongfei Tian[1], Philip Milosevski[1] and Masami Nakano[2]

[1]School of Science, Technology and Engineering, University of the Sunshine Coast
90 Sippy Downs Dr, Sippy Downs, Queensland, 4556, Australia
(E-mail: ttian@usc.edu.au, philipmilosevski15@gmail.com)
[2] SmartTECH Lab. Inc., Material Solutions Center, Tohoku University
2-1-1, Katahira, Aoba-ku, Sendai, Miyagi, 980-8577, Japan
(E-mail: mnakano@smarttech-lab.com)

Short abstract: Magnetorheological elastomers (MREs) are composite materials consisting of a silicone rubber matrix embedded with ferromagnetic microparticles, offering tunable viscoelastic properties under an applied magnetic field. This study synthesizes MREs with isotropic and two types of anisotropic particle orientations and evaluates their rheological properties using quasi-static compression and dynamic vibration tests. Results indicate that vertically aligned anisotropic MREs exhibit the most significant tunability in elastic modulus and damping properties. These findings highlight the potential of MREs for adaptive applications in vibration control, seismic isolation, and haptic feedback systems.
Keywords: magnetorheology, particle alignment, dynamic viscoelasticity, equivalent damping coefficient, hysteresis loop

1. INTRODUCTION

MREs are functional materials composed of a silicone rubber matrix with dispersed ferromagnetic microparticles [1,2]. These materials exhibit tunable viscoelastic properties under an applied magnetic field. By utilizing the variable viscoelasticity of MREs, various applications such as multi-layer MRE sheets for seismic isolation, MRE joints for rotating shaft bearings, and MRE mounts for vibration control have been developed [3-5]. Furthermore, MREs show potential applications in haptic feedback systems. This study aims to develop high-performance MREs and evaluate their variable viscoelastic properties to determine their suitability for such applications.

2. OBJECTIVES

- To synthesize MREs with enhanced tunable viscoelastic properties.
- To design and fabricate a testing system for evaluating MREs in compression mode.
- To analyze the impact of magnetic field strength on the elastic modulus of MREs.
- To explore the frequency dependence of the viscoelastic properties of MREs.

3. MATERIAL AND METHODOLOGY

3.1 Fabrication of MREs

MREs were fabricated using heat-curable silicone rubber (KE-1241, Shin-Etsu Chemical) as the matrix and carbonyl iron particles (CS, BASF) with an average particle size of 6 μm as the dispersed phase. The materials were mixed in a 30 wt% silicone rubber to 70 wt% carbonyl iron ratio, degassed, and poured into a brass mold (30 mm diameter, 10 mm depth). The elastomers were cured using a heat gun, producing disk-shaped samples of 30 mm in diameter and 10 mm in thickness. As shown in Figure 1, MREs with three different particle orientations types of were prepared: isotropic MREs, anisotropic MREs (Vertically Aligned), and anisotropic MREs (Horizontally Aligned).

3.2 Testing Methods

In Quasi-Static compression test, the near-static viscoelastic properties were evaluated. MREs were compressed to 10% strain at a slow, constant rate (10% strain/1 min) and then released back to 0% strain. The vertical stress σ versus strain ε hysteresis loop was recorded, and the elastic modulus was determined from the hysteresis slope during strain increase. In dynamic vibration test, sinusoidal displacement vibration tests were conducted at a fixed frequency (f = 1 Hz) with different strain amplitudes (1% to 5%). The stress-strain hysteresis loop was analyzed to determine the dynamic elastic modulus E_d and equivalent damping coefficient C_{eq}. In frequency-dependent dynamic tests, the frequency dependence of MREs was evaluated by varying the vibration frequency from 1 Hz to 20 Hz while measuring the strain-stress response. The impact of frequency on E_d and C_{eq} was investigated.

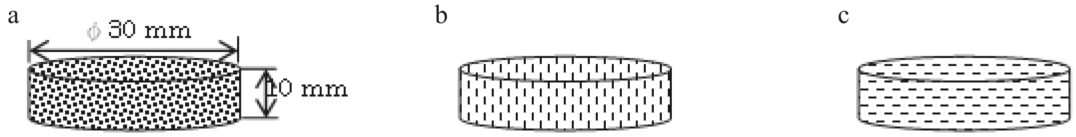

Figure 1: Different orientations of iron particles: a) isotropic; b) vertically anisotropic; c) horizontally anisotropic.

4. RESULTS AND DISCUSSION

In Quasi-Static compression tests, the stress-strain curve of isotropic MREs shifted upward with increasing magnetic field, but the elastic modulus showed minimal change. For vertically aligned anisotropic MREs, the elastic modulus significantly increased with the applied magnetic field, with a change of approximately 66% for B = 0.7 T. Horizontally aligned anisotropic MREs exhibited similar behavior to the isotropic samples, with minimal changes in stiffness. In the strain amplitude sweep tests, the dynamic elastic modulus, E_d, increased by approximately 2.4 times for vertically aligned anisotropic MREs at B = 0.7 T, particularly at a strain amplitude of 1%. The equivalent damping coefficient, C_{eq}, increased by about three times under the same conditions. In contrast, isotropic and horizontally aligned MREs exhibited only minor changes in stiffness and damping. In frequency dependence tests (f = 1-20 Hz), the results showed that E_d remained largely independent of vibration frequency, indicating that stiffness was primarily influenced by the applied magnetic field and strain amplitude. In contrast, C_{eq} decreased with increasing frequency, demonstrating that MREs exhibit non-viscous damping behavior. The hysteresis loop area remained nearly constant across frequencies, confirming that damping behavior is not velocity-dependent.

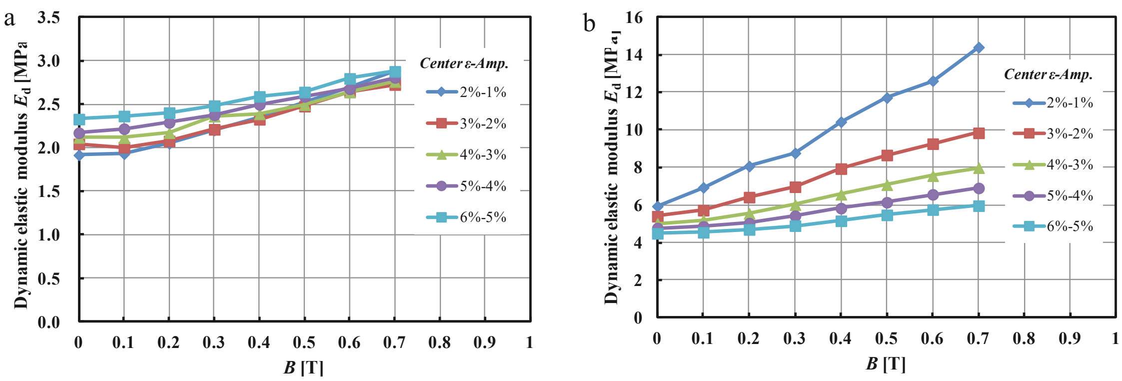

Figure 2: Dynamic elastic modulus under different magnetic flux densities: a) isotropic MRE; b) vertically aligned MRE

5. CONCLUSIONS

This study demonstrated that MREs with vertically aligned anisotropic particle structures exhibit the highest tunability in elastic modulus and damping properties under a magnetic field. The findings suggest that these materials are highly suitable for applications requiring variable stiffness and adaptive damping. However, the frequency-dependent analysis indicates that MREs are more effective for low-frequency damping applications rather than high-frequency vibration control.

REFERENCES

[1] Díez AG, Tubio CR, Etxebarria JG, Lanceros-Mendez S. Magnetorheological elastomer-based materials and devices: state of the art and future perspectives. Advanced Engineering Materials. 2021;23(6):2100240.
[2] Kang SS, Choi K, Nam JD, Choi HJ. Magnetorheological elastomers: fabrication, characteristics, and applications. Materials. 2020;13(20):4597.
[3] Wang Q, Shen Y, Peng L, Liu H, Hua D, Liu X. Preparation of high mechanical performance magnetorheological elastomer for engine mount. Smart Materials and Structures. 2025.
[4] Costi L, Georgopoulou A, Mondal S, Iida F, Clemens F. 3D printable self-sensing magnetorheological elastomer. Macromolecular Materials and Engineering. 2024;309:2300294.
[5] Stewart EM, Anand L. Magnetostriction of soft-magnetorheological elastomers. Journal of the Mechanics and Physics of Solids. 2025;194:105934.

On the fracture mechanism of magnetic microparticle structures in quasi-static shear

Dmitry Borin[1] and Stefan Odenbach[2]

[1, 2] Chair of Magnetofluiddynamics, Measuring and Automation Technology, TU Dresden, 01069 Dresden, Germany
(E-mail: dmitry.borin@tu-dresden.de, stefan.odenbach@tu-dresden.de)

Short abstract: The study is devoted to attempts to find experimental conditions in which a non-monotonic dependence of the shear stress on quasi-static shear strain is observed for a structured magnetorheological (MR) fluid of known composition. Such parameters as the concentration and size of magnetic particles, the size of the working gap between the rheometer static and shear plates, the strength of the external magnetic field, material and surface roughness of the plates are varied. Rheometric measurements are supported by the observation of the microstructure of the field structured low concentrated specimens using X-ray computed microtomography.
***Keywords*:** MR fluid, breaking, microstructure, quasi-static creep.

1. INTRODUCTION AND OBJECTIVES

Despite more than half a century of active research on magnetorheological (MR) fluids, there are still a number of important but unresolved aspects of the macroscopic response of these materials to external influences from a fundamental physics point of view. One of these is the clarification of the mechanism of fracture of the MR fluid structured in the magnetic field under shear stress. A number of theoretical models and computer simulations have been published on this subject, considering both aggregates of magnetic microparticles in the form of simple linear chains, cylinders or ellipsoids, and branched labyrinth structures [1-3]. The expected response under quasi-static shear of a structured MR fluid is a monotonic stress growth, the slope of which determines the regions of pre- and post-yield behaviour [2]. It has been reported that under certain conditions the models show a non-monotonic dependence of the shear stress on the macroscopic shear [1, 3]. As pointed out in [3], the state of the system with a decreasing dependence of stress on shear strain is mechanically absolutely unstable, since the smallest internal deformation fluctuations should grow rather than dissipate. Hence the difficulty in detecting such a state in experimental studies. In fact, almost all published experimental studies show a monotonic dependence of shear stress on strain/time. However, in some cases (see e.g. Fig. 3a in [4]) an overshoot can also be observed in the plots of the measured results presented, but has not been taken into account by the researchers. In this context, the present study is devoted to attempts to find experimental conditions under which a non-monotonic dependence of shear stress vs. quasi-static strain is observed for a structured MR fluid of the simplest possible and known composition. At the same time, since the conditions of interaction between the MR fluid and the working surfaces vary in the work, the study is also relevant to application-oriented aspects.

2. MATERIALS AND METHODOLOGY

In the above context, MR fluid made from silicon oil, BASF CC grade carbonyl iron powder and Sigma-Aldrich iron and magnetite powders was investigated. Parameters such as the concentration and size of the magnetic particles (~0.5-40 vol%, ~0.1-50μm), the size of the working gap between the static and rotating plates (0.1-1 mm) and the strength of the external magnetic field (flux density up to 500 mT) were varied. An Anton Paar Physica MCR 502 WESP rheometer equipped with an MRD cell was used. Both standard titanium plates and modified surfaces with different roughness and magnetic properties were used as measurement geometries. To evaluate a quasi-stationary shear deformation of the MR fluid, the sample was first structured, i.e. placed under the influence of a magnetic field for a certain time. The sample was then loaded with a slowly increasing strain from 0 to 300% and the corresponding shear stress was measured on the moving rotor.

In order to clarify and visualise the morphology of structures formed by magnetic particles of low concentration MR fluid, the silicone oil of the carrier medium was replaced by a two-component PDMS polymerised in a magnetic field in a configuration representing the working gap of the rheometer. Corresponding microstructural investigations were carried out using the laboratory X-ray microtomography setup, and the reconstruction process was performed using in-house developed software packages [5].

4. EXPERIMENTAL RESULTS

Quasi-static strain-stress curves obtained for the structured MR fluids are presented in Figures 1 and 2. When using magnetic PLA plates for low concentration samples (ϕ<3 vol.%) a non-monotonic shear stress change is observed. Under other conditions (MR fluid composition and plate material) a monotonic response is noticed. Microstructural observations show that samples with a concentration of ϕ<3 vol.% contain single chain-like aggregates rather than dense clusters, which are characteristic of samples with higher particle concentrations. However, for another type of rheometer plates, non-monotonic behavior is not observed as well for MR fluid with single chain-like aggregates. This suggests a different interaction of particle structures with different types of surfaces. Further results of the experimental analysis will be presented at the conference.

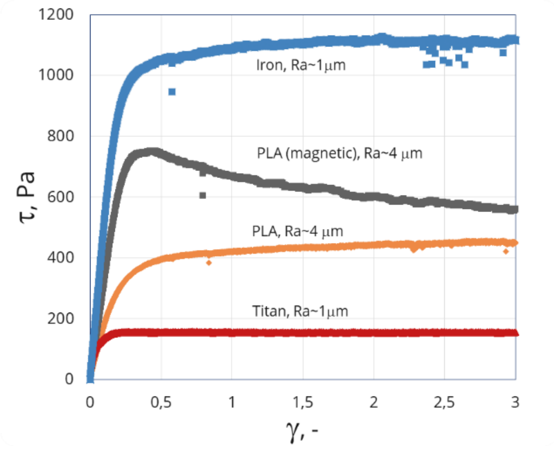

Figure 1: Quasi-static strain-stress curves obtained for the structured MR fluid with 1.5 vol.% particles using measuring geometry with different magnetic properties and surface roughness.

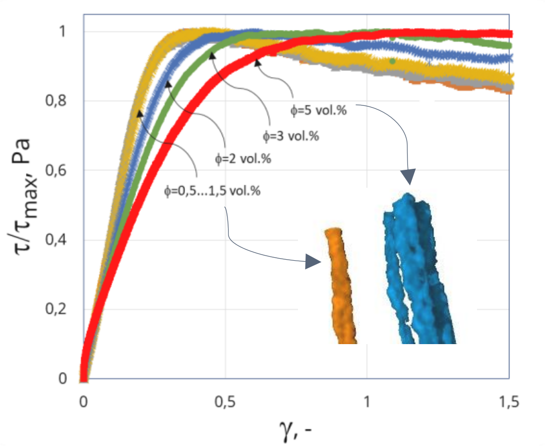

Figure 2: Normalized quasi-static strain-stress curves obtained for the structured MR fluid with different particle concentrations using a measuring geometry made of magnetic PLA. The inset shows the particle clusters at two different powder concentrations (structuring field is 250 mT).

5. SUMMARY

The response of a field-structured MR fluid to applied quasi-static shear differs for different measurement geometry surfaces used, for samples with different concentrations of magnetic particles and for different gap sizes between the plates of the measurement geometry. The experimental results indicate that the observed differences are related to different slip conditions of the particle structures under different settings rather than to different mechanisms of particle aggregate failure, although the morphology of the structures is an important aspect to consider in addition to the properties of the surface geometry. In addition to the fundamental importance, from an applied point of view, the results are essential for the choice of MR fluid and operating conditions for devices using magnetic control of the static yield stress. In particular, it is stated that the rheological characterisation of the MR fluid should use a measurement geometry with magnetic properties and roughness identical to the intended working surface of the MR device.

ACKNOWLEDGEMENT

The financial support by German Federal Ministry of Education and Research within the KMU-innovativ - collaborative project "COGNAC" under contract number 13GW0632D is gratefully acknowledged. The authors would like to thank Mr Y. Jiang for the preliminary measurements.

REFERENCES

[1] Bossis G. et al 1997, J. Rheol. 41, 68.
[2] Gandhi F., Bullough A. 2005, J. Int. Mat. Sys. Str. 16, 237.
[3] Zubarev A. et al 2020 Eur. Ph. J. ST 229, 2967–79.
[4] Li W.H, Zhang X.Z. 2008, Kr.-Astr. Rheol. J. 20, 45-50.
[5] Borin D., Odenbach S. in Magnetic Soft Matter, ed. J. de Vicente, The Royal Society of Chemistry, 2023, ch. 8, pp. 213-228.

Magneto-Rheology Helps Us to Cure Hypertension

Rongjia Tao

Department of Physics, Temple University, Philadelphia, PA 19122, USA
(E-mail: rtao@temple.edu)

Short abstract: Hypertension is a silent killer. Curing hypertension requires lowering blood viscosity and suppressing turbulence. Unfortunately, these tasks conflict with each other. A lower isotropic viscosity leads to higher Reynold number, worse turbulence. When a strong magnetic field is applied along patients' blood flow, red cells are polarized and aggregated into short chains. The blood viscosity becomes anisotropic, reduced significantly along the flow direction but increased substantially in perpendicular directions. Turbulence is suppressed; stable laminar blood flow lowers patients' blood pressure quickly and effectively. Our clinical trial has confirmed that this magnetorheological technology is safe and effective to cure hypertension.
***Keywords*:** Blood viscosity, turbulence, disturbed blood flow, magneto-rheology, hypertension.

1. INTRODUCTION

According to World Health Organization, hypertension is a major cause of premature death worldwide [1]. Sever hypertension comes with headaches, chest pain, shortness of breath, flushing, and visual changes etc. Left untreated, high blood pressure can lead to dangerous complications like heart attack or stroke. Despite medications and lifestyle changes, many hypertensive patients do not achieve adequate blood pressure control. As there are billions of people suffering hypertension, effective medical treatment to cure hypertension is always in high demand.

What causes hypertension? Hypertension patients are classified into two categories: primary and secondary hypertension. Secondary hypertension occurs quickly and can become severe as it is triggered by some other health conditions such as kidney disease, obstructive sleep apnoea, congenital heart defects etc. Primary hypertension, also called essential hypertension, is the one for most patients, developing over time with no identifiable health cause. However, from fluid dynamics, the cause of high blood pressure is high blood viscosity and turbulence in blood flow. While the health situation for hypertension patients may be different, all of them must have high blood viscosity and turbulent blood flow.

Unfortunately, these two tasks conflict with each other under conventional approaches. For example, when the blood viscosity is reduced and isotropic, the turbulent blood flow becomes worse because the Reynold number $R_e = \rho v D / \eta$ is increased. Presently neither medicine nor treatment is available to suppress turbulence in blood flow.

It is thus clear that unconventional scientific approach is critically needed. Here we report our new approach with magneto-rheology (MR) [2]. Instead of conventional viscosity reduction, we will make blood viscosity anisotropic: it is significantly reduced along the flow direction but substantially increased in the directions perpendicular to the flow. Hence, the blood flow becomes stable laminar, turbulence is suppressed, and the high blood pressure can be lowered effectively,

2. OBJECTIVES

Utilizing magneto-rheology (MR) to reduce patients' blood viscosity and suppress turbulence in their blood circulation as the treatment to cure their hypertension.

3. MATERIAL AND METHODOLOGY

In our new MR approach, a strong magnetic field is applied along the blood flow direction (Fig.1). The red blood cells are polarized by the magnetic field and aggregated into short chains parallel to the blood flow. The blood viscosity along the flow direction is thus significantly reduced, while the viscosity in the directions perpendicular to the blood flow is increased substantially, so that the turbulence is suppressed, and a steady laminar blood flow is achieved. With such anisotropic viscosity, the blood circulation is greatly improved and the workload for heart is reduced. Hence the blood pressure is lowered down to the normal range quickly. To implement such therapy, we invented a magnetic hematology device, which can apply a strong magnetic field along patients' blood flow direction to optimize blood flow and cure hypertension (Fig.2a).

Our clinical trials have 215 subjects in the second stage of hypertension participated in. Our magnetic hematology device has a bore of 10 cm diameter made to go through the frame and poles of the electromagnet. The device can have a stable magnetic field close to 1.0 T inside the bore along the bore's axis direction. The trial for each subject takes about 20-30 minutes. We measure the subject's blood pressure first. Afterwards, the subject places his/her right arm into the bore of the electromagnet for treatment while we monitor the blood pressure with the left arm. The magnetic treatment will last about 15 minutes. To see how long the effect lasts and check any side effect, we ask the subject to return and measure the blood pressure again 24 hours after the treatment

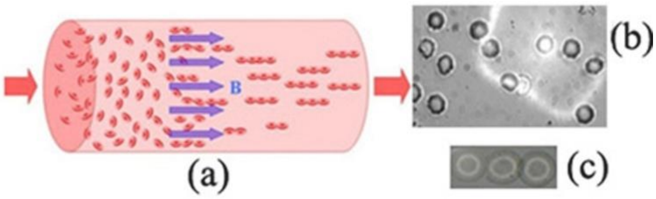

Fig.1. Magneto-rheology improves blood flow. (a) As the blood passes a strong magnetic field parallel to the flow, the red cells are aggregated into short chains along the flow direction. (b) Microscopic image showing that the red blood cells are randomly distributed in plasma before the magnetic field is applied. (c) Microscopic image of a short red-cell chain formed under 1.3T magnetic field.

4. RESULTS AND DISCUSSION

In Fig. 2b, a typical blood pressure reduction pattern under the magnetic treatment is plotted. The subject initially had blood pressure 150/88 mmHg. Within 11 minutes of magnetic treatment, his blood pressure was down to 111/70 mmHg; reduced 26% for systolic pressure and 21% for diastolic pressure. Next day, 24 hours after the treatment, he returned for the follow up, finding his blood pressure 129/78 mmHg, still 12-14% lower than the original blood pressure. There were no side effects. The subject told us that he enjoyed the therapy. All 215 tests are quite like this one. The MR technology is safe and effective for everyone. On average, in 15-20 minutes the therapy lowers the blood pressure by 21.4%, 24 hours after the treatment, the blood pressure is still 12.6% lower than the original one. Our placebo tests have also confirmed that without magnetic field, the blood pressure cannot be lowered. The effect is produced by improvement of blood flow with magnetic field. The MR treatment also improves blood oxygen function. We expect that this technology will effectively help people to cure hypertension, preventing cardiovascular diseases. The device is 100% safe and effective.

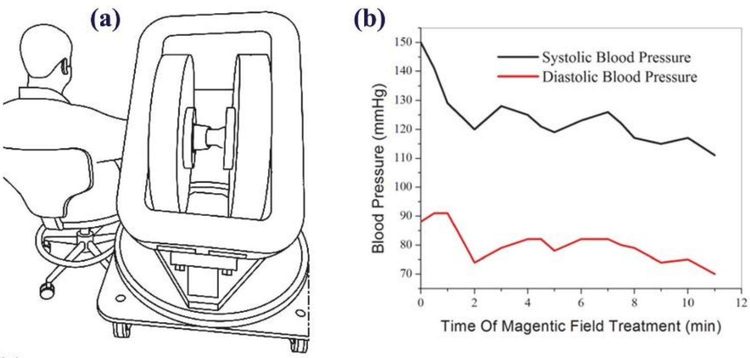

Fig.2 Clinical trial results. (a) The magnetic hematology device for clinical trials. (b) A typical blood pressure reduction under the magnetic field treatment.

5. CONCLUSIONS

The magneto-rheology and magnetic hematology device are safe and effective in lowering blood pressure for hypertension patients.

ACKNOWLEDGEMENT

The research was supported by American Heart Association and Temple University.

REFERENCES

[1] World Health Organization, “Global report on hypertension: the race against a silent killer”, ISBN: 978-92-4-008106-2. (9/19/2023).
[2] R. Tao, *et al.*, Systems and methods for reducing the viscosity of blood, suppressing turbulence in blood circulation, and curing rouleaux. US Patent 11,406,840, B2 (2022).

Intercomponent Synergetic Effect of Carbon-based Materials for Electro- and Magneto- Response

Ke Zhang*, Sai Chen, Tong Zhang

MIIT Key Laboratory of Critical Materials Technology for New Energy Conversion and Storage, School of Chemistry and Chemical Engineering, Harbin Institute of Technology, Harbin 150001, China
(E-mail: zhangke@hit.edu.cn)

Short abstract: In this context, we present the synthesis and investigation of a novel double-layered hollow nanoparticle, consisting of hollow carbon spheres coated with a titanium dioxide layer (HCs@TiO_2). The hollow carbon spheres serve as the "core", effectively reducing the overall density of the material and improving its sedimentation resistance. The amorphous TiO_2 shell was strategically designed to function as a vital buffer layer, thereby reducing leakage current density and increasing yield stress. Furthermore, we synthesized a core-shell structure of C@Fe_3O_4 composite particles with an urchin-like morphology, facilitating remarkable electrorheological (ER) and magnetorheological (MR) performance.

***Keywords*:** core-shell structure; electrorheological; magnetorheological; carbon material; smart material

1. INTRODUCTION

Electrorheological (ER) and magnetorheological (MR) materials are stimuli-responsive smart materials that have been used in various applications, including smart actuators[1], haptic devices[2], fluid transportation systems[3], and vibration isolators[4]. Due to the induced microstructural transitions[5], the shear stress, shear viscosity, and shear modulus of ER fluids (ERF) and MR fluids (MRF) can be reversibly altered in response to an electric field or magnetic field. However, ERF and MRF have recently encountered significant limitations due to their restricted stability and yield stress.

Carbon-based materials, known for their low density and remarkable chemical, thermal, and mechanical stability, have emerged as promising candidates for improving the performance of the ERF. Nonetheless, the intrinsic electron hopping motion inherent in carbon materials results in a significant leakage current density, which adversely affects the ER performance. This study prepared a hollow carbon spheres coated with a titanium dioxide layer (HCs@TiO_2), where the hollow carbon spheres serve as "core". The hollow structure effectively reduces the overall density of the ER material and improves its sedimentation resistance. The amorphous TiO_2 shell was strategically designed to function as a vital buffer layer, thereby contributing to a reduction in leakage current density and an increase in yield stress. Transmission electron microscopy (TEM) images indicate that both the thickness of the shell and the dimensions of the spheres can be adjusted. Additionally, dielectric and nuclear magnetic resonance (NMR) spectroscopy were employed to demonstrate that the TiO_2 shell not only restricts electron mobility but also significantly improves the wettability of silicone oil. Furthermore, core-shell-structured C@Fe_3O_4 composite particles with an urchin-like morphology were synthesized. This design enhances the interaction forces among the particles due to the presence of spiny structures. Consequently, the C@Fe_3O_4 suspension simultaneously facilitates impressive ER and MR response.

2. OBJECTIVES

A novel ER and MR material was designed and synthesized to simultaneously achieve elevated yield stress and extended lifetime by incorporating a heterostructure shell and a core-shell structure.

3. MATERIAL AND METHODOLOGY

First, polystyrene (PS) particles were synthesized to serve as sacrificial templates[6]. Subsequently, the obtained PS particles and dopamine were added to a Tris-HCl buffer solution. After stirring for 24 hours, the PS@PDA particles were formed. Following this, the hollow carbon particles (HCs) were synthesized through a high-temperature pyrolysis process of the PS@PDA particles. Finally, the prepared HCs were coated with a titanium dioxide shell (HCs@TiO_2) through the hydrolysis of tetrabutyl titanate[7].

4. RESULTS AND DISCUSSION

4.1. FIGURE AND FORMULA EXAMPLES

As shown in Figure 1, the maximum shear stress of the HCs@TiO_2 ERF reaches 7.8 kPa at an electric field strength of 3 kV/mm, which contains 15 wt.% of the ER material. This enhancement is attributed to improved polarization and additional electrostatic accumulation within the hybrid shells. Furthermore, the yield stress of this ERF is the highest reported to date among studies involving carbon -based materials.

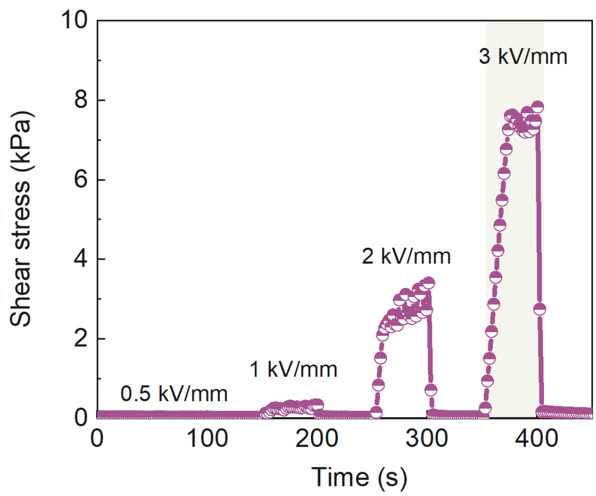

Figure 1: Shear stress vs time of HCs@TiO_2 ERFs.

5. CONCLUSIONS

Carbon nanomaterials-based composites with abundant morphology and excellent physicochemical properties have been reported as potential candidates for developing ER activity. Carbon shells, as derivatives, have been utilized to prepare electrorheological (ER) materials or to combine with magnetic substances for the creation of ER/magnetorheological (MR) bifunctional particles, due to their tunable surface properties.

ACKNOWLEDGEMENT

The work was financially supported by the Fujian Institute of Research on the Structure of Matter (Grant No. 20230008). The authors also acknowledge support from the Key Laboratory of Earthquake Engineering and Engineering Vibration, Institute of Engineering Mechanics, China Earthquake Administration (2023D16).

REFERENCES

[1] Chou P C, Lin F P, Hsu H L, Chang C J, Lu C H, Chen J K. (2020). Electrorheological sensor encapsulating microsphere media for plague diagnosis with rapid visualization. *ACS Sensors*, *5*(3): 665-673.

[2] Mazursky A, Koo J H, Yang T H. (2020). A compact and compliant electrorheological actuator for generating a wide range of haptic sensations. *Smart Materials and Structures*, *29*(5): 055028.

[3] Tao R, Tang H, Tawhid Al Islam K, Du E, Kim J. (2016). Electrorheology leads to healthier and tastier chocolate. *PNAS*, *113*(27): 7399-7402.

[4] Sun J, Zhang L, Hui X, Huang Y, Chen J, Hu C, Guo H, Qi S, Wang Z L. (2023). Self-powered in-phase sensing and regulating mechanical system enabled by nanogenerator and electrorheological fluid. *Advanced Functional Materials*, *33*(9): 2212248.

[5] Levine D J, Turner K T, Pikul J H. (2021). Materials with electroprogrammable stiffness. *Advanced Materials*, *33*(35): 2007952.

[6] Oh H G, Shin H, Jung H, Lee B H, Choe S. (2011). Control of molecular weight of polystyrene using the reverse iodine transfer polymerization (RITP)-Emulsion technique. *Journal of colloid and interface science*, *353*(2): 459-466.

[7] Yin J, Xia X, Xiang L, Zhao X. (2010) Coaxial cable-like polyaniline@titania nanofibers: facile synthesis and low power electrorheological fluid application. *Journal of Materials Chemistry*, *20*(34): 7096-7099.

Super Macroporous Hydrogel Foam with Rapid Electro-Response for Soft Actuators

Sara Badr[1,3], Vincent Lévesque[2] and Ali Ahmadi[1,3*]

[1] Department of Mechanical Engineering, École de technologie supérieure, Canada
(sara.badr.1@ens.etsmtl.ca, ali.ahmadi@etsmtl.ca)
[2] Department of Software and Information Technology Engineering, École de technologie supérieure, Canada
(vincent.levesque@etsmtl.ca)
[3] Biomaterials and BioFabrication Laboratory, University of Montreal Hospital Research Centre, Canada

***Short abstract*:** We present a super macroporous hydrogel foam actuator designed for rapid actuation. We investigate the effects of macroporosity on its physical, viscoelastic, and electroresponsive properties, achieving significantly faster response times compared to conventional hydrogels actuators.
***Keywords*:** *electroactive, porous, conductive, hydrogel, actuator*

1. INTRODUCTION

Soft actuators have emerged as promising alternatives to conventional rigid metallic electronics for bioelectronic and human-machine interfaces [1,3]. Stimuli-responsive hydrogels are promising candidates for actuators due to their biocompatibility, inherent softness, and responsiveness to various external stimuli. Among them, electro-responsive hydrogels have gained significant interest due to their controllable and remote actuation [1-3]. However, current hydrogel-based actuators suffer from slow response times (minutes to hours) due to diffusion-limited water transport within the hydrogel matrix [3]. Therefore, the development of a hydrogel-based actuator with rapid response times (~s) is required [2-4]. Herein, we propose a super macroporous (SMP) hydrogel foam actuator driven by electroosmosis, exhibiting significantly enhanced actuation speed.

2. OBJECTIVES

The main objective of this study is to develop an SMP hydrogel and investigate the effects of super macroporosity on actuation response, swelling, and viscoelastic properties.

3. MATERIAL AND METHODOLOGY

Acrylamide (AAm), 2-Acrylamido-2-methylpropanesulfonic acid (AMPS), N, N′-Methylenebis(acrylamide) (MBAA crosslinker), and photoinitiator (V50) were dissolved in Milli-Q water to prepare hydrogel precursors. Subsequently, the foaming agent, albumin, was added to the hydrogel precursor solution and vortexed at 3200 rpm for 120 seconds to form hydrogel precursor foams with final concentrations of 1, 2, 4, 8, and 16 $w \cdot v^{-1}$%. The hydrogel precursor foams were then injected into a mold (20×10×1 mm^3) and immediately exposed to ultraviolet light (395 nm, 90 s) to initiate free-radical photopolymerization (Fig. 1a). The hydrogel foam precursors were stained with Rhodamine B (1 µg/mL) to enhance visualization. Foam air bubbles were characterized using fluorescence imaging (Revolve), and their diameters were measured with Fiji. The porosity of the hydrogels was characterized by using scanning electron microscopy. Furthermore, the effects of super macropores on the hydrogel actuation response, swelling properties and viscoelastic properties were studied.

4. RESULTS AND DISCUSSION

The hydrogel foam actuator is highly porous (air bubble sizes ~100-300 µm), which was hypothesized to enhance actuation response times by facilitating ion mobility and diffusion. While bubble size was not affected by varying albumin concentration (Fig. 1b), it significantly influenced foam formation and phase separation. Low concentrations (<2 $w \cdot v^{-1}$%) were insufficient to fully foam the hydrogel precursor, whereas higher concentrations (8-16 $w \cdot v^{-1}$%) resulted in poor-quality foams with reduced stability. Therefore, albumin concentrations of 2 and 4 $w \cdot v^{-1}$% were selected for further studies. The SMP hydrogel foam actuator exhibited a threefold increase in bending rate ($\theta \cdot s^{-1}$) (Figs. 1c and d) and higher swelling properties (200%) (Fig. 1.e). Finally, inducing macropores resulted in a lower storage modulus, indicating reduced elastic stiffness, which further enhanced the bending deformation response (Fig. 1f).

5. CONCLUSIONS

The developed SMP hydrogel foams exhibit enhanced rapid response and, therefore, have the potential for use in advanced soft actuators, soft robotics, and human-machine interface applications.

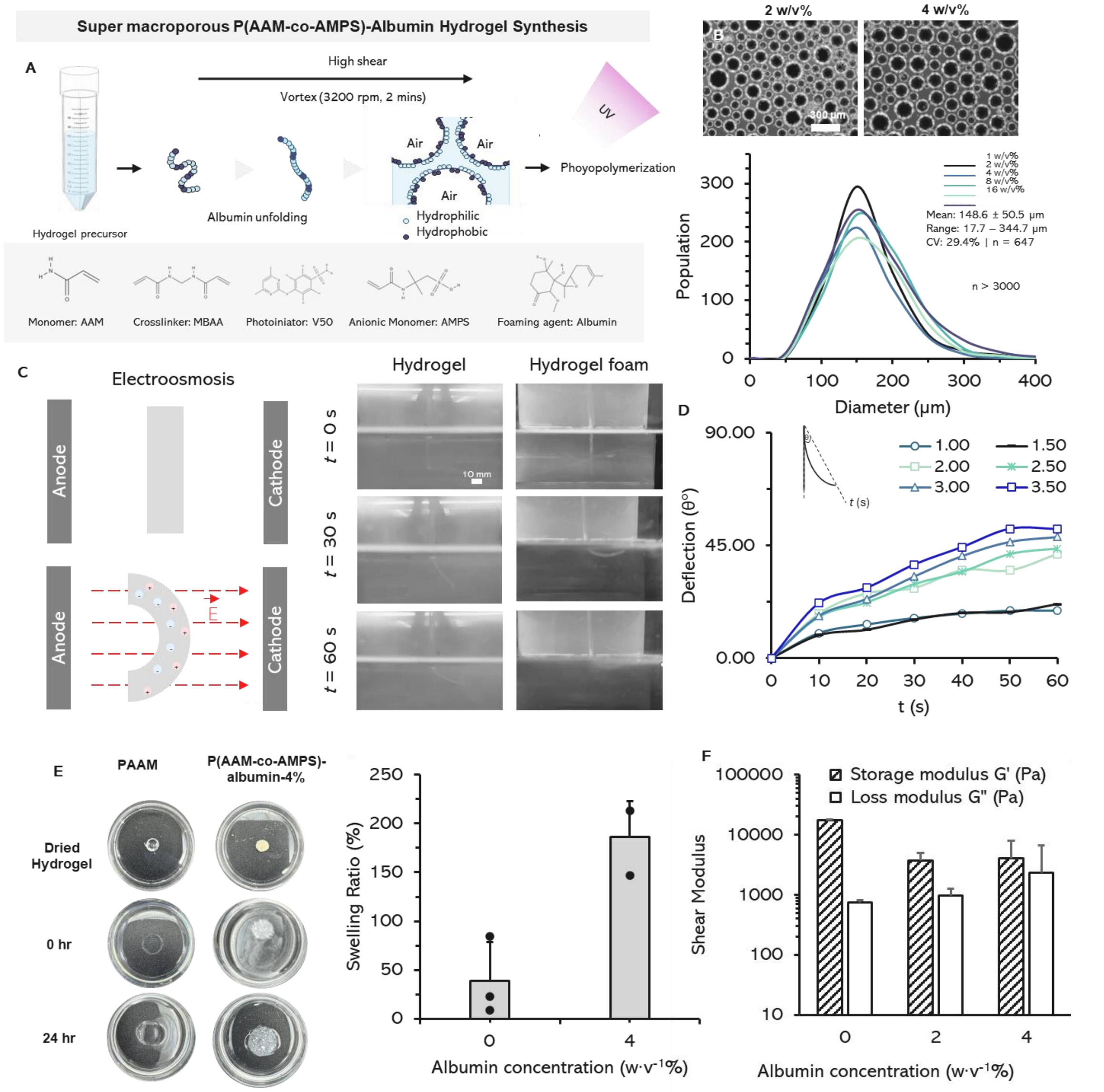

Figure 1: SMP foam hydrogel actuator. a) Hydrogel foam precursor preparation. b) Representative fluorescence images of hydrogel foam precursors with varying albumin concentrations (Scale bar represents 300 µm) and quantification of foam air bubble diameter distribution. c) Experimental set-up and hydrogel bending behavior experiments at 3.5 V/cm. d) The effects of electric fields on the bending behavior of hydrogel foam 4 w·v-1%. e) Swelling properties of hydrogel and hydrogel foam. f) The effect of foaming and various albumin concentrations on the shear moduli the hydrogels.

ACKNOWLEDGEMENT

This works was supported by Natural Sciences and Engineering Research Council of Canada (NSERC) and the Fonds de Recherche du Québec Nature et technologies (FRQNT).

REFERENCES

[1] Park J, Lee Y, Cho S, Choe A, Yeom J, Ro YG, Kim J, Kang DH, Lee S, Ko H. Soft Sensors and Actuators for Wearable Human–Machine Interfaces. Chemical Reviews. 2024 Feb 5;124(4):1464-534.

[2] Na H, Kang YW, Park CS, Jung S, Kim HY, Sun JY. Hydrogel-based strong and fast actuators by electroosmotic turgor pressure. Science. 2022 Apr 15;376(6590):301-7.

[3] Hu H, Li D, Salim T, Li Y, Cheng G, Lam YM, Ding J. Electrically driven hydrogel actuators: working principle, material design and applications. Journal of Materials Chemistry C. 2024;12(5):1565-82.

[4] Li CY, Zheng SY, Hao XP, Hong W, Zheng Q, Wu ZL. Spontaneous and rapid electro-actuated snapping of constrained polyelectrolyte hydrogels. Science Advances. 2022 Apr 13;8(15):eabm9608.

Development of a viscoelastic model for predicting the behavior of Hybrid Magnetorheological Elastomer-Fluids

Karl Adams-Gillstrom[1], Hossein Vatandoost*[2], Seyed Alireza Moezi[1], Ramin Sedaghati[1], Subhash Rakheja[1]

[1]Department of Mechanical, Industrial and Aerospace Engineering, Concordia University, Montreal, QC
(E-mail: karlag159@gmail.com, ramin.sedaghati@concordia.ca, seyedalireza.moezi@concordia.ca, subhash.rakheja@concordia.ca)
[2]National Research Council of Canada, Boucherville, QC, Canada
(E-mail: hossein.vatandoost@nrc-cnrc.gc.ca)

Abstract In the present study, a phenomenological based viscoelastic model has been formulated to predict the behavior of hybrid magneto-rheological (MR) elastomeric-fluid composites, namely MRF-MRE, in Cylinder and Cube shapes. For this purpose, the hybrid MREs, incorporating MR fluid within pure elastomeric matrices (MRF-Es) as well as within MRE matrices (MRF-MREs) were characterized under various loading conditions, including strain amplitudes (2.5–15%), frequencies (0.088–10Hz), and currents (0–8 A). The proposed viscoelastic model accurately predicts the field-dependent behavior of these hybrid MRF-Es, and MRF-MREs as function of applied current, loading frequency, and strain amplitude.

Keywords: Magnetorheological (MREs), Magnetorheological Fluids (MRFs), Viscoelastic Models, Characterization

1. INTRODUCTION

The development of a material model to predict the dynamic behavior of MR materials is of paramount importance for the development and design of MR-based adaptive systems, as well as for synthesizing control strategies. A field-dependent viscoelastic model based on the modified Kelvin-Voigt model has been developed to predict stress-strain response behaviour of the hybrid MREs. Under the harmonic strain excitation $\varepsilon(t) = \varepsilon_0 \sin(2\pi f t)$, the generated total stress based on the Kelvin-Voigt model consists of elastic and viscous parts $\sigma(t) = E'(f, I, \varepsilon_0)\, \varepsilon(t) + E''(f, I, \varepsilon_0)\, \dot{\varepsilon}(t)$. In contrast to conventional viscoelastic models based on excitation frequencies (f) [1, 2], storage modulus (E') and loss modulus (E'') are additionally functions of strain amplitude (ε_0) and applied current (I) as well. Based on the model found by Vatandoost et al. [3], and the observed experimental data from characterization, a phenomenologically based model is developed to reasonably predict the dynamic viscoelastic and hysteresis behaviour of the hybrid MREs with embedded MR fluid in compression mode while considering the variation in excitation frequency, strain amplitude, and applied current. The proposed phenomenological model to describe the elastic and loss moduli can be presented in Eqs. (1) and (2):

$$E'(f, I, \varepsilon_0) = (\beta_1' I^2 + \beta_2' I + \beta_3') \left(\frac{f}{f_0}\right)^b \varepsilon_0^{(\beta_4' I + \beta_5')} \tag{1}$$

$$E''(f, I, \varepsilon_0) = (\beta_1'' I^2 + \beta_2'' I + \beta_3'') \left(\frac{f}{f_0}\right)^{1+e} \left(e^{-\beta_4'' \varepsilon_0}\right) \tag{2}$$

2. OBJECTIVES

The main goal of this research is to develop a material model for predicting the field-dependent viscoelastic behaviour of various types of hybrid MREs, including MRF-MREs and MRF-Es, as well as MREs of different shape and shape factors, under a wide range of excitation frequencies, strain amplitudes, and applied magnetic fields.

3. METHODOLOG

The proposed phenomenological model consists of six constant parameters for the elastic modulus (β_1', β_2', β_3', b, β_4', β_5') and five constant parameters for the loss modulus (β_1'', β_2'', β_3'', e, β_4''). These parameters are subsequently identified through minimization of the merit functions J' and J'' to minimize the error between the predicted and the respective experimental measured moduli. The error minimization problem is solved using a combination of the genetic algorithm (GA) and the Sequential Quadratic Programming (SQP) technique. GA is first executed to obtain a solution near the global minimum. Using the solution from GA as the initial point, the SQP technique, which is a gradient based nonlinear optimization algorithm, is subsequently employed to accurately capture the precise global minimum solution. The above-mentioned methodology was performed for all different MR samples and corresponding coefficients were identified and tabulated.

4. RESULTS

Fig. 1 as an example compares the measured elastic modulus of Cube MRF-MRE data with the values predicted by the phenomenological model at a strain amplitude of 2.5% and frequencies of 1Hz and 10Hz across varying levels of applied current. Fig. 2 compares the measured and modelled stress-strain hysteresis characteristics of Cube MRF-MRE sample at a strain amplitude of 2.5% and current of 6 A for frequencies of 1Hz and 10Hz. Examination of the results in Fig. 1 and Fig. 2 show that the proposed model for elastic modulus can reasonably predict the variation of storage modulus with respect to the applied current and correctly represent the magnetic field stiffening effect. Furthermore, as the frequency increases, the elastic modulus increases, indicating the presence of a strain-rate stiffening effect also seen through the increase in slope in Fig. 2. Additionally, the impressive tunability of the MRF-MRE sample is demonstrated, where at a frequency of 10Hz, the elastic modulus increases from 0.3 MPa at 0 A to almost 1.73 MPa at 8 A, a relative increase of 475%. It should be noted that relatively similar predictions were also observed for MRF-E samples. Furthermore, the proposed model predicts the elastic modulus with an average error of less than 5% across all MR samples.

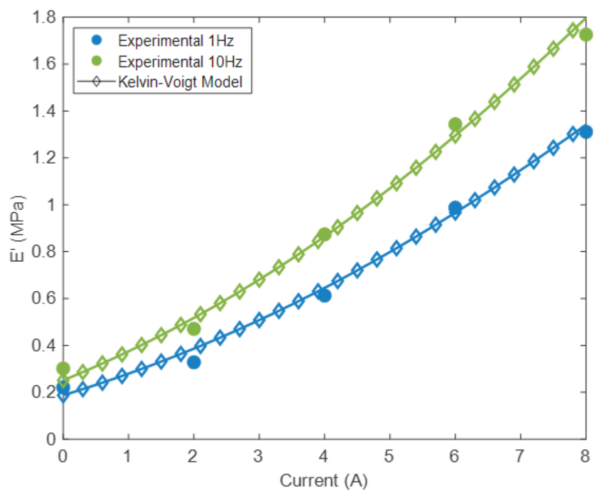

Figure 1: Effects of current on the elastic modulus at a strain amplitude of 2.5% and frequencies of a)1Hz and b)10Hz for the Cube MRF-MRE 30mm sample

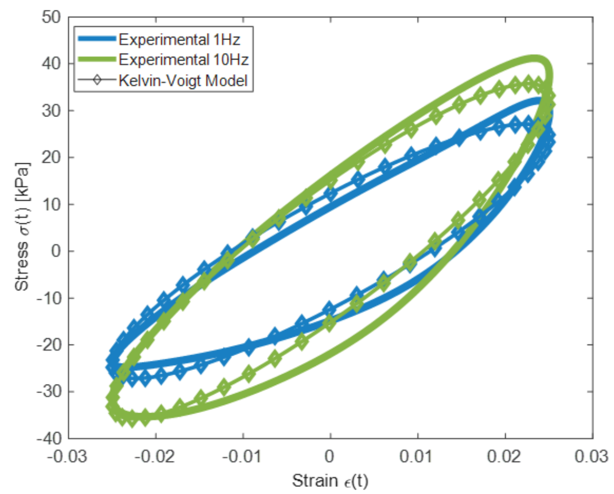

Figure 2: Experimental vs. Kelvin Voigt modelled stress-strain hysteresis at a strain amplitude of 2.5% and current of 6A for frequencies of a)1Hz and b) 10Hz for the Cube MRF-MRE sample

5. CONCLUSION

The results show that the proposed viscoelastic model can reasonably predict the dynamic properties of the MRF-E and MRF-MRE samples with minimal error. For future research, exploring the modeling of hybrid MRE samples in shear mode, as well as in combined shear and compression modes, remains largely unexplored and could offer valuable insights.

REFERENCES

[1] R. Ma, M. Ni, Q. Chen, Y. Zhou and J. Han, "Viscoelastic Fractional Model Based on Harmonic Excitation," *Mathematical Problems in Engineering,* vol. 2022, no. 1, 2022.

[2] T. Huu Ham, I. Petrikova and B. Marvalova, "Experimental Characterization and Viscoelastic Modeling of Isotropic and Anisotropic Magnetorheological Elastomers," *Polymer Testing,* vol. 81, 2020.

[3] H. Vatandoost, "Fabrication and Modeling of Magnetorheological Elastomer (MRE)," Shahrood University of Technology, 2015.

Soft MRE Gripper: Preliminary Study

D. Gutenko[1], J. Gołdasz[2], B. Sapiński[1] and P. Orkisz[1]

[1] Chair of Process Control, AGH University of Kraków, Poland
(E-mail: denys.gutenko@doktorant.pk.edu.pl, deep@agh.edu.pl, orkisz@pk.edu.pl)
[3] Chair of Automation and Information Technology, Cracow University of Technology, Poland
(E-mail: janusz.goldasz@pk.edu.pl)

Short abstract: Recently, soft flexible robotic grippers have attracted research and engineering interest. Such gripper can be used for tasks which are beyond the reach of conventional rigid body ones. A variety of materials and actuation technologies incl. magnetorheological (MR) materials have been used for developing grippers for grasping and object manipulation purposes. The study explores the development of using a magnetorheological elastomer based gripper that is capable of adapting to a variety of objects shapes. In the study the authors reveal the gripper's operating principle, the actuation mechanism and the results of a testing programme to examine the soft gripper's performance with respect to loads and shapes.
Keywords: *magnetorheological elastomer, gripper, soft, robotic*.

1. INTRODUCTION

To begin with, robotic end-effectors provide robots with the capability to interact with the environment. They give robots particular functions without which they would be useless in the industrial environment. End-effectors are referred to as End-Of-Arm-Tooling (EOAT). Various types of robotic end effectors include tools, magnets, clamps, grippes and the like. Grippers have given robots the abilities similar to human hands. In general, grippers are used in applications that require, e.g. lifting, touching, manipulating, grabbing, etc. Material handling, assembly, component transfer, loading, etc. can be managed by means of capable (pneumatic, mechanical, hydraulic, electrical, magnetic) robotic grippers. Therefore, a soft gripper whose actions are driven by applying magnetic fields of sufficient strength ot it belongs to a category of specific EOATs. In comparison with conventional rigid grippers, the soft grippers allow to reduce the robotic system's complexity, minimize the risk of damaging the objects, are capable of accommodating a variety of shapes while maintaining the same level of control as the rigid ones [1-3].

Thus, the purpose of the work undertaken by the authors was to examine the possibility of manufacturing a low-cost soft soft MRE gripper that can be used for a variety of tasks. The authors reveals the gripper's underlying concept, the prototype, and demonstrate the gripper's basic operating principles.

2. RESULTS

Briefly, the authors developed a soft MRE based gripper that can be used for handling objects with irregular shapes.

a) b)

Figure 1: Soft MRE gripper: a) undeformed, b) deformed

The MRE composite material was manufactured in-house using the silicone elastomer (Ecoflex Gel) that was mixed with carbonyl iron powder (CIP) particles with an average particle size of 3 μm, stirred and poured into the 3D-printed mould. The prepared material sample was then cured for 12 h hours. The design of the gripper is based on the idea of a hexagon-shaped MRE shell that gets deformed in the presence of magnetic field. The shape of the shell with the solenoid is illustrated in Fig. 1a. In the absence of magnetic field the opening at the top of the shell is at its maximum aperture. The solenoid when activated induces magnetic flux in the solenoid-shell structure that produces a force acting on the MRE material pulling it towards the core surface of the solenoid. At the same time, as the material gets deformed, the shell opening cross-section area is significantly reduced – see Fig. 1b. The solenoid is cylindrical – 100 mm in dia., core diameter – 40 mm, no. of wire turns – 500. The pulling current was found to be 3 A (or 1500 AT). The current level is sufficient to ensure the gripper is operated in a reversible and repeatable manner. Moreover, a rig was prepared for testing the gripper's ability to handle various loads and objects.

3. CONCLUSIONS

The purpose of this study was to examine the possibility of manufacturing a low-cost soft soft MRE gripper that can be used for a variety of tasks and load handling. The gripper was manufactured out of a MRE material (based on the mixture of silicon gel and CIP particles). The prototyped device was found to operate in a reversible and repeatable manner, thus confirming the initial concept.

REFERENCES

[1] Xu, Meng, et al. Review of Flexible Robotic Grippers, with a Focus on Grippers Based on Magnetorheological Materials. Materials. 2024, 17.19: 4858.
[2] Choi, Dong-Soo, et al. Beyond human hand: shape-adaptive and reversible magnetorheological elastomer-based robot gripper skin. ACS Applied Materials & Interfaces. 2020, 12.39: 44147-44155.
[3] Chung, Hyun-Joong, Andrew M. Parsons, and Lelin Zheng. Magnetically controlled soft robotics utilizing elastomers and gels in actuation: A review. Advanced Intelligent Systems. 2021, 3.3: 2000186.

Composition of Electrolytic Iron Particle for Performance Improvement of Magnetorheological Grease

Nur Adilah Adanan[1], Abdul Yasser Abd Fatah[1], Saiful Amri Mazlan[2,3], Nur Azmah Nordin[2,3], Mohd Aidy Faizal Johari[2,3], Ramesh V Upadhyay[4]

[1] Faculty of Artificial Intelligence (FAI), Universiti Teknologi Malaysia, Jalan Sultan Yahya Petra, 54100, Kuala Lumpur, Malaysia.
(E-mail: yasser.kl@utm.my, adilah00@graduate.utm.my)
[2] Engineering Materials and Structures (eMast) iKohza, Malaysia-Japan International Institute of Technology (MJIIT), Universiti Teknologi Malaysia, Jalan Sultan Yahya Petra, 54100, Kuala Lumpur, Malaysia.
(E-mail: amri.kl@utm.my, nurazmah.nordin@utm.my, ma.faizal@utm.my)
[3]Automotive Development Centre, Institute for Sustainable Transport (IST), Universiti Teknologi Malaysia, 81310 Skudai, Johor, Malaysia.
(E-mail: amri.kl@utm.my, nurazmah.nordin@utm.my, ma.faizal@utm.my)
[4]K.C. Patel Research and Development Centre, Charotar University of Science and Technology, Charusat Campus, Changa 388421, Gujarat, India.
(E-mail: rvu.as@charusat.ac.in)

Short abstract: Magnetorheological grease (MRG) is a smart material that exhibits tuneable rheological properties in response to magnetic fields. However, its high initial viscosity can limit performance. This study investigates MRG formulated with irregular flake-shaped electrolytic iron particles (EIP) to enhance its properties. MRG samples with 30-70 wt.% EIP were tested under varying magnetic fields. Results show that rheological properties depend on EIP concentration, with MRG containing 70 wt.% EIP exhibiting a greater magnetoviscous effect and storage modulus than MRG with 70 wt.% carbonyl iron particles. This suggests that EIP can improve MRG efficiency, making it suitable for potential applications such as seismic damper, brakes, and clutches.
Keywords: electrolytic iron particle; magnetorheological grease; magnetoviscous effect; viscosity, storage modulus

1. INTRODUCTION

MRG was first discovered by Rankin et al. in 1999 [1] by introducing grease as the viscoplastic medium in MRF to overcome sedimentation issue of MRF. It consists of magnetic particles dispersed in a carrier grease, which serves as a thixotropic medium to suspend the magnetic particles. The main drawback of MRG is its high initial viscosity [2] which reduces the storage modulus on the performance of material, leading to inefficiency of the devices during operation. The rheological properties of magnetorheological grease (MRG), including viscosity and storage modulus can be improved by optimizing the composition of magnetic particles. Therefore, in this study, a new MRG was made featuring irregular flake-shaped electrolytic iron particles (EIP) to study the effects of EIP composition in improving the performance of MRG.

2. OBJECTIVES

This study explores how the incorporation of irregular flake shaped EIP affects the rheological behavior of MRG, focusing on viscosity and viscoelastic properties. The overarching goal is to optimize EIP composition to achieve MRG with superior magnetorheological performance.

3. MATERIAL AND METHODOLOGY

A series of MRG with different ratios, varying from 30 to 70 wt.% were prepared in order to examine the behaviour of varied composition of magnetic particles on rheological properties. Irregular shape of EIP purchased from Industrial Metal Powder (India) and grease (NPC Highrex HD-3 Grease, Nippon Koyu Ltd., Japan) as medium were used to fabricate MRG using a high-speed mechanical stirrer (HS-30 D, DAIHAN Scientific Co., Ltd.). In order to fabricate the MRG, 30 wt.% of grease is stirred for 5 minutes to loosen the internal structures of the base grease. Then, different ratios of EIP were added into the stirred grease and continuously stirred with mechanical mixing stirrer at 300 rpm for 2 hours to ensure homogenous distribution of MRG. It is remarked that all the samples preparation conducted in this study was carried out at room temperature. The summary of the fabricated samples in this study as tabulated in Table 1.

Table 1: Compositions of MRG samples

Samples	% by weight of EIP	% by weight of grease
MRG-E 30	30	70
MRG -E 50	50	50
MRG -E 70	70	30

4. RESULTS AND DISCUSSION

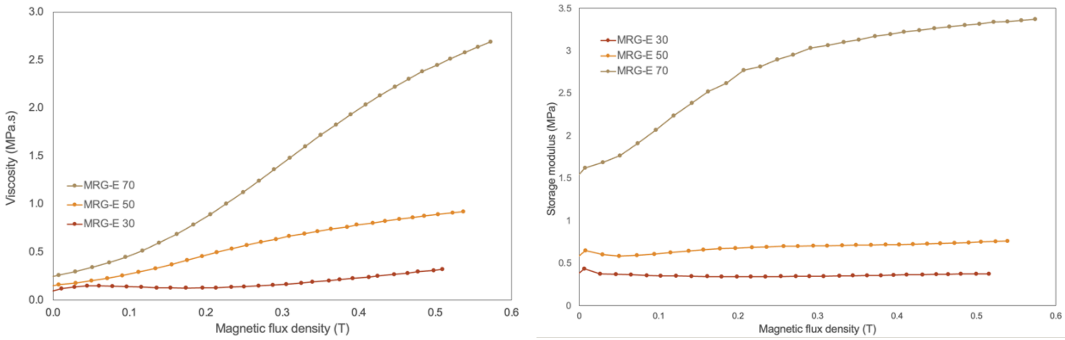

Figure 1: Effect of varying EIP composition on MRG properties: (a) Magnetoviscous effect and (b) relationship between storage modulus and magnetic flux density.

The relationship between viscosity and magnetic flux density was determined using rotational mode. Figure 1(a) illustrates the magnetoviscous effect of MRG at different EIP compositions, analyzed using rotational mode. The results show that viscosity increases with both magnetic flux density and EIP fraction at constant shear rates, attributed to the formation of a more structured particle network as EIP concentration rises.Furthermore, in oscillatory mode, the relationship between storage modulus and magnetic flux density was investigated. As shown in Figure 1(b), MRG-E 70 exhibits a noticeable increase in storage modulus with increasing magnetic field strength. In contrast, MRG-E 30 and MRG-E 50 maintain a steady storage modulus between 0.1 T and 0.5 T. This stability is likely due to the lower EIP concentration in MRG-E 30 and MRG-E 50, which prevents the formation of strong chain-like structures and results in a low yield stress that is easily surpassed under oscillatory shear. In contrast, MRG-E 70 demonstrates a significant increase in storage modulus due to its higher magnetic particle concentration, leading to stronger inter-particle interactions and a more pronounced response to the applied magnetic field.

5. CONCLUSIONS

The performance of MRG with the irregular shaped EIP was expressed in terms of magnetoviscous effect and storage modulus. Experimental results showed that the rheological properties of irregular shape MRG in terms of viscosity and storage modulus were dependent on the wt.% of EIP dispersed in the grease medium. The findings indicated that the incorporation of 70 wt.% of EIP can enhance the performance of MRG.

ACKNOWLEDGEMENT

This work was supported by the Higher Institution Centre of Excellence (HiCOE) program of the Ministry of Higher Education (MOHE) Malaysia under the HiCOE Research Grant. This research work also supported and funded by Universiti Teknologi Malaysia (UTM) under Fundamental Research (Vot. No. 31J85).

REFERENCES

[1] P. J. Rankin, A. T. Horvath, and D. J. Klingenberg, "Magnetorheology in viscoplastic media," *Rheol. Acta*, vol. 38, no. 5, pp. 471–477, 1999, doi: 10.1007/s003970050198.

[2] X. Ye, J. Wang, X. Wang, G. Zhang, and Q. Ouyang, "An experimental study on thermo-field rheological properties of lithium-based magnetorheological grease," *Colloids Surfaces A Physicochem. Eng. Asp.*, vol. 648, no. April, p. 129047, 2022, doi: 10.1016/j.colsurfa.2022.129047.

Magneto-Mechanical-Thermal Coupled Behavior of Transversely Isotropic Magnetorheological Elastomers: A continuum-mechanics Approach

Amin Saber*[1], Ramin Sedaghati[2]

[1, 2] Department of Mechanical, Industrial and Aerospace, Concordia University, Montreal, QC H3G 1M8, Canada
(E-mail: amin.saber@mail.concordia.ca, ramin.sedaghati@concordia.ca)

Short abstract: This study presents an analytical model, formulated within the framework of nonlinear continuum mechanics, to predict the coupled magneto-mechanical-thermal behavior of transversely isotropic magnetorheological elastomers (MREs). The model is based on a modified Helmholtz free energy function, extended to explicitly incorporate temperature as an independent variable. Consequently, the total free energy is expressed as a function of temperature, the deformation gradient, the magnetic field, and the particle orientation parameters. Through the derived constitutive equations, the proposed model can accurately capture the response of MREs under various combinations of magnetic, mechanical, and thermal loading conditions.
***Keywords*:** Magnetoreological Elastomer, continuum-based model, temperature effect.

1. INTRODUCTION

Magnetorheological elastomers (MREs), a class of smart functional materials, have attracted considerable attention in recent years. MREs possess the remarkable ability to alter their mechanical properties in response to an externally applied magnetic field, making them highly suitable for a broad spectrum of advanced engineering and biomedical applications. These materials are composed of a soft elastomeric matrix embedded with microscale ferromagnetic particles. The unique magnetorheological (MR) properties of MREs arise from the presence of these ferromagnetic inclusions, a phenomenon commonly referred to as the MR effect. Research has demonstrated that MREs with aligned particles—referred to as transversely isotropic MREs—exhibit enhanced MR behavior, particularly when the external magnetic field is applied in the same direction as the particle alignment. To fully exploit the potential of MREs, it is essential to develop accurate constitutive models capable of capturing their magneto-mechanical coupling behavior. Such models must reliably describe the material response across a broad range of magnetic field strengths, mechanical loading conditions, and temperatures. A comprehensive review of the major modeling approaches for MREs has been presented in a recent study [1]. Among these, the continuum-based modeling approach stands out by offering a robust, physics-based mathematical framework for predicting the nonlinear behavior of MREs under diverse conditions. Ultimately, integrating constitutive modeling with experimental data will facilitate more reliable and cost-effective design processes for magnetorheological systems.

2. OBJECTIVES

Motivated by existing gaps in the literature, this study aims to develop a robust continuum-based model to predict the coupled magneto-mechanical-thermal response of transversely isotropic magnetorheological elastomers, explicitly incorporating temperature as an independent variable.

3. MATERIAL AND METHODOLOGY

In this study, a modified Helmholtz free energy function is formulated to incorporate magnetic induction $\boldsymbol{B}$ and the particle alignment direction $\boldsymbol{a}$, in addition to the deformation gradient $\boldsymbol{F}$ [2]. By applying the first and second laws of thermodynamics, the corresponding constitutive equations are derived, and the dependence of the total modified energy function on temperature T is established. Once the dependence of the total energy function on temperature is established, it becomes necessary to determine the temperature distribution throughout the MRE sample. The system under consideration is a cylindrical, transversely isotropic MRE specimen with a height of 10 mm and a diameter of 20 mm. To obtain the temperature as a function of the material coordinates, the heat conduction problem is solved in cylindrical coordinates. It is worth noting that a practical thermal boundary condition is adopted: the bottom surface of the cylinder is maintained at a prescribed temperature, while all other surfaces are subjected to free convection boundary conditions. Incorporating the temperature distribution function enables the proposed model to capture the response of MREs under varying thermal gradients. Moreover, in addition to the influence of magnetic induction on the shear modulus, the steady-state temperature also affects the off-field stiffness of MREs—such as in scenarios where the sample is placed in a thermal chamber and allowed to reach thermal equilibrium. Consequently, the shear modulus can be expressed as a function of both magnetic induction and temperature. In this study, both the effects of temperature gradients and steady-state temperature conditions are taken into account.

4. RESULTS AND DISCUSSION

The solution of heat conduction results if temperature distribution function as following equation:

$$T(r,z) = \sum_{n=1}^{\infty} E_n J_0(\lambda_n r)\sinh(\lambda_n z) - \frac{h}{hL + \kappa_{eff}} z + 1 \qquad \text{(Eq. 1)}$$

Thus, the modified energy function can be defined as:

$$\psi(\boldsymbol{F},\boldsymbol{B},T,\boldsymbol{A}) = c_0\left[T - T_0 - T\ln\left(\frac{T}{T_0}\right)\right] - (T - T_0)M_1(\boldsymbol{F}) + \frac{T}{T_0}W_2(\boldsymbol{F},\boldsymbol{B},\boldsymbol{A}) \qquad \text{(Eq. 2)}$$

By applying the constitutive equations in conjunction with the mechanical boundary conditions corresponding to torque–twist loading, the material constants can be identified, and the overall response of transversely isotropic MREs under coupled magneto-mechanical-thermal conditions can be predicted. The resulting torque–twist response, along with the corresponding temperature distribution within the MRE, is presented in Figure 1.

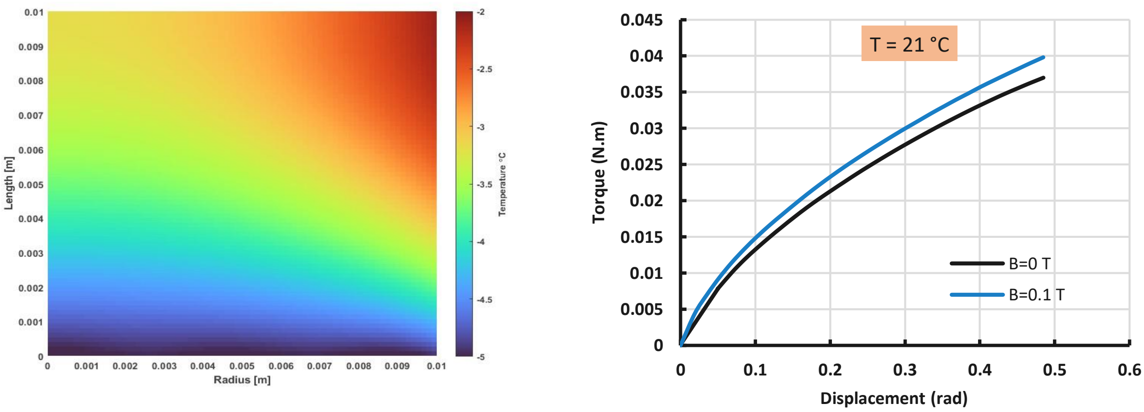

Figure 1: a) The temperature distribution for fixed base temperature of -5°C, b) Torque-twist response under different B at fixed room temperature

5. CONCLUSIONS

The proposed continuum-based model is capable of capturing the coupled magneto-mechanical-thermal behavior of transversely isotropic MREs under quasi-static loading conditions.

ACKNOWLEDGEMENT

Support from the Natural Sciences and Engineering Research Council of Canada (NSERC) is gratefully acknowledged.

REFERENCES

[1] Saber A, Sedaghati R. The Modeling of Magnetorheological Elastomers: A State-of-the-Art Review. *Adv Eng Mater* (2023);25.

[2] Bustamante R. Transversely isotropic nonlinear magneto-active elastomers. *Acta Mech* (2010);210:183–214.

Proposal of Hybrid Smart Structure with Magnetorheological Fluid / Elastomer

Kyusei Shimoma[1], Rihiro Fukuyama[2] and Takehito Kikuchi[3]

[1] Graduate School of Science and Technology, Oita University, Japan
[2] Graduate School of Engineering, Oita University, Japan
[3] Faculty of Science and Technology Oita University, Japan
(E-mail: t-kikuchi@oita-u.ac.jp)

Short abstract: In this study, we proposed a hybrid smart structure with a combination of magnetorheological (MR) fluid and elastomer by using a soft ultraviolet-reactive resin (UVR) and magnetic particles. In this method, a key material is an MR ultraviolet resin (MRUVR) that is a mixture of the soft UVR and magnetic particles. As a basic study, we experimentally investigated the manufacturability of its cure process and elastic properties of the cured MRUVR. The results of the compression tests show significant increasement of the elastic modulus for some prepared MRUVR.
Keywords: Magnetorheological fluid, Magnetorheological elastomer, Ultraviolet cure

1. INTRODUCTION

Soft robotics [1] is an attractive field for many applications of robot hands targeting to manipulate delicate objects, e.g., natural products or biological objects. In the soft robotics, several types of smart materials and smart structure have been utilized to achieve lightweight and flexible handling devices. For example, magnetorheological (MR) fluid [2] is a candidate for fluidic soft robot owing to its rapid response, wide range of its viscosity change and simple structure. However, leakage of the fluid is one of drawbacks for the MR fluid-based mechanisms. On the other hand, MR elastomer [3] is a flexible solid material. Its elastic properties can be controlled with intensity of external magnetic field. This material is also attractive as a 3D printable material [4] for the soft robots. However, the range of its elastic change is relatively low due to the limitation of volume fluxion that can be applicable for stable material production.

2. OBJECTIVES

To overcome the above drawbacks of the MR fluids / elastomers, and utilized their advantages in the soft robot devices, we propose a hybrid smart structure with a combination of the MR Fluid and Elastomer in this study. In this smart structure, an MR fluid is completely packed with an MR elastomer without air cavity. To achieve this goal, a 3D printing technique is utilized. The conceptual drawing of its production process is shown in Fig.1. In this method, a key material is an MR ultraviolet resin (MRUVR) that is a mixture of a soft ultraviolet-reactive resin (UVR) and magnetic particles. Before its curing, it works as an MR fluid. On the other hand, it becomes an MR elastomer after curing.

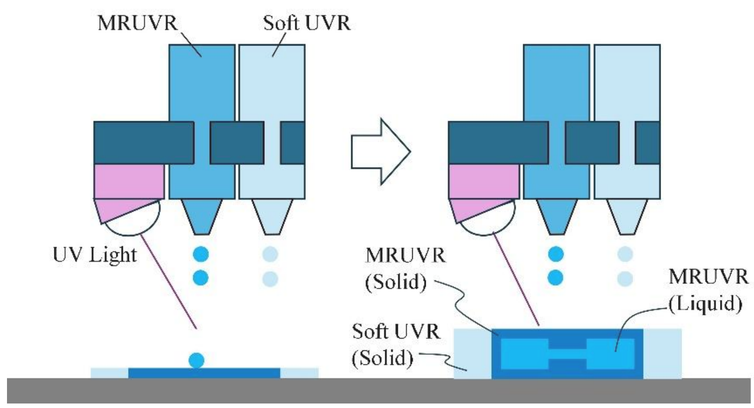

Figure 1: Conceptual drawing of 3D printable Hybrid Smart Structure with Magnetorheological Fluid / Elastomer.

3. MATERIAL AND METHODOLOGY

As a basic study, we experimentally investigated the manufacturability of cure processes of the MRUVR and elastic properties of the cured MRUVR. Figure 2 shows the magnetic particles used in this study. Five to fifteen vol% of iron particles (Iron powder, Kyowa Pure Chemical, average diameter: 74 µm (#200) and 47µm (#300, Fig.2)) are mixed in a soft UV resin (SK Rubber-like Resin, SK Honpo, shore hardness: A45), and stirred with an overhead stirrer (RW16, IKA). After stirring, ultraviolet ray was exposed to the mixture for 0.5 – 3.0 minutes with a LED handy light (light diameter: 30 mm). After curing, compression tests were conducted with a universal testing machine (MCT-1150; AND Corp.).

4. RESULTS AND DISCUSSION

After the exploration of the curing process, 5 − 10 vol% were selected as stable preparation conditions for both particle sizes. Figure 3 shows experimental results of the compression tests for 5 vol% of #200 and curing time of 1 minute. Horizontal and vertical axes show strain and stress on the MRUVR sample. The results of the compression tests show significant increasement of the elastic modulus.

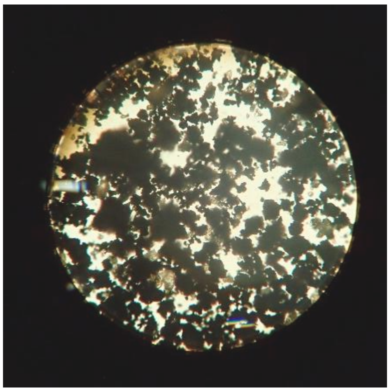

Figure 2: Magnetic particle (#300)

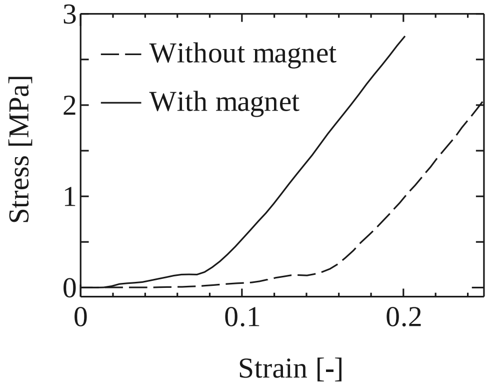

Figure 3: Experimental result for #200

5. CONCLUSIONS

In this study, we proposed a hybrid smart structure with a combination of MR fluids and elastomers by using a soft UVR and magnetic particles. As a basic study, we experimentally investigated the manufacturability of its cure process and elastic properties of the cured soft MRUVR.

ACKNOWLEDGEMENT

This study was partially supported by Kurata Grants of the Hitachi Global Foundation (1555) and the Fund Program for Creating Research-based Startups from Academia (Grant Number JPMJSF23DW).

REFERENCES

[1] Jakub Bernat, Piotr Gajewski, Jakub Kołota, Agnieszka Marcinkowska, Review of Soft Actuators Controlled with Electrical Stimuli: IPMC, DEAP, and MRE, Applied Sciences. 2023; 13 (3), 1651.

[2] Kevin McDonald, Abigail Rendos, Stephanie Woodman, Keith A. Brown, Tommaso Ranzani, Magnetorheological Fluid-Based Flow Control for Soft Robots, Advanced Intelligent Systems. 2020; 2 (11), 2000139.

[3] Peizhi Zhang, Mitsuhiro Kamezaki, Zhuoyi He, Hiroyuki Sakamoto and Shigeki Sugano, EPM–MRE: Electropermanent Magnet–Magnetorheological Elastomer for Soft Actuation System and Its Application to Robotic Grasping, IEEE Robotics and Automation Letters. 2021; 6 (4), pp. 8181-8188.

[4] Leone Costi, Antonia Georgopoulou, Somashree Mondal, Fumiya Iida, Frank Clemens, 3D Printable Self-Sensing Magnetorheological Elastomer, Macromolecular Materials and Engineering. 2023; 309 (2), 2300294.

Quantitative Analysis of Mechanical Properties in GO/rGO-Reinforced PDMS Nanocomposites

Ghazaleh Ramezani [1], Ion Stiharu * [2], Theo G.M. van de Ven [3]
[1,2] Concordia University, Montréal, CA
(ghazaleh.ramezani@mail.concordia.ca; ion.stiharu@concordia.ca)
[3] McGill University, Montreal, CA
(theo.vandeven@mcgill.ca)

Short abstract: This study investigates the mechanical properties of polydimethylsiloxane (PDMS) nanocomposites reinforced with graphene oxide (GO) and reduced graphene oxide (rGO). PDMS (15:1 base-to-curing agent ratio) was reinforced with varying GO concentrations (0.3%-0.6% by weight) and 0.3% rGO. Using an Instron mini tensile testing machine, enhancements in Young's modulus, tensile strength, ultimate tensile strength, and elongation at break were evaluated. Results revealed optimal performance at 0.5% GO and superior reinforcement with 0.3% rGO compared to equivalent GO concentrations. This work builds on prior studies highlighting the role of nanofillers in improving elastomer strength for advanced applications.

Keywords: PDMS nanocomposites, graphene oxide, reduced graphene oxide, mechanical properties, tensile testing

1. INTRODUCTION

Polydimethylsiloxane (PDMS) is a widely used elastomer known for its excellent flexibility, low modulus, and thermal stability, making it a preferred material in applications ranging from biomedical engineering to microfluidics and coatings. However, its relatively low mechanical strength and stiffness often limit its use in high-performance applications. To address these challenges, the incorporation of nanofillers such as graphene oxide (GO) and reduced graphene oxide (rGO) has emerged as an effective strategy to enhance the mechanical properties of PDMS. These nanofillers provide superior reinforcement due to their high surface area, excellent mechanical properties, and strong interfacial interactions with the PDMS matrix. Recent advancements in nanocomposite technology have demonstrated significant improvements in tensile strength, Young's modulus, and elongation at break for PDMS reinforced with GO and rGO. For instance, studies have shown that GO can act as a multifunctional filler, improving not only the mechanical properties but also the thermal stability and self-healing capabilities of PDMS-based composites(Krishnakumar et al., 2020; Moorthi et al., 2022). Moreover, rGO has been highlighted for its superior reinforcement capabilities compared to GO due to its higher electrical conductivity and better dispersion within the polymer matrix(Bellier et al., 2022; Khan et al., 2020). These enhancements make GO- and rGO-reinforced PDMS nanocomposites promising candidates for advanced engineering applications such as flexible electronics, coatings, and sensors. This study evaluates the mechanical properties of PDMS nanocomposites with varying concentrations of GO (0.03g–0.06g) and rGO (0.03g) using an Instron mini tensile testing machine, aiming to quantify improvements and determine optimal filler concentrations for maximizing performance.

2. OBJECTIVES

The objective of this study is to investigate the development of electro-active elastomers with tunable properties responsive to electric current. Building upon previous research, including our own work demonstrating significant strength improvements in nano-cellulose matrices with low graphene oxide (GO) content, this study aims to evaluate the mechanical properties of polydimethylsiloxane (PDMS) nanocomposites reinforced with varying concentrations of GO (ranging from 0.3% to 0.6% by weight) and reduced graphene oxide (rGO) (0.3% by weight). Using an Instron mini tensile testing machine, we will quantify enhancements in Young's modulus, tensile strength, ultimate tensile strength, and elongation at break. The study seeks to identify optimal GO concentration for maximum performance, compare the reinforcement efficacy of GO and rGO in PDMS nanocomposites, and establish a relationship between filler concentration and mechanical property improvement. This research contributes to the development of high-performance, electrically responsive PDMS-based materials for advanced engineering applications, with potential implications for smart materials and adaptive structures.

3. MATERIAL AND METHODOLOGY

The study utilized polydimethylsiloxane (PDMS) Sylgard 184, graphene oxide (GO) synthesized via a modified Hummers' method, and reduced graphene oxide (rGO) prepared through chemical reduction of GO, with isopropyl alcohol (IPA) as the dispersing agent. The nanocomposite preparation involved dispersing GO and rGO in IPA through ultrasonication, mixing with PDMS base at various concentrations (0.03g, 0.04g, 0.05g, and 0.06g for GO; 0.03g for rGO), mechanical stirring, and addition of curing agent at a 15:1 base-to-curing agent ratio. The mixture was then cured at 80°C for 30 minutes in an oven to produce the final nanocomposite samples.

4. RESULTS AND DISCUSSION

Table 1 shows the improved mechanical properties of PDMS (15:1) when reinforced with graphene oxide (GO) and reduced graphene oxide (rGO). The best results were achieved with 0.05g GO and 0.03g rGO.

Table 1: Mechanical Properties of PDMS (15:1) Reinforced with Graphene Oxide (GO) and Reduced Graphene Oxide (rGO)

Property	Base PDMS (15:1)	+0.3% GO	+0.4% GO	+0.5% GO	+0.6% GO	+0.3% rGO
Young's Modulus (MPa)	1.1	1.8	1.9	2	1.85	2.2
Tensile Strength (MPa)	3.5	4.2	4.3	4.4	4.25	4.7
Ultimate Tensile Strength (MPa)	4	5	5.1	5.2	5.05	5.5
Elongation at Break (%)	160	170	172	175	173	175

The work will be further extended to evaluate if a current circulating through the elastomer will modify in any way the strain or the strength of the material when subjected to tensile forces. Further work will be directed towards the scaling the stiffness of the material when subjected to compressive forces.

5. CONCLUSIONS

In conclusion, this study demonstrates the significant enhancement of PDMS mechanical properties through the incorporation of GO and rGO nanofillers. Specifically, a GO concentration of 0.05g yielded optimal performance among GO-reinforced samples, while 0.03g rGO exhibited superior reinforcement compared to the equivalent GO concentration. Future work could explore the long-term durability and stability of these nanocomposites, as well as investigate the effects of different reduction methods on rGO's reinforcement capabilities to further optimize the mechanical properties of PDMS-based materials.

REFERENCES

Bellier, N., Baipaywad, P., Ryu, N., Lee, J. Y., & Park, H. (2022). Recent biomedical advancements in graphene oxide- and reduced graphene oxide-based nanocomposite nanocarriers. *Biomaterials Research*, *26*(1), 65. https://doi.org/10.1186/S40824-022-00313-2

Khan, F., Khan, M. S., Kamal, S., Arshad, M., Ahmad, S. I., & Nami, S. A. A. (2020). Recent advances in graphene oxide and reduced graphene oxide based nanocomposites for the photodegradation of dyes. *Journal of Materials Chemistry C*, *8*(45), 15940–15955. https://doi.org/10.1039/D0TC03684F

Krishnakumar, B., Singh, M., Parthasarthy, V., Park, C., Sahoo, N. G., Yun, G. J., & Rana, S. (2020). Disulfide exchange assisted self-healing epoxy/PDMS/graphene oxide nanocomposites. *Nanoscale Advances*, *2*(7), 2726. https://doi.org/10.1039/D0NA00282H

Moorthi, K. ;, Saxena, V., Prasanna Sanka, R. V. S., & Rana, S. (2022). Self-healing epoxy/PDMS/graphene oxide nanocomposites for anti-corrosive applications. Chemical and Process Engineering-Inzynieria Chemiczna i Procesowa. *Chemical and Process Engineering*, *43*(2), 137–145. https://doi.org/10.24425/cpe.2022.140816

Active natural frequency tuning of a magnetorheological membrane

Seyyedmohammad Aghamiri[1], Ramin Sedaghati[1]

[1] Mechanical Engineering Department, Concordia University, Montreal, QC, Canada
(E-mail: seyyedmohammad.aghamiri@concordia.ca, ramin.sedaghati@concordia.ca)

Short abstract: In this study, the vibration characteristics of a magnetorheological elastomer (MRE) membrane under a varying magnetic field are analytically investigated. The MRE membrane, with a known magnetization, deforms into a spherical cap under a uniform magnetic field, inducing tension proportional to the magnetic field. This magnetic-induced tension alters the membrane's natural frequencies. By modeling the field as a pressure acting perpendicularly to the membrane, we analyze how changes in the magnetic field modify the tension and, consequently, the natural frequencies. The results aim to elucidate the tunability of MRE membranes for adaptive structural applications.

Keywords: Membrane, Magnetorheological Elastomers, Tension, Natural Frequency, Pressure.

1. INTRODUCTION

Membranes are thin and flexible structures that primarily resist loads through in-plane tension rather than bending stiffness. These lightweight structures are widely applied in acoustic devices, sensors, and adaptive structures due to their high sensitivity and tunability. Membranes offer advantages such as low mass and responsiveness to external stimuli, making them ideal for dynamic environments. Fabricating the membrane from a magnetorheological elastomer imparts magnetic properties that complement its inherent mechanical characteristics. This integration transforms the membrane into an active component capable of modifying its mechanical and dynamic responses under an applied magnetic field, enabling it to function as a remotely adjustable element. Such adaptability enhances its utility in applications requiring precise control over vibrational and structural behaviour.

Numerous studies have explored magnetoactive membrane designs for various applications, particularly acoustic metamaterials [1-3]. This shows the importance of investigating the dynamic behaviour of such systems. In this paper, we examine a thin, circular membrane made from a magnetorheological elastomer, analyzing the influence of an applied magnetic field on its dynamic properties. The research aims to indicate how magnetic stimuli can modulate the membrane's vibrational characteristics, contributing to the advancement of adaptive material technologies.

2. OBJECTIVES

The primary factor influencing the vibration propagation properties of MRE membranes is the applied tension. The first type of tension is externally imposed through boundary conditions using a fixture. However, with the introduction of magnetic effects, the magnetic field can also modify the internal tension of the membrane, thereby altering its stiffness or flexibility. The natural frequencies can be effectively tuned by adjusting the membrane's tension. The following section will employ a linear analytical approach to derive equations describing magnetically induced tension and its impact on the membrane's natural frequencies.

3. MATERIAL AND METHODOLOGY

A circular, flat, thin MRE membrane is considered. Upon applying a magnetic field perpendicular to the membrane, the magnetic field can be treated as an equivalent pressure field, denoted as P_0 [3]:

$$P_0 = \mu_0 h M \nabla H \tag{1}$$

where μ_0 is the vacuum permeability, h is the membrane's thickness (0.5mm), M is the magnetization of the material (assumed to be a constant and equal to 300 $\frac{kA}{m}$), and ∇H is the magnetic field gradient. This equation can be derived from magnetic energy density. On the other hand, by considering wave equation in membranes[1] and solving the eigenvalue problem with fixed boundary conditions, the first natural frequency can be expressed as:

[1] $T\nabla^2 w = \rho \frac{\partial^2 w}{\partial t^2}$

$$f_n = \frac{2.405}{2\pi a}\sqrt{\frac{T}{\rho h}} \tag{2}$$

where T, ρ, and a are tension (10 $\frac{N}{m}$), density (2800 $\frac{kg}{m^3}$), and radius of the membrane (50mm), respectively. Assuming linear stress and strain in the deformed membrane, which is assumed to take the shape of a spherical cap, and using Hook's law, the magnetically induced tension may be derived as:

$$T_{mag} = [\frac{Eha^2P_0^2}{24(1-\nu)}]^{\frac{1}{3}} \tag{3}$$

where E and ν are Young's modulus (1 MPa) and Poisson's ratio (0.49), respectively. Based on the principle of superposition, the total tension in the membrane is the sum of the magnetically induced tension and the mechanically applied pre-tension. As the strength of the magnetic field changes, the equivalent pressure field P_0 is altered, allowing for control over the membrane's overall tension.

4. RESULTS AND DISCUSSION

The variation of the first natural frequency of the MRE membrane concerning the applied magnetic field gradient is presented in Figure 1. The trend demonstrates a clear increase in natural frequency as the magnetic field gradient increases. This behaviour indicates that the induced magnetic tension plays a significant role in altering the membrane's dynamic characteristics and suggests that the additional magnetic-induced tension enhances the membrane's stiffness, leading to a higher resistance to deformation and, consequently, an increase in natural frequency. The nonlinearity arises from the nonlinearity of the equations. This result highlights the feasibility of tuning the membrane's vibrational properties through external magnetic control, which is particularly beneficial for applications requiring adaptive frequency response, such as vibration control, tunable resonators, and smart material systems.

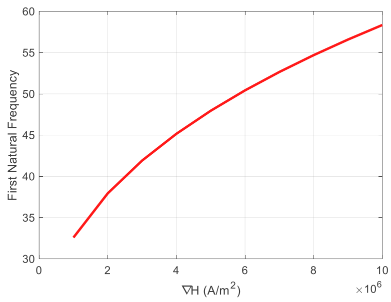

Figure 1: First natural frequency shift under varying magnetic field gradient

5. CONCLUSIONS

This study demonstrates that the natural frequency of an MRE membrane can be effectively tuned by adjusting the applied magnetic field. The induced magnetic tension increases the membrane's stiffness, leading to a higher resistance to deformation and a corresponding rise in natural frequency. The results highlight the potential of MRE membranes for adaptive structural applications, enabling precise control over vibrational properties in smart material systems.

ACKNOWLEDGEMENT

Support from the Natural Sciences and Engineering Research Council of Canada (NSERC) is gratefully acknowledged.

REFERENCES

[1] Sun C, Cao X, Zhou X, Gong X, Xuan S. Deformation dependent sound absorption property of a novel magnetorheological membrane sound absorber. Frontiers in Materials. 2020 Oct 30;7:598973.
[2] Xia P, Lai Y, Liu X. Adjustable magnetic-control design of a metasurface for sound insulation. Frontiers in Mechanical Engineering. 2022 Jan 19;7:829149.
[3] Chen X, Xu X, Ai S, Chen H, Pei Y, Zhou X. Active acoustic metamaterials with tunable effective mass density by gradient magnetic fields. Applied Physics Letters. 2014 Aug 18;105(7).

Adhesion and Detachment of Spherical Particles on Microstructures of Permanent Magnet Elastomers

S. Suzuki[1], R. Kuwada[2], M. Hayashi[2], Y. Ido[1], D. Ishii[2], M. Kamezaki[3], Y. Iwamoto[1]

[1] Department of Mechanical Engineering, Nagoya Institute of Technology, Japan
(E-mail: iwamoto.yuhiro@nitech.ac.jp)
[2] Department of Soft Materials, Nagoya Institute of Technology, Japan
[3] Graduate School of Engineering, The University of Tokyo, Japan

Short abstract: Biomimetics is gaining increasing attention, particularly in applications such as solar panel cleaning and spacecraft maintenance. Among these developments, gecko-inspired robots that utilize adhesion mechanisms to traverse surfaces are being actively researched. However, contamination significantly deteriorates the adhesion performance of these mechanisms. This study investigates the use of ridge-shaped permanent magnet elastomers that combine flexibility with magnetic properties to facilitate particle adhesion and detachment. By measuring adhesion and detachment quantities of particles, we found that the ridged structure allowed particles to be removed and self-cleaning to be realized compared to smooth surfaces.
Keywords: Permanent magnet elastomer, Gecko robot, Self-cleaning, Biomimetics.

1. INTRODUCTION

Gecko-inspired robots that utilize van der Waals forces can climb walls and ceilings[1]. These robots hold promise for applications such as cleaning solar panels and inspecting buildings. However, maintaining adhesion, especially on contaminated surfaces, remains a significant challenge.

Previous studies have explored the use of magnetorheological elastomers with micro-ridge structures. Such microstructures can realize self-cleaning by applying magnetic fields[2]. Although the shape of such a microstructure changes when an external magnetic field is applied, it returns to its original shape by relying solely on its elastic force. This is because the dispersed magnetic particles are soft magnetic materials. In order to realize more effective self-cleaning, this study proposes the use of permanent magnet elastomers containing neodymium particles, which provide residual magnetization, flexibility, and shape control.

Figure 1 demonstrates the particle capture and release using the ridge-shaped permanent magnet elastomer. The ridges of permanent magnet elastomers can capture particles when tilted and release them when they are returned to their original shape. In the present study, to understand the self-cleaning mechanism, the amount of particles captured and released was evaluated by measuring the weight of detached glass particles with varying ridge dimensions.

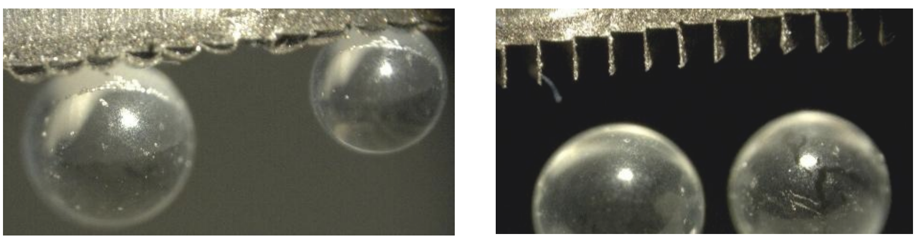

Figure 1: Particle adhesion and detachment using ridge-shaped permanent magnet elastomer.

2. MATERIAL AND METHODOLOGY

In this study, permanent magnet elastomers were fabricated using SILPOT184 (manufactured by Dow TORAY) as the dispersing medium and neodymium particles (manufactured by Magnepunch) with an average size of 5 μm as the dispersed phase. To create the ridge structures, molds were made by precisely carving grooves of equal height and width into PTFE using a design knife. The dispersing medium and particles were mixed, poured into the molds, and thermally cured to produce micro-ridges.

The self-cleaning ability of micro-ridge permanent magnet elastomers was evaluated using glass particles as simulated contaminants. Adhesion and detachment of the glass particles were assessed using the following procedure. First, a magnetic field was applied to tilt the ridges, allowing glass particles to adhere to the surface, and the weight of the attached particles was measured. Then, by adjusting the magnetic field to return the ridges to an upright position, the weight of the detached particles was measured to evaluate self-cleaning performance. Four types of permanent magnet elastomers were tested: three with ridge heights and widths of 200 µm, 300 µm, and 350 µm, and one without ridges. Glass particles with sizes ranging from 0.500 to 0.710 mm were used in the experiments.

3. RESULTS AND DISCUSSION

The measured adhesion and detachment amounts are shown in Figure 2. These values represent the averages of five measurements conducted under each condition. In the case of w = 0 and h = 0, where no ridges are present and the surface remains smooth, detachment due to surface shape changes does not occur, resulting in adhesion measurements only.

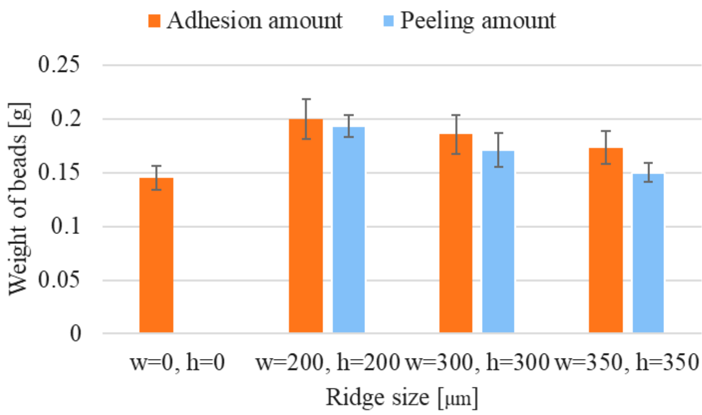

Figure 2: Results of the experiment measuring adhesion and detachment amounts.

The experimental results indicated that, for the tested particle sizes, adhesion increased as ridge size decreased in samples with ridges. Similarly, the ratio of detached to adhered particles was higher for smaller ridge sizes. These findings suggest that reducing ridge size enhances both particle adhesion and detachment, thereby improving the self-cleaning performance of micro-ridge permanent magnet elastomers. Furthermore, the ridge-free sample exhibited the lowest adhesion, indicating that the presence of ridges promotes particle attachment. However, since adhesion still occurred in the ridge-free sample, micro-ridge permanent magnet elastomers, which facilitate particle detachment, are considered effective for self-cleaning applications.

4. CONCLUSIONS

The experimental results confirmed that modifying the ridge size affected both particle adhesion and detachment. Additionally, it was demonstrated that micro-ridge permanent magnet elastomers are effective for self-cleaning applications. While this study focused on self-cleaning, the ability to control particle attachment and detachment has potential applications in various fields.

ACKNOWLEDGEMENTS

This work was supported in part by Integrated Research, Frontier Research Institutes, Nagoya Instiute of Technology, Japan.

REFERENCES

[1] Ozgur.Unver, Ali Uneri, Alper Aydemir, M.Sitti. Geckobot: A Gecko Inspired Climbing Robot Using Elastomer Adhesives. IEEE International Conference on Robotics and Automation. 2006 May;2329-35.
[2] Andrew G. Gillies, Jonghun Kwak and Ronald S. Fearing. Controllable Particle Adhesion with a Magnetically Actuated Synthetic Gecko Adhesive. Advanced Functional Materials. 2013 Feb;26(23):3256-61.

Influence of microstructure on magnetic properties of anisotropic magnetic elastomers

Dmitry Borin[1], Nils Magin[2] and Stefan Odenbach[3]

[1, 2, 3] Chair of Magnetofluiddynamics, Measuring and Automation Technology, TU Dresden, 01069 Dresden, Germany
(E-mail: dmitry.borin@tu-dresden.de, nils.magin@tu-dresden.de, stefan.odenbach@tu-dresden.de)

Short abstract: The magnetic properties of elastomers based on silicone matrix and iron microparticles assembled in aggregates of different morphology are experimentally investigated. For this purpose, elastomer samples with various concentrations of magnetic filler are structured in a magnetic field of various strength. The influence of the shape and size of the particle aggregates on the magnetic characteristics of the samples is revealed. Moreover, the influence of the angle between the direction of particle aggregates, i.e. the field applied in the process of crosslinking the polymer matrix, and the direction of the field applied during magnetic measurements on the macroscopic magnetic properties of the composite is investigated. Magnetic measurements are supported by the evaluation of the real microstructure of the samples using X-ray computed microtomography and corresponding digital image processing methods.
Keywords: elastomer, magnetization, microstructure, anisotropy, field angle.

1. INTRODUCTION AND OBJECTIVES

Composites based on magnetic particles and an elastic polymer matrix are called magnetic elastomers. Depending on the size and concentration of magnetic particles and the elasticity of the matrix, such materials can have a significant magnetorheological (MR) effect and are traditionally referred to as MR elastomers [1]. Regardless of the above parameters and the magnitude of the MR effect, the presence of a magnetic component makes such composites magnetically sensitive. The application of an external homogeneous magnetic field during the polymerisation process makes it possible to obtain anisotropic material due to the structuring of particles in the initially liquid polymer matrix. It is obvious that the induced anisotropy significantly changes the magneto-mechanical response of composites to an external magnetic field. Recently, the influence of the mutual orientation of particle aggregates and the external magnetic field applied during magneto-mechanical tests on the macroscopic mechanical properties of MR elastomers was systematically investigated, see e.g. [2]. At the same time, the known results of measuring magnetization curves and determining the corresponding magnetic properties of magnetic elastomers as a function of the mutual orientation of the particle structures and the external field are limited to theoretical predictions, see e.g. [3]. The known experimental publications consider parallel and perpendicular orientations only [4,5]. On the other hand, varying the concentration of magnetic filler and the magnitude of the magnetic field applied during material crosslinking makes it possible to obtain a composite with different morphology of particle aggregates, see e.g. [6]. However, the relationship between the morphology of particle aggregates and the macroscopic properties of the material has not been sufficiently investigated to date. The question of the influence of the spatial orientation of different particle structures relative to the direction of the magnetic field applied in the experiment remains open. Accordingly, this study examines the influence of the angle between the direction of particle aggregates of different morphologies and the direction of the field applied during magnetic measurements on the macroscopic material response. Measurements of the magnetic characteristics of various composite samples are accompanied by microstructural studies.

2. MATERIAL AND METHODOLOGY

The study examines elastomeric composite samples based on two-component polydimethylsiloxane matrix (silicone and crosslinker NEUKASIEL RTV 230 and A149). Sigma-Aldrich iron powder with a particle average diameter of 44 µm are used as magnetic filler. The specimens are fabricated by mechanical mixing of all components, vacuum degassing and crosslinking at room temperature. The structuring magnetic field is provided by the electromagnet of a vibrating sample magnetometer (Lake Shore VSM 7407s), which is further used for magnetic measurements. The spatial orientation of particle structures relative to the direction of the external field in magnetic measurements was changed by rotating the VSM rod with the sample holder around the vertical axis. Microstructural investigations are conducted using the own laboratory X-Ray microtomography setup and reconstruction process is performed calculating a three-dimensional model from the individual radiographs with a software package developed in house [7].

3. RESULTS AND DISCUSSION

Figure 1 shows visualization of the different internal microstructure of a magnetic elastomer with the same microparticle content. A composite with short chains formed by structuring in a low (<10 A/m) magnetic field (b) and a composite with long chains formed by structuring in a high magnetic field (>) (c) are shown next to the isotropic sample (a). Figure 2 shows the dependence of the initial magnetic susceptibility χ_{ini} on the tilt angle of the particles α relative to the direction of the magnetic field applied during the magnetic measurements. The values of χ_{ini} are obtained from the magnetization curves of these samples. The smaller the tilt angle of chain aggregates relative to the applied field, the higher the initial magnetic susceptibility. The composite with long chains has the highest susceptibility. At higher tilt angle (α>60°), the susceptibility of anisotropic composites is comparable to that of isotropic material. The obtained results are obviously related to the demagnetizing factor of chain aggregates and its variation with the change of the tilt angle of the chains. It should also be noted that a similar trend is observed for filled composites (~10 vol.%) with thick clusters and/or network-like aggregates of particles, i.e. composites with a morphology fundamentally different from individual chains. These results will be demonstrated at the conference.

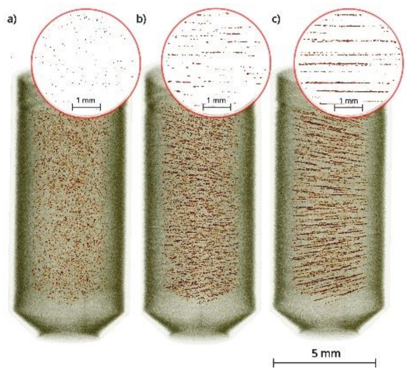

Figure 1: Microstructure of specimens with ~0.13 vol.% particles in VSM specimen holder: a) isotropic composite, b) short chain composite, c) long chain composite.

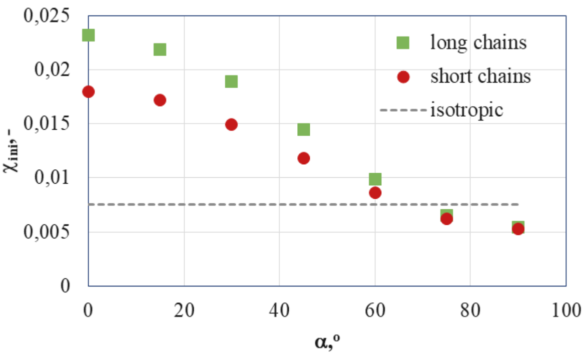

Figure 2: Initial magnetic susceptibility of samples with ~0.13 vol.% particles as a function of the angle of spatial orientation of particle chains relative to the external magnetic field.

4. SUMMARY AND OUTLOOK

The morphology of the structures of magnetic microparticles and their orientation relative to the external field has a significant influence on the magnetic properties of anisotropic magnetic elastomers. Quantitative correlations between the size of the structures and the obtained dependencies of the magnetic properties of the composite on the spatial orientation of the structures remain to be carried out.

ACKNOWLEDGEMENT

This work was supported by the Deutsche Forschungsgemeinschaft (DFG) under Grant OD 18/35-1 within Research Unit FOR5599. The authors thank Dr. Dirk Romeis for detailed discussion of the results.

REFERENCES

[1] Wereley N. (ed.), Magnetorheology, RSC Publishing, Cambridge, 2014.
[2] Yao J. et al. Magnetorheological elastomers with particle chain orientation: modelling and experiments. Smart Mater. Struct. 2019; 28, 095008.
[3] Romeis D, Saphiannikova M. Effective magnetic susceptibility in magnetoactive composites. J. Magn. Magn. Mater. 2023; 565, 170197.
[4] Stepanov G.V. et al. Motion of ferroparticles inside the polymeric matrix in magnetoactive elastomers. J. Phys. Condens. Matter, 2008; 20, 204121.
[5] Borin D., Odenbach S. Initial magnetic susceptibility of the diluted magnetopolymer elastic composites. J. Magn. Magn. Mater. 2017; 431, 115-119.
[6] Borin D. Targeted patterning of magnetic microparticles in a polymer composite. Phil. Trans. R. Soc. A 2020; 378: 20190256.
[7] Borin D., Odenbach S. in Magnetic Soft Matter, ed. J. de Vicente, The Royal Society of Chemistry, 2023, ch. 8, pp. 213-228.

A New Compact Magneto-Rheological Torque Feedback Device with Comb-Shaped Channel for Steer-by-Wire Systems

Long-Vuong Hoang[1], Quoc-Duy Bui[2,*], Van Cuong Vo[3] and Quoc Hung Nguyen[4,*]

[1, 2, 3] Faculty of Mechanical Engineering, Industrial University of Ho Chi Minh City, Vietnam
(E-mail: hoanglongvuong@iuh.edu.vn, buiquocduy@iuh.edu.vn, vovancuong@iuh.edu.vn)
[4] Institute of Engineering, Ho Chi Minh City University of Technology, Ho Chi Minh City, Vietnam
(E-mail: nq.hung@hutech.edu.vn)
* Corresponding author. Tel.: +84 938485812 (Q. H. Nguyen)

Short abstract: This paper develops a new magneto-rheological (MR) torque feedback device (TFD) for Steer-by-Wire (SbW) systems. The new MRTFD utilizes a comb profile MRF channel to extend the operational area of the fluid, thereby improving performance characteristics. Modeling and optimization are conducted to achieve a compact and optimal design. Experiments and assessments are planned to validate the feasibility of the MRTFD. The study is expected to provide an effective and compact MRTFD for SbW systems in particular and green haptic technology in general.
Keywords: brake, comb-shaped, feedback, magneto-rheological, Steer-by-Wire.

1. INTRODUCTION

It is widely recognized that SbW systems offer safety and fuel efficiency benefits over traditional mechanical steering systems. However, it lacks tactile steering feedback, which impacts driver control. Therefore, it is necessary to integrate an TFD into SbW systems for enhanced steering feel experiences.

MRF, a smart material responsive to magnetic fields, has recently emerged as a promising candidate for semi-active feedback systems. Most MRF-based TFDs operate similarly to MR brakes, enabling precise torque control according to steering angle by adjusting magnetic field strength. Over the past years, extensive research on MRBs has been conducted by numerous scholars [1-4], serving as a basis for the advancement of MRTFDs. In this study, we develop a new compact MRTFD with superior performance characteristics for SbW systems. This new MRTFD features a comb-shaped channel configuration to increase the active area of MRF in a specific operational space, producing improved feedback torque and dynamic range.

2. OBJECTIVES

Based on the previous analyses, the objectives of paper are as follows:

- Develop a new MRTFD with comb-shaped channel to enhance feedback torque and dynamic range.
- Conduct the modeling and optimization to achieve the compact and optimal design for a specific SbW system.
- Validate the feasibility of the comb-shaped channel MRTFD through experiments and evaluations.

3. MATERIAL AND METHODOLOGY

Figure 1 shows the configuration of the new comb-shaped channel MRTFD. A magnetic sleeve with axial comb profile is securely attached to a non-magnetic material shaft, serving as the rotor element. Comb teeth are positioned on the inner face of the cylinder, engaged with the corresponding profile on the rotor to form a comb-shaped MRF channel. Upon exposure to magnetic field, the MRF solidifies, resulting in the expected feedback torque generated by heightened friction between the rotor and MRF.

The total feedback torque T_f is determined as the sum of yield stress torque T_τ, viscous torque T_η and Coulomb friction torque at lip seal T_{ls} [4]:

$$T_f = T_\tau + T_\eta + 2T_{ls} \tag{1}$$

$$T_\tau = 2\sum T_{\tau.j} = \frac{\pi}{3}\sum l_j\left(3r_j^2 + 3r_j l_j \sin\theta + l_j^2 \sin^2\theta\right)\tau_{y.j} \tag{2}$$

$$T_\eta = 2\sum T_{\eta.j} = \pi\left[\sum l_j\left(4r_j^3 + 6r_j^2 l_j \sin\theta + 4r_j l_j^2 \sin^2\theta + l_j^3 \sin^3\theta\right)\right]\eta\frac{\omega}{t_g} \tag{3}$$

where τ_y and η are the MRF properties, ω is the spindle speed, and r, l, θ and t_g are geometric dimensions.

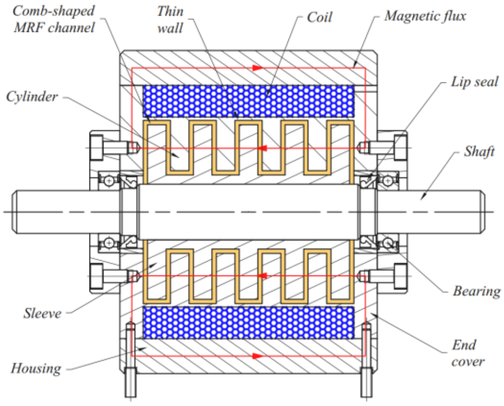

Figure 1: Configuration of the comb-shaped channel MRTFD.

The methodologies planned to be implemented in the paper are as follows:

– Analysis and review. Configurations of MRTFDs are first reviewed, followed by analyses of their respective advantages and disadvantages, then the comb-shaped channel structure is proposed.

– Modeling, simulation and comparison. Based on the mathematical model, a design optimization problem is formulated. The comb-shaped channel MRTFD model is then simulated and optimized using ANSYS software, and the results are subsequently compared with previous studies.

– Experimental validation. The MRTFD is designed, prototyped and experimentally verified on a test rig.

4. RESULTS AND DISCUSSION

Figure 2 shows the simulation results for the comb-shaped channel MRTFD. The distribution of magnetic flux is observed to extend across the MRF channel segments, consequently enhancing the feedback torque. Based on these modeling and simulation, a design optimization is planned to be conducted, considering performance criteria such as feedback torque, dynamic range, time constant and power consumption.

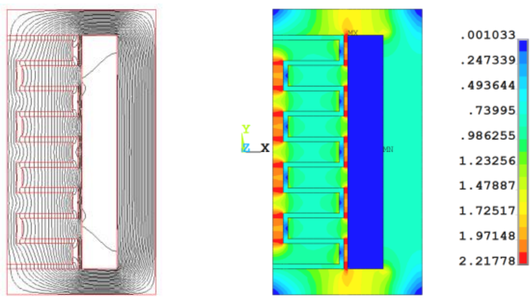

Figure 2: Simulation of magnetic flux lines and magnetic flux density.

5. CONCLUSIONS

In this study, a new compact MRTFD featuring comb-shaped channel for SbW systems is presented. The modeling and simulation results show the feasibility of this concept. In the next phase, the MRTFD will undergo optimization, prototyping, testing, and comprehensive evaluation to validate its functionality.

REFERENCES

[1] Attia EM, Elsodany NM, El-Gamal HA, Elgohary MA. Theoretical and experimental study of magneto-rheological fluid disc brake. Alexandria Engineering Journal. 2017;56(2):189-200.
[2] Mousavi SH, Sayyaadi H. Optimization and testing of a new prototype hybrid MR brake with arc form

surface as a prosthetic knee. IEEE/ASME Transactions on Mechatronics. 2018;23(3):1204-1214.
[3] Nguyen ND, Nguyen TT, Le DH, Nguyen QH. Design and investigation of a novel magnetorheological brake with coils directly placed on side housings using a separating thin wall. Journal of Intelligent Material Systems and Structures. 2021;32(14):1565-1579.
[4] Nguyen VB, Le HD, Nguyen QH, Duyen DQ, Hieu DHM, Choi S. Design and experimental evaluation a novel magneto-rheological brake with tooth shaped rotor. Smart Materials and Structures. 2022;31(1):015015.

Performance of Magnetorheological fluid in a novel composite system of flake-shaped Amorphous particles and carbonyl iron particles

Tianxiang Du[1], Ning Ma[2], Xufeng Dong[1, *]

[1] School of Materials Science and Engineering, Dalian University of Technology, Dalian, 116024, P. R. China.
[2] School of Infrastructure Engineering, Dalian University of Technology, Dalian, 116024, China
(E-mail: 875973609@mail.dlut.edu.cn, maning@dlut.edu.cn, dongxf@dlut.edu.cn.)

Short abstract: To address the inherent trade-offs among key performance indicators of magnetorheological fluids (MRFs), such as shear yield strength, sedimentation stability, zero-field viscosity, and redispersibility. This research investigates the development of a bidisperse particle system MRF by directly compounding flake-shaped FeSiCr amorphous alloy particles with carbonyl iron particles. The results demonstrate that the incorporation of flake-shaped FeSiCr particles not only enhances the shear yield strength of the MRFs across the entire magnetic field range but also significantly improves sedimentation stability and wear resistance characteristic during long-term operation. Most importantly, the combination of superior comprehensive performance and a simple manufacturing process significantly enhances the engineering applicability of the bidisperse particle system MRFs, making it a promising candidate for practical applications in intelligent vibration control systems.
Keywords: magnetorheological fluids, flake-shaped particles, FeSiCr amorphous alloy, bidisperse particle system, comprehensive performance.

1. INTRODUCTION

Magnetorheological fluids (MRFs) are intelligent fluids whose rheological parameters such as viscosity and shear yield strength can be instantaneously and reversibly controlled by a magnetic field. Typically composed of soft magnetic particles, carrier liquids and functional additives. Particles are the key components that determine the properties of MRFs. The element, morphology, particle size, content and dispersibility of soft magnetic particles are widely regarded as the starting point of particle regulation. However, the influence of these factors on the key performance indicators is extremely complex, typically resulting in the improvement of one or two performance indicators accompanied by the deterioration of other performance indicators. Therefore, resolving the contradiction between key performance indicators of MRFs and preparing MRFs with high shear yield strength, satisfactory zero-field viscosity and excellent sedimentation stability is an urgent bottleneck problem that needs to be addressed for the development of MR damping technology.

2. OBJECTIVES

The main purpose of this research is to solve the contradiction between shear yield strength, zero-field viscosity and sedimentation stability of MRFs by particle systems control.

3. MATERIAL AND METHODOLOGY

3.1. Preparation of MRFs

For the preparation of bidisperse MRFs, flake-shaped FeSiCr particles and CIPs were pre-mixed in varying proportions and added together to a beaker containing dimethyl silicone oil, maintaining a particle content of 65 wt.%. The mixture was thoroughly stirred at room temperature to achieve uniform suspension, thereby preparing a series of MRFs for experimental research.

3.1. Characterization of particles and MRFs

The morphology and compositional analysis of particles were thoroughly investigated using a JSM-7900F ultra-high resolution field-emission scanning electron microscope (FE-SEM) coupled. The phase structure of particle was extensively characterized using a Bruker D8 Advance X-ray diffractometer (Cu target and 2.2 kW ceramic X-ray tube) produced by Bruker Corporation. The magnetic properties of particles evaluated over a range of -15000 to 15000 Oe using a Lakesore-7400s vibrating sample magnetometer (VSM) at 40°C. The rheological performance of MRFs containing varying concentrations of bidisperse particles were investigated at 40°C using an Anton Paar MCR-301 rheometer (parallel plate system with PP-20 geometry, 1 mm test gap distance, and magnetic field intensity ranging from 0 mT to 545 mT).

4. RESULTS AND DISCUSSION

Figure 1a shows that the flake-shaped FeSiCr particles have a typical amorphous structure and are consistent with PDF cards numbered 34-0396. Figure 1b shows that the flake-shaped FeSiCr particles have excellent soft magnetic properties, and the saturation magnetization is comparable to that of CIPs. Figure 1c shows that the MRFs prepared by simple flake-shaped FeSiCr particles has extremely high shear yield strength under low magnetic field, and also has a shear yield strength comparable to that of CIPs-based MRFs phase under high magnetic field. In general, the superiority of flake-shaped FeSiCr as MRFs particles is demonstrated. Figure 1d and 1e respectively show that with the addition of flake-shaped FeSiCr particles, the sedimentation stability and zero-field viscosity of MRFs are improved to varying degrees. Figure 1f shows that the shear yield strength increases first and then decreases with the increase of the relative content of flake-shaped FeSiCr in the bidisperse particle system. The shear yield strength can be improved under the full magnetic field at a specific ratio. Figure 1g shows that MRFs-50/50 has excellent operational stability under both high and low magnetic fields. Figure 1h shows that the particle morphology of MRFs-50/50 does not change after 72 h of ball milling, indicating that the flake-shaped FeSiCr has excellent wear resistance.

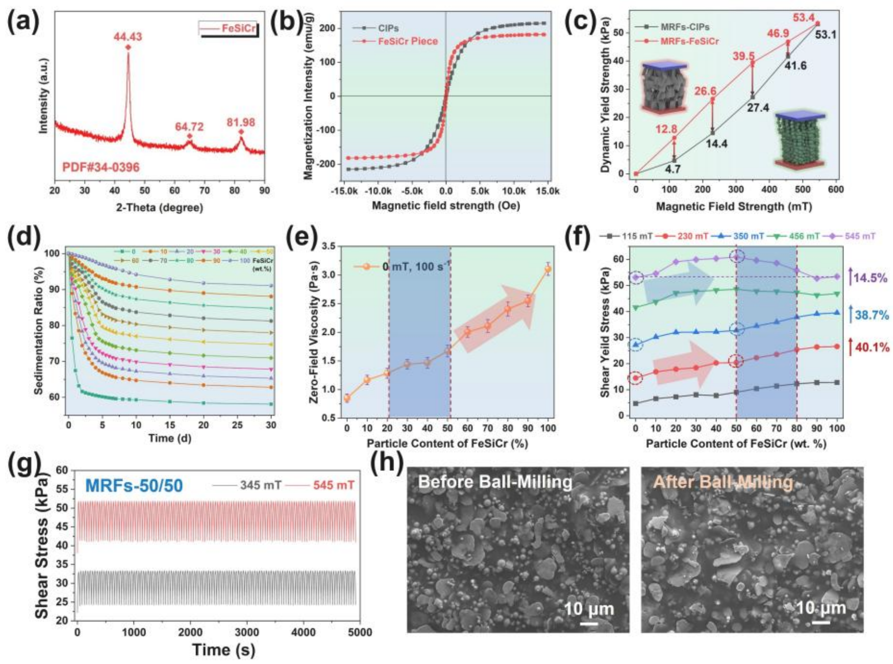

Figure 1: Properties of flake-shaped FeSiCr particles and bidisperse MRFs composed with CIPs. XRD (a), VSM (b), shear yield strength of monodisperse MRFs (c), sedimentation stability of bidisperse MRFs (d), zero-field viscosity of bidisperse MRFs (e), shear yield strength of bidisperse MRFs (f), operational stability of MRFs-50/50 (g), wear resistance of MRFs-50/50 (h).

5. CONCLUSIONS

This study employs a micro-size FeSiCr amorphous alloy flake, which is directly compounded with CIPs to form a bidisperse particle system MRFs. The results demonstrate that the incorporation of flake-shaped FeSiCr not only achieves high yield stress under both low and high magnetic fields but also ensures sedimentation stability over long-term storage. The large-sized FeSiCr particles, which possess wear-resistant characteristics, enhance the durability of the MRF while preventing excessive increases in zero-field viscosity. This study's straightforward preparation method for MRFs with high comprehensive performance lays a foundation for industrial development of predominant performance MRFs.

ACKNOWLEDGEMENT

This research is funded by the National Natural Science Foundation of China under Grant Number 52178459.

Design of a Test Bench Emulating Aircraft Primary Flight Control Operating Conditions to Study Magnetorheological Fluid Aging

J. Moorhead[1], F. Thérien[1], J-S. Plante[1], and D. Rancourt[1]

[1] Faculté de génie, Université de Sherbrooke, Createk, Canada
(E-mail: jeanne.moorhead@usherbrooke.ca, francis.therien@usherbrooke.ca)
(E-mail: jean-sebastien.plante@usherbrooke.ca, david.rancourt2@usherbrooke.ca)

Short abstract: As the aerospace industry shifts to electrifying aircraft, magnetorheological actuators are promising replacements for flight control. They offer high torque density, and high dynamic motion possibilities while being free of jam failure modes exhibited by conventional electromechanical actuators. However, wear mechanisms of magnetorheological fluid have only been tested in controlled laboratory environments. These tests do not accurately reflect realistic operating conditions in aircraft flight control applications. To address this, a new test bench was designed to evaluate the fluid's wear in realistic conditions and provide a clearer understanding of the actuator's durability.

Keywords: Testing, Wear, Magnetorheological Fluid, and Magnetorheological Actuator.

1. INTRODUCTION

Aircraft control surfaces are currently actuated by hydraulic actuators due to their robustness, reliability, and high force-to-weight ratio. However, these actuators use corrosive fluids and require expensive maintenance [1]. The aerospace industry is shifting towards More Electric Aircraft (MEA), requiring the development of electrical actuators for control surfaces [1]. Existing electromechanical actuators are not ideal replacements due to risks of mechanical jamming, which can immobilize control surfaces and compromise reliability [2]. Magnetorheological actuators (MRA) are promising alternatives, as they eliminate mechanical contact between the input and output and thus the risk of jamming [2]. While prior durability studies have validated the feasibility of MRA technology [3] and studied its primary wear mechanisms [3,4], the test conditions employed do not accurately reflect the operational environments encountered in aerospace. In order to fill existing knowledge gap, the research proposes a novel test bench design that is able to simlulate magnetorheological fluid (MRF) wear in aircraft operating conditions. Table 1 compares operating conditions of real-world flight controls applications, test benches described in previous work on MRF aging and the proposed test bench.

Table 1 : Differences between operating conditions of real-world flight controls applications, previous work on MRF aging and the proposed test bench

	Realistic Conditions	**Previous Work** [3,4]	**Proposed Test Bench**
Temperature	Fluctuating	Constant	Controlled
	-40°C to 80°C [5]	>0°C	-15°C to 80°C
Output shaft rotation	Yes	No	Yes
MR clutch	Reliable design	MRF leaks observed	Commercial design

2. KEY FEATURES OF THE TEST BENCH

Figure 1 illustrates the main components of the test bench in a simplified schematic. The MR clutch is immersed in a heat-transfer fluid (HTF) within a sealed chamber.

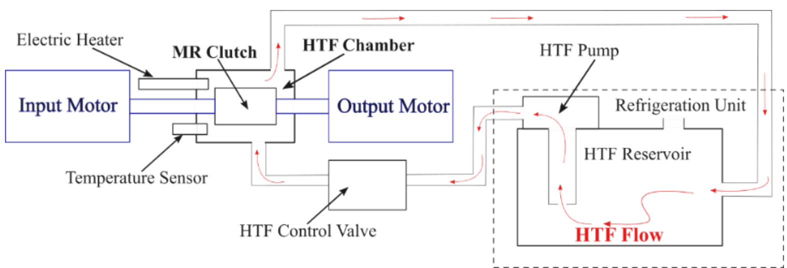

Figure 1 : Main components of the test bench

A mixture of ethylene glycol and distilled water is used as the heat-transfer fluid. A temperature sensor is installed inside the chamber to monitor the heat-transfer fluid's temperature. The temperature regulation system is comprised of two independent sub-systems for heating or cooling, depending on the desired operating temperature for a given aging test. The heating subsystem is provided by an electric heater, and a solid-state relay is used to modulate heating power between 0 and 100%. The heater inside the chamber heats the HTF surrounding the MR clutch. A refrigeration unit, which contains the HTF's reservoir and pump, is installed separately to circulate cold heat-transfer fluid inside the chamber. Commercial temperature control units (Red Lion PXU) use standard PID control to always keep the HTF at the desired temperature during an aging test. The temperature controllers can activate either the heating system or the cooling system, depending on the desired operating temperature (setpoint). The input and output rotation speeds of the clutch are controlled independently with electric motors. A wireless pressure sensor is added to the MR clutch to monitor pressure increase inside the clutch caused by out-gassing as the fluid wears.

3. ASSEMBLY OF THE TEST BENCH

Figure 2 below illustrates the fully assembled test bench.

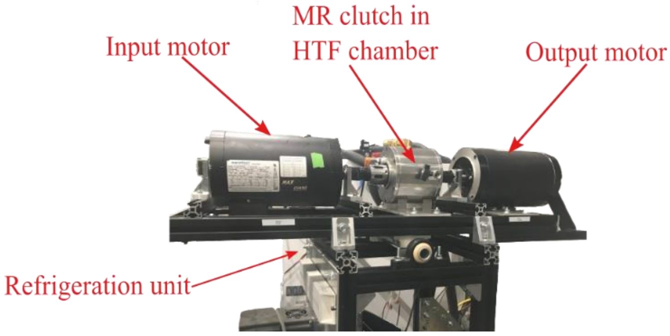

Figure 2 : Assembled test bench

Preliminary tests were conducted to validate the proper integration of each subsystem.

Before wear tests begin, the test bench's physical limitations must be evaluated. Indeed, the true range of torque, rotational speed, and HTF temperature will be determined to observe heat and mechanical losses. These evaluations will ensure the test bench's capacity to meet its requirements. Future presented results will also include real-time MRF wear curves obtained during the test bench's operation.

4. CONCLUSIONS

A test bench was designed and assembled to respond to the discrepancies in MRF wear studies between the laboratory testing and the real operating conditions of an aircraft. A test sequence was elaborated with the project's partners and the test bench will shortly conduct initial MRF wear tests.

ACKNOWLEDGEMENTS

This project is funded through a CRIAQ Exploring Innovation grant (MRFS+) and NSERC Alliance grant (ALLRP 567155-21).

REFERENCES

[1] Boglietti A, Cavagnino A, Tenconi A, Vaschetto S, di Torino P. The safety critical electric machines and drives in the more electric aircraft: a survey. IECON 2009 – 35th Annual Conference of IEE Industrial Electronics. 2009 Nov;2587-94.
[2] Chouinard P, Denninger M, Plante JS. Reliable and lightweight primary flight control actuation using magneto-rheological clutches in slippage. 2015 IEEE International Conference on Robotics and Automation (ICRA). 2015 Jul;213-19.
[3] Desrosiers JF, Lucking Bigué JP, Denninger M, Julió G, Plante JS, Charron F. Preliminary investigation of magneto-rheological fluid durability in continuous slippage clutch. Journal of Physics: Conference Series. 2013 Feb;412(1):012022.
[4] Lucking Bigué JP, Landry-Blais A, Pin A, Pilon R, Plante JS, Xining C, Andrews M. On the relation between the Mason number and the durability of MR fluids. Smart Materials and Structures. 2019 Sep; 28(9):094003.
[5] Bell Textron Canada Limited. Bell 505: Specifications. 2019 Feb.

Simulation Analysis of Whole-spacecraft Vibration Isolation Platform Based on Magnetorheological Fluid Porous Fabric Dampers

Di Xu[1],Xiaomin Dong[2] and Pingyang Li[3]

[1,2,3] State Key Laboratory of Mechanical Transmission, Chongqing University, People's Republic of China
(E-mail: yakamixd@163.com, xmdong@cqu.edu.cn, 20170713098t@cqu.edu.cn)

***Short abstract*:** To effectively enhance the vibration isolation performance of magnetorheological whole-satellite isolation systems under micro-amplitude working conditions, this study designed a novel damper based on magnetorheological fluid porous fabric (MRF-PF). Prototype development and performance analysis were systematically conducted. The vibration isolation capability was ultimately validated through the establishment of a two-degree-of-freedom (2-DOF) simulation platform for whole-satellite vibration isolation..

***Keywords*:** Magnetorheological fluid porous fabric, Whole-spacecraft vibration isolation, Vibration control, Magnetorheological damper.

1. INTRODUCTION

Intense broadband micro-amplitude vibrations throughout the life cycle of a satellite can seriously affect the safety of load-sensitive components such as satellites. The complex mechanical environment causes local damage and failure of key components, which in turn greatly affects the function and service life of the satellite. Whole-spacecraft vibration isolation (WSVI) technology has been proposed and thoroughly studied.

Currently, the WSVI technology mainly consists of two ways of realisation, the first one is to add damping materials on the basis of the traditional cone-shell adapter. The second one is to change the structure of the cone shell adapter to improve the vibration isolation performance of the platform. The method of changing the structure of the cone-shell adapter generally replaces the original rigid cone-shell adapter with a multi-degree-of-freedom active or semi-active vibration isolation platform. Semi-active vibration isolation systems can be classified into galvanic, magnetorheological, solenoidal and pneumatic forms according to their operating principles. where the magnetorheological material can be controlled by an external magnetic field. A reversible change in output damping is achieved within a few milliseconds. It can be used in semi-active vibration isolation systems.

In this paper, a shear magnetorheological broadband micro-amplitude damper is designed based on MRF-PF. The damper was designed to construct a WSVI platform. The machining and assembly of the relevant damper prototype are carried out in this paper. Finally, the vibration isolation performance of the platform is verified by simulation.

2. MRF-PF DAMPER

Magnetorheological materials are the most important working medium in dampers and our team has developed a high performance MRF-PF(Li et al, 2023, 2024; Yan et al, 2022). Using a conventional magnetorheological fluid as a base, the porous nature of the MRF-PF composite was exploited to enhance the performance. Figure 1 illustrates a magnetorheological composite damper structure designed for a WSVI platform.

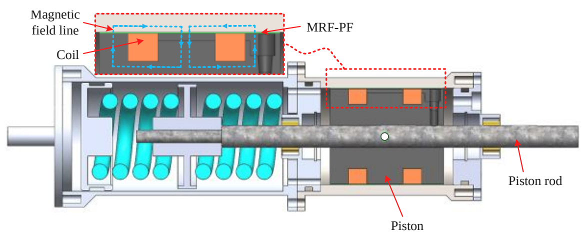

Figure 1: Example graph for the extended abstract.

Performance testing of damper is mainly based on Materials Test Systems (MTS). Take the excitation frequency of 5Hz under the working condition of 0.5mm amplitude as an example. The damping force curves for different current outputs are shown in Figure 2. It can be seen that the damper is capable of a wide range of damping force variations.

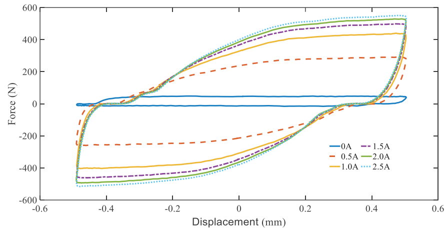

Figure 2: Partial damper test data under 0.5mm amplitude excitation.

3. WSVI PLATFORM DESIGN AND VALIDATION

A six-degree-of-freedom Stewart magnetorheological WSVI platform is designed, and its structural design and simplified mechanical model are shown in Figure 3. The vibration isolation platform is a multi-degree-of-freedom Stewart platform consisting of six MRF-PF dampers. The dampers are mounted and fixed at a specific tilt angle between the upper and lower platforms. An interference fit at the articulation is used to fully transmit the micro-amplitude vibrations to the flexible satellite.

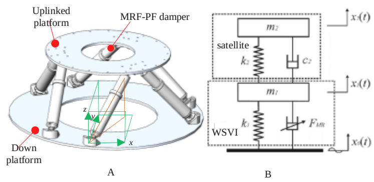

Figure 3:A:Structure of WSVI; B: Simplified dynamic model of WSVI

In this paper, the acceleration response under random excitation is simulated and analysed using the Sky-hook damping Control (SH) algorithm as well as the Acceleration Driven Damper Control (ADD) algorithm. In order to quantitatively evaluate the vibration isolation effect of different control algorithms under random acceleration excitation, the root-mean-square (RMS) values of acceleration under different operating conditions are listed in Table 1.

Table 1: RMS value of satellite acceleration under random excitation

Direction	0A	SH (rate of change)	ADD (rate of change)
Horizontal	3.443	2.411 (29.97%)	2.519 (26.87%)
Vertical	7.053	5.283 (25.1%)	5.329 (24.44%)

The vibration isolation effect of both control strategies on satellite vertical/horizontal wide-frequency random excitation is greater than 24%, indicating that the proposed magnetorheological damper and vibration isolation platform have good wide-frequency vibration isolation performance.

5. CONCLUSIONS

In this paper, the performance of the MRF-PF damper is verified and the micro-amplitude vibration isolation performance of the WSVI platform is simulated and analysed. In the next work, the WSVI experimental platform will be built to experimentally verify the vibration isolation performance of the platform.

REFERENCES

[1] LI PY, DONG XM, RAN JC, et al. Performance evaluation of a novel semi-active absorption and isolation co-control strategy with magnetorheological seat suspension for commercial vehicle. Smart Materials and Structures. 2024 OCT;33(10): 105016.

[2] LI PY, DONG XM, YAN H, et al. Performance evaluation of magnetorheological fluid porous fabric composite based on a novel constitute model. 2023 OCT; 322: 117363.

[3] YAN H, WU LF, LI PY, et al. Performance Analysis of Magnetorheological Porous Fabric Composite. APPLIED SCIENCES-BASEL. 2022 DEC;12(23): 12062.

Experimental study of centrifugal pumping of magnetorheological fluid

Tim Dumais[1], Jean-Sébastien Plante[2] and David Rancourt[3]

[1,2,3]Interdisciplinary Institute for Technological Innovation (3IT), Université de Sherbrooke, Canada
(E-mail: Tim.Dumais@Usherbrooke.ca, Jean-Sebastien.Plante@USherbrooke.ca, David.Rancourt2@USherbrooke.ca)

***Short abstract*:** This study investigates the potential of using a centrifugal pump to handle magnetorheological fluid with the ultimate goal of integrating such a pump directly into a magnetorheological clutch to increase magnetorheological clutch life and stabilize performance over time. Experimental characterization reveals that the standard scaling laws for centrifugal pumps provide accurate predictions of performance with changes in rotation speed, but do not fully account for geometric effects when scaling pump size. Results also suggest that a centrifugal pump of 46 mm in diameter such as tested here could effectively circulate magnetorheological fluid at 540 mL/min on a commercial magnetorheological clutch.
***Keywords*:** Magnetorheological, pump, centrifugal, sedimentation, durability

1. INTRODUCTION

Magnetorheological (MR) actuators have shown great potential to replace high-maintenance and environmentally harmful hydraulic actuators in aerospace flight control applications [1]. However, some challenges remain to be mitigated: (1) MR fluid have a finite lifetime [2], and (2) the density difference between carbonyl iron powder and carrier fluids leads to sedimentation [3]. Theses two challenges results in an actuator performance that can vary over time depending on the state of the fluid. A mitigation is to force MRF circulation in the shear interfaces of the clutch to distribute wearing on the entire fluid volume within the clutch and to mitigate the impact of sedimentation by continuously remixing the fluid.

In this study, a centrifugal pump is investigated to circulate MRF with the ultimate goal of integrating such a pump directly into a magnetorheological clutch in the future. This paper has two objectives of: (1) determining whether MRF pumping adheres to the usual centrifugal pump scaling laws despite high particle concentrations to ease the design of MRF centrifugal pump, and (2) assessing the feasibility of centrifugal pumping in a 70 mm diameter, commercial drum-type MR clutch.

2. METHODOLOGY AND EXPERIMENTAL TEST BED

A theoretical model of the hydraulic circuit formed by the shear interfaces of the commercial MR clutch is produced to set a targeted pressure versus flow rate curve. A matching centrifugal pump design is proposed and shown in Figure 1a. The pump design is scaled to two different sizes, built, and tested. The diameters of the tested impellers are 23 mm (D1) and 46 mm (D2). The two pump prototypes are characterized on the pump characterization test bed shown in Figure 1b. The MRF flow rate is measured in open loop with a load cell while the head is measured with a differential pressure sensor. The pump curves are measured by starting the pump with the restrictor valve wide open and gradually closing it.

Four pump curves are measured (1050, 1250, 1500 and 2000 RPM) for the D2 impeller, and two are measured (2250 and 2750 RPM) for the D1. Three of the D2 pump curve (1050, 1500 and 2000RPM) are used to develop a semi-empirical model. The other D2 pump curve (1250 RPM) is used to validate the developed model. Dimensionless pump curves are generated from the experimental results with the dimensionless capacity coefficient C_Q and heat coefficient C_H. The pump curve obtained from the semi-empirical model of the D2 impeller and the hydraulic system model are plotted together to determine the operating point and consequent flow rate through a shear interface of the commercial drum clutch.

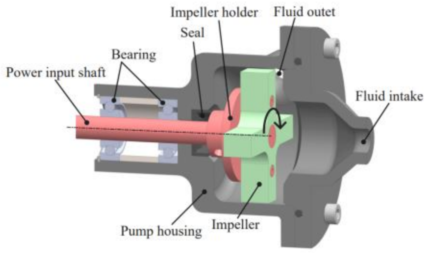

(a)

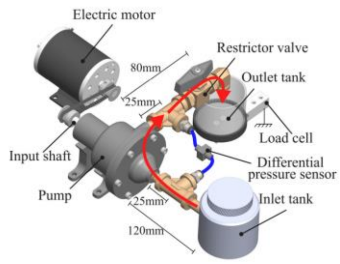

(b)

Figure 1: (a) MRF centrifugal pump (b) Pump characterization test bed.

3. RESULTS AND DISCUSSION

The dimensionless pump curves for different rotation speeds are presented in Figure 2a. Since the D1 and D2 pump design are geometrically similar, all curves should overlap regardless of impeller size or rotational speed. However, the results show a noticeable difference between the D1 and D2 curves with the bigger pump, D2, demonstrating better performance. It is hypothesized that the pump efficiency varies non-linearly when using two-phase fluids like MRF. Nevertheless, for a given impeller size, the curves are similar, confirming that scaling laws can accurately predict performance changes with varying rotation speeds.

The D2 pump curves are used to generate a semi-empirical pressure-flow model of a pump. Figure 2b shows the pump curves obtained from the model and the pressure-flow data at 1250 RPM that was kept for validation (not used for model calibration). The agreement between the model and validation data is strong, with a relative error of only 2%. Finally, Figure 2b also shows the pressure losses of a MRF flow across the shear interfaces of the commercial MR clutch. The pressure range produced by the pump would enable high flow rates in the clutch. For example, at 1500 RPM, the flow rate would be 540 mL/min which is, for a clutch with internal cavity volume of 30 mL, is plenty sufficient to assure fluid mixing.

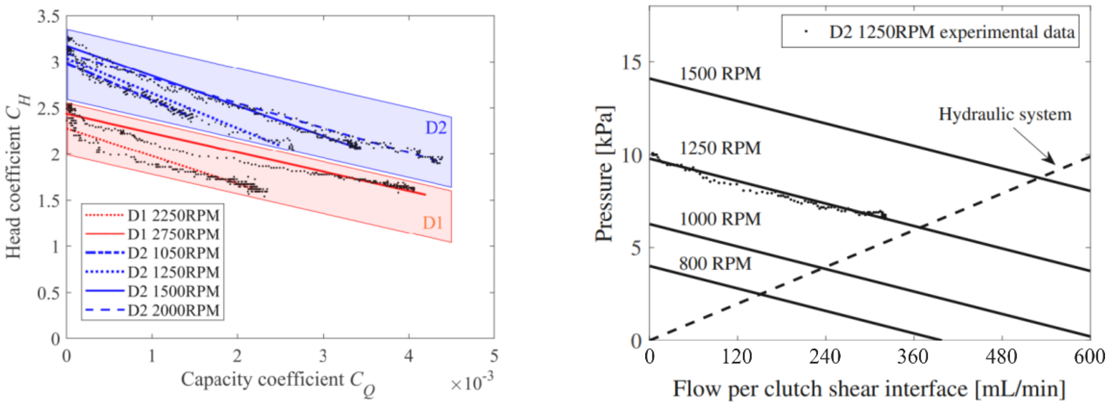

(a) (b)

Figure 2: (a) Dimensionless pump curve for centrifugal pump with MRF (b) Operating point of centrifugal pump with D2 impeller in a commercial MR clutch.

4. CONCLUSIONS

This work studied the potential of centrifugal pumping MRF. Two centrifugal pumps have been designed and bench-tested. Usual centrifugal pump scaling laws accurately predict performance changes with varying rotation speeds. However, they are less reliable for predicting performance variations when the impeller diameter is scaled, here by a factor of two, because of significant changes in pumping performance. Further investigations should validate the effect of flow rate on fluid mixing and explore two-phase flow computational fluid dynamics to better understand pump performance.

ACKNOWLEDGEMENT

This project is funded through a CRIAQ Exploring Innovation grant (MRFS+), NSERC Alliance grant (ALLRP 567155-21), Université de Sherbrooke.

REFERENCES

[1] Chouinard P, Denninger M and Plante J (2015) Reliable and lightweight primary flight control actuation using magneto-rheological clutches in slippage. 2015 IEEE International Conference on Robotics and Automation (ICRA), pp. 213–219.
[2] Carlson JD (2002) What makes a good MR fluid? Journal of Intelligent Material Systems and Structures, 13(7-8), 431-435.
[3] Kikuchi T, Kumagae T, Abe I and Inoue A (2017) Particle sedimentation in magnetorheological fluid and its effect. 2017 IEEE International Conference on Advanced Intelligent Mechatronics (AIM), pp. 767–772.

Effect of Magnetic Fields on the Melting Process of Magnetic Fluids

Argeena A. Agao-Agao[1], Kazuto Yamashiro[1], Shunta Masuda[1], Yuhiro Iwamoto[1], Yasushi Ido[1], Ignat Tolstorebrov[2], Trygve M. Eikevik[2], Yasutake Hirota[3] and Takuya Miyazaki[3]

[1] Department of Electrical and Mechanical Engineering, Nagoya Institute of Technology, Gokiso-cho, Showa-ku, Nagoya, Aichi, 466-8555, Japan
(E-mail: a.agao-agao.607@stn.nitech.ac.jp)
[2] Department of Energy and Process Engineering, Norwegian University of Science and Technology, Høgskoleringen 1, 7034 Trondheim, Norway
[3] Ferrotec Material Technologies Corporation, Nihonbashi 2-3-4, Chuo-ku, Tokyo, 103-0027, Japan

***Short abstract*:** This study explores the influence of magnetic fields on the melting process of temperature-sensitive magnetic fluid (TSMF) for phase change thermal energy storage applications. Without a magnetic field, melting occurs primarily through conduction, resulting in a slower process. However, the melting rate significantly increases under both uniform and non-uniform magnetic fields due to magnetically driven convection enhancing heat transfer. The findings highlight the potential of TSMF to improve phase transition efficiency, making it a promising material for adaptive thermal management and energy-efficient cooling systems.
***Keywords*:** Magnetic fields, melting process, phase-change, temperature-sensitive magnetic fluid.

1. INTRODUCTION

The increasing demand for cooling, driven by urbanization and rising global temperatures, underscores the need for efficient thermal energy storage solutions [1]. Cold thermal energy storage (CTES) systems improve cooling efficiency by shifting energy consumption away from peak periods, reducing grid strain and operational costs [2]. Phase change materials (PCMs) are widely used in CTES for their high latent heat storage capacity, but their low thermal conductivity limits heat transfer efficiency [3].

To enhance PCM performance, researchers have explored nanofluids, including magnetic nanofluids, which enable heat transfer control via external fields [4,5]. Temperature-sensitive magnetic fluids (TSMF), composed of ferromagnetic nanoparticles with a low Curie temperature, exhibit magnetization changes with temperature, making them a promising material for thermal management [6]. While TSMFs have been studied for heat transfer applications, their melting behavior under external magnetic fields remains largely unexplored.

2. OBJECTIVES

This study aims to investigate the potential of TSMF as a PCM for CTES systems by examining its melting behavior under uniform and non-uniform magnetic fields. Specifically, the research will focus on measuring temperature variations and analyzing the thermomagnetic convection effects to assess the feasibility of TSMF for enhanced thermal energy storage applications.

3. MATERIAL AND METHODOLOGY

This experiment investigates the behavior of TC3030W, a water-based TSMF from Ferrotec Materials Technology, under different magnetic field conditions.

As shown in Figure 1, the setup comprises a Peltier controller (1) that regulates temperature, a computer (2) and data logger (3) for monitoring, and a constant temperature bath (4) serving as a heat sink. A magnetic field generator (5) applies uniform or non-uniform fields to analyze thermomagnetic convection. Insulation (6) reduces external thermal interference, while the measurement section (7) houses the TSMF in a Teflon container. The setup investigates heat transfer during the melting process under magnetic influence.

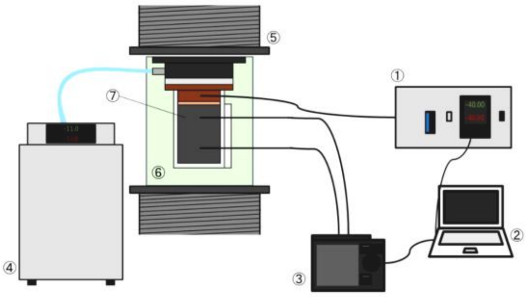

Figure 1: Schematic diagram of the experimental set-up.

4. RESULTS AND DISCUSSION

In the analysis of the melting behavior of TC3030W, the presence of a magnetic field significantly influences heat transfer. The melting time for the TSMF (TC3030W) is shown in Table 1 for different magnetic fields. Without a magnetic field, the material melts in 90.1 min, indicating a slower heat transfer mechanism mainly driven by conduction. However, when a uniform magnetic field is applied, the melting time drastically decreases to 20.5 min, demonstrating a substantial 77.2% reduction. This implies that the magnetic field induces strong internal convection within the TSMF, enhancing thermal transport. Similarly, a non-uniform magnetic field results in a melting time of 20.7 min, showing a comparable 77.0% decrease. The minimal difference between uniform and non-uniform fields suggests that both configurations effectively improve heat transfer, likely by generating fluid motion through magnetically driven convection. The movement of magnetic particles under the field facilitates a more efficient redistribution of heat, thus speeding up the melting process. This behavior highlights the potential of ferrofluids for adaptive thermal management applications, where regulated heat transfer is essential.

Table 1: Comparison of the melting time for the TSMF (TC3030W).

Magnetic Field	Time (min)	Abs. Diff. w/ no magnetic field (min)	Rel. Diff. w/ no magnetic field (%)
Without	90.1	-	-
Uniform	20.5	-69.6	-77.2
Non-uniform	20.7	-69.4	-77.0

5. CONCLUSIONS

This study demonstrated that the application of a magnetic field significantly enhances the heat transfer efficiency of TSMF by inducing thermomagnetic convection. Both uniform and non-uniform magnetic fields accelerated the melting process, reinforcing the potential of TSMF for adaptive thermal management in cooling applications. Future research should explore on developing the properties of TSMF and optimizing magnetic field configurations and thermal properties for improved performance. Additionally, investigating the effects of different magnetic field strengths and orientations, as well as integrating TSMF into real-world thermal energy storage systems, will further enhance its practical applications.

ACKNOWLEDGEMENT

The research mobility was supported by the Interdisciplinary Education and Research Platform in Cold-Chain of Fish: From Norway to Japan, Research Council of Norway (Project code: 309841).

REFERENCES

[1] International Energy Agency (IEA). The Future of Cooling. 2018.
[2] Dincer I, Rosen M. Thermal energy storage: systems and applications. John Wiley & Sons; 2002.
[3] Farid MM, Khudhair AM, Razack SA, Al-Hallaj S. A review on phase change energy storage: materials and applications. Energy Conversion and Management. 2004 Jun;45(9):1597–1615.
[4] Harikrishnan S, Devaraju A, Rajesh Kumar G, Kalaiselvam S. Improved thermal energy storage behavior of a novel nanofluid as phase change material (PCM). Materials Today: Proceedings. 2019 Jan 1;9:410–421.
[5] Rosensweig RE. Ferrohydrodynamics. Cambridge University Press; 1985.
[6] Rong Z, Iwamoto Y, Ido Y. Thermal flow analysis of self-driven temperature-sensitive magnetic fluid around two cylinders arranged in tandem. Results in Engineering. 2022 Dec 1;16:100660.

A Giant Electrorheological Fluid Damper Prototype Functions in Shear-Flow Hybrid Mode and Its Performance

Zihao Qiu[1], Hongliang Dou[1], Xiaorui Cui[1], Siyu Yang[2] and Weijiw Wen[1,2]

[1] The Advanced Material Thrust, The Hong Kong University of Science and Technology (Guangzhou), Guangzhou 511458, China
(E-mail: zqiu452@connect.hkust-gz.edu.cn(Z. Qiu))
[2] Department of Physics, The Hong Kong University of Science and Technology, Hong Kong 999077, China
(E-mail: phsidney@ust.hk(S. Yang), phwen@hkust-gz.edu.cn(W. Wen))

Short abstract: This paper introduced the structure and force versus shear/flow-rate/electric-field test results of a damper prototype based on giant electrorheological fluid(GERF). Unlike most ER dampers have been investigated, this prototype functions in a hybrid mode of shear and flow. Tension test results show that the damping force of this prototype has a strong dependence on shear/flow rate and applied electric field - with low shear/flow rate, applied electric field dominates the damping force; while with high shear/flow rate, the effect applied electric field on damping force gradually dwindles.
Keywords: electrorheological(ER) fluid, damper, damping force, shear mode, flow mode.

1. INTRODUCTION

ER Technology has entered a new era since the development of GERF[1][2]. Although ER fluids possessing novel properties have been emerging in recent years, GERF consisting Ba-Ti-O nano-particles coated with urea is still one of the most widely used ER materials in research and industry due to the well-designed synthesis process and commercialized fabrication.

In this paper we proposed a damper prototype functions in a hybrid mode of shear and flow with GERF as the working medium, followed by a series of preliminary tests concerning the relationship between damping force, shear/flow rate and electric field. It is worth a mention that the peak velocity in the test has reached 0.6m/s, which is very close to an authentic velocity an automotive damper would be dealing with in practice, thus the results might be of reference value to engineering applications.

2. OBJECTIVES

This paper aims to provide a brief introduction to the structure of a ER damper prototype and its performance under different shear/flow rate and electric field. The design and data could, if effective, provide a deeper insight into the mechanism of ER dampers and be reference for further researches.

3. MATERIAL AND METHODOLOGY

3.1. STRUCTURE AND PROTOTYPE

Fig.1 shows the internal structure of the prototype with the shell being translucent. In this prototype, the shell works as the negative electrode and the positive electrode is set within the piston head. There are 6 insulating, smooth cylinders embedded on the positive electrode to keep the 0.8 mm gap between electrodes. Besides, the effective area of the electrode is approximate 1,778 mm^2.

When the damper being stretched or compressed, electrodes move relative to each other while GERF flows through the gap in-between them, thence the ER fluid is working in a hybrid mode of shear and flow.

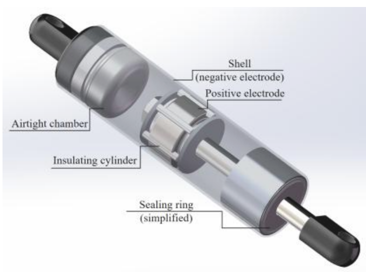

Figure 1: Structure of the prototype.

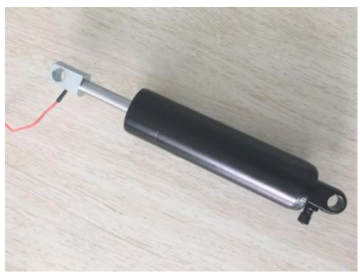

Figure 2: Photograph of the prototype.

3.2. TEST METHODOLOGY

The damper prototype was tested with an automotive shock absorber testing system. Four sets of quasi-sinusoidal waves with an amplitude of 50mm(± 25mm) were applied, the peak velocity of each reaches 0.05, 0.1, 0.3 and 0.6m/s, respectively. Within each set, forces without electric field and with applied voltage from 1k to 3kV were recorded.

4. RESULTS AND DISCUSSION

Fig.3 shows the relationship between damping force and displacement with peak velocities mentioned above, while Fig.4 provides a deeper look into the dependence damping force on shear/flow rate and applied electric field.

Results show that the damping force of this prototype has a strong dependence on shear/flow rate and applied electric field - with low shear/flow rate, applied electric field dominates the damping force; while with high shear/flow rate, the effect applied electric field to damping force gradually dwindles.

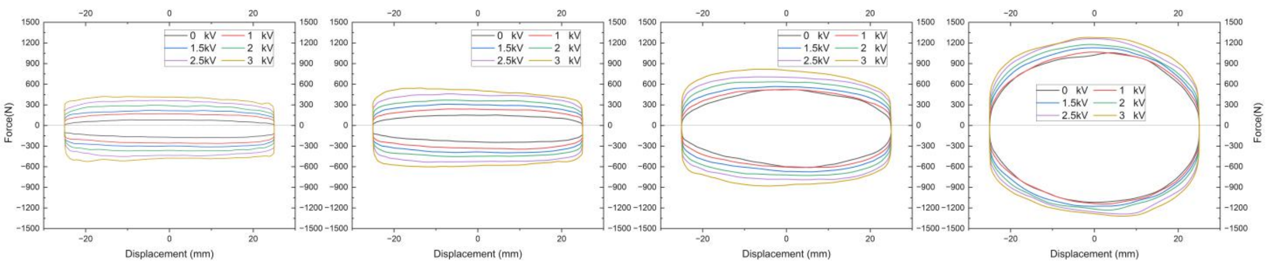

Figure 3: Damping force results with peak velocity of 0.05/0.1/0.3/0.6 m/s (from left to right).

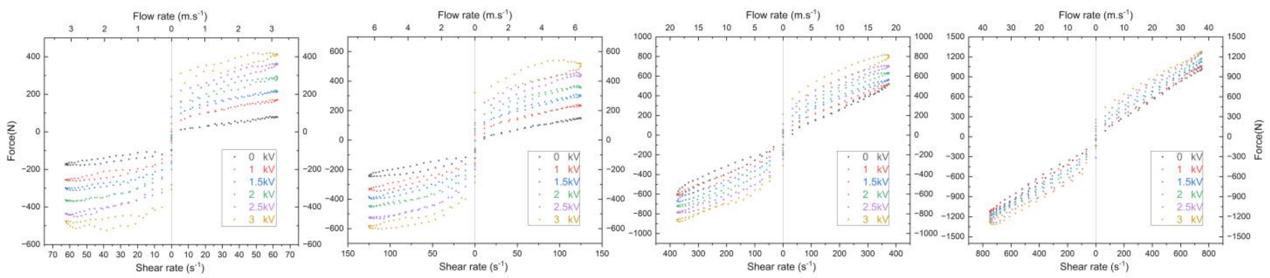

Figure 4: Damping force results with shear/flow rate derived from velocity and prototype dimensions.

5. CONCLUSIONS

Knowing that high shear/flow rate has an innegligible effect on the performance of an ER damper, further investigations concerning ER fluids as well as damper designs for potential shocks should take high rate into consideration. How to decrease the shear/flow rate at which ER fluids work so as to make the damping force more tunable and controllable could be as well another important issue in future researches.

ACKNOWLEDGEMENT

Thanks for Tingyong LU for his work in the fabrication and tests of the prototype. This research is supported by the postgraduate scholarship provided by the Hong Kong University of Science and Technology(Guangzhou).

REFERENCES

[1]Wen, W., Huang, X., Yang, S., Lu, K., & Sheng, P. (2003). The giant electrorheological effect in suspensions of nanoparticles. Nature Materials, 2(11), 727–730.

[2]Liang, Y., Huang, D., Zhou, X., Wang, Z., Shi, Q., Hong, Y., Pu, H., Zhang, M., Wu, J., & Wen, W. (2023). Efficient Electrorheological Technology for Materials, Energy, and Mechanical Engineering: From Mechanisms to Applications. Engineering, 24, 151–171.

On the operational speed limit of magnetorheological clutches

Frédérick Bérubé, Jean-Sébastien Plante and David Rancourt
Interdisciplinary Institute for Technological Innovation (3IT), Université de Sherbrooke, Canada
(E-mail: Frederick.Berube@USherbrooke.ca, Jean-Sebastien.Plante@USherbrooke.ca, David.Rancourt2@USherbrooke.ca)

Short abstract: Using magnetorheological clutches in power transmission applications, such as automotive powertrains, implies that the fluid enters solid-body rotation for relatively long durations, with or without magnetic field influence. In such conditions, centrifugal acceleration could cause sedimentation and thus, affect intended functionality. Preliminary observations suggest that sedimentation occurs when crossing a threshold of centrifugal acceleration. This paper quantitatively assesses the threshold behavior under controlled laboratory conditions and investigates the influence of the fluid's formulation on the threshold occurrence. Experimental results indicate a 100g threshold for the tested proprietary fluid, whereas centrifugal acceleration always triggered sedimentation for a fluid without additives.
Keywords: Magnetorheological Fluid, Clutch, Centrifugal, Sedimentation, Additives

1. INTRODUCTION

Magnetorheological (MR) clutches have been studied extensively in robotics [1] and vibration control applications [2]. However, there is comparatively much less research in power transmission applications, even though their high torque controllability suggests a strong potential for vibration control and/or impact management. Compared to robotics and vibration control applications, power transmission applications such as found in automotive powertrains present unique operating conditions, with higher rotating speeds and where fully-locked or fully-unlocked modes may be held for extended periods of time (hours vs seconds). Preliminary experiments with overspeeding various MR clutch designs beyond the operating limits seen in robotics and vibration control suggests the existence of a clutch-specific "speed threshold". Once such a threshold is exceeded, a significant increase in viscous drag torque is measured. As shown in Figure 1 (a), upon disassembling an over speeded clutch, it is found that the fluid had became a near solid-state ("hard cake") in the clutch's outer periphery. The normally homogenously suspended carbonyl iron particles (CIPs) separate to form distinct solid and liquid phases. The mechanism responsible for this behaviour is the centrifugal acceleration that acts on the particles, throwing them out to the outer wall of the fluid cavity, as illustrated in Figure 1b.

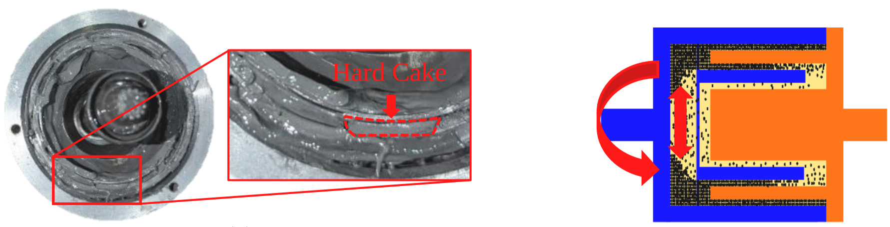

(a) (b)

Figure 1: (a) Resulting hard cake between the clutch drums **(b)** Clutch cross-section schematic of centrifugation

The objective of this paper is to conduct an experimental study of the behaviour of the speed threshold phenomenon in simplified laboratory conditions. The test conditions replicate centrifugal acceleration found in a clutch for power transmission applications, but in a centrifuge machine. Different fluid formulations are also tested in order to understand possible effects of MR fluid additives on the rotational speed threshold. Operating variables of clutch geometry, slippage speed, and magnetic field are left out for future work.

2. MATERIAL AND METHODOLOGY

Two fluid formulations are tested. Both fluids have a target value of 40%v/v CIP concentration. The first fluid is a proprietary fully formulated fluid, incorporating conventional MRF additives such as antiwear, thixotropic and surfactant agents. The second fluid contains no additives other than a minimal quantity of dispersant, which facilitates the process of remixing prior to each test. This manipulation ensures repeatable properties between samples. Nevertheless, owing to the simplicity of its formulation, the second fluid is regarded as a fluid without additives.

Centrifugation of both fluids is conducted using the LUMiSizer, a centrifuge equipped with a light transmission sensor. At each timestamp, the LUMiSizer measures the amount of light passing through the fluid sample and outputs a curve. The presence of solid content results in the obstruction of the light passing through the vial, which decreases the local measurement of light transmission. An example of the LUMiSizer output is shown in Figure 2 (a). The results are presented in a color gradient, with the red lines indicating the beginning of the test and the green lines marking the end. The red dash lines indicate the meniscus of fluid and the bottom of the vial, to measure the total height of fluid. The green dash line indicates the CIP sedimentation front, and the blue dash line indicates the additives sedimentation front. Given that the height of fluid remains constant and the sedimentation front progresses towards the bottom, it is possible to calculate the evolution of the CIP concentration in the hard cake. This metric is illustrated in Figure 2 (b), and helps understanding the sedimentation speed, the time before sedimentation starts and the final concentration in the cake compare to the initial homogeneous concentration (red dash line).

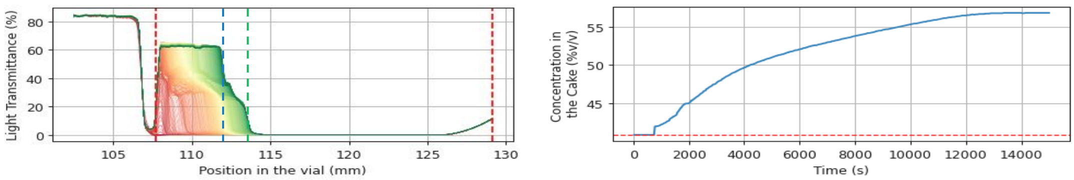

(a) (b)

Figure 2: (a) LUMiSizer's raw result - Fluid with additives at 40g for 15ks **(b)** Extracted sedimentation metric

3. RESULTS AND DISCUSSION

The evolution of the concentration of CIP in the hard cake is compared for both fluid under increased centrifugal acceleration up to 100g. Results are shown in Figure 3 for a 1 hr (3600 s) timeframe.

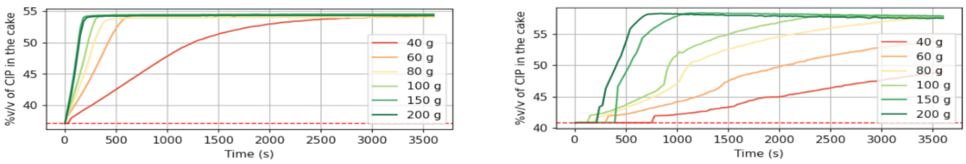

(a) (b)

Figure 3: Evolution of CIP concentration in the cake for **(a)** Fluid Without Additives **(b)** Fluid with Additives

As shown in Figure 3 (b), there is a time delay before sedimentation actively starts. The delay gradually reduces as centrifugal acceleration increase, eventually becoming almost null at about 100g. On the contrary, all samples of the fluid without additives on Figure 3 (a) started to sediment as soon as centrifugal acceleration is applied. For the curves below 100g for the fluid with additives, sedimentation progresses gradually until a maximum sedimentation concentration is reached. Above 100g, the sedimentation starts suddenly and quickly reaches its maximum concentration, with a comparable speed to the fluid without additives. The additives therefore have a significant ability to resist or retard centrifugal sedimentation, setting a speed threshold above which sedimentation is instantaneous.

4. CONCLUSION

As shown by the centrifugation tests, the additives have the ability to retard the onset of sedimentation for some time delay. For the tested fluid with additives, a delay is observed until a threshold of 100g is reached, beyond which sedimentation starts suddenly with a rate comparable to the fluid without additives. Results suggests that the fluid formulation and presence of additives explains, at least in part, the rotational speed threshold observed in rotary MR clutches. Future work should focus on the impact of the clutch geometry and magnetic field on centrifugal sedimentation.

ACKNOWLEDGEMENT

This project is funded through a CRIAQ Exploring Innovation grant (MRFS+) and NSERC Alliance grant (ALLRP 567155-21). The team would also like to highlight the contribution of Infineum UK Ltd. in providing the MRF and laboratory test equipment that were used in this study.

REFERENCES

[1] A. St-Jean, F. Dorval, J.-S. Plante, and A. Lussier-Desbiens, "Magnetorheological-Actuators: An Enabling Technology for Fast, Safe, and Practical Collaborative Robots," *IEEE Trans. Robot.*, vol. 40, pp. 1261–1272, 2024, doi: 10.1109/TRO.2023.3341573.

[2] W. East, J. Turcotte, J.-S. Plante, and G. Julio, "Experimental assessment of a linear actuator driven by magnetorheological clutches for automotive active suspensions," *J. Intell. Mater. Syst. Struct.*, vol. 32, no. 9, pp. 955–970, May 2021, doi: 10.1177/1045389X21991237.

Development of Autonomous Mobile Robot with Semi-active Universal Joint using Rotational Magnetorheological Fluid Damper

Taiki Mieda[1], Yudai Moriki[2], Zhu Hongzhou[2], Isao Abe[3] and Takehito Kikuchi[3]

[1] Graduate School of Science and Technology, Oita University, Japan
[2] Graduate School of Engineering, Oita University, Japan
[3] Faculty of Science and Technology Oita University, Japan
(E-mail: t-kikuchi@oita-u.ac.jp)

Short abstract: Autonomous Mobile Robots (AMRs) typically travel on level ground, but some are designed and developed to operate in uneven environments. We have developed a magnetorheological fluid (MRF)-based semi-active universal joint (SAUJ) as a horizontal stabilization unit for stable delivery equipment that can be attached to AMRs. Furthermore, an optimal path planning approach was conducted to match the characteristics of the SAUJ. In the optimal path planning, the trajectory was generated considering changes in ground angle and sway caused by centrifugal acceleration.

Keywords: Magnetorheological fluid, Rotational MR fluid damper, Autonomous mobile robot, Path planning

1. INTRODUCTION

AMRs are typically designed to operate on level terrain. However, some AMRs are specifically developed to navigate uneven and challenging environments, such as those encountered in agriculture, disaster response, and hazardous conditions that pose risks to humans. Navigating such rugged terrain presents significant challenges from various perspectives, including locomotion methods, structural design, sensing technologies, and path planning strategies.

2. OBJECTIVES

As shown in Fig. 1, we have developed an AMR capable of traversing uneven terrain, with the long-term goal of utilizing it as a charging station for unmanned aerial vehicles (UAVs). This paper reports on the development of a semi-active universal joint (SAUJ) using magnetorheological fluid (MRF) as a horizontal stabilization mechanism for the charging spot, as well as the optimal path planning for the AMR equipped with this mechanism. MRFs exhibit reversible and highly responsive MR effects, making them suitable for various engineering applications. We have previously developed MRF devices with rotor configurations [1] and utilized them as posture control elements, which serve as the basis for this study.

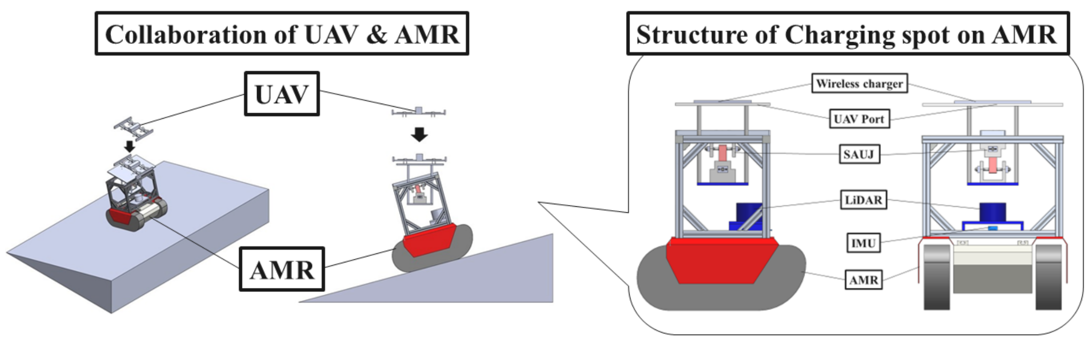

Figure 1: Goal of this study

3. METHODOLOGY

3.1. SAUJ on AMR

The SAUJ is a swing control unit that can be mounted on AMRs. Its basic structure consists of a universal joint equipped with rotational MR fluid dampers, which are placed on both the pitch and roll axes. The gap between the MRF layers has been optimized to improve torque performance [2]. The system uses an Arduino

Due for control, and by performing serial communication with ROS2, it can suppress swings during acceleration and deceleration. Due to its pendulum motion, the SAUJ is significantly affected by acceleration and centrifugal forces.

3.2. Path planning for SAUJ

To achieve swing-suppressing path planning based on the map created by SLAM, the A* algorithm [3] was improved by considering the following elements. First, angle swing was introduced as a cost to reduce swing risks. Additionally, angle constraints were applied to avoid slopes steeper than 20 degrees, and vehicle width was considered to enhance safety. Finally, the generated paths were smoothed using spline interpolation, and constraints were added to ensure that centrifugal acceleration does not exceed a certain threshold, resulting in a path suitable for the SAUJ.

4. RESULTS AND DISCUSSION

Figures 2 and 3 show the paths without/with the SAUJ control. From the results, it was observed that with SAUJ control, the system could handle relatively sharp curves, whereas without SAUJ control, the generated trajectory tended to follow gentler curves. Additionally, although the trajectory without SAUJ control was shorter in distance, it deviated significantly from the original path, suggesting that the trajectory with SAUJ control is preferable in terms of safety.

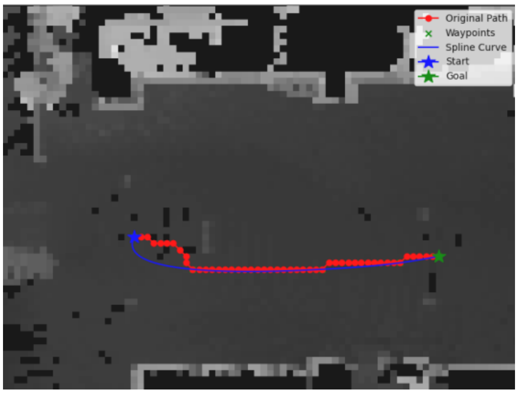

(a) Without SAUJ control

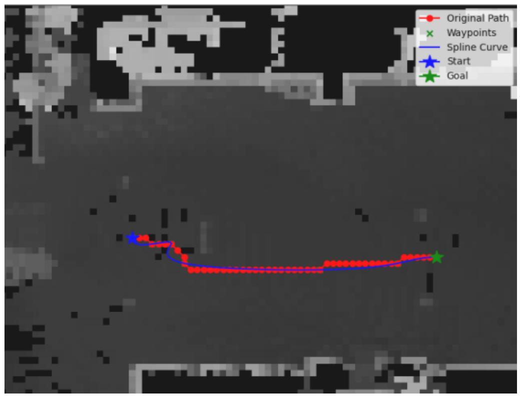

(b) With SAUJ control

Figure 2: Results of path planning with/without SAUJ control

5. CONCLUSIONS

In this study, we proposed the development of an all-terrain AMR equipped with a charging function for UAVs. In this report, we developed the swing control unit (SAUJ), and an optimal path was planned considering its characteristics. As a result of the path planning, a path was created that suppresses the swing caused by the pendulum characteristics of the SAUJ and uneven ground.

ACKNOWLEDGEMENT

This study was partially supported by Kurata Grants of the Hitachi Global Foundation (1555) and the Fund Program for Creating Research-based Startups from Academia (Grant Number JPMJSF23DW).

REFERENCES

[1] Takehito Kikuchi, Kikuko Otsuki, Junji Furusho, Hiroya Abe, Junichi Noma, Makio Naito and Nicolas Lauzier, "Development of compact MR fluid clutch for human-friendly actuator", Advanced Robotics, 24 (10), pp.1489-1502, 2010

[2] Yudai Moriki, Isao Abe, Takehito Kikuchi, "Development of Semi-active Universal Joint with Rotational Magnetorheological Fluid Damper for Unmanned Ground Vehicle", IEEE International Conference on Advanced Intelligent Mechatronics, pp.609-614, 2024

[3] Bo Zhang, Guobin Li, Qixin Zheng, Xiaoshan Bai, Yu Ding, Awais Khan, "Path Planning for Wheeled Mobile Robot in Partially Known Uneven Terrain", Sensors, 22 (14), 5217, 2022

Magnetorheological fluids under perturbating magnetic fields

Guillermo Camacho[1], Jesús García-Gutiérrez[1], Óscar Martínez-Cano[1], José R. Morillas[1], Stefania Nardecchia[1] and Juan de Vicente[1]

[1] Magnetic Soft Matter Group. Applied Physics Department. University of Granada, Spain
(E-mail: guillermocamacho@ugr.es, jesusjgg@ugr.es, omcano@ugr.es, jmorillas@ugr.es, stefania@ugr.es, jvicente@ugr.es)

Short abstract: This study investigates the mechanisms underlying self-assembly in MR fluids under the influence of a perturbing magnetic field. By combining a static field with an orthogonal oscillatory component, we explore the assembly process through experiments conducted using a custom-made device operating at high frequency, particle-level simulations, and energy minimization calculations. The manuscript concludes by highlighting the role of time-varying magnetic fields in enhancing the magnetorheological effect and guiding cell growth within hydrogels.
***Keywords*:** Time-dependent field, Perturbating fields, Layer formation, Biocompatible Hydrogel, Self-assembly.

1. INTRODUCTION

Magnetorheological (MR) fluids subjected to steady magnetic fields are well known to form aligned columnar structures that impart yield stress [1]. However, the application of time-varying magnetic fields facilitates the assembly of novel microstructures, enhancing their overall physicochemical properties. The interplay between hydrodynamic forces and magnetic interactions in these dynamic environments gives rise to complex self-assembly mechanisms, enabling new functionalities that go beyond conventional MR effects [2]. In this study, we investigate the formation mechanisms of magnetic mesostructures in MR fluids under a perturbating magnetic field, specifically by combining a static field with an orthogonal oscillatory component (Figure 1a) [3].

2. OBJECTIVES

This study aims to understand the mechanisms governing the formation of magnetic layers in MR fluids subjected to perturbating magnetic fields. The objective is to explore the role of interparticle interactions and field parameters in determining the material's structural and mechanical responses for biomedical applications. To achieve this, we conducted experiments, energy landscape analyses, and particle-level simulations.

3. MATERIAL AND METHODOLOGY

Perturbating magnetic fields are generated using a custom-built triaxial magnetic field generator [4] that is connected to a fractal capacitor bank and capable of producing time-dependent magnetic fields along the three spatial dimensions, with frequencies up to 4 kHz. Through high-speed and confocal microscopy, we studied how field parameters and sample confinement influence the morphology of the assembled layers. Langevin Dynamics were also performed to predict the phase diagram in MR fluids self-assembly under perturbating magnetic fields and to explain the spacing between layers as a function of sample height. Additionally, energy landscape calculations were carried out to further elucidate the layered structure. Finally, these layered structures were embedded within a hydrogel matrix to serve as an anisotropic scaffold for directed cell growth.

4. RESULTS AND DISCUSSION

4.1. Self-assembly and phase diagram

The final assembled structure under perturbating magnetic fields is essentially governed by two parameters: the perturbation angle (the ratio of the unsteady to static components) and the Mason number (the ratio of hydrodynamic to magnetic forces). At very low and high angles, the effective interaction is similar to that of a uniaxial steady field, leading to the formation of classical columnar structures. However, at intermediate angles, the effective interactions cause the particles to assemble into parallel layers along the field plane. Based on the Mason number we can distinguish between dynamic layer assembly (where magnetic forces dominate) and time-averaged interactions (where hydrodynamic forces dominate). See Figure 1b.

4.2. Influence of confinement

Through experiments, particle-level simulations, and energy minimization calculations, we demonstrate that the separation between layers can be controlled by sample confinement. Our results reveal a positive power-law relationship between layer spacing and sample height.

4.3. MR effect and directed cell growth

Finally, we demonstrate that time-dependent magnetic fields serve as a powerful tool to enhance the magnetorheological response (Figure 1c), as well as to utilize magnetic layered patterns as scaffolds for directed cell growth within hydrogels (Figure 1d). When these layers are embedded in gelatin/laminarin hydrogels, the structures induce a high degree of cellular alignment, offering promising opportunities for engineering tissues with anisotropic organization.

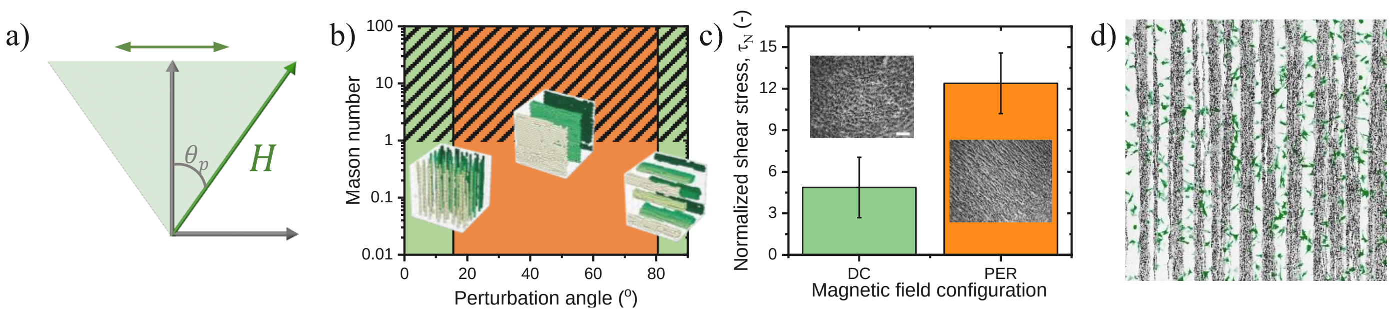

Figure 1: a) Perturbating magnetic field configuration, consisting of the superposition of a steady and an orthogonal oscillatory field component. b) Particle level simulations phase diagram. Orange for layered structures and green for chains and columns. Dashed zones correspond to dynamic structures (magnetic force dominated). c) MR effect enhancement under perturbating magnetic fields. Normalized shear stress for steady (DC) and perturbating fields (PER), plotted along with rheo-microscopy images showing the different internal structures while shearing d) Confocal micrograph of the layered structures assembled along the oscillatory field plane within a hydrogel matrix. Fibroblasts, dyed in green, grow along the direction of the structure.

5. CONCLUSIONS

Perturbating magnetic fields offer a novel approach to controlling microstructure formation and enhancing the magnetorheological response. The findings suggest promising applications in biomedical engineering, particularly in developing anisotropic tissue structures.

ACKNOWLEDGEMENT

This work was supported by projects PID2022-138990NB-I00 and TED2021.129384B.C22 funded by MCIN/AEI/10.13039/501100011033 and by EU NextGenerationEU/ PRTR. G. C. acknowledges the financial support by the FPU20/04357 fellowship. J. R. M. acknowledges the financial support by (EFST)-H2020-MSCA-IF-2020 (Grant 101030666) fellowship.

REFERENCES

[1] Morillas, J. R., de Vicente, J. Magnetorheology: a review. Soft Matter. 2020;16(42);9614–9642.
[2] Martin, J. E., Snezhko, A. Driving self-assembly and emergent dynamics in colloidal suspensions by time-dependent magnetic fields. Reports on Progress in Physics. 2013;76;126601.
[3] Terkel, M., de Vicente, J. Magnetorheology of exotic magnetic mesostructures generated under triaxial unsteady magnetic fields. Smart Materials and Structures. 2021;30;014005.
[4] Tajuelo, J., Martínez-Cano, O., Morillas, J.R., Yang, J., de Vicente, J. Generation of synchronized high-frequency triaxial magnetic fields using fractal capacitor banks. Physical Review Applied. 2023;20;044063.

Modeling of Abrasive Magnetorheological Fluids for Drag Finishing

Fabian Sordon[1], Jürgen Maas[2]

[1, 2] Mechatronic Systems Lab EMK, Technische Universität Berlin, Germany
(E-mail: f.sordon@tu-berlin.de)

Short abstract: The application of abrasive magnetorheological fluids for the cutting edge preparation of milling tools has been previously investigated. In this study, the behavior of abrasive MR fluids is analyzed through two modeling approaches: on the one hand a microscopic framework based on the well-established model of dipole-dipole interaction, and on the other hand from a macroscopic perspective using the Bingham-Papanastasiou model for the behavior of non-Newtonian fluids. A computational fluid dynamics model is developed and implemented using COMSOL Multiphysics, enabling the approximation of the overall material removal rate during the process.
Keywords: Abrasive magnetorheological fluids, drag finishing, computational fluid dynamics.

1. INTRODUCTION

Polishing applications utilizing magnetorheological fluids (MRF) have gained significant attention in recent years [1]. Previous studies have introduced MRF drag finishing, also referred to as immersed tumbling, as an innovative method for the cutting-edge preparation of milling tools [2, 3]. The fundamental principle of MRF drag finishing involves the rotational and translational movement of a workpiece through a container filled with an abrasive MRF fluid following a circular trajectory. The lapping medium, composed of magnetorheological fluid and abrasive particles, is subjected to magnetic excitation via a magnetic circuit. Given the inherent inhomogeneities at the cutting edges of milling tools, MRF drag finishing has demonstrated promising results in achieving high surface quality, reduced processing times, and controllable grinding effects.

This study aims to model the behavior of abrasive MR fluids during the MRF drag finishing process under the influence of the magentic field. A microscopic model based on the dipole-dipole interaction theory is developed following [4] to characterize the magnetically induced yield stress. Additionally, a macroscopic modeling approach employing the Bingham-Papanastasiou model is established to account for the non-Newtonian rheological behavior of the fluid. A CFD model is subsequently developed using COMSOL Multiphysics to estimate the overall material removal rate, utilizing a predictive material removal model from [6].

2. MODELING APPROACH

A dipole-dipole interaction model is applied in accordance with [4] to determine the yield point of the MRF. The force exerted by a particle chain against shear $F_{\hat{s}}$ is given by

$$F_{\hat{s}} = \frac{8}{3} \cdot \mu_0 \cdot \pi \cdot r_\mathrm{p}^6 \cdot \chi_\mathrm{eff}^2 \cdot H_0^2 \cdot \frac{\gamma}{(\gamma^2+1)^{3/2}} \cdot \sum_{j \neq i}^{n} \frac{1}{r_{ij}^4} \cdot \left(3 + \frac{2}{r_{ij}^3} \cdot \chi_\mathrm{eff} \cdot r_\mathrm{p}^3\right), \tag{1}$$

where r_p represents the particle radius, r_{ij} denotes the distance between two arbitrary particles, χ_eff is the effective magnetic susceptibility, γ is the shear strain and H_0 is the applied magnetic field. The magnetically induced yield stress τ_0^M is subsequently calculated as $\tau_0^\mathrm{M} = P_\mathrm{max} \cdot F_{\hat{s}}$, where P_max represents the maximum number of particle chains per unit area.

For macroscopic modeling, a Bingham-Papanastasiou-model is employed following [5], as expressed by

$$\tau = \eta \cdot \dot{\gamma} + \tau_0 \cdot [1 - \exp(-m \cdot \dot{\gamma})]. \tag{2}$$

Here, τ denotes the shear stress within the fluid, η the dynamic viscosity, τ_0 the yield stress and m describes a constant exponent. The material removal $\mathrm{MRR}_\mathrm{MRF}$ is computed using the predictive equation from [6], given with

$$\mathrm{MRR}_\mathrm{MRF} = C_\mathrm{p,MRF} \cdot \frac{E}{K_\mathrm{c} {H_\mathrm{V}}^2} \cdot \tau \cdot v_\mathrm{r}, \tag{3}$$

where $C_\mathrm{p,MRF}$ is a modified Preston's coefficient, E is the Young's modulus, H_V is the Vickers hardness, K_c represents the fracture toughness and v_r is the relative velocity.

3. EXPERIMENT SETUP FOR ABRASIVE MAGNETORHEOLOGICAL FLUIDS

The rheological properties of the utilized abrasive MRF are determined using a specialized rheometer introduced in [3]. Within the rheometer, the MRF is subjected to axial shear in a magnetic field ranging from $0\ \mathrm{T} < B < 0.5\ \mathrm{T}$. A schematic diagram of the rheometer test bench is presented in **Figure 1** a). For abrasive processing experiments, a dedicated test bench for MRF drag finishing, as described in [2], is utilized. The setup, illustrated in **Figure 1** b), consists of high-speed steel workpieces being traversed through a container filled with abrasive MRF lapping medium, which is magnetically excited via a controlled magnetic circuit.

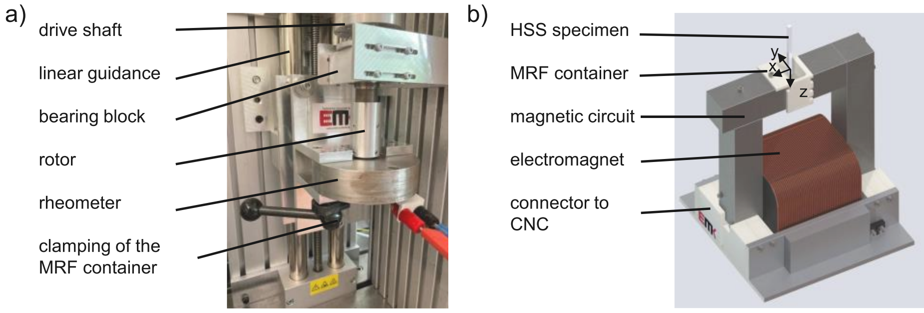

Figure 1: a) Rheometer for abrasive MRF [3] and b) MRF drag finishing test bench introduced in [2].

4. RESULTS AND DISCUSSION

Experimental investigations are conducted using an abrasive MRF with volume fractions $\varphi_{\mathrm{cip}} = 45\%$ and $\varphi_{\mathrm{ap}} = 15\%$, incorporating monocrystalline diamond abrasives with a particle diameter of $d_{\mathrm{ap}} = 252\ \mu\mathrm{m}$. The results indicate a strong correlation between the measured and modeled yield stresses for the examined MRF compositions, as depicted in **Figure 2** a).

CFD simulations reveal that an increase in magnetic flux density leads to a corresponding increase in shear stress while significantly reducing the velocity field near the moving workpiece, as illustrated in **Figure 2** b) and c). Future studies will extend the analysis to include abrasive experiments and validate material removal rate predictions based on Equation (3).

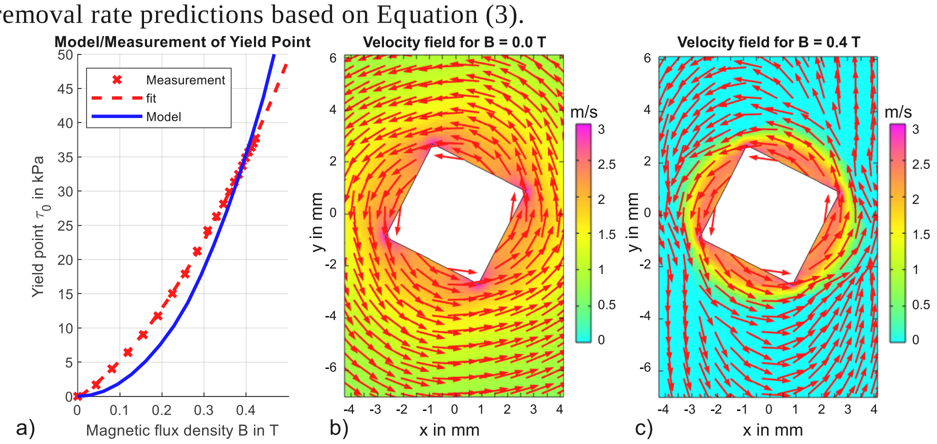

Figure 2: a) Measured and modeled yield point of the abrasive MRF. b) Modeled velocity field around the specimen within the MRF container for $B = 0.0$ T and c) for $B = 0.4$ T.

REFERENCES

[1] Denkena B, Köhler J, Schindler A. Behavior of the magnetic abrasive tool for cutting edge preparation of cemented carbide end mills. Prod. Eng. Res. Devel. 8, 2014: 5, p. 627 – 633.
[2] Sordon F, Ludwig J, Hocke T, Uhlmann E, Maas J. Abrasive properties of magnetorheological fluids for immersed tumbling processes. ASPE Proceedings, 2023: 81, p. 304-309.
[3] Sordon, F., Lahoda, C., Uhlmann, E., Maas, J. Rheological properties of abrasive magnetorheological fluids for immersed tumbling processes. ACTUATOR, 2024: 110, p. 64-67.
[4] Gueth, D., Maas, J. Characterization and modeling of the behavior of magnetorheological fluids at high shear rates in rotational systems. JIMSS 27, 2016: 5, p. 689-704.
[5] Papanastasiou TC. Flows of Materials with Yield. Journal of Rheology 31, 1987: 5, p. 385-404.
[6] Miao C, Shafrir S, Lambropoulos J, Mici J & Jacobs S. Shear stress in magnetorheological finishing for glasses. Applied Optics, 2009: 48, p. 2585-2594.

Model-based Investigation of the Sedimentation Behavior of Magnetorheological Fluids under the Influence of Magnetic and Acceleration Fields

Valentin Schreiner[1], Ina Bregu[2] and Jürgen Maas[3]

[1, 2, 3] Mechatronic Systems Lab EMK, Institute of Machine Design and Systems Technology, Technische Universität Berlin, Germany
(E-mail: valentin.schreiner@emk.tu-berlin.de, ina.bregu@emk.tu-berlin.de, juergen.maas@tu-berlin.de)

***Short abstract*:** The sedimentation behavior of magnetorheological fluids under acceleration fields is investigated by analyzing the relationship between magnetic flux density and the acceleration at which particle settling begins. An analytical approach based on the dipole-dipole model is employed to describe the forces acting at the particle level and to define a critical equilibrium state for calculating the chain stability criteria. Finally, experimental validation is conducted, providing insights into the fundamental mechanisms governing MRF sedimentation stability.
***Keywords*:** Sedimentation of magnetorheological fluids, stability criteria, centrifugal force and rotational speed.

1. INTRODUCTION

A critical characteristic of magnetorheological fluids (MRFs) is the tendency of suspended particles to settle under gravitational or other external forces over time. This process, known as sedimentation, can affect the performance and long-term stability of MRF-based systems, which is undesirable in most applications. However, it can also be used to precisely influence the mass distribution, such as in the balancing of rotors. The targeted manipulation of MRFs can be achieved by controlling a magnetic field, which allows the formation of particle chains and facilitates the transfer of shear stress, enabling controlled sedimentation.

While several studies have examined this phenomenon experimentally, as shown in [1] and [2], this study utilizes an analytical approach using the dipole-dipole interaction model, as proposed in [3]. First, the chain formation under static loading conditions is investigated, where gravity is the only force driving sedimentation. Once the critical parameters for static conditions are defined and calculated, they establish the thresholds above which the particle chain remains stable. The model is then extended to account for dynamic rotational conditions, where centrifugal forces dominate and become the primary factor determining stability. The objective of this study is therefore to determine the relationship between the magnetic flux density and the centrifugal acceleration at which sedimentation occurs.

2. ANALYTICAL APPROACH TO SEDIMENTATION STABILITY

The system considered in this study consists of a chamber filled with MRF. The chamber can rotate around a fixed axis, and is therefore subjected to both gravitational and centrifugal forces. Additionally, a homogeneous magnetic field, parallel to the axis of rotation, is applied throughout the entire chamber. The superposition of gravitational, centrifugal, and magnetic forces creates a dynamic regime, which determines the behavior of the MRF inside the chamber. To analyze this behavior, a representative volume element consisting of a single chain of particles is considered, and its stability is investigated.

The derivation of the magnetic forces acting on the particle chain is based on previous work using the dipole-dipole model [3]. Assuming uniform spherical particles of radius r_p and a quasi-static applied magnetic field $\boldsymbol{H}_0$, the resulting magnetic force on particle j from particle i can be expressed as:

$$\boldsymbol{F}_j^i = \mu_0 \cdot \frac{8}{3} \cdot \pi \cdot r_\mathrm{p}^3 \cdot \chi_\mathrm{eff} \cdot \boldsymbol{H}_i \nabla \left\{ \boldsymbol{H}_0 + \chi_\mathrm{eff} \cdot r_\mathrm{p}^3 \sum_{j \neq i}^{n} \left[\frac{(\boldsymbol{H}_0 \cdot \boldsymbol{r}_{ij}) \boldsymbol{r}_{ij}}{r_{ij}^5} - \frac{\boldsymbol{H}_0}{3 r_{ij}^3} \right] \right\}. \tag{1}$$

Here $\mu_0 = 4\pi \cdot 10^{-7}\ \frac{\mathrm{N}}{\mathrm{A}^2}$ represents the vacuum permeability, χ_eff is the effective magnetic susceptibility, and $\boldsymbol{r}_{ij}$ is the position vector between particles i and j in the chain. Since the position vector clearly depends on the form of the chain, the chain's configuration is derived to parametrize the position of each particle. To determine the chain's form, the chain is modeled as a continuum, and the forces acting on a differential element of the chain are analyzed. The chain's behavior is described using Newton's laws of motion, where each loading scenario results in a distinct second-order nonlinear differential equation. The results show that the chain adopts a hyperbolic cosine shape under static loading conditions, and an approximately parabolic shape under the influence of centrifugal forces. Once the position vectors are defined, the magnetic force can be computed using (1), and a critical equilibrium state can be established to calculate the critical parameters for the stability of the particle chain.

3. EXPERIMENTAL SETUP OF THE PARTICLE CHAIN STABILITY

Two different experiments were conducted for each loading scenario. In the first experiment, a C-shaped electromagnet was used to generate the required external magnetic field. To prevent particle clustering, the particle chain was placed between the two tapered ends of the electromagnet. The applied magnetic field was gradually decreased and the critical value $H_{0,crit}$ at which the chain loses its stability is determined experimentally.

The second experiment involved a rotor with three chambers, each connected to the rotor, and only one housing the MRF. The chambers are rotated at a low angular velocity, with the imbalance vector recorded as a baseline. The angular velocity is incrementally increased while monitoring changes in the imbalance vector. A shift in the imbalance indicated the onset of sliding in the particle chain, which, as the form of loss of stability caused by Ω_{crit}, is calculated using the rotor's imbalance vector. The experimental results and their comparison with the analytical model are presented in **Figure 1**.

4. RESULTS, DISCUSSION AND CONCLUSIONS

A decrease in particle size enhances the sedimentation stability. Similarly, higher magnetic fields improve the sedimentation behavior and particle chain stability. Under dynamic conditions, a higher coefficient of friction results in greater chain stability, while an increase in angular velocity accelerates the sedimentation process, as shown in **Figure 1** b).

A key finding regarding the sedimentation behavior and stability of particle chains in both static and dynamic scenarios is that the optimal number of particles—slightly exceeding that of a straight chain—minimizes the system's total energy. This results in a slight sag in the static case and small oscillation amplitudes in the dynamic case, with the latter being further dampened by the viscosity of the carrier oil. These results are depicted in **Figure 1** a), where, at small particle numbers, there is strong correspondence between the experimental and modeled critical magnetic flux, while greater discrepancies are observed at higher particle numbers. This outcome highlights the mathematical limitations of the dipole-dipole model in accurately predicting the behavior of particle chains, particularly at higher particle numbers where chain sag becomes more pronounced.

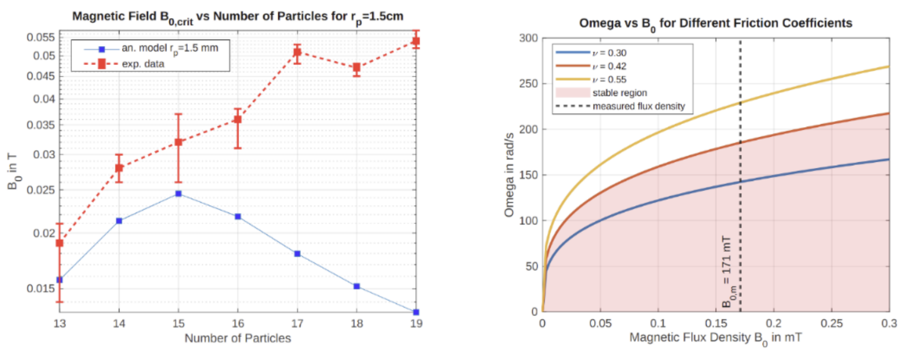

Figure 1: a) Analytical and experimental results for sedimentation stability under static and b) dynamic conditions.

REFERENCES

[1] Ashtiani, M., Hashemabadi, S.H., & Ghaffari, A. (2015). A review on the magnetorheological fluid preparation and stabilization. *Journal of Magnetism and Magnetic Materials*, *374*, 716–730.
[2] Kumar, J. S., Paul, P. S., Raghunathan, G., & Alex, D. G. (2019). A review of challenges and solutions in the preparation and use of magnetorheological fluids. *International Journal of Mechanical and Materials Engineering*, *14*(1).
[3] Güth, D., & Maas, J. (2015). Characterization and modeling of the behavior of magnetorheological fluids at high shear rates in rotational systems. *Journal of Intelligent Material Systems and Structures*, *27*(5), 689–704.

Comparing ER and MR Dampers: Bouc-Wen vs. Spencer Models

Mohammed Mujeeb[1], Robert Langlois[2] and Fred Afagh[3]

[1, 2, 3] Department of Mechanical and Aerospace Engineering, Carleton University, Canada
(E-mail: MohammedMujeeb@cmail.carleton.ca, RobertLanglois@cunet.carleton.ca,
FredAfagh@cunet.carleton.ca)

Abstract: This study compares the hysteresis characteristics of two typical commercial Electrorheological and Magnetorheological dampers using Bouc-Wen and Spencer models. It examines the influence of mechanical analogues in these parametric models on the force-velocity curves of both dampers, reasoning why these curves take their characteristic shapes. Results indicate that the Spencer model captures hysteresis most effectively for both the dampers, particularly in high-velocity regions.
***Keywords*:** Mechanical analogues, hysteresis, parametric models, hybrid optimization.

1. INTRODUCTION

To capture the response of an Electrorheological (ER) or Magnetorheological (MR) damper, several parametric models such as the Bingham, Bouc-Wen and Spencer models have been studied extensively. These models include mechanical analogues, such as springs, dashpots, and friction elements, a combination of which aims to represent the physical behaviour of these dampers and individually capture a specific characteristic of force-velocity behaviour. However, the ability of these models in capturing hysteresis loops varies, making comparative analysis crucial. Therefore, this study analyzes the influence of mechanical analogues on force-velocity hysteresis curves to better understand their role in shaping damper behaviour.

2. METHODOLOGY

Two experimental datasets were analyzed, corresponding to an MR damper (López Boada, 2023) and an ER damper. Using this data, these dampers were characterized using two widely studied parametric models: Bouc-Wen and Spencer models. For parameter identification, a hybrid optimization combining Particle Swarm Optimization (PSO) with gradient descent was employed to improve optimization time and efficiency. Additionally, the force-velocity hysteresis curves obtained from each model were compared with experimental data to determine their accuracy in representing ER and MR damper behaviour.

3. RESULTS AND DISCUSSION

Table 1 presents Bouc-Wen and Spencer model parameters for force-velocity plots in Figures 1-4 for both ER and MR dampers. The superscript ($^{\text{ER/MR}}$) will be used to distinguish between the ER and MR damper parameters. Analyzing the parameter values in Table 1 shows a notably small stiffness value of k_0^{ER}. Low stiffness causes gentler force slopes, indicating a gradual increase in force with displacement. In contrast, high stiffness results in steeper slopes, leading to abrupt force increments for smaller displacements. This distinction is seen in the Bouc-Wen force-velocity plots of ER (Figure 1) and MR (Figure 2) dampers.

Table 1: Identified parameters for selected experimental data (Mujeeb, 2025).

Damper	Model	Parameters								
		c_0 (Ns/m)	k_0 (N/m)	c_1 (Ns/m)	k_1 (N/m)	α (N/m)	B (m^{-2})	γ (m^{-2})	A	n
ER	Bouc-Wen	5106.60	0.01	-	-	6128.34	494.58	0.01	118.38	1
	Spencer	5748.03	0.01	11214.72	0.01	1152.57	311.12	0.01	1322.02	1
MR	Bouc-Wen	1108.03	1718.24	-	-	740.92	268.70	99.64	61.52	1
	Spencer	963.63	484.85	7648.72	7238.15	527.62	513.38	190.28	280.13	1

In low-velocity regions $[-0.1,0.1]$ m/s, the ER damper's force-velocity loop is elliptical, inclined to the x-axis and has sharply tapered corners at higher velocities. The low stiffness ($k_0^{\text{ER}} = 0.01$ N/m) results in a less pronounced steepness at low velocities, ensuring smooth force transition even in the post-yield region, leading to smoother damping behaviour. Conversely, the MR damper's hysteresis loop forms a rectangular shape, exhibiting a steep and abrupt force increase due to its high stiffness ($k_0^{\text{MR}} = 1718.24$ N/m). This causes rapid force changes at low velocities before transitioning to a gentler slope in the post-yield region.

Area covered by hysteresis loops reflect energy dissipation, larger loops indicate higher dissipation. This depends on hysteresis stiffness α, which influences loop size, while damping coefficient c_0 controls force transition smoothness during changes in operational states. Thereby, for the ER damper, larger values of

$\alpha^{\mathrm{ER}} = 6128.34$ N/m and $c_0^{\mathrm{ER}} = 5106.60$ Ns/m create a large and smooth loop. In contrast, the MR damper, with lower values of $c_0^{\mathrm{MR}} = 1108.03$ Ns/m and $\alpha^{\mathrm{MR}} = 740.92$ N/m, forms a smaller loop with sharper force transitions. Hence, for MR damper, the dominant influence of high stiffness k_0^{MR} causes a steep pre-yield force increase, followed by an abrupt force transition in the small rectangular region controlled by α^{MR}.

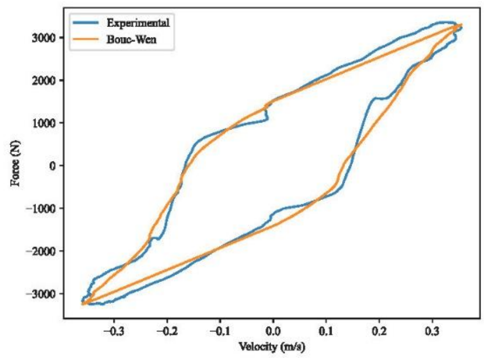

Figure 1 Bouc-Wen model predicted versus experimental force-velocity plots of ER damper.

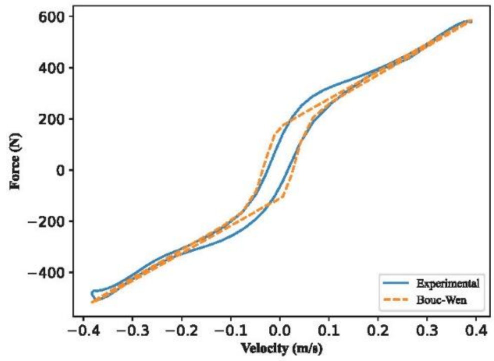

Figure 2 Bouc-Wen model predicted versus experimental force-velocity plots of MR damper.

While the Bouc-Wen model effectively captures low-velocity force transitions, it struggles at high velocities. The hysteresis loops become narrower and sharper towards extremities, failing to accurately capture the force transition when piston direction changes. To address this, the Spencer model enhances the Bouc-Wen formulation by introducing an additional stiffness k_1 and damping c_1, producing larger, rounder, and better-fitted hysteresis curves, particularly towards the extremities as seen in Figures 3 and 4.

For the MR damper, a high damping coefficient ($c_1^{\mathrm{MR}} = 7648.72$ Ns/m) smooths the mid-velocity region, while a large stiffness value ($k_1^{\mathrm{MR}} = 7238.15$ N/m) maintains sharp transitions at high velocities. For the ER damper, a low stiffness ($k_1^{\mathrm{MR}} = 0.01$ N/m) results in blunter extremities, whereas a large damping coefficient ($c_1^{\mathrm{MR}} = 11214.72$ Ns/m) ensures smoother force transitions throughout the velocity range.

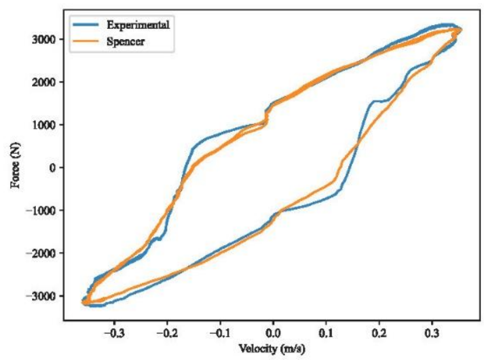

Figure 3 Spencer model predicted versus experimental force-velocity plots of ER damper.

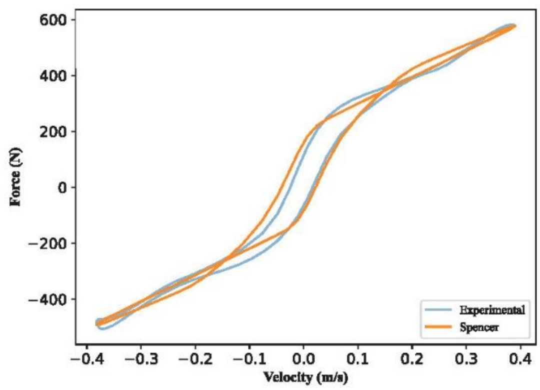

Figure 4 Spencer model predicted versus experimental force-velocity plots of MR damper.

4. CONCLUSION

The study explains the effects of mechanical analogues in Bouc-Wen and Spencer models, demonstrating that the Spencer model provides a more accurate representation of ER and MR damper hysteresis, particularly in high-velocity regions due to the inclusion of additional damping and stiffness elements.

REFERENCES

[1] López Boada, M. J. (2023). Experimental magnetorheological (MR) damper curves for different levels of applied current, amplitudes, and frequencies of excitation. e-cienciaDatos.
[2] Mujeeb, M. (2025). Rheological Damper Characterization and Control with Application to a Drop Tower for Replicating the Impact Profiles of High Speed Craft. Carleton University.

Understanding Self-Organization from Permanently Encoded Ferrofluid Spike Patterns

Michel Laforest Mongeau[1], Mark Andrews[1], Tina Lam[1], Tianyu Zhong[1]

[1] Department of Chemistry, McGill University, Montréal, Québec, Canada
(E-mail: michel.laforestmongeau@mail.mcgill.ca, mark.andrews@mcgill.ca, tina.lam@mcgill.ca, tianyu.zhong@mail.mcgill.ca

Short abstract: We live in a world and in a universe that are marked by systems of evolving patterns and structures. When energy is put into the constituents that make up these systems, remarkable transformations occur that cause the patterns, structures and their properties to appear different from the unchanging state that we call equilibrium. In this work, we discuss our findings on how control variables govern self-organization that manifests as pattern formation in ferrofluids. We use measurables such as Voronoi entropy to interrogate the evolution of order in these patterns.
Keywords: Ferrofluids, self-organization, Voronoi entropy

1. INTRODUCTION

Ferrofluids consist of stable suspensions of ferrimagnetic (magnetite) nanoparticles (MNPs) in a liquid. The fluid responds to an external magnetic field in a symmetry-breaking event that features lattices of spikes. But the patterns disappear when the field is removed. This is a hallmark of a dissipative system. All life forms are self-organized and dissipative. This underscores our interest to explore the nanoscale origins of ferrofluid-based self-organized patterns as models for more complex systems. The history of patterning is encoded through surface ligand soft-soft interactions and kinetic barriers to dissipation imposed by low molecular weight poly(vinylpyrrolidone) (PVP). We report on the impact of control variables like alkane carbon number, magnetic field strength and nanoparticle loading. Measures of the Voronoi entropy are used to quantify order. With accompanying videos, we explain how we record the dynamic trajectories of the unusual ferrofluid patterns by a motion tracking algorithm that allows us to determine the time dependent evolution of the Voronoi entropy.

2. OBJECTIVES

In this work, we explain how we use evaporating alkane and alcohol-water fluids to permanently trap patterns that emerge when the fluids are exposed to different external magnetic field strengths. We also aim to uncover trends in the time evolution of the Voronoi entropy.

2. Material and Methodology

3.1. Preparation of aqueous and alkane-based Fe_3O_4 ferrofluids

The MNPs are prepared via a basic co-precipitation reaction of ferrous and ferric chloride in water [1]. The resulting aqueous ferrofluid is blended with a small volume of PVP/n-butanol solution prior to the patterning experiment. The alkane based ferrofluid is prepared by precipitating the particles with ethanol, then collecting them with a magnet. The dried particles are then redispersed in octane via sonication [2].

3.2. Acquisition of ferrofluid patterning videos and data processing details.

The ferrofluid is deposited onto a glass substrate. A cylindrical magnet is raised from underneath the sample until the desired field strength is reached. The pattern formation is recorded with a microscope and a CMOS camera. The recordings are fed to a motion tracking software, wherein each spike is individually tracked. Manual adjustments to the trajectories are performed if the tracking is inaccurate. A Python script is used to load the coordinates, compute the Voronoi entropy and render a Voronoi diagram for each frame.

4. RESULTS AND DISCUSSION

Alkane-based ferrofluid patterns experience large fluctuations in Voronoi entropy, most evident when the lattice transitions from a square to hexagonal phase. PVP-containing ferrofluids experience gradual changes in entropy. These changes appear to be due to motions impeded by the mutual polymer-MNP interactions. Ultra-high resolution scanning electron microscopy reveals that spikes derived from alkane media comprise rhombic lattice assemblies of MNPs. PVP-MNP composites are disordered. The encoded spikes from both matter classes are permanent magnets, despite the latent superparamagnetism of the MNPs.

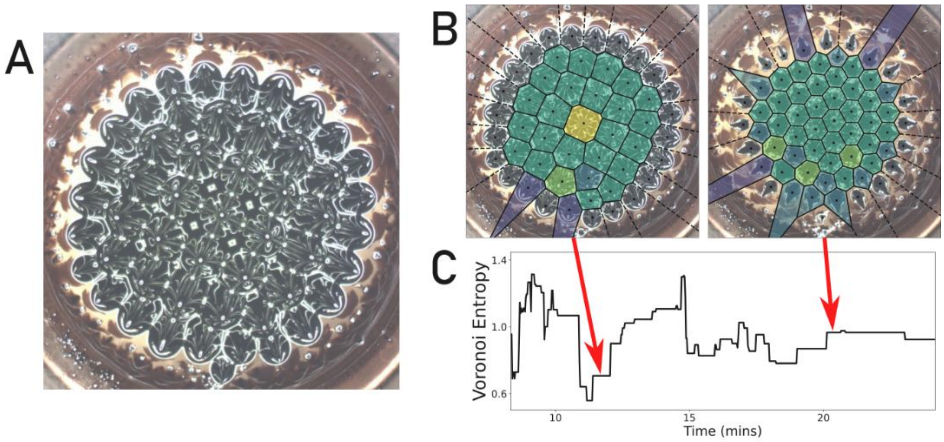

Figure 1: Micrograph of alkane-based ferrofluid pattern (A). Micrographs with superimposed Voronoi diagrams of the square and hexagonal phases (B). The time index of these spike arrangements are indicated on the time evolution of the Voronoi entropy (C).

5. CONCLUSIONS

In brief, this work outlines a novel method for gathering insights into pattern formation in ferrofluids. We observed trends in the dynamic evolution of Voronoi entropy in both aqueous and alkane based ferrofluid pattern. In future work, we wish to explore the prediction of Voronoi entropy evolution with the aid of machine learning.

ACKNOWLEDGEMENT

This work is supported under the Natural Sciences and Engineering Research Council of Canada (NSERC) and NSERC alliance. We extend our thanks to the McGill Chemistry Characterization (MC2), the McGill Institute for Advanced Materials (MIAM) and the Facility for Electron Microscopy Research (FEMR).

REFERENCES

[1] Petcharoen, K., Sirivat, A. Synthesis and characterization of magnetite nanoparticles via the chemical co-precipitation method. Materials Science and Engineering: B. 2012 Feb 4;177(5):421–7.
[2] Zhong, T., Andrews, M., Fournier, P., Dion, M. Permanent encoding of nano- to macro-scale hierarchies of order from evaporative magnetic fluids. Nano Select. 2021 Jan 15;2(3):591–9.

Magnetorheological Elastomer-Based Smart Structures Fabricated through Additive Manufacturing Route

I. Handa[1], Sh. Foroughi[1] and M. Packirisamy[1]

[1] Department of Mechanical, Industrial, and Aerospace Engineering, Concordia University, Canada

(E-mail: iris.handa@mail.concordia.ca, s_foroug@encs.concordia.ca, m.packirisamy@concordia.ca)

Short abstract: Micro-cantilevers are crucial in sensing applications due to their high sensitivity, enabling precise detection of forces and biomolecules. This study presents the fabrication of a magnetorheological elastomer (MRE) microcantilever consisting of 2 different ratios of Carbonyl Iron particles (CIP) with Polydimethylsiloxane using a 3D printed mold, leveraging the flexibility and cost-effectiveness of additive manufacturing. To evaluate its mechanical response, we measured the deflection of the cantilever under the influence of a permanent magnet. The results show more sensitivity of the microcantilever with higher ratio of CIP under the variable magnetic field.

Keywords: Magnetorheological elastomer, Microcantilever, MRE, Magnetic field.

1. INTRODUCTION

Magnetorheological Elastomer (MRE) is a rubber-like solid material that is composed of a non-magnetic elastomeric matrix loaded with magnetic particles and the additives [1]. MREs can be regarded as the solid analog of Magnetorheological fluids. MREs are used in various applications where stiffness changeability is desired, such as vibration absorbers, vibration isolators, and sandwich beams [1]. The conventional method for fabricating MREs involves using matrix materials such as silicone rubber or thermosetting/thermoplastic polymers in their liquid form. Magnetic particles such as carbonyl Iron powders (CIP), along with any additional additives, are mixed into the liquid matrix—typically at room temperature. The resulting mixture is then poured into a mold and cured at an elevated temperature to form the final MRE structure [2]. In this paper, we present an easy method to fabricate isotropic MRE microcantilevers using 3D printed molds. Microcantilevers are increasingly being used in a variety of microelectromechanical systems (MEMS) like micro transducers, sensors, switches, actuators, resonators, and probes [3].

2. OBJECTIVES

The main goal of this paper is to present an easy method for fabricating MRE microcantilevers in two different concentrations of carbonyl Iron powder and validate their performance under an external magnetic field.

3. MATERIAL AND METHODOLOGY

3.1. MATERIALS

Materials: The polydimethylsiloxane (PDMS) and its corresponding curing agent were purchased from Dow Corning (Midland, US). CIP was purchased from Sigma Aldrich. Permanent Magnet (NdFeB, Grade N52, 400 mT) was purchased from K&J Magnetics Inc. (PA, US). **MRF Preparation**: The PDMS monomer and curing agent were mixed in a 10:1 ratio. CIP was added to the weight percentages of 10 and 20 in PDMS. The mixture was degassed using a vacuum for 10 mins. **Mold preparation**: The mold was 3D printed using a Formlabs 3D printer from clear resin.

3.2. METHODOLOGY

The MRF was poured into the mold and kept in the oven at 70 °C for 20-30 minutes. The MRE in the shape of a microcantilever was then extracted from the mold with the dimensions of 2.5×0.5×0.3 mm (Length×Width×Thickness). Subsequently, the microcantilever was attached to a support, mounted on a CNC, and exposed to an external magnetic field generated by a permanent magnet, as shown in Figure 1. The distance to the magnet is then varied, and the resulting beam deflection is captured using the camera. At each step the magnetic field intensity was measured using the gauss meter probe (HSOKEW, China.) The same process was carried out for both the cantilevers with different mixing ratios of CIP and PDMS

4. RESULTS AND DISCUSSION

Both the cantilevers exhibited increasing deflections as they moved closer to the magnet, which is plotted in Figure 2, with deviations from linearity becoming more evident at higher steps. This non-linearity suggests a stronger magnetic influence at closer proximities, likely due to material properties and nonlinear magnetic effects, which impact the mechanical response of the microcantilevers. Among the samples, the MRE cantilever with 20 wt% CIP demonstrated the highest deflection, confirming that higher iron content enhances magnetic responsiveness. A particularly interesting observation was that the 10 wt% MRE displayed deflections comparable to those of the 20 wt% for a substantial portion of the experiment. This finding implies that even a relatively low iron content (10 wt% CIP in PDMS) is sufficient for the material to exhibit smart material behaviour under a magnetic field. This could have practical implications for optimizing material composition in applications requiring flexible yet magnetically responsive structures.

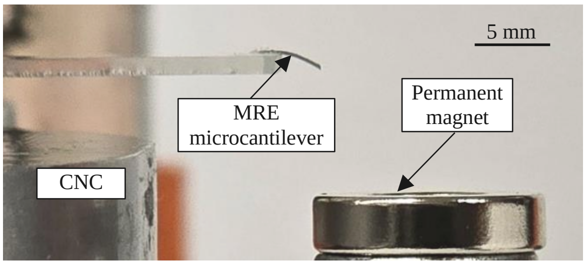

Figure 1: Setup for deflection measurement of the MRE microcantilever in magnetic field.

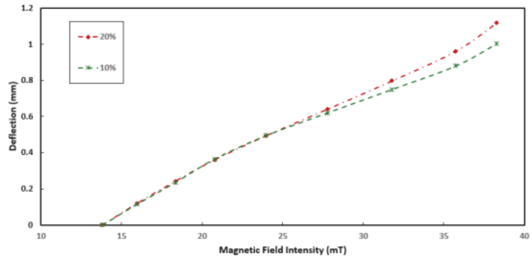

Figure 2: Deflection of the microcantilevers with varying magnetic field intensity.

5. CONCLUSIONS

Soft lithography using a 3D printed Mold is a fast and cheap approach to manufacture MREs. The microcantilevers fabricated using the described method showed expected behaviour of an MRE. This fabrication method offers a fast fabrication process, and cost effectiveness. Future work involves the direct 3D printing of micro-cantilevers, which presents challenges such as the sedimentation of magnetic particles and the limited penetration of light in opaque media. Addressing these issues will require optimizing material compositions, refining printing parameters, and exploring alternative light delivery techniques to enhance precision and structural integrity.

REFERENCES

[1] “Li, Y., Li, J., Li, W., & Du, H. (2014). A state-of-the-art review on magnetorheological elastomer devices. Smart materials and structures, 23(12), 123001.”.

[2] “Puente-Córdova, J. G., Reyes-Melo, M. E., Palacios-Pineda, L. M., Martínez-Perales, I. A., Martínez-Romero, O., & Elías-Zúñiga, A. (2018). Fabrication and characterization of isotropic and anisotropic magnetorheological elastomers, based on silicone rubber and carbonyl iron microparticles. Polymers, 10(12), 1343.”.

[3] “Manvi M, Swamy KM. Microelectronic materials, microfabrication processes, micromechanical structural configuration based stiffness evaluation in MEMS: A review. Microelectronic Engineering. 2022 Jul 15;263:111854.”.

Rheological, microscopic and statistical analysis of elastomers made with silicone and ferromagnetic powder for application as *honeycomb* core filling in sandwich beams

Pedro Yanaze[1], Felipe de Souza Eloy[2], Antonio José Faria Bombard[3] and Regina Celia Reis Nunes[4]

[1, 2] Institute of Mechanical Engineering (IEM), UNIFEI, Itajubá, Brazil
(E-mail: d2021024035@unifei.edu.br, felipeeloy@unifei.edu.br)
[3] Institute of Physics and Chemistry (IFQ), UNIFEI, Itajubá, Brazil
(E-mail: bombard@unifei.edu.br)
[4] Professor Eloisa Mano Institute of Macromolecules (IMA), UFRJ, Rio de Janeiro, Brazil
(E-mail: rcnunes@ima.ufrj.br)

Short abstract: Magnetorheological materials are widely used in engineering due to their ability to modify rheological properties under magnetic fields. This study evaluated the use of additives to improve the distribution of ferromagnetic particles in silicone elastomers, preventing accumulation at the sample's bottom. Three additives were tested: silica, muscovite mica and kynar powder. The results show that up to 134kA/m, the sample with mica showed the greatest variation in storage and loss modulus. Above this field, silica demonstrated better reactivity. Microscopic and statistical analyses confirmed that additives ensured homogeneous particle distribution, with silica showing the most uniform dispersion along the sample's thickness.

Keywords: Ferromagnetic elastomer, smart sandwich beams, rheology, microscopy, magnetic field.

1. INTRODUCTION

Smart materials, such as magnetorheological ones, exhibit adjustable rheological properties under magnetic fields, making them widely used in damping, vibration control systems [1] and as sandwich beam cores. However, a key challenge in producing such elastomers lies in the accumulation of ferromagnetic particles at the silicone base due to their higher density, that compromises the dynamic response of the structure [2].

This study investigates the influence of different additives in fabricating elastomers composed of silicone and ferromagnetic powder. Samples were naturally cured, without external orientation to avoid interference with particle deposition and then subjected to rheological, microscopic and statistical analyses. Previous studies using ABS and PLA square cross-linked cores were made and demonstrated that elastomers with 60% ferromagnetic powder by weight effectively altered dynamic behavior [2]. However, this work aims to adapt the concept for commercial honeycomb cores, where uniform particle distribution is even more critical.

2. OBJECTIVES

The main objective of the study is to identify the best additive for the silicone and ferromagnetic powder composite, for each magnetic field range applied (up to 600kA/m), which results in a desirable variation in the rheological properties of the final composite. Finally, the study also checks whether the sample's rheological applicability matches the main reason for adding an additive to the elastomer, which is to improve the distribution of the ferromagnetic powder throughout the core.

3. MATERIAL AND METHODOLOGY

The samples were produced using metal and acrylic molds (both ⌀20x1.6mm). Their compositions are silicone-based (100:3) and a further 3% by mass of additives was added. Finally, magnetic iron powder (MIP) was added to account for 60% by mass of the final composite, so that the results obtained would be significant in the magneto-rheological analysis, as experienced in previous work.

Table 1: Density of the samples produced

Sample	Mass [g]	Density [g/cm³]
Silicone + MIP	1.5629	2.6248
Silicone + Silica + MIP	1.6339	2.8907
Silicone + Mica + MIP	1.2348	2.7799
Silicone + Kynar Powder + MIP	1.2972	2.8183

3.1. RHEOLOGICAL, MICROSCOPIC AND STATISTICAL ANALYSIS

After the samples were fully cured and demolded, they were subjected to a rheological analysis using the ANTON PAAR PHYSISCA MCR-301 rheometer, equipped with an MRD-180/1T magnetic cell capable of applying a magnetic field of 0.05 to 600 kA/m. The main interest of the test is to analyze and compare the storage and loss modulus in relation to the deformation caused by shear, at a constant temperature of 25ºC.

To analyze the influence of the heterogeneous deposition of magnetic iron, the samples had to be viewed microscopically using an Olympus SZ61 stereoscope at 45x magnification and then a statistical analysis was carried out using *ImageJ* software to verify the influence of each additive on the deposition of MIP throughout the thickness of the sample.

4. RESULTS AND DISCUSSION

One of the main results obtained when adding additive compounds to the final elastomer composition was an increase in the specific mass of the elastomer, as shown in Table 1, and consequently a better distribution of the ferromagnetic powder throughout the thickness of the test specimen, as shown in the histograms below.

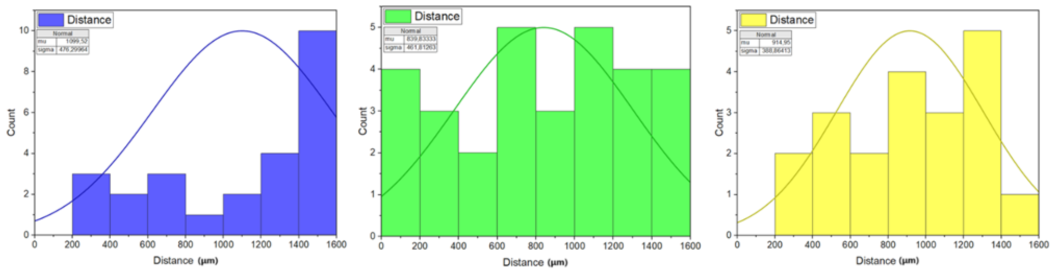

Figure 1: Histograms of ferromagnetic powder distribution along the thickness of the sample without additives (left), with silica (center) and with muscovite mica (right)

In addition, the rheological behavior of the samples was analyzed, where points of interest within the elastic regime of the material were studied, whose behavior is relatively predictable. Therefore, average values of storage and loss modulus were calculated for all the parameters found, and were compared with the values found for 0.05 kA/m (reference). The difference from the reference, in percentage, was compared between all the materials and the one with the greatest variation is the one most recommended for use under the conditions imposed by the test.

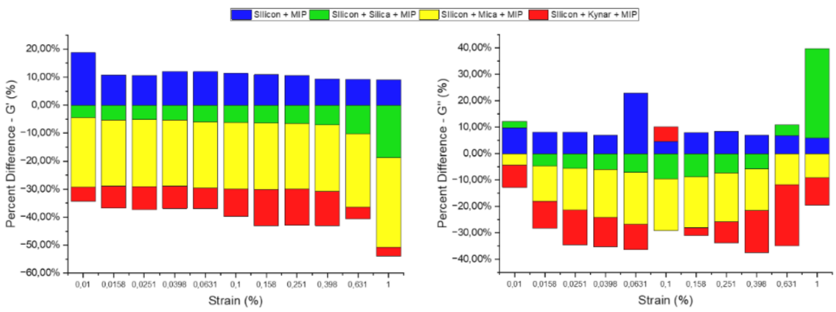

Figure 2: Percentage difference in G' and G" in the elastic regime of the samples at 134 kA/m

5. CONCLUSIONS

Microscopic and statistical analyses revealed that additives improve the distribution of ferromagnetic particles, with silica offering the most homogeneous result. For fields up to 134 kA/m, mica is preferred due to its low density, while silica is ideal for higher fields despite its slightly greater weight. Now the challenge is to develop a manufacturing method of the sandwich beam that ensures that this homogeneity is maintained.

REFERENCES

[1] JOLLY, Mark R et al. A model of behaviour of magnetorheological materials. 1996 Smart Mater. Struct. 5 60
[2] ELOY, F. S. Estudo do Comportamento Dinâmico de Vigas Sanduíche com Núcleo Honeycomb preenchido com Elastômero Magneto Reológico. Itajubá, 2018. Tese de Doutorado em Projeto, Materiais e Processos. Instituto de Engenharia Mecânica, Universidade Federal de Itajubá.

Analysis on the Transmission Principle of Eccentric Squeezed Magnetorheological Fluids

Qingchao Chen, Fangping Yan, Jiajie Li, Guanqi Wang and Xuli Zhu

College of Mechanical and Electronic Engineering, Shandong University of Science and Technology, China
(E-mail: 18263821719@163.com, yfp232086@163.com, 13968351044@163.com, wgq18005447781@163.com, zhuxuli@tsinghua.org.cn)

Short abstract: A transmission structure based on the squeeze mode of magnetorheological fluids was proposed. The flow function of magnetorheological fluids and the potential function of magnetic field were derived, and the conjugate characteristics of the two functions were deduced. The distributions of stress and magnetic field were analyzed by solving the functions, and the transmission principle of eccentric squeezed magnetorheological fluids was concluded.
***Keywords*:** Magnetorheological fluid, Squeeze mode, Eccentric structure, Transmission principle

1. INTRODUCTION

Magnetorheological transmission devices (MRTDs) use magnetorheological fluids (MRFs) as the transmission medium. The transmitted torque is controlled by adjusting the external magnetic field[1]. Lu designed a squeeze shear mode magnetorheological brake with multiple fluid channels[2]. Quamar proposed a model applied the compressive forces of MRFs[3]. Wang designed a brake in which MRFs worked at compression and shear mode[4].

2. OBJECTIVES

The purpose of this paper is to get hold of the principle of eccentric squeezed magnetorheological transmission through basic theoretical analysis. The dependences of output torque and speed on structural parameters and magnetic field will be concluded by numerical calculation in order to propose a design method for more efficient and reliable MRTDs.

3. THEORETICAL ANALYSIS

Eccentric squeezed magnetorheological transmission is a kind of MRTDs that utilizes the rheological properties of MRFs to achieve transmission control. There is an eccentric rotor inside the device, which rotates to make the MRF in the squeeze mode as shown in Fig. 1. The motion of MRFs was simplified as a two-dimensional incompressible potential flow by analyzing the relative motion of the device structure, and the flow function is

$$\psi = \frac{Q}{4\pi}(lnr_A - lnr_B) \tag{1}$$

The magnetic potential function was derived according to the characteristics of passive magnetic fields.

$$\varphi = \frac{Br}{\mu}(\theta_B - \theta_A) \tag{2}$$

The stress distribution of MRFs was analyzed based on the conjugate properties of the two functions and the constitutive equation of MRFs, and then the transmission law of eccentric magnetorheological transmission was obtained.

4. RESULTS AND DISCUSSION

1) The distribution of streamlines of MRFs and magnetic force lines is shown in Fig. 2(a), while the distribution of squeezed MRFs induced shear stress and pressure is shown in Fig. 2(b). Streamlines and magnetic lines are perpendicular everywhere because the flow function and potential function are conjugated. The shear stress on the outer surface of the inner ring and the inner surface of the outer ring are generated, thereby the torque can be transmitted.

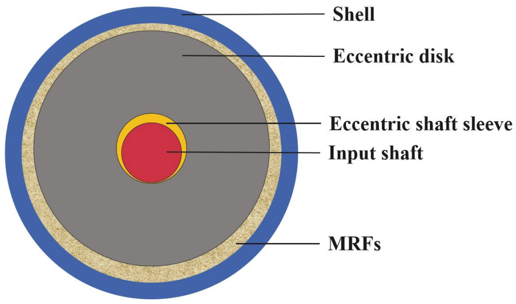

Figure 1: Schematic diagram of eccentric squeezed magnetorheological transmission

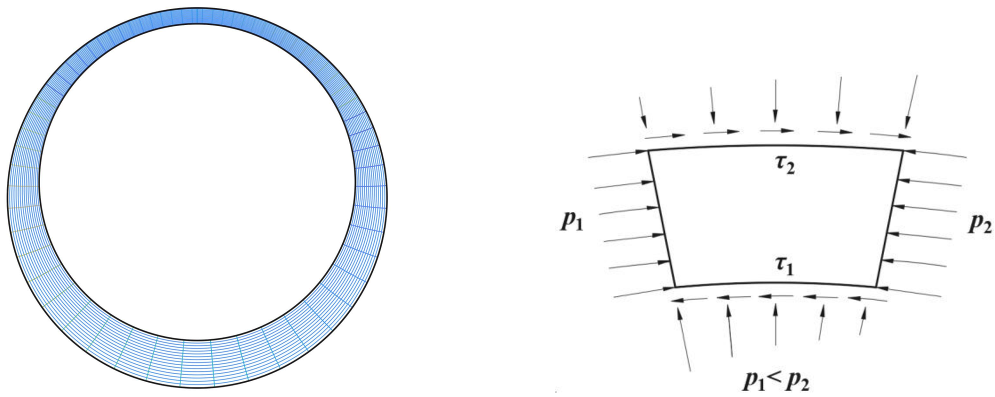

(a) (b)

Figure 2: Distribution diagram of streamline and potential lines (a) and shear stress and pressure distributions (b).

2) The larger the eccentricity, the greater the transmitted torque when other parameters are fixed.

3) The output torque and speed can be controlled by adjusting the magnetic field.

5. CONCLUSIONS

The output torque mainly depends on the magnetic field, eccentricity and the performance of MRFs. The output speed of eccentric squeezed MRTDs can be controlled by the external magnetic field.

ACKNOWLEDGEMENT

The Project Supported by National Natural Science Foundation of China No. 52375192.

REFERENCES

[1] Acharya S, Saini T R S, Kumar H. Optimal design and analyses of T-shaped rotor magnetorheological brake. IOP Conference Series: Materials Science and Engineering, 2019 Jul;624(1):012024.

[2] Lu H, Wang Q, Dai L, et al. Design and optimization of squeeze-shear mode MR brake with multi-fluid flow channels based on multi-objective sooty tern optimization algorithm. Smart Materials and Structures, 2024 Oct 17;33(11):115032.

[3] Quamar D, Sarkar C. Optimal Design of Hydraulic Disc Brake for Magnetorheological (MR) Application. Defence Science Journal, 2022 Nov;72(6):783792.

[4] Wang H, Bi C. Study of a magnetorheological brake under compression-shear mode. Smart Materials and Structures, 2019 Nov 29;29(1):017001.

Micro thermo-electromagnetic actuator platform design for Littrow monolithic coupled system

Mehdi Kharazmi[1], Muthukumaran Packirisamy[2]

[1, 2] Mechanical, Industrial, and Aerospace Engineering Department, University of Concordia. Canada
(E-mail: m_kharaz@encs.concordia.ca, M.Packirisamy@concordia.ca)

***Short abstract*:** Light propagation in photonic integrated circuits (PICs) without gaps minimizes power loss, though it requires robust actuation forces. Recent progress in integrating MEMS with silicon photonics has enabled novel techniques for tuning light propagation. Micro thermo-electromagnetic actuators, which exploit electromagnetic forces and thermal expansion, provide an efficient solution for waveguide beam steering. In this study, numerical analyses of a thermo-electromagnetic actuator platform for a monolithic coupled system, where a straight waveguide is seamlessly integrated with a concave diffraction grating, have been presented.
***Keywords*:** Micro-actuator platform, Thermo-electromagnet actuator, MEMS, Monolithic coupled system.

1. INTRODUCTION

Guiding light along a desired path without altering material properties can be achieved by mechanically moving optical components [1]. This adjustment is made possible through MEMS actuators, which modify properties such as length, direction, and coupling angle. Thermo-electromagnetic actuators are particularly promising for integration with optical systems due to their capability to generate significant force and operate bidirectionally [2]. Despite these advantages, challenges such as managing power consumption and controlling temperature rise are critical and require careful consideration. This paper introduces an actuator platform capable of achieving a significant ±2.5 μm deflection (total 5 microns) in a monolithic Littrow coupled system, as illustrated in Fig. 1. The platform successfully displaces the system's intersection of the straight waveguide to trapezoidal waveguide to direct light toward a concave diffraction grating (CDG) [3], and has been extensively simulated using COMSOL Multiphysics to verify its effectiveness.

2. MATERIAL AND METHODOLOGY

The thermo-electromagnetic actuator platform, shown in Fig. 1, utilizes a permanent magnet to generate a Lorentz force when power is applied. This, combined with current-induced temperature increases in the wires, causes thermal expansion that helps achieve the desired deflection, as detailed in the system's load diagram (Fig. 2) and governing equations (Eq. 1) [4–6]. Using MATLAB, we developed initial design parameters, with subsequent refinement through COMSOL Multiphysics FEM analyses focusing on temperature rise, stress at supports, and displacement control to maintain the platform within a 4.3*4.3 mm² area. We designed wire widths narrower than their thickness to avoid out-of-plane displacements from thermal expansion. The project incorporates solid mechanics, electric current, and heat transfer, enhanced by Joule heating and thermal expansion interactions, assuming natural convection with the surrounding air. This platform interfaces with a Littrow monolithic coupled system, ending at a concave diffraction grating (CDG), effectively manipulating the spectral response by adjusting the optical intersection position.

$$EI_{beam}\frac{d^2}{dx^2}\left(\frac{d^2y(x)}{dx^2}\right)+P\left(\frac{d^2y(x)}{dx^2}\right)+\frac{K_s}{n}*y(x)=q(x)=I_{current}*B \tag{1}$$

3. RESULTS AND DISCUSSION

This paper presents a thermo-electromagnetic actuator capable of achieving precise displacement at a designated intersection, requiring a minimal current of 0.0016 mA. Key design factors include the trade-offs between current increase, which boosts force but risks nonlinear behaviour and exceeds silicon's current density limits, and actuator lengthening, which raises both force and stress while expanding the platform's area, causing unwanted size increments in the wire extremities and elevated temperatures. Adding more wires also necessitates increased power and enlarges the platform further. With a magnetic field flux set at 1 Tesla, the platform's specifications are a length of 2430 microns, a width of 3 microns, and 680 wires, aiming for a monolithic system with approximately 645 N/m stiffness at the middle. These considerations are crucial for optimizing performance and minimizing the footprint in photonic systems, as detailed in Figures 3-5.

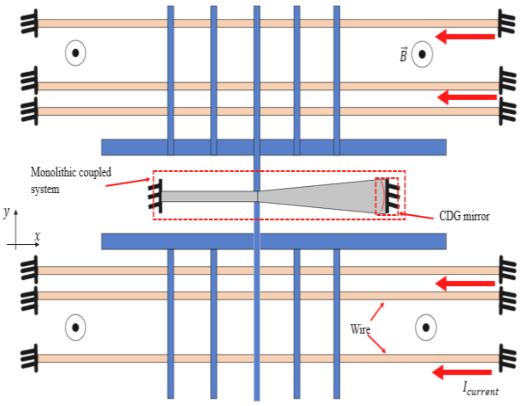

Figure 1: Schematic of the Littrow monolithic coupled system.

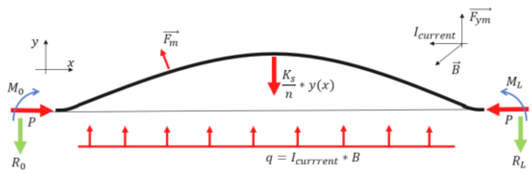

Figure 2: One of the top wires under the upward magnetic pressure (q(x)), thermal induced (P), and spring force (Ks/n).

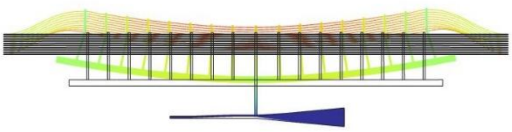

Figure 3: Simulation of the platform for 10 wires.

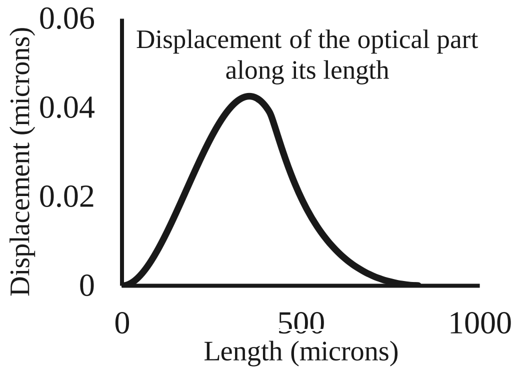

Figure 4-Deflection of the optical component alongside its length with 10 wires.

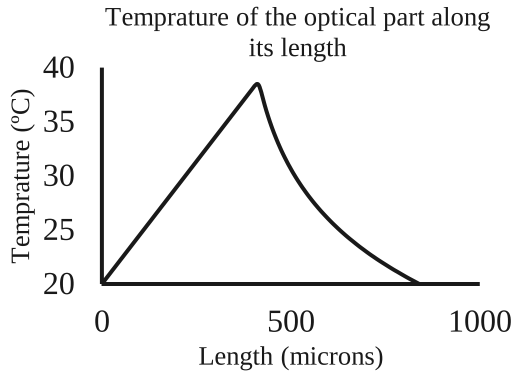

Figure 5-Temprature profile of the optical component alongside its length.

5. CONCLUSIONS

In conclusion, we have presented a thermo-electromagnetic actuator that delivers substantial force to reposition the intersection of the straight waveguide and trapezoidal waveguide of a Littrow monolithic coupled system, enabling effective steering of light propagation over a broad spectral range. Owing to its monolithic design, the platform minimizes concerns related to system rotation. However, as the temperature increases, nonlinear behaviour becomes evident, and operation before the buckling threshold may alter the reflective index, potentially affecting system efficiency. Future investigations should consider alternative actuator designs to address these challenges while preserving the high-force capabilities demonstrated here.

REFERENCES

[1] F. Chollet, Devices based on co-integrated MEMS actuators and optical waveguide: A review, Micromachines 7 (2016) 18.
[2] A. Cao, J. Kim, L. Lin, Bi-directional electrothermal electromagnetic actuators, Journal of Micromechanics and Microengineering 17 (2007) 975.
[3] M. Fasihanifard, M. Packirisamy, Methods and systems of mechanical tuning multi channel optical components, (2023).
[4] A. Potekhina, C. Wang, Review of electrothermal actuators and applications, in: Multidisciplinary Digital Publishing Institute, 2019: p. 69.
[5] Y. Zhu, A. Corigliano, H.D. Espinosa, A thermal actuator for nanoscale in situ microscopy testing: design and characterization, J. Micromech. Microeng. 16 (2006) 242. https://doi.org/10.1088/0960-1317/16/2/008.
[6] X. Lv, W. Wei, X. Mao, Y. Chen, J. Yang, F. Yang, A novel MEMS electromagnetic actuator with large displacement, Sensors and Actuators A: Physical 221 (2015) 22–28.

Formation and Shielding Effectiveness of Ferrosoliton in the Presence of Dynamic Magnetic Field

Huan-Kuang Kuan[1], Hsin-Chieh Hsieh[1] and Yan-Hom Li [1]
Department of Mechanical and Aerospace Engineering, Chung-Cheng Institute of Technology, National Defense University, Taiwan
(E-mail: ruly5201314@gmail.com, belle820908@gmail.com, athomeli@ccit.ndu.edu.tw)

***Short abstract*:** This work is aimed to study the relationship between layer thickness and ferrosoliton behavior in the presence of an oscillating magnetic field and to enable the design of lightweight and material-efficient shielding systems. The experimental results indicate that taller ferrosolitons, which form at lower oscillation frequencies, possess a higher effective cross-section and generate stronger magnetization gradients. This enhances both the absorption and reflection of electromagnetic interference (EMI). In contrast, at higher frequencies, the reduced height of ferrosolitons results in weaker interactions, leading to a decrease in EMI shielding effectiveness (SE).
***Keywords*:** *ferrofluid, ferrosoliton, oscillating magnetic field, EMI, shielding effectiveness*.

1. INTRODUCTION

Ferrofluids, colloidal suspensions of nanoscale ferromagnetic or ferrimagnetic particles in a carrier fluid, have a wide range of applications due to their unique magnetic and fluidic properties. These applications span across engineering, medicine, and technology [1]. Ferrofluids find widespread usage in magnetic sealing, dynamic loudspeakers, computer hardware, electronic packaging, aerospace, bioengineering, and EMI shielding [2]. Ferrosolitons are nonlinear wave phenomena that can occur in ferrofluids under the influence of magnetic fields. These localized, stable wave structures are significant because they represent a unique interplay between the fluid dynamics and the magnetic properties of ferrofluids. Ferrofluid-based systems can offer tunable shielding properties, particularly valuable in adaptive shielding applications by adjusting the oscillating frequency and layer thickness. This work investigates the relationship between layer thickness and ferrosoliton behavior in an oscillating magnetic field. The EMI SE for the Ku-band frequency is measured to determine the optimal layout of the ferrofluid thickness and magnetic field conditions.

2. MATERIAL AND METHODOLOGY

A coil with 2000 turns of copper wire is connected to an AC/DC power supply, generating both a static magnetic field and a dynamic magnetic field by adjusting the input current and oscillating frequency. The ferrofluid used in the experiment, EMG905, is oil-based and consists of nanoscale magnetite (Fe_3O_4) particles suspended in petroleum with an oleic acid dispersant. EMG905 has a saturation magnetization of 44 mT, a density (ρ) of 1200 kg/m³, and a surface tension (γ) of 25.6 mN/m. The prepared ferrofluid is introduced into a Petri dish with a flat circular bottom measuring 20 mm in diameter and 10 mm in thickness. To observe the splitting patterns of the ferrofluid under various magnetic field conditions, cameras are positioned above and at the sides of the setup. A pair of linearly polarized antennas were installed inside an EMI shielding box with dimensions of 100 cm × 100 cm × 100 cm. The electromagnetic parameters of the sample were measured using a vector network analyzer (R&S ZNB40) connected to the box.

3.RESULTS AND DISCUSSION

Figure 1 shows the images of the formation of the ferrofluid spikes subjected to an oscillating magnetic field with verious frequency. In a ferrofluid layer with a thickness of 3 mm, the ferrofluid spike number decreases from 8 to 3 when the frequency increases from 15 Hz to 105 Hz. When the thickness increases to 5 mm, the single spike (or so-called ferrosilicon) starts emerging at frequencies between f=45 Hz to 105 Hz. For the thickness of 7 mm, ferrosoliton is observed at a frequency between f=15 to 85. It's noted that the spike is diminished at a higher frequency of 105 Hz because of the significant phase lag between the oscillating magnetic field and the superparamagnetic ferrofluid. Figure 2 (a) compares the formation of ferrosolitons under various experimental conditions, focusing on oscillating frequency, layer thickness, and ferrosoliton height. At low frequencies, the ferrofluid has sufficient time to align with the magnetic field, forming taller spikes even in thicker layers. At high frequencies, the combination of phase lag and distributed magnetic force in thicker layers leads to shorter and insigificant spikes. Figure 2 (b) shows the EMI SE for the ferrosoliton generated from 9-mm thickness ferrofluid layer subjected to various oscillating magnetic fields. It's known that the SE is affected by the thickness of the layer, oscillating frequency, and height of the ferrosoliton. Thicker layers generally improve EMI SE. However, excessive thickness may cause energy dissipation through secondary mechanisms like heat generation, reducing the efficiency of shielding at higher frequencies. Taller ferrosolitons, formed at lower oscillating frequencies, have a higher effective cross-section and introduce stronger gradients in magnetization, improving both absorption and reflection of EMI. At higher frequencies, the reduced ferrosoliton height leads to weaker interactions, thereby lowering the EMI SE. The effects of the ferrofluid thickness, height of the ferrosoliton, and oscillating frequency on the EMI SE will be discussed comprehensively in the full manuscript.

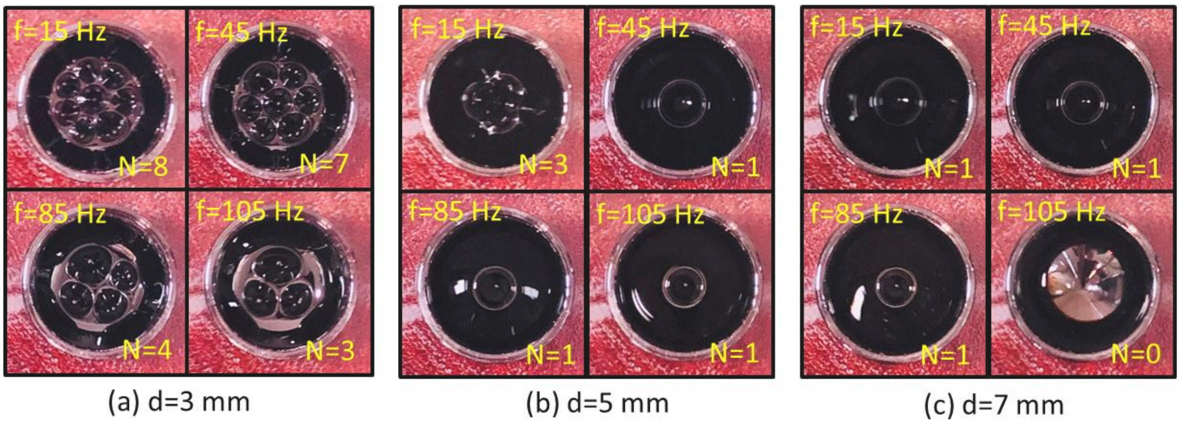

Figure 1: Instability of a ferrofluid layer with a thickness of (a) d=3 mm (b) d=5 mm (c) d=7 mm subjected to an oscillating magnetic field with a frequency of 15 Hz, 45 Hz, 85 Hz, and 105 Hz.

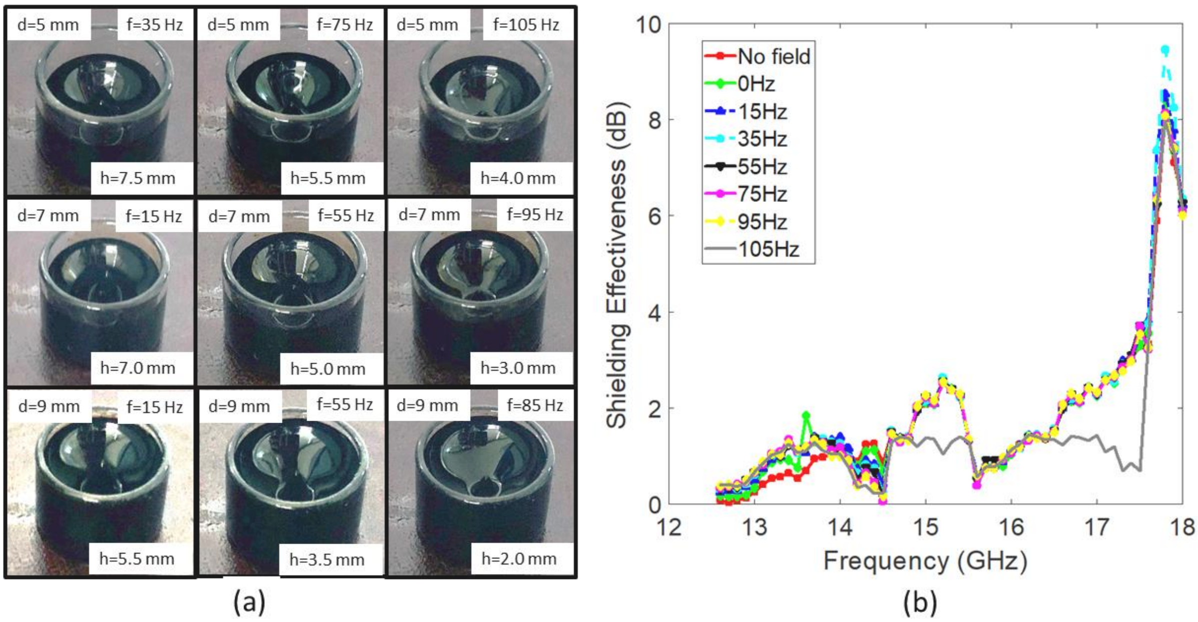

Figure 2: (a) Formation of the ferrosoliton under various experimental conditions. (b) Measurement of EMI shielding effectiveness for a 9-mm thickness ferrofluid layer with different types of ferrosoliton. The h in figure (a) stands for height.

4. CONCLUSIONS

The thickness of ferrofluid and ferrosoliton's height play crucial roles in optimizing the shielding effectiveness. Applications requiring high EMI SE should operate under conditions favoring taller and more stable ferrosolitons. The insights on frequency and thickness optimization can contribute to the development of energy-efficient shielding materials by reducing excess material usage while maximizing effectiveness.

REFERENCES

[1]Kole, M., Khandekar, S. Engineering applications of ferrofluids: A review. Journal of Magnetism and Magnetic Materials. 2021, 537:168222.

[2]Malaescu I, Marin CN, Fannin PC, Experimental Investigations on the Ferromagnetic Resonance and Absorbing Properties of a Ferrofluid in the Microwave Range. Magnetochemistry. 2024; 10: 7.

Development of a Rotary Liquid Inerter with Negative Stiffness and Variable Damping Characteristics

Wenlang Xie[1], Lei Deng[2] and Weihua Li[1]

[1] School of Mechanical, Materials, Mechatronic, and Biomedical Engineering, University of Wollongong, Australia
(E-mail: wx528@uowmail.edu.au, leideng@uow.edu.au)
[2] School of Electrical, Computer & Telecommunications Engineering, University of Wollongong, Australia
(E-mail: weihuali@uow.edu.au)

Short abstract: An inerter is a single-port, two-terminal device generating inertance proportional to relative acceleration and delivering force aligned with motion. A helical-tube fluid inerter achieves inertance via external fluid motion, though only linear versions have been reported. This study introduces a rotary fluid inerter with two critical features: negative stiffness and variable damping. Meanwhile, by integrating a magnetorheological unit, the inerter can deliver variable damping characteristics in addition to its negative stiffness feature. This integration also enables magnetorheological devices to deliver force aligned with motion, improving vibration attenuation. A prototype was tested to verify these features.
***Keywords*:** rotary inerter, negative stiffness, variable damping, magnetorheological device, mathematical modelling

1. INTRODUCTION

Vibrations challenge mechanical engineering applications, prompting diverse passive control solutions. Among these, inerters—one-port, two-terminal elements generating forces proportional to relative acceleration—can impart negative stiffness, lowering natural frequencies [1]. Inerters are broadly classified as flywheel- or non-flywheel-based ones. Flywheel-based inerters convert linear motion into flywheel rotation but degrade over time due to component wear. Non-flywheel fluid inerters, like helical-tube designs, rely on fluid mass in an external channel yet remain limited to linear setups [2]. This restricts their suitability for rotary vibrations, such as in robotic arms. Due to adaptability to broad frequency scenarios, the effectiveness of passive systems is severely constrained [3]. Meanwhile, active and semi-active systems address multiple frequencies by providing adjustable forces. Magnetorheological fluid (MRF) dampers, for example, offer variable damping with low power demands and rapid response but cannot produce negative stiffness forces, reducing their control effectiveness [4]. To overcome these limitations, this paper introduces a novel rotary liquid inerter featuring both negative stiffness and adjustable damping via an integrated MRF element, enabling even more advanced rotary vibration control.

2. OBJECTIVES

1. Design and prototype the proposed rotary fluid inerter.
2. Evaluate the negative stiffness and variable damping characteristics by experiments.

3. MATERIAL AND METHODOLOGY

As indicated in Figure 1(a), the variable damping rotary fluid inerter (VDRFI) is designed. When no current is applied to the coils, the MRFs remain in a fluid state, allowing unrestricted rotation between the rotor and casing. Conversely, when current is supplied, a perpendicular magnetic flux forms across the MRF gap, causing the MRFs to transition into a semi-solid state within milliseconds. This transformation generates a damping torque opposing the relative motion of the rotor and casing. By adjusting the input current, the magnetic field strength can be varied, thus regulating the damping level in the variable damping (VD) unit.

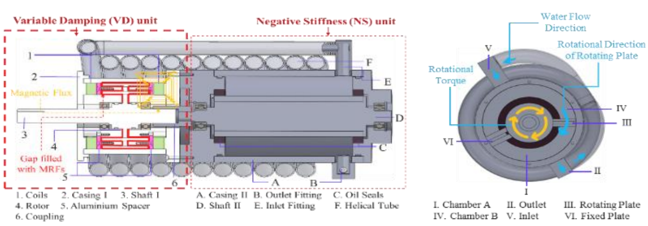

(a) (b)

Figure 1: The design of the proposed VDRFI: (a) the section view, (b) the schematic of the NS unit

Being detailed in Figure 1(a), the negative stiffness (NS) unit features two plates—one mounted on the shaft, the other on the casing—that partition its interior into two water-filled chambers connected by a helical tube. Seal grooves ensure water flows exclusively through the tube rather than around the plates. As detailed in Figure 1(b), when the rotating plate turns clockwise, the volume of chamber A contracts, pushing water out through the helical tube, and accelerating the fluid. After overcoming frictional and pressure losses, the water enters chamber B. This acceleration establishes inertance, which applies an inertial torque in the same direction as the shaft's motion. Hence, the NS unit provides a negative stiffness effect.

4. RESULTS AND DISCUSSION

The evaluation of the prototyped VDRFI includes frequency and current dependency tests. In the frequency test, the device is tested under harmonic displacement excitations with a fixed amplitude A= 40° and various frequencies f = 0.5, 0.75, 1.0, 1.25, and 1.5 Hz, while the supplied current is I = 0.5 A. In the current dependency test, the device is tested under various currents I= 0, 0.5, 1.0, 1.5, and 2.0 A, and the harmonic displacement signal is set with an amplitude A = 40° and a frequency f = 1.25 Hz.
The response of the whole VDRFI to different frequencies is depicted in Figure 2(a). It is observed that all torque-displacement loops incline left, appearing a negative stiffness characteristic. Following the increase of the excitation frequency, this tendency becomes more obvious. Figure 2(b) shows the results of the current dependency tests. It is seen an expansion of the torque-displacement loop in the vertical direction as the current increases, demonstrating the damping variability. The torque-displacement loops also behave with a negative stiffness feature, while no clockwise revolve is observed.

(a) (b)

Figure 2: Experimental results to evaluate the VD unit under: (a) frequency dependency test, and (b) current dependency test

5. CONCLUSIONS

To fill the gap of missing in rotary liquid ineters and overcome the limitation of variable damping devices in generating forces aligned with the relative motion, this paper proposes a rotary VDRFI, which can simultaneously exhibit variable damping and negative stiffness characteristics. The proposed design has been prototyped and tested. The experimental results have verified its features.

ACKNOWLEDGEMENT

This research is supported by the Australian Research Council Linkage Grant (LP210301054), the Australian Research Council Discovery Grants (DP200100149 and DP240101050), the Australian Research Council DECRA Grant (DE250100190) and the University of Wollongong and China Scholarship Council (CSC) joint scholarship (202308200019).

REFERENCES

[1] M. C. Smith. Synthesis of mechanical networks: the inerter. IEEE Transactions on Automatic Control. 2002 47(10):1648-1662.
[2] Y. Shen, L. Chen, Y. Liu, X. Zhang and X. Yang. Optimized modeling and experiment test of a fluid inerter. Journal of Vibroengineering. 2016 08/15;18(2789-2800.
[3] T. T. Soong and B. F. Spencer. Supplemental energy dissipation: state-of-the-art and state-of-the-practice. Engineering Structures. 2002 2002/03/01/;24(3):243-259.
[4] L. Deng, S. Sun, M. D. Christie, J. Yang, D. Ning, X. Zhu, H. Du, S. Zhang and W. Li. Experimental testing and modelling of a rotary variable stiffness and damping shock absorber using magnetorheological technology. Journal of Intelligent Material Systems and Structures. 2019 30(10):1453-1465.

Rheological and piezoresistive properties of anisotropic magnetorheological elastomers based on gelatine

Robert Moucka[1], Josef Osicka[1], Michal Sedlacik[1], and Michal Kocak[1]

[1] Centre of Polymer Systems, Tomas Bata University in Zlín, Czech Republic
(E-mail: moucka@utb.cz, osicka@utb.cz, msedlacik@utb.cz, m_kocak@utb.cz)

Abstract:

Magnetorheological elastomers (MREs) have garnered significant attention due to their tunable mechanical properties under the influence of magnetic fields [1-3]. This study explores the rheological and piezoresistive behaviour of anisotropic MREs synthesized using gelatine as the polymer matrix and magnetic iron particles as the dispersed phase. The anisotropic gelatine-based MREs were prepared by dispersing varying concentrations of iron particles within the gelatine matrix. Anisotropy was introduced by aligning the iron particles while the gelatine was still in a liquid state.

Rheological measurements were conducted to evaluate the viscoelastic properties of the MREs under different magnetic field strengths. The results demonstrated a substantial increase in storage modulus with the application of a magnetic field, indicating enhanced stiffness and improved mechanical performance. Additionally, the influence of particle concentration on the rheological properties was systematically analysed, revealing a direct correlation between particle content and the magnetorheological effect.

Piezoresistivity tests were performed on the anisotropic MREs to assess their electrical resistance changes under mechanical deformation. The aligned particles within the gelatine matrix exhibited significant piezoresistive behaviour, with resistance decreasing under compression. This property underscores the potential of these MREs for use in sensors and adaptive systems where both mechanical and electrical responses are critical.

The findings of this study highlight the potential of gelatine-based MREs for applications in adaptive damping systems, soft robotics, and biomedical devices [4]. The biocompatibility of gelatine further extends the applicability of these MREs in medical and pharmaceutical fields. Future work will focus on optimizing the particle dispersion, alignment, and cross-linking density to enhance the performance and stability of the MREs.

***Keywords*:** Piezoresistivity, Magnetorheological elastomers, Anisotropy, Gelatine.

ACKNOWLEDGEMENT

The authors wish to thank the Czech Science Foundation [23-07244S] for the financial support.

REFERENCES

[1] Y. Kim and X. H. Zhao, "Magnetic Soft Materials and Robots," Chemical Reviews, vol. 122, pp. 5317-5364, Mar 2022.

[2] Y. C. Li, J. C. Li, W. H. Li, and H. P. Du, "A state-of-the-art review on magnetorheological elastomer devices," Smart Materials and Structures, vol. 23, Dec 2014.

[3] Y. Fu, J. J. Yao, H. H. Zhao, G. Zhao, Z. S. Wan, and R. Z. Guo, "A muscle-like magnetorheological actuator based on bidisperse magnetic particles enhanced flexible alginate-gelatin sponges," Smart Materials and Structures, vol. 29, Jan 2020.

[4] X. H. Liu, P. P. Yan, R. Cui, Y. Wu, B. Xu, W. T. Zhou, et al., "Controllable Damping Magnetorheological Elastomer Meniscus," Acs Biomaterials Science & Engineering, 2022 Dec 2022.

Effect of the spatial distribution of magnetic filler on the effective electromagnetic interference shielding of magnetorheological elastomers

Michal Sedlacik[1], Andrei Munteanu[1] and Martin Cvek[1]

[1] Centre of Polymer Systems, Tomas Bata University in Zlín, Czech Republic
(E-mail: msedlacik@utb.cz, munteanu@utb.cz, cvek@utb.cz)

Short abstract: The current study is concerned with the electromagnetic interference shielding of magnetorheological elastomers (MREs). More specifically, the correlation between the spatial distribution of magnetic particles and the resulting electromagnetic shielding efficiency is studied. During preparation, both isotropic and anisotropic structures were obtained. For the isotropic MREs, the particles were coated with a thin layer of organosilane, using a surface-initiated atom transfer radical polymerization with the magnetic properties being preserved. Both the internal arrangement and the surface modification of the particles significantly affected the shielding properties. The best results were obtained for the isotropic MREs.

Keywords: Particle modification, Electromagnetic interference shielding, Magnetorheological elastomers, Anisotropy.

1. INTRODUCTION

This work deals with a promising application of MREs in the form of radioabsorbers [1]. Such materials are able to absorb electromagnetic (EM) waves due to electrical/magnetic dipoles that interact with them [2]. Another method is the utilization of multireflection and absorption taking place on the interfaces of the radioabsorber [3]. The conventional radioabsorbers are usually hard and heavy materials. Today, there is a need for soft materials, i.e., clothes with EM shielding properties [4]. Such soft materials include composites filled with micro/nanoparticles, which are effective due to the high surface area of the filler leading to a high interface between filler and matrix, thus interaction with EM signal [5]. Magnetorheological elastomers (MREs) can be a good candidate due to their magnetic and conductive fillers. However, MREs share some drawbacks, such as bad compatibility of the polymeric matrix and the filler, consequently insufficient dispersion of the particles, and the possibility of the filler's corrosion, both of which affect the EM shielding. Creating core-shell structured particles with a polymeric surface layer on the surface of carbonyl iron (CI) particles can be a good solution [1]. The polymeric layer improves both the particles' compatibility with a matrix and their resistance against corrosion agents. So far, there are not many studies based on MREs with EM shielding properties, and the current study fills critical gaps in the field, including the effect of particle distribution, coating, and filler concentration.

2. OBJECTIVES

The objectives of the presented paper include:

- To successfully coat the CI particles with a very thin layer of organosilane using a novel method.
- The investigation of spatial distribution of particles and their concentration on the EM shielding.
- The investigation of the effect of the coating on the EM shielding of the most promising MREs.

3. MATERIAL AND METHODOLOGY

The coating of the particles was poly(trimethylsilyloxyethyl methacrylate), which was performed via surface-initiated atom transfer radical polymerization. The coating of the CI particles was confirmed via transmission electron microscopy (TEM). The magnetic properties of the bare and coated particles were investigated via vibrating sample magnetometry. The MREs were prepared by mixing the CI particles with a silicone elastomer under constant mixing, while for the anisotropic samples, the elastomers were cured under the presence of a magnetic field of 300 mT. The shielding efficiency of the MREs under investigation was determined using a PNA-L network analyzer and waveguide method. Rectangular samples with dimensions fitting the insert of the corresponding waveguide were measured in the frequency range of 2.6–18 GHz.

4. RESULTS AND DISCUSSION

The magnetic properties of the bare and coated samples are shown in Figure 1a. As can be seen, both bare and coated samples have almost identical magnetization curves, with coated particles having a slightly higher susceptibility at lower fields but a slightly lower saturation magnetization, which is, however, insignificant (bottom inset). Usually, organic coatings hinder the magnetic properties of magnetic particles; however, due to the very thin layer of the coating (top inset), the particles preserved their original saturation magnetization.

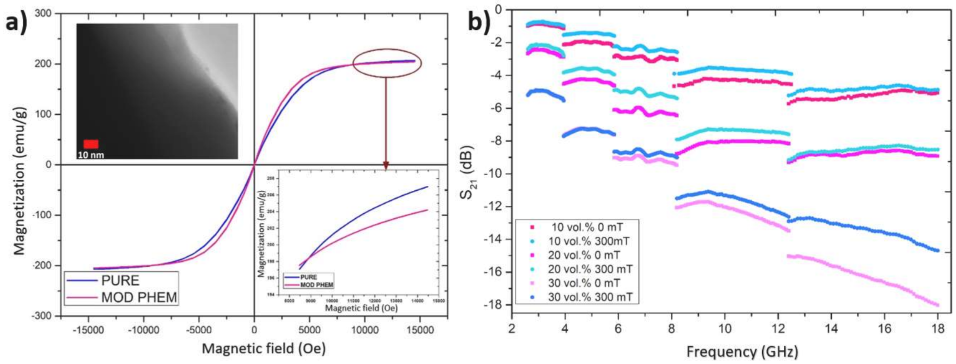

Figure 1: a) The magnetic curve of the bare CI (blue) and coated (purple) particles. The bottom inset magnifies the saturation region while the top shows a TEM. b) The EM efficiency for isotropic and anisotropic MREs as a function of frequency for different particle concentrations.

Figure 1b displays the influence of the particle concentration and orientation on the shielding properties of the MREs. As can be seen, the samples with higher concentrations display better shielding properties. Furthermore, isotropic samples were able to block more signal. A possible explanation would be the better dispersibility/spatial distribution of the particles, which allows the absorption of more waves due to the higher number of reflections. Moreover, the particles of the anisotropic samples are arranged in chains, in the same direction as the EM wave, thus it can be assumed that the waves pass through them easier. As revealed in Figure 1b, the shielding properties increase with growing frequency; e.g., the isotropic MRE can interfere ~ 98 % (–16.3 dB) of incident electromagnetic signal, while the anisotropic only ~ 95 % (–13.4 dB) of incident electromagnetic signal. Results on coated particles are preserved for the presentation.

5. CONCLUSIONS

We investigated the effect of particle orientation within MREs on electromagnetic shielding. Isotropic samples proved to have a higher efficiency. Capitalizing on the latter result, we improve the distribution by coating the filler with a thin layer of organosilane, which does not hinder the magnetic properties of the sample. Although the shielding efficiency does not reach commercial values, our material is soft, bendable and much lighter than existing solutions.

ACKNOWLEDGEMENT

The authors wish to thank the Czech Science Foundation [23-07244S] for the financial support. M.C. would like to acknowledge project DKRVO [RP/CPS/2024-28/007] supported by the Ministry of Education, Youth and Sports of the Czech Republic.

REFERENCES

[1] Cvek M, Moucka R, Sedlacik M, Pavlinek V. Electromagnetic, magnetorheological and stability properties of polysiloxane elastomers based on silane-modified carbonyl iron particles with enhanced wettability. Smart Materials and Structures. 2017 Oct;26(10):105003.
[2] Lee HR, Ryu SH, Kwon SJ, Choi JR, Lee SB, Park B. Absorption-Dominant mmWave EMI Shielding Films with Ultralow Reflection using Ferromagnetic Resonance Frequency Tunable M-Type Ferrites. Nano-Micro Letters. 2023 Dec;15(1):76.
[3] Cheng ML, Ying MF, Zhao RZ, Ji LZ, Li HX, Liu XG, Zhang J, Li YX, Dong XL, Zhang XF. Transparent and Flexible Electromagnetic Interference Shielding Materials by Constructing Sandwich AgNW@MXene/Wood Composites. Acs Nano. 2022 Oct 25;16(10):16996-17007.
[4] Wei YF, Luo JB, Yang WF, Gong W, Li YG, Zhang QH, Li KR, Hou CY, Wang HZ. Superflexible hybrid aerogel-based fabrics enable broadband electromagnetic wave management. Chemical Engineering Journal. 2023 Apr 15;462:142169.
[5] Moucka R, Sedlacik M, Prokes J, Kasparyan H, Valtera S, Kopecky D. Electromagnetic interference shielding of polypyrrole nanostructures. Synthetic Metals. 2020 Nov;269:116573.

Semi-conducting microspheres prepared from a glucose: A way to sustainable electrorheological fluids

Tomas Plachy, Tereza Cermakova and Erika Pavlikova

(E-mail: plachy@utb.cz, t_cermakova@utb.cz; epavlikova@utb.cz)
Centre of Polymer Systems, University Institute, Tomas Bata University in Zlín, The Czech Republic, třída Tomáše Bati 5678, Zlín 760 01

Short abstract: In this study, a glucose was used as a renewable precursor for preparation of a dispersed phase for electrorheological fluids. Using in sequence hydrothermal and thermal carbonization, the semi-conducting microspheres were prepared using only water and heat without excessive chemicals. Moreover, using thermal carbonization enabled tuning of the particle conductivity and thus optimize performance of their electrorheological fluids. This approach led to electrorheological fluids with sufficient electrorheological effect using sustainable system at the same time.
Keywords: Glucose; electrorheology; dielectric properties, sustainable.

1. INTRODUCTION

Electrorheological (ER) fluids (ERFs) are well-known intelligent systems, whose rheological properties can be controlled through application of an external electric field. They are commonly composed of a dispersed phase consisting of particles with specific electric and/or dielectric properties, and a dispersed medium with low dielectric permittivity (for example silicone oil).

Due to increasing effort on sustainability and a use of renewable sources for production of goods, this work is focused on utilization of glucose, as an abundant matter, as a precursor for production of a particulate material suitable for its usage as a dispersed phase for ERFs. One of the main drawbacks of ERFs is their low yield stress, which is commonly not sufficient for industrial applications. This study joins together a sustainable dispersed phase for ERFs exhibiting high yield stresses at relatively low particle concentration.

2. OBJECTIVES

The presented paper deals with possibility of preparation of particles suitable for their use as a dispersed phase in ERFs from renewable source. The precursor, glucose, is hydrothermally treated using only demineralized water and heat without any excessive chemicals. The hydrothermally heated glucose is further carbonized in an inert atmosphere at elevated temperatures giving arise to semi-conducting particles, whose conductivity can be further controlled by the carbonization temperature. Unique ERFs with high yield stresses at relatively low loading level of the particles can be thus prepared using renewable source as a dispersed phase. Moreover, the synthesis considering a usage only of demineralized water and heat source can be considered as a green synthesis.

3. MATERIAL AND METHODOLOGY

For synthesis of the particles a glucose (α-D-Glucose, anhydrous, 96%; Sigma-Aldrich) and demineralized water were used. For preparation of electrorheological fluids (5wt% particle concentration) silicone oil Lukosoil M200 (η = 200 mPa s) was used.

The electrical conductivity of the prepared particle was measured using a two-point method and a Kethley 6517K electrometer. Scanning electron microscopy (SEM; Tescan VEGA) was involve to observe morphology and size of the prepared particles. Further, electrorheological properties of prepared ERFs were investigated using a rotational rheometer Anton Paar and impedance spectroscopy was used to evaluate dielectric properties of the prepared ERFs.

3.1. Particle preparation

A glucose (α-D-Glucose, anhydrous, 96%; Sigma-Aldrich) was mixed with a demineralized water and poured into an autoclave as demonstrated elsewhere [1]. The mixture was heated at 180 °C for 12 hours and the particles were then filtered with demineralized water and ethanol. The sample is further labelled as HTC-Glucose. Dried HTC-Glucose was then thermally treated using a tubular furnace at various temperatures. The average heating rate was 3.3 °C/min and the sample was held at the final temperature for one hour.

4. RESULTS AND DISCUSSION

Figure 1a depicts HTC-Glucose particles and Figure 1b their carbonized analogues treated at 500 °C. Both particles exhibited spherical shape with a diameter of the particles below 500 nm, making them suitable candidates for use as a dispersed phase in ERFs also from the point of view of sedimentation stability. Moreover, the possibility to tune their conductivity according to carbonization temperature is shown in Figure 2. While HTC-Glucose possessed electric conductivity 8.45×10^{-13} S/cm, their carbonized analogues exhibited electric conductivity about several orders of magnitude higher (Figure 2).

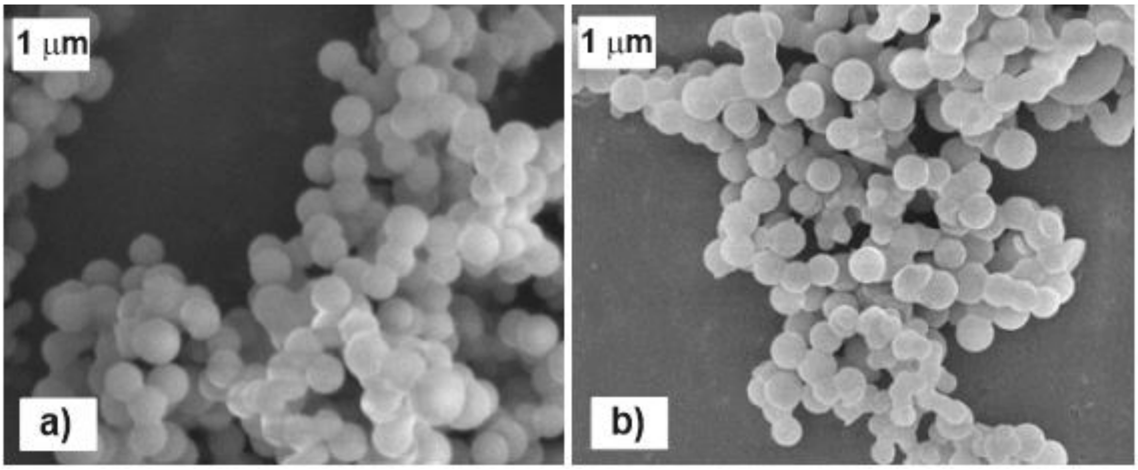

Figure 1: SEM Image of the prepared particles: (a) hydrothermally treated glucose and (b) its thermal carbonized analogues treated in an inert gas at 500 °C.

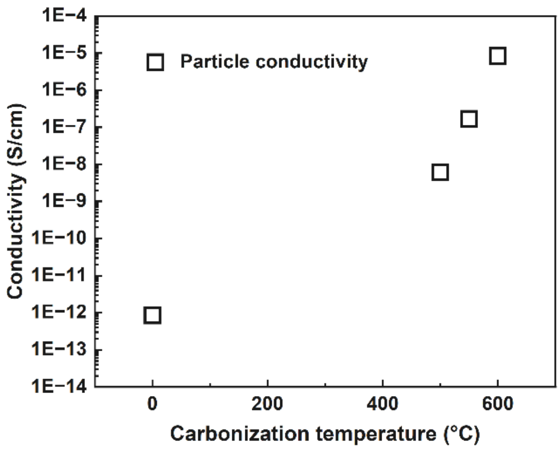

Figure 2: A dependence of particle conductivity on the carbonization temperature.

5. CONCLUSIONS

The study confirms the possibility to use glucose as a renewable source for preparation of dispersed phase with tuneable conductivity for electrorheological fluids. The electrorheological fluids based prepared particles exhibited outstanding properties with a yield stress over 150 Pa at particle loading 5 wt%.

ACKNOWLEDGEMENT

The authors would like to thank for financial support provided by the Ministry of Education, Youth and Sports of the Czech Republic – DKRVO (RP/CPS/2024-28/003).

REFERENCES

[1] Pavlikova E, Plachy T, Urbanek M, Cvek M. Engineering Conductivity and Performance in Electrorheological Fluids Using a Nanosilica Grafting Approach. ACS Applied nano materials. 2023 6:9768-9776.

Electro-rheo-imaging of a non-equilibrium emulsion: microstructures and a multi-state switchable viscous response

Majid Bahraminasr *[1] and Anand Yethiraj [1,2]

[1] Department of Physics and Physical Oceanography, Memorial University of Newfoundland, Canada
(E-mail: mbahraminasr@mun.ca, ayethiraj@mun.ca)
[2] Department of Physics, University of Guelph , Canada
(E-mail:ayethira@uoguelph.ca)

Short abstract: We introduce a novel technique combining electric forcing, rheology and microscopy – Electro-Rheo-Imaging (ERI) – and apply it to an oil-in-oil emulsion. Using a modified rheometer and a low-threshold castor oil–motor oil emulsion, we demonstrate reversible, field-tunable viscosity shifts—with shear-induced banding, droplet deformation, and phase transitions driven by AC and DC electric fields.

Keywords: Electrohydrodynamics, Emulsion, Rheology, Banding, ERI

1. INTRODUCTION

Complex fluids such as emulsions exhibit diverse rheological behaviors under flow, particularly when driven by external fields. Electrohydrodynamic (EHD) effects provide a means to manipulate microstructure and thus control macroscopic viscosity. In this study, we present ERI—a technique that combines rheology with real-time imaging, enabling correlation between structure and flow properties in an oil-in-oil emulsion system.

2. OBJECTIVES

The aim is to investigate the electric-field-induced structural transitions and viscosity modulation in emulsions using ERI. We target both DC and AC field regimes to understand the interplay between shear, droplet dynamics, and field-driven microstructural changes.

3. MATERIAL AND METHODOLOGY

The emulsion consists of castor oil droplets dispersed in motor oil. The ERI setup modifies an Anton Paar MCR 301 rheometer by integrating optical microscopy with ITO-coated electrodes for electric field application. DC and AC fields up to 500 Hz and 3.7 V/μm were applied across a 270 μm gap. Microscopy captured quarter-disk views of the sample to resolve both individual and collective droplet behaviors. Shear rates varied from 1 to 600 s^{-1} to explore flow regimes.

4. RESULTS AND DISCUSSION

Our results reveal a strong frequency-dependent modulation of emulsion viscosity under applied electric fields, characterized by three distinct regimes:

Regime I (DC and AC, $f < 10$ Hz): Dominated by electrohydrodynamic (EHD) flows. Droplet breakup and dynamic coalescence lead to a dramatic reduction in viscosity, reaching as low as 0.03 Pa·s at 2 Hz—nearly a sixfold drop compared to the quiescent state. Micrographs show irregular, fluctuating droplet distributions consistent with convective electroflows. A similar viscosity drop is observed under DC fields (3.7 V/μm), confirming the EHD nature of this regime.

Regime II (10 Hz < f < 30 Hz): Marked by a balance between EHD and dipolar forces. Droplets flatten and accumulate near electrodes, resulting in a partial clearing of the bulk region. Viscosity rises back toward the zero-field value, and the system exhibits quasi-static behavior with slow structural reconfiguration. Notably, DC field responses lie within this regime, showing modest shear thinning and coalescence-driven effects without banding.

Regime III ($f > 60$ Hz): Dipolar interactions dominate. Droplets form prolate chains that align along the flow direction, increasing resistance and generating a yield stress. The apparent viscosity reaches values exceeding 1 Pa.s, highlighting the tunability of the system across nearly two orders of magnitude.

Two qualitatively distinct types of banding emerge depending on field parameters. **Dipolar banding**, observed at high frequencies and low shear rates, features regularly spaced droplet chains aligned in the vorticity direction. In contrast, **EHD banding** arises at low frequencies and high shear rates, displaying diffuse bright-dark bands due to radial segregation of droplet density. Both modes are linked to changes in light scattering and correlate strongly with measured viscosity trends.

The transition between regimes is fully reversible and can be actuated simply by toggling the field frequency. This enables **multi-stable rheological states**—a rare feature in soft matter—which is promising for active material design and flow-on-demand applications.

4.2. FIGURE AND FORMULA EXAMPLES

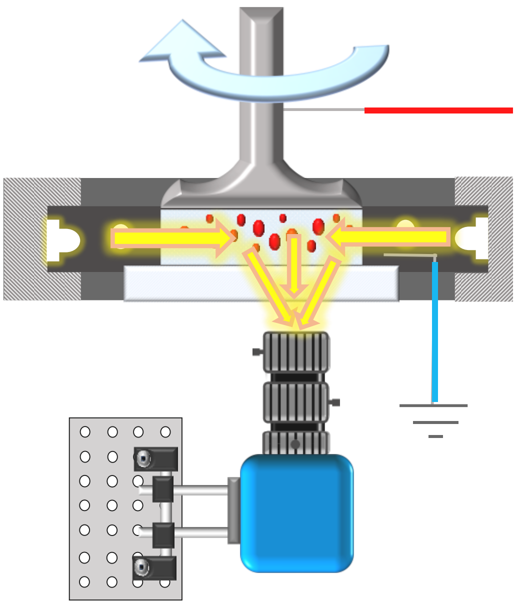

Figure 1: Schematic of the ERI setup showing imaging and field configuration

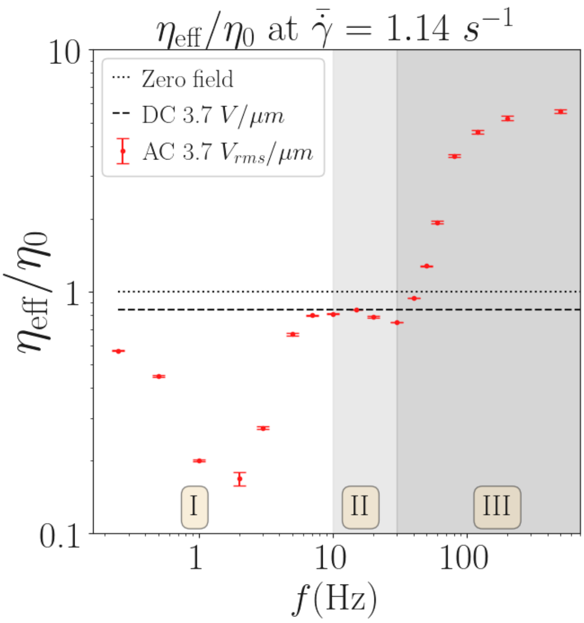

Figure 2: η_{eff}/η_0 at low shear rate ($\dot{\gamma} \approx 1\ s^{-1}$) as a function of AC field frequency (red points, 3.7 $V_{rms}/\mu m$), compared with zero-field (dotted line) and DC field (dashed line) responses. Three regimes are identified:
Regime I: (EHD-dominated, viscosity reduction),
Regime II: (transition zone with coalescence-dominated response), and
Regime III: (dipolar-dominated, viscosity enhancement).

5. CONCLUSIONS

We demonstrate an electric-field-controlled, reversible switch in emulsion viscosity using ERI. Shear-induced banding and field-driven phase reconfiguration offer insights into tunable soft matter systems with potential applications in smart rheological materials.

ACKNOWLEDGEMENT

The authors acknowledge the support of the National Science and Engineering Research Council of Canada (RGPIN-2019-04970). All design and construction were completed in-house, with extensive support from the Memorial University Physical Sciences Machine Shop.

REFERENCES

[1] Vlahovska, P. M. (2019). Electrohydrodynamics of drops and vesicles. *Annual Review of Fluid Mechanics*, *51*(1), 305-330.
[2] Varshney, A., Ghosh, S., Bhattacharya, S., & Yethiraj, A. (2012). Self organization of exotic oil-in-oil phases driven by tunable electrohydrodynamics. *Scientific Reports*, *2*(1), 738.
[3] Kesy, Z., Medrek, G., Osowski, K., Olszak, A., Migus, M., Musiałek, I., Musiałek, K., & Kesy, A. (2022). Characteristics of electrorheological fluids. In A.-G. Olabi (Ed.), *Encyclopedia of smart materials*, 114–139. Elsevier.

Integration of a Magnetorheological Actuator into an Elbow Rehabilitation Orthosis for Patients with Spasticity

Henri Pagé, Carolane Guay-Tanguay, François Michaud, and Jean-Sébastien Plante

Interdisciplinary Institute for Technological Innovation (3IT), Faculty of Engineering, Université de Sherbrooke, 3000 Universite´ Blvd, Sherbrooke, QC J1K 0A5, Canada.
(E-mail: Henri.Page@usherbrooke.ca, Carolane.Guay-Tanguay@usherbrooke.ca, Francois.Michaud@usherbrooke.ca, Jean-Sebastien.Plante@usherbrooke.ca)

Short abstract: Stroke survivors with spasticity face limited access to rehabilitation due to the need for specialized staff and equipment. To address this, portable orthoses that are user-friendly, safe, and tolerant of erratic spastic movements are needed for home use. This paper investigates the integration of a magnetorheological (MR) actuator into an elbow orthosis. Results demonstrate that the MR-based design is lightweight, responsive, and capable of safely accommodating involuntary motion, making it a promising solution for home-based rehabilitation of patients with spasticity.
Keywords: Orthosis, rehabilitation, spasticity, magnetorheological, actuators.

1. INTRODUCTION

Cerebrovascular accidents (CVAs), or strokes, are a leading cause of long-term physical disability [1]. Resulting neurological damage often leads to hemiparesis—partial paralysis on one side of the body—typically manifesting as spasticity, an involuntary increase in muscle tone that limits activities of daily living (ADLs). In severe cases, spasms further reduce voluntary muscle control. Therapeutic interventions include physical rehabilitation, electrostimulation, and botulinum toxin injections. Among these, physical rehabilitation remains the most effective and widely used, involving daily sessions where clinicians manually stretch spastic muscles to encourage motor recovery [2]. However, a growing shortage of trained clinicians limits access to therapy, resulting in fewer treated patients and shorter sessions, which may reduce motivation and recovery. One solution is the integration of mechatronic orthoses for post-stroke rehabilitation [3]. These devices automate elbow rehabilitation exercises and improve consistency. Yet, many lack the force capacity to manage spasticity effectively [4]. For example, while 12 N·m is typical, at least 20 N·m is often required. Muscle spasms (clonus) can occur at 5–8 Hz, or 160–200 ms intervals. Actuators must therefore offer both high torque and rapid response—beyond clonus frequency—to meet rehabilitation safety standards.

2. OBJECTIVES

The objective of this study is to evaluate the actuator's ability to deliver the torque and responsiveness required for effective spasticity management in post-stroke upper-limb rehabilitation. The Magnetorheological Rehabilitation Orthosis (MRO) aims to replicate clinician-guided motion through high-bandwidth torque control and rapid dynamic response, ensuring both therapeutic efficacy and patient safety.

3. CONCEPTION

The developed MRO, shown in Figure 1, was designed with simplicity, portability, and torque performance in mind. Mechanically, it consists of a lightweight exoskeletal frame supporting a custom MR actuator positioned

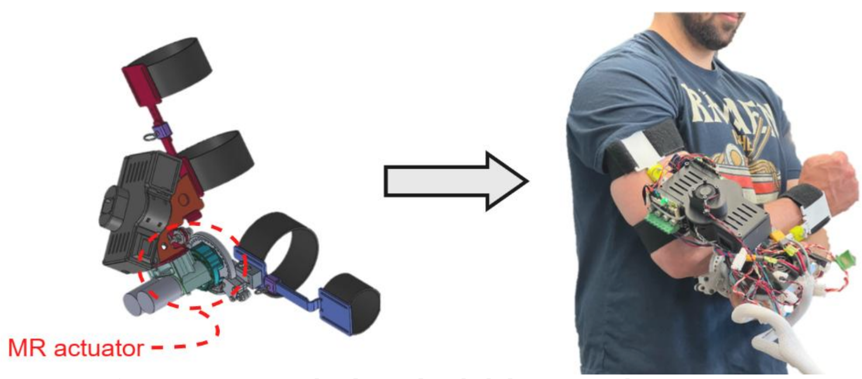

Figure 1: Magnetorheological Rehabilitation Orthosis (MRO).

at the elbow joint to provide flexion-extension assistance. The actuator combines a brushless motor with a magnetorheological clutch to deliver both active and passive torque control, allowing for responsive interaction and backdrivability. Electrically, the system is powered by a compact setup that includes dedicated motor and coil drivers, enabling independent control of the motor torque and the clutch locking effect. A low-cost Arduino UNO R4 Minima microcontroller handles real-time control and signal processing. This minimalist hardware configuration favorize portability and low power consumption while still achieving responsive control. On the software side, a fully open-loop strategy was implemented to maintain simplicity and ensure fast response. Torque commands are sent from a main PC interface, processed by the Arduino, and translated into motor and clutch actuation. Though calibration is required to maintain accuracy, the absence of feedback loops reduces system complexity and latency. Together, these design elements create an efficient, user-friendly orthosis capable of generating clinically relevant torque levels, while maintaining the transparency and safety needed for rehabilitation outside clinical environments.

4. RESULTS AND DISCUSSION

The system was validated through three experimental tests: open-loop torque control, backdrivability, and human interaction under perturbation. The first two tests, illustrated in Figure 2, assessed the system's accuracy and passive behavior. Results showed a fast torque response of ≈14 ms and good tracking accuracy (MAE = 0.3175 N·m), with minimal overshoot and steady-state error. Backdrivability evaluation confirmed low passive resistance across varying speeds, modeled by a nonlinear friction-velocity relationship. During human testing, the orthosis maintained the desired torque with an R^2 of 0.759, despite disturbances up to ±75 deg/s. These results confirm the orthosis's responsiveness, transparency, and suitability for safe upper-limb rehabilitation.

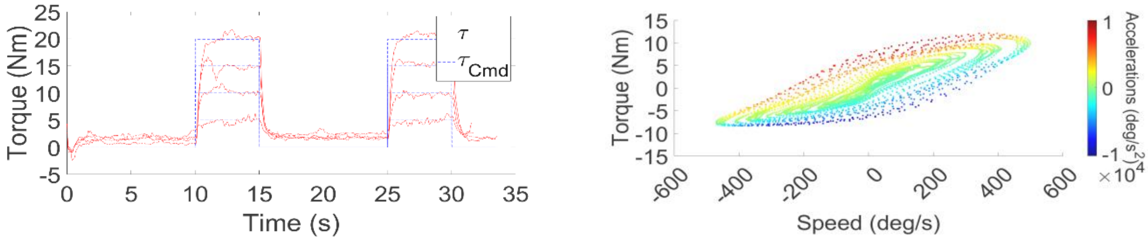

(a) (b)

Figure 2: Open-loop torque response vs. commanded torque **(a)** Output torque as a function of output speed **(b)**

5. CONCLUSIONS

Mechanical and electrical validation was carried out through a series of experiments, including temporal response evaluation, backdrivability assessment, and real-world testing with a human subject. Combined with the implementation of a closed-loop control architecture, this MRO would be a strong candidate for practical, patient-ready use in elbow, wrist and hand rehabilitation contexts.

ACKNOWLEDGEMENT

The authors would like to thank the physical therapist at Raymond Poincaré Hospital, Garches, France, for their involvement in this project.

REFERENCES

[1] V. L. Feigin *et al.*, « Global, regional, and national burden of neurological disorders, 1990–2016: a systematic analysis for the Global Burden of Disease Study 2016 », *Lancet Neurol.*, vol. 18, nº 5, p. 459-480, mai 2019, doi: 10.1016/S1474-4422(18)30499-X.

[2] L. Kerr, V. D. Jewell, et L. Jensen, « Stretching and Splinting Interventions for Poststroke Spasticity, Hand Function, and Functional Tasks: A Systematic Review », *Am. J. Occup. Ther.*, vol. 74, nº 5, p. 7405205050p1-7405205050p15, sept. 2020, doi: 10.5014/ajot.2020.029454.

[3] M. Babaiasl, S. H. Mahdioun, P. Jaryani, et M. Yazdani, « A review of technological and clinical aspects of robot-aided rehabilitation of upper-extremity after stroke », *Disabil. Rehabil. Assist. Technol.*, p. 1-18, janv. 2015, doi: 10.3109/17483107.2014.1002539.

[4] J. Brackenridge, L. V. Bradnam, S. Lennon, J. J. Costi, et D. A. Hobbs, « A Review of Rehabilitation Devices to Promote Upper Limb Function Following Stroke », *Neurosci. Biomed. Eng.*, vol. 4, nº 1, p. 25-42, mai 2016, doi: 10.2174/2213385204666160303220102.

Author Index

X

Y

Z